Assessing pulmonary ventilation and perfusion properties with ^{19}F-MRI

Benjamin John Pippard

BSc MRes MBBS MRCP CertMedEd

Newcastle Magnetic Resonance Centre

Translational and Clinical Research Institute

Thesis submitted in partial fulfilment of the requirements for the degree of

Doctor of Philosophy

November 2021

Supervisors

Prof Peter E Thelwall

Prof A John Simpson

Abstract

Pulmonary imaging with conventional MRI remains challenging, owing to the low proton density of lung tissue and magnetic susceptibility gradients that exist at ubiquitous air-tissue interfaces. The use of exogenous gas agents can overcome these challenges by direct visualisation of inhaled gases within the airways, facilitating assessment of regional ventilation properties. To date, this has largely been achieved in research settings using hyperpolarised-gas MRI, a well-established technique that is capable of providing clinically useful metrics of lung function (e.g. the percentage ventilated lung volume, %VV). However, the requirement for specialised gas polarising equipment and expertise remains a barrier to widespread clinical adoption. Recently, ^{19}F-MRI of inhaled perfluoropropane (PFP) has emerged as a viable approach to human ventilation imaging, offering an alternative to hyperpolarisation with potential for translation to clinical practice.

This thesis presents methods for performing human ^{19}F-MR ventilation imaging, focussing on the application of novel scan procedures in healthy volunteers, patients with asthma, and patients with chronic obstructive pulmonary disease (COPD). Initial experiments were conducted within the framework of a dual-centre study (LIFT), enabling the establishment of reproducible imaging methods in healthy volunteers for the evaluation of static %VV measurements across different study sites. The utility of these methods to quantify ventilation defects in patients with asthma and COPD, including bronchodilator response, is reported and discussed. In addition, this thesis explores the feasibility of performing dynamic ventilation and perfusion imaging, employing ^{19}F-MRI of inhaled PFP in combination with a widely used intravenous gadolinium-based contrast agent. Experiments were conducted within the framework of two small feasibility studies (VQ MRI and LungGas). Initial results of these studies are presented, alongside a discussion of the wider implications for future assessment of regional pulmonary ventilation/perfusion properties. This work supports the use of ^{19}F-MRI as a novel imaging modality for the assessment of respiratory disease.

Acknowledgements

The work presented in this thesis is multidisciplinary by nature, involving close collaboration with colleagues based in Newcastle upon Tyne and Sheffield. Where relevant, the specific contributions of others are referred to throughout this thesis. The following people deserve special mention:

Newcastle upon Tyne

- Prof Pete Thelwall (Primary Supervisor): for his role in devising the experimental studies and associated scan protocols, obtaining relevant funding (Medical Research Council awards), providing data processing and analysis input, and for his support, enthusiasm and generosity of time over the course of this research

- Prof John Simpson (Secondary Supervisor): for his support during my PhD, providing valuable insight regarding the ethical applications and approvals process, and for acting as Chief Investigator for all human studies performed

- Dr Mary Neal: for her direct role in supporting the day-to-day running of experimental studies, providing MR Physics expertise, development of scan protocols, and contribution to data processing and analysis

- Dr Kieren Hollingsworth: for his role in developing the compressed sensing methods employed in this research, and for freely sharing his time, enthusiasm and MR Physics expertise

- Prof John Matthews and Dr Holly Fisher: for their invaluable contribution to the statistical analyses performed as part of the LIFT study, and wider discussions relating to the processing of study data

- Tim Hodgson, Dorothy Wallace, Louise Ward (Radiographers) and Debra Galley (Radiographers assistant): for their help and support in conducting all MRI scans performed in Newcastle upon Tyne during the course of this research

- Prof Andy Blamire and Dr Sophie West: for overseeing my annual PhD progression reviews and providing valuable opportunity to discuss ideas

- Dr Ian Forrest and Dr Graham Burns: for providing clinical support throughout the course of my PhD, and encouraging me to pursue both my interest in respiratory medicine and this period of research

Table of Contents

List of Figures

List of Tables

List of Abbreviations

ADC	Apparent diffusion coefficient
ATS	American Thoracic Society
B_0	External magnetic field
BD	Bronchodilator
BMI	Body mass index
BTS	British Thoracic Society
BW	Bandwidth
CF	Cystic fibrosis
CF_4	Carbon tetrafluoride
C_2F_6	Hexafluoroethane
CI	Confidence interval
CiC	Confidence in Concept
CO_2	Carbon dioxide
COPD	Chronic obstructive pulmonary disease
CoV	Coefficient of variation
COVID-19	Coronavirus disease 2019
CS	Compressed sensing
CT	Computed tomography
CTPA	CT pulmonary angiography
DCE-MRI	Dynamic contrast enhanced magnetic resonance imaging
DSC	Dynamic susceptibility contrast
ERS	European Respiratory Society
^{19}F	Fluorine-19 isotope
^{19}F-MRI	Fluorinated-gas magnetic resonance imaging
FD-MRI	Fourier decomposition magnetic resonance imaging
$FEF_{25-75\%}$	Forced mid expiratory flow
FeNO	Fractional exhaled nitric oxide
FEV_1	Forced expiratory volume in 1 second
FEV_1/FVC	Forced expiratory ratio
FID	Free induction decay
FOV	Field of view

FRC	Functional residual capacity
FVC	Forced vital capacity
GBCA	Gadolinium-based contrast agent
^{1}H	Hydrogen nuclei (protons)
^{1}H-MRI	Proton magnetic resonance imaging
^{3}He	Helium-3 isotope
HP-MRI	Hyperpolarised-gas magnetic resonance imaging
HRA	Health Research Authority
IC	Inspiratory capacity
ICC	Intraclass Correlation Coefficient
IQR	Interquartile range
KCO	Transfer coefficient for carbon monoxide
LCI	Lung clearance index
MRC	Medical Research Council
MRI	Magnetic resonance imaging
N_2	Nitrogen
NHS	National Health Service
NMRC	Newcastle Magnetic Resonance Centre
NSA	Number of signal averages
NUTH	Newcastle upon Tyne Hospitals NHS Foundation Trust
O_2	Oxygen
OE-MRI	Oxygen-enhanced magnetic resonance imaging
PE	Pulmonary embolism
PEFR	Peak expiratory flow rate
PET	Positron emission tomography
PFP	Perfluoropropane (C_3F_8)
PIS	Participant information sheet
ppm	Parts per million
r	Pearson correlation coefficient
R_2^*	Transverse relaxation rate
RAW	Airway resistance
REC	Research ethics committee
RF	Radiofrequency
RMSE	Root mean square error

ROI	Region of interest
RV	Residual volume
SAR	Specific absorption rate
SD	Standard deviation
SF_6	Sulphur hexafluoride
SIGN	Scottish Intercollegiate Guidelines Network
SNR	Signal-to-noise ratio
SPECT	Single photon emission computed tomography
SPGR	Spoiled gradient echo
sRAW	Specific airway resistance
SSFP	Steady state free procession
STH	Sheffield Teaching Hospitals NHS Foundation Trust
T	Tesla
T_1	Longitudinal relaxation time
T_2	Transverse relaxation time
T_2^*	Reduced transverse relaxation time
TE	Echo time
TLC	Total lung capacity
T_LCO	Transfer factor for carbon monoxide
TR	Repetition time
TV	Tidal volume
UK	United Kingdom
UTE	Ultrashort echo time
VC	Vital capacity
VDP	Ventilation defect percentage
VV	Ventilated lung volume
%VV	Percentage ventilated lung volume
^{129}Xe	Xenon-129 isotope
χ	Magnetic susceptibility
2D	Two dimensional
3D	Three dimensional

Chapter 1.

Introduction

1.1   Overview and clinical context

Respiratory diseases, such as asthma and chronic obstructive pulmonary disease (COPD), are a leading cause of morbidity and mortality worldwide (Wang *et al.*, 2016). Asthma is characterised by reversible airway obstruction secondary to bronchial wall hypersensitivity and inflammation, and is thought to affect between 5% and 16% of individuals globally (Martinez and Vercelli, 2013). In the United Kingdom (UK), approximately five million people are known to have the condition, translating to 1 in every 12 adults (Asthma UK, 2017). COPD is predominantly caused by smoking and encompasses emphysema (the destruction and enlargement of distal airways and alveoli) and chronic bronchitis, leading to progressive and largely irreversible airflow obstruction (Rabe and Watz, 2017). Over 1 million people in the UK have a diagnosis of COPD, although it is estimated a further 2 million may remain undiagnosed (British Lung Foundation, 2017). The condition has now become the third leading cause of death worldwide (World Health Organisation, 2020).

Given the substantial contribution towards global healthcare burden, there is a pressing need to establish robust measures of pulmonary function that permit early detection of respiratory disease and effective monitoring of treatment response. Although widely used in clinical practice, conventional spirometric lung function tests are relatively insensitive to early disease changes (Petousi *et al.*, 2019) and provide little information regarding regional lung abnormalities, despite the heterogeneous nature of pulmonary pathology. The development of modern imaging techniques has opened the door to improved assessment of not only lung structure, but also a range of functional parameters, which may serve as quantitative biomarkers of disease (Trivedi *et al.*, 2017; Washko and Parraga, 2018). In particular, the use of magnetic resonance imaging (MRI) to assess lung ventilation properties represents a nascent area of research with potential for translation to the clinical environment.

This thesis concerns the development and application of ^{19}F-MRI of inhaled perfluoropropane (PFP) as a novel imaging modality for the assessment of respiratory disease.

The present chapter begins by outlining the normal structure and function of the lungs, highlighting the central role of pulmonary ventilation and perfusion in facilitating effective gas exchange. Specific reference is made to the pathophysiological features associated with asthma and COPD; these two conditions represent the primary focus for the patient studies presented in this thesis. An overview of the common clinical methods used to assess lung function is provided, leading to a more detailed discussion of the potential role of MRI in the investigation of pulmonary disease. The chapter concludes by summarising the principal aims and hypotheses relating to this research, including an outline of the experimental work conducted in subsequent chapters.

1.2   Structure and function of the lungs

The primary function of the lungs is to bring about the exchange of oxygen (O_2) from the atmosphere with carbon dioxide (CO_2) from the body (West and Luks, 2016). This is achieved through the process of ventilation and perfusion of respiratory bronchioles and alveoli – the main site of gas exchange. The average adult human lung contains approximately 480 million alveoli, each with a diameter of ~200 μm (Ochs *et al.*, 2004). The dichotomous branching structure of the lungs (Figure 1.1) facilitates maximal contact between the alveoli and pulmonary capillary bed, providing a vast surface area – approximately 130 m^2 (Weibel, 2009) – for the diffusion of O_2 and CO_2 across the respiratory membrane (Figure 1.2).

Respiratory disease may arise when there is a disturbance of one or more of the constituent components of the lung; namely, the airways, the vasculature, or their supporting tissue (the lung parenchyma). As such, there exists an inherent relationship between lung structure and function: structural changes associated with respiratory pathology may impact functional capacity (i.e. effective gas exchange), while clinical tests of lung function may be used to provide important information regarding underlying lung structure and disease.
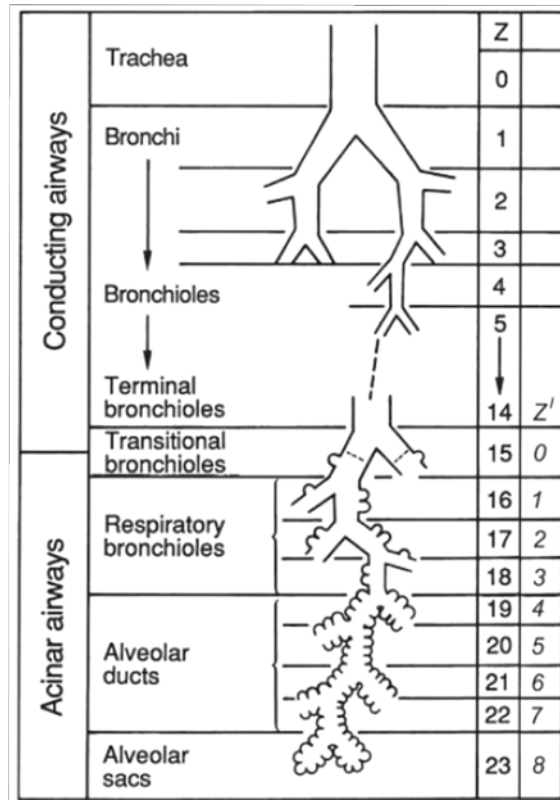
Figure 1.1: Branching structure of the lungs, demonstrating successive airway generations. A total of 23 bifurcations are typically present between the trachea and alveoli. The conducting zone serves to transport air to the respiratory zone (or acinus), the main site of gas exchange. Adapted from Weibel (2009).
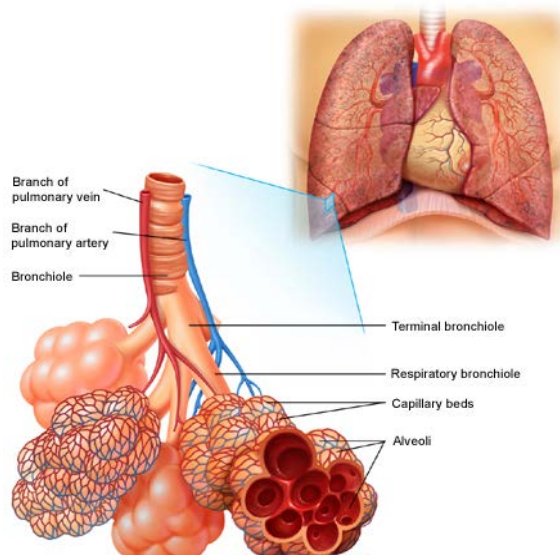
Figure 1.2: Representation of the respiratory zone, showing the close proximity of the alveoli and associated pulmonary capillary network. Adapted from https://www.myvmc.com/diseases/chronic-obstructive-pulmonary-disease-copd.

1.2.1 *Ventilation*

Ventilation refers to the movement of air in to and out of the lungs, brought about by inspiratory and expiratory manoeuvres. Whilst inspiration is governed principally by diaphragmatic contraction (increasing the volume of the thoracic cavity to create a negative intra-pulmonary pressure gradient), relaxed expiration is a largely passive process arising from the intrinsic elastic recoil properties of the lungs. This natural elasticity is balanced by an opposing action of the chest wall, returning the lungs to their resting state following a normal tidal (i.e. relaxed) breath. During forced expiration, the abdominal wall muscles play a greater role, increasing intra-abdominal pressure and raising the diaphragm to actively expel air from the lungs. Likewise, during forced inspiratory manoeuvres, the external intercostal and sternocleidomastoid muscles act synergistically with the diaphragm to enable greater depth of inhalation.

It is well established that ventilation is not entirely homogeneous in health and is increased in the most dependent parts of the lung (West, 1962; Milic-Emili *et al.*, 1966). Specifically, in the upright position, the influence of gravity has been shown to produce an apical-basal gradient of approximately 1:1.6 (Bryan *et al.*, 1964), resulting in relatively enhanced ventilation towards the bases of the lung. Similar apical-basal distribution has been observed in the supine position, where the change in orientation also produces an evident anterior-posterior gradient secondary to gravitational effects (Amis *et al.*, 1984; Musch *et al.*, 2002). This degree of natural ventilation heterogeneity may be exaggerated by the presence of underlying respiratory pathology, leading to marked regional differences in ventilation distribution. For instance, in asthma the combination of local airway inflammation, smooth muscle contraction and increased mucus production in response to provocative stimuli gives rise to varying levels of airway narrowing (i.e. bronchoconstriction) (Doeing and Solway, 2013), which may manifest as an obstructive ventilation defect (see Section 1.3, below). Similarly, in COPD, the effects of chronic inflammation and scarring within the small airways (defined as less than 2 mm in diameter) result in persistent airway narrowing and airflow limitation (Baraldo *et al.*, 2012); this may be exacerbated by an increase in lung compliance (i.e. tissue distensibility) stemming from the loss of elastic recoil in emphysematous regions of the lung, resulting in spatially localised 'gas trapping' during expiration (Sheikh *et al.*, 2016).

Increased airway resistance represents a key feature of obstructive airway diseases (Bonini and Usmani, 2015). Notably, the Hagen-Poiseulle equation states that airway resistance is inversely proportional to the fourth power of the airway radius (Kaminsky, 2012). As such, even modest changes to airway calibre can have a substantial impact on airflow within individual respiratory bronchioles (i.e. < 2 mm diameter). Nonetheless, owing to the vast total cross-sectional area of the small airways, the main site of airway resistance in health lies more proximally between generations six and eight (Bossé *et al.*, 2009). This has important implications for the early identification of peripheral airways diseases like asthma and COPD, since extensive pathology may already exist prior to detectable changes in airflow resistance. For this reason, the small airways are often referred to as the 'silent zone' of the lungs (Hogg *et al.*, 2017).

The efficacy of pulmonary ventilation is also inherently influenced by the speed and volume of breath performed (Milic-Emili *et al.*, 1966; Hughes *et al.*, 1972), such that deeper inspiratory manoeuvres are likely to facilitate airflow and minimise natural ventilation inhomogeneities that exist within the lungs. It has previously been demonstrated that airway resistance increases as lung volume declines (Briscoe and Dubois, 1958), chiefly through reduced traction of surrounding lung tissue on the small airways: the subsequent compression of peripheral airways (which lack the cartilaginous support of larger airways) limits airflow during expiration and is a key feature of the obstructive deficit seen in COPD in particular (Hogg, 2004).

Pulmonary ventilation is therefore governed by several interdependent factors, including the elasticity of the lungs and chest wall, airway resistance and lung compliance, all of which contribute to the efficacy of both regional and global gas distribution.

1.2.2 Perfusion

Perfusion refers to the flow of blood to an organ and is intrinsically linked to its functional capacity; namely, for the lungs, gas exchange. The pulmonary circulation arises from the right ventricle as the pulmonary artery, splitting into left and right pulmonary trunks which follow a branching structure mirroring that of the bronchial tree. This facilitates the transport of deoxygenated blood to the pulmonary capillary beds, where the exchange of CO_2 and O_2 occurs within the distal airways and alveoli (see Figure 1.2). Newly oxygenated blood is

subsequently returned to the left atrium via the pulmonary veins, from which it enters the systemic circulation for distribution to the rest of body. In parallel, bronchial arteries arise from the descending aorta to provide a direct supply of oxygenated blood to the bronchial tissue down to the level of the respiratory bronchioles; these eventually drain into the capillary circulation, creating a slight physiological 'shunt' (i.e. delivery of a small amount of deoxygenated blood to the pulmonary veins) that is present even in health (Petersson and Glenny, 2014).

As with pulmonary ventilation, there exists a natural perfusion gradient within the lungs, driven primarily by the effect of gravity and the comparatively low pressure of the pulmonary vascular system (West and Dollery, 1960; Kaneko *et al.*, 1966). This gives rise to a relative increase in blood flow towards dependent parts of the lungs, matching the global pattern of ventilation distribution and promoting efficient gas exchange (Petersson and Glenny, 2014). The resulting ratio of alveolar ventilation to pulmonary perfusion across the entire lungs is approximately 0.8 (Sarkar *et al.*, 2017), reflecting the slightly greater apical-basal perfusion gradient compared to the corresponding ventilation gradient (i.e. ventilation typically exceeds perfusion at the lung apices, whereas perfusion exceeds ventilation at the lung bases).

Several additional factors are thought to influence the pattern of regional pulmonary blood flow, including intrinsic variations in microvascular structure (Galvin *et al.*, 2007), as well as local fluctuations arising from differences in lung volume or phase of respiration (Hughes *et al.*, 1968). The constriction of pulmonary arterioles in response to hypoxia (hypoxic vasoconstriction) is a further characteristic feature of the lung vasculature (Dunham-Snary *et al.*, 2017), serving to maintain ventilation/perfusion matching by directing blood flow away from alveoli that are poorly oxygenated. This effect likely contributes to the increased vascular resistance that is commonly observed in COPD (Sakao *et al.,* 2014), though previous studies suggest alteration to regional microvasculature structure may also predate, and occur independently of, significant small airways disease and emphysema (Peinado *et al.*, 2008; Hueper *et al.*, 2015). By comparison, asthma is often associated with an increase in regional blood flow, angiogenesis and vascular permeability which may promote the delivery of inflammatory mediators to the most hyper-responsive airways (Harkness *et al.*, 2014).

Where the lungs are subject to impaired regional perfusion and/or ventilation, a ventilation/perfusion mismatch may occur, leading to the disruption of normal gas exchange;

this effect is fundamental to the reduction in lung function that characterises respiratory disease.

1.3   Clinical tests of lung function

The previous section provided an overview of pulmonary ventilation and perfusion as the primary physiological mechanisms underpinning effective gas exchange. This section outlines the established approaches to lung function assessment in clinical practice, focussing on the use of spirometric measurements and body plethysmography. The role of medical imaging in the investigation of lung disease is introduced further in Section 1.4.

1.3.1   Spirometry

Spirometry is the most commonly employed clinical test of lung function and remains central to the diagnosis and monitoring of respiratory disease. It provides a marker of ventilatory function by measuring the volume of air expelled from the lungs following a full inspiration; principally, the forced expiratory volume in 1 second (FEV_1) and forced vital capacity (FVC), representing the total volume of air that can be exhaled. Obstructive airways diseases, such as asthma and COPD, predominantly affect the FEV_1, resulting in a reduced forced expiratory ratio (FEV_1/FVC). The normal FEV_1/FVC varies with age (Thomas *et al.*, 2019); however, a value of less than 0.7 is generally considered to represent an obstructive deficit and forms the basis of current diagnostic guidelines (NICE, 2017; GOLD, 2020). In contrast, restrictive lung diseases (characterised by a failure to achieve full inspiration) impact both the FEV_1 and FVC, maintaining an essentially normal forced expiratory ratio (i.e. > 0.7). This may reflect extra-pulmonary disease (such as chest wall deformity) or intrapulmonary pathology (such as pulmonary fibrosis). Typical patterns of obstructive and restrictive ventilation, represented by volume–time curves, are illustrated in Figure 1.3.
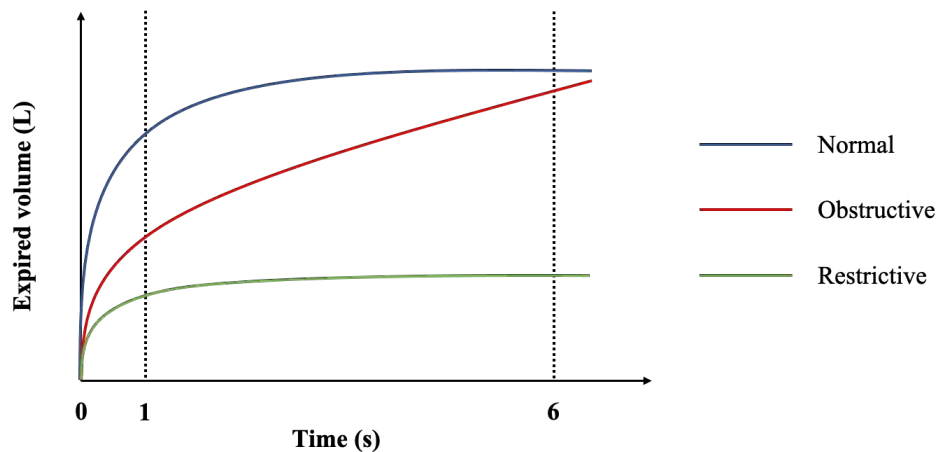
Figure 1.3: Patterns of normal (blue), obstructive (red) and restrictive (green) ventilation, represented by volume-time curves.

Spirometry may be used both to support the diagnostic process and to inform the severity of underlying disease, directly influencing management and treatment decisions. For example, the hallmark feature of asthma is reversible airflow obstruction, manifest as a measurable change in FEV_1 and/or FVC over time or following bronchodilator (BD) administration (e.g. salbutamol) (NICE, 2017; GINA, 2020). In contrast, spirometric values in COPD typically show little variability or response to BD therapy: this can help distinguish the condition from asthma, although it is important to recognise that some patients with COPD may demonstrate significant BD reversibility even in the absence of co-existent asthma (Hanania *et al.*, 2011). Likewise, in longstanding and severe asthma, a degree of 'fixed' airway obstruction can exist (Yii *et al.*, 2014; Konstantellou *et al.*, 2015), which may be mistaken for COPD.

Notably, there is no single diagnostic test that confirms the presence of either asthma or COPD, and the diagnoses are generally made clinically using a combination of typical symptoms and supportive investigations. It is quite possible for patients with asthma to exhibit 'normal' lung function according to spirometric measurements (GINA, 2020), particularly if already receiving treatment. As such, the severity of asthma is generally based upon the extent of therapy required to bring about the control of symptoms (see BTS, 2019), rather than a specific quantitative measurement. By comparison, once an obstructive FEV_1/FVC ratio has been confirmed, the severity of COPD is typically classified according to the degree of airflow limitation as assessed by FEV_1 (Table 1.1).

Severity of COPD	FEV_1 (% predicted)
Mild	> 80
Moderate	50–79
Severe	30–49
Very severe	< 30

Table 1.1: Classification of COPD severity according to criteria outlined by the Global Initiative for Chronic Obstructive Lung Disease (GOLD, 2020).

Spirometric parameters are conventionally compared to mean reference values from a demographically similar healthy population, enabling individual measurements to be expressed as a percentage of the predicted value (% predicted) (Pellegrino *et al.*, 2005). However, it is well established that lung function declines with age (Fletcher and Peto, 1977; Kim *et al.*, 2015), such that the prevalence of respiratory disease in older populations may be overestimated if an FEV_1/FVC of 0.7 is assumed to be correct for everyone. The lower limit of normal (LLN) for FEV_1 and FEV_1/FVC represents an alternative threshold that may be more applicable to older age groups in particular (Swanney *et al.*, 2008; Fisher *et al.*, 2016). Moreover, FEV_1 is generally considered insensitive to early pathology of the small airways, since it is influenced largely by airflow resistance in mid-generation airways (see Section 1.2.1, above). Additional spirometric indices, such as the forced mid-expiratory flow ($FEF_{25-75\%}$) or maximal mid-expiratory flow (MMEF) – derived from the mid-point of the flow-volume loop (i.e. at 50% of FVC) – may provide a more reliable indicator of peripheral airways physiology by measuring airflow at lower lung volumes (Katsoulis *et al.*, 2016; Petousi *et al.*, 2019), where the contribution of small airway resistance may be more apparent. For example, the ratio of MMEF to FVC has previously been shown to reveal early airflow limitation ('pre-COPD') in smokers with preserved FEV_1/FVC (Mirsadraee *et al.*, 2013). Similarly, Stockley *et al.* (2017) demonstrated the utility of MMEF to identify small airway dysfunction, as well as disease progression, in non-smokers with alpha-1 antitrypsin deficiency (a genetic condition predisposing to COPD), where FEV_1 and FVC were within the normal range. As such, these measurements may offer a simple global assessment of small airways disease. Nonetheless, the detection of early regional lung pathology remains challenging with spirometry alone, especially as a heavily technique-dependent procedure.

1.3.2   *Plethysmography*

Plethysmography is a complementary method that can provide information on static lung volumes, beyond what is available by conventional spirometry (Figure 1.4). The procedure involves performing respiratory maneuvers inside an airtight box: as the lungs expand, pressure rises within the enclosed box and lung volume can subsequently be determined by applying Boyle's Law (Wanger *et al.*, 2005). The acquired measurements are useful indicators of respiratory function and can be beneficial in distinguishing underlying restrictive and obstructive airways disease. Specifically, both the functional residual capacity (FRC) and residual volume (RV) are frequently reduced in the presence of restrictive pathology (such as pulmonary fibrosis), secondary to reduced lung compliance. By contrast, these parameters are typically elevated in obstructive lung diseases (such as asthma and COPD) relating to early airway closure and gas trapping during expiration (Sorkness *et al.*, 2008). Previous studies have demonstrated that RV, in particular, correlates well with measures of small airways resistance and inflammation in both asthma and COPD (Kraft *et al.*, 2001; Turato *et al.*, 2002), providing a robust marker of lung hyperinflation (i.e. increased end-expiratory volume) associated with these conditions. For patients with significant emphysema, this can have a dramatic impact on the degree of breathlessness experienced, since it is necessary to perform tidal breathing at a relatively higher baseline volume; such patients may benefit from intervention with lung volume reduction surgery, or endobronchial valve or coil placement, to reduce the level of hyperinflation that exists (Sciurba *et al.*, 2010, 2016; Ginsburg *et al.*, 2011).

Other plethysmography-derived measures have been developed that may be used to report on clinically important disease outcomes. Notably, a reduction in the ratio of inspiratory capacity, IC (the maximal volume that can be inhaled following a relaxed expiration) to TLC (IC/TLC) is recognised as an independent predictor of mortality in COPD (Casanova *et al.*, 2005). Measures of airway resistance – namely, the specific airway resistance, sRAW (calculated from the relationship between changes in box-pressure and flow-rate) and RAW (equal to sRAW/FRC) – can also be readily obtained by plethysmography; it has been suggested these measurements provide improved sensitivity to BD response compared to conventional spirometry (Criée *et al.*, 2011), offering an alternative approach to the evaluation of small airways disease. Even so, plethysmography remains a technique-dependent procedure with potential for variable performance both within and between

participants. Moreover, lung volumes (such as TLC) are likely to be overestimated in situations where substantial airflow-obstruction exists, owing to poor equilibration of mouth and alveolar pressure changes (O'Donnell *et al.*, 2010; Criée *et al.*, 2011). These factors must be considered when interpreting results.
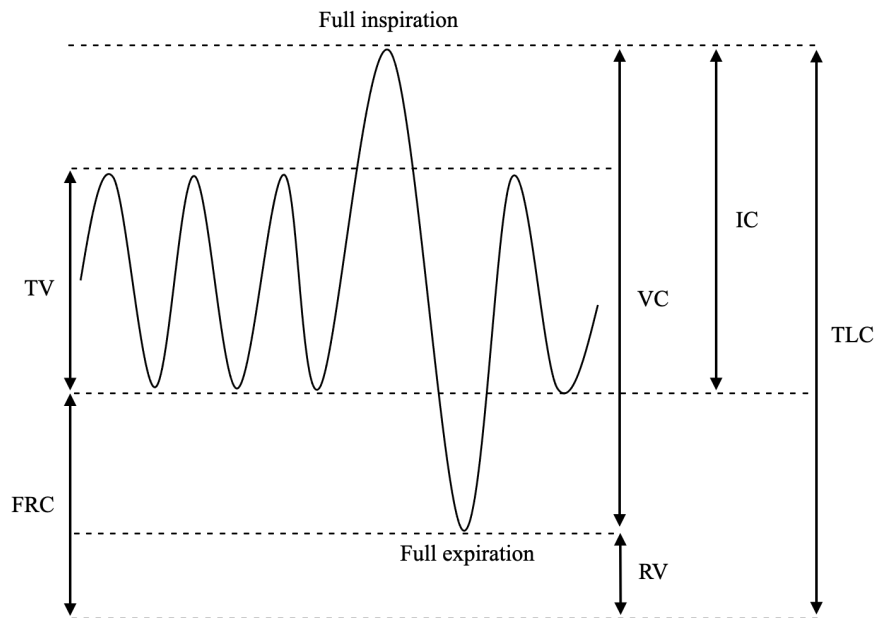
Figure 1.4: Representation of dynamic lung volumes.
TV = tidal volume; FRC = functional residual capacity; VC = vital capacity; RV = residual volume; IC = inspiratory capacity; TLC = total lung capacity.

1.3.3   Additional measures

Several other lung function tests have been adopted in clinical practice, which can offer additional information regarding the nature of respiratory disease. In particular, the transfer coefficient for carbon monoxide (KCO) and its derivative transfer factor (T_LCO, equal to KCO × the alveolar gas volume, V_A) provide a measure of gas exchange (namely, CO) across the respiratory membrane and are frequently performed alongside spirometry and plethysmography: the values, which serve as a surrogate for O_2 transfer, are typically reduced in COPD (secondary to emphysematous destruction of alveolar walls) but remain normal or even supranormal in asthma (secondary to increased pulmonary blood flow) (Petousi *et al.*, 2019). Importantly, these measurements are usually acquired during a 10 s breath-hold following inhalation of a helium/CO gas mixture, which some patients (e.g. those with significant breathlessness) may find difficult to perform. In addition, both T_LCO and KCO are dependent on having an accurate (corrected) haemoglobin concentration available, while

KCO is also governed by extra-thoracic factors, such as obesity (Petousi *et al.*, 2019). Nevertheless, these basic measurements remain important indicators of parenchymal lung disease characterised by impaired gas exchange (such as emphysema or pulmonary fibrosis).

The use of nitrogen (N_2) gas wash-out and helium dilution techniques (see Wanger *et al.*, 2005) represents an alternative approach to the measurement of static lung volumes, which may be beneficial for patients unable to perform plethysmography (e.g. secondary to claustrophobia). In the case of N_2 wash-out, FRC is calculated by measuring the alveolar gas concentration at the start of the wash-out period (achieved by breathing 100% O_2) and the volume of gas exhaled within a specified timeframe (typically 7 minutes); in the case of helium dilution, the FRC is calculated based on equilibration of a known, fixed volume of gas containing helium within the lungs. There is currently no accepted 'gold standard' approach concerning the measurement of static lung volumes; however, it should be noted that the techniques may produce slightly varying results stemming from inherent differences in how they are performed (Tantucci *et al.*, 2016). Specifically, while whole body plethysmography has a tendency to *overestimate* lung volume in the presence of severe airflow obstruction (see Section 1.3.2, above), gas dilution techniques typically *underestimate* lung volume as the proportion of ventilated lung regions (i.e. those involved in gas equilibration) reduces (O'Donnell *et al.*, 2010). Correct interpretation of lung volume measurements must therefore take into account the particular method adopted, as well as the extent of underlying pathology (e.g. gas trapping in emphysema).

Although not used routinely, both single-breath and multiple-breath inert gas wash-out techniques (using inhaled nitrogen or sulphur hexafluoride, SF_6) are capable of detecting ventilation heterogeneity associated with early airways disease (Robinson *et al.*, 2013) and have shown particular promise for the evaluation of childhood cystic fibrosis (CF) (Aurora *et al.*, 2004; Gustafsson *et al.*, 2008). Specifically, the lung clearance index (LCI) has been widely adopted in research settings as a marker of ventilation heterogeneity (or abnormal gas-mixing), based on the time-course of gas wash-out from the lungs (i.e. the number of respiratory cycles) to reach $1/40^{th}$ of its original concentration (Horsley, 2009). Previous studies have demonstrated improved sensitivity of LCI to detect small airways disease in patients with asthma (Macleod *et al.*, 2009) and CF (Horsley *et al.*, 2008) compared to conventional spirometry. Other indices – namely, S_{cond} and S_{acin}, derived from analysis of gas exhalation slopes – have been used to distinguish ventilation inhomogeneity arising from the

conducting airways (S_{cond}) or the acinar airways (S_{acin}), respectively; in patients with COPD, these measurements have previously shown good correlation with both FEV_1 and T_LCO (Verbanck *et al.*, 1998). It is important to appreciate, however, that gas wash-out techniques are unable to characterise the specific structural abnormalities leading to local ventilation heterogeneity. Moreover, at present, there remains some uncertainty regarding appropriate standardisation of the technique for routine clinical adoption (Robinson *et al.*, 2013).

Impulse oscillometry represents an additional technique that is emerging as a non-invasive method for assessing airway resistance, utilising the absorption of sound waves at different frequencies to distinguish airway size and calibre (Bickel *et al.*, 2014). This approach has been used successfully to identify small airways obstruction relating to asthma and COPD (Cavalcanti *et al.*, 2006; Kolsum *et al.*, 2009). Importantly, the technique does not rely on forced maneuvers, making it a relatively straightforward test to perform; however, analysis of parameters is complex and, at present, standardised procedures and reference values have not been established (Petousi *et al.*, 2019).

In practice, the peak expiratory flow rate (PEFR) offers a simple alternative to FEV_1 that allows patients to self-monitor airflow limitation over time; alongside measurement of the fractional exhaled nitric oxide (FeNO) – a surrogate marker of eosinophilic inflammation – these tests may help to clarify the presence of airway obstruction and inflammation relating to asthma (BTS, 2019). Nonetheless, a common limitation of all these approaches – including spirometry and plethysmography – is the reliance on a single global measurement that is unable to report directly on regional lung function. As such, alternative techniques are necessary to inform about regional pathophysiology in greater detail.

1.4   Functional lung imaging in clinical practice

Medical imaging technologies can aid the diagnosis and management of respiratory disease by providing both structural and functional information about the lungs, beyond what is offered by conventional pulmonary function tests. This section outlines two key imaging modalities used clinically in the investigation of lung disease; namely, computed tomography and nuclear medicine techniques. The use of MRI as a novel pulmonary imaging modality is considered in greater detail in the following section of this chapter (Section 1.5).

1.4.1 Computed tomography

Computed tomography (CT) is widely considered the 'gold standard' of thoracic imaging and remains a cornerstone in the investigation of structural lung pathology, such as pulmonary fibrosis (Gotway *et al.*, 2007) and bronchiectasis (Pasteur *et al.*, 2010). Images are based on the relative attenuation of different body tissues to X-ray radiation, using multiple measurements to create a highly-detailed three dimensional (3D) map of the lungs. The resulting spatial resolution is typically in the region of 0.5 mm (Kakinuma *et al.*, 2015), permitting assessment of respiratory pathology down to the level of the peripheral airways. Recent technological advances with dual-energy and multi-detector systems (McCollough *et al.*, 2015) have enabled further improvements in image quality and are increasingly used for a range of clinical applications. It is now feasible to detect changes in the structure and number of small airways indicative of early-stage COPD (Kirby *et al.*, 2018), as well as phenotype patients according to airway- or emphysema-predominant disease (Subramanian *et al.*, 2016). In asthma, the assessment of airway wall thickness and expiratory gas-trapping has previously shown to correlate strongly with the degree of airflow limitation observed by spirometry (Gono *et al.*, 2003), emphasising the inherent link that exists between lung structure and function.

The use of xenon-enhanced CT (employing inhaled ^{133}Xe) has enabled investigation of additional functional properties of the lungs that relate directly to pulmonary ventilation. This includes the assessment of regional gas distribution and dynamic wash-in/wash-out measurements in COPD (Kong *et al.*, 2014), as well as monitoring ventilation defects in response to therapeutic intervention in patients with asthma (Kim *et al.*, 2012). Notably, Park *et al.* (2010) demonstrated the ability to distinguish emphysematous lung regions from airway-centred disease in patients with COPD, based on the presence of retained gas signal during wash-out imaging. Such functional information may be utilised in the identification of patients suitable for lung volume reduction procedures, where the role of CT in general remains a key component of assessment (Washko *et al.*, 2008). Importantly, CT can also be used to acquire measurements of lung perfusion following administration of intravenous contrast agents, offering potential for combined assessment of ventilation/perfusion properties (Zhang *et al.*, 2013). Previous studies have demonstrated regional perfusion deficits and early microvascular changes in patients with COPD, even in the absence of other CT features of emphysema (Ley, 2015), highlighting the ability to detect subtle

pathophysiology. In practice, CT pulmonary angiography (CTPA) remains the imaging modality of choice for the investigation of pulmonary embolism (PE) (Moore *et al.*, 2018), owing to its high sensitivity and rapid image acquisition time.

Despite these benefits, CT is limited by its reliance on ionising radiation. This impacts the ability to perform repeated or longitudinal studies, where cumulative radiation exposure is associated with an increased risk of malignancy (Hall and Brenner, 2008). The advent of low and ultra-low dose CT imaging protocols (Hammond *et al.*, 2017) may reduce this radiation burden somewhat. Nonetheless, the potential to acquire high quality structural images must remain balanced by the need to avoid unnecessary harm.

1.4.2   *Nuclear medicine*

Nuclear medicine represents a group of functional imaging techniques, including single photon emission computed tomography (SPECT) and positron emission tomography (PET). Both are based on the detection of radioactive properties of tracer elements (radionuclides) introduced into the body, whose emitted energy is subsequently converted into a signal for image production. Typically, SPECT is used to measure regional ventilation and/or perfusion properties in the lungs, using the inhaled gases ^{133}Xe, krypton-81m (^{81m}Kr), or technetium-99m (^{99m}Tc) in combination with injected 99mTc-macroaggregated albumin (Petersson *et al.*, 2007). The technique has previously shown potential to differentiate healthy and emphysematous lungs, permitting quantitative measures of ventilation heterogeneity (Nagao *et al.*, 2000; Xu *et al.*, 2001). Combined ventilation/perfusion imaging is often employed clinically in the diagnosis of PE (Stein *et al.*, 2009; Bajc *et al.*, 2019), where it provides benefits over CTPA relating to its high sensitivity and comparatively lower radiation dose (Roach *et al.*, 2013). However, SPECT is characterised by lengthy scan times (in the order of tens of minutes) and relatively low spatial resolution (approximately 10–20 mm) (Petersson *et al.*, 2007), which represent limitations for routine use.

PET typically employs nitrogen-13 (^{13}N), fluorine-18 (^{18}F) or neon-19 (^{19}Ne) isotopes as a source for functional imaging of ventilation and/or perfusion properties (Rhodes and Hughes, 1995; Vidal Melo *et al.*, 2003; de Prost *et al.*, 2015). Previous work has demonstrated the ability to identify changes in regional perfusion in response to bronchoconstriction in asthma (Harris *et al.*, 2006), as well as increased ventilation/perfusion heterogeneity in patients with

COPD compared to healthy volunteers (Vidal Melo *et al.*, 2010). The use of ^{18}F-FDG (fluorodeoxyglucose) uptake has shown particular promise for assessing inflammatory activity in various respiratory pathologies, including COPD and fibrotic lung disease (Chen *et al.*, 2017). In practice, PET is often combined with CT, permitting improved spatial resolution and functional capabilities; the approach is now widely utilised in the evaluation of lung nodules (Callister *et al.*, 2015) and for radiological staging of lung cancer (Kandathil *et al.*, 2018). Nonetheless, as with CT and SPECT, the use of PET is limited by its reliance on radiation exposure, in addition to its relative complexity and high cost. As such, there is a pressing need to establish alternative means of assessing pulmonary disease, which can be applied clinically without recourse to ionising radiation.

1.5   Pulmonary MRI

MRI is a comparatively new approach to the investigation of respiratory disease which, at present, is not used routinely in clinical practice. A number of challenges exist in relation to pulmonary MRI (discussed in the following sub-sections of this chapter), which have undoubtedly contributed to its slow uptake. However, research interest has grown considerably over the past two decades, not least because of its potential to provide non-invasive and radiation-free assessment of both lung structure and function. This has clear implications for the diagnosis and longitudinal monitoring of chronic diseases, such as asthma and COPD, as well as childhood conditions like CF, where the avoidance of excessive radiation exposure is paramount.

While lung perfusion imaging has become increasingly prominent in recent years (Johns *et al.*, 2017a), the bulk of pulmonary MRI research has centred on ventilation imaging. As such, this represents the primary focus for the following discussion.

The section begins by providing a brief overview of MRI, including a description of the basis of MR image production: this discussion draws in large part on the review paper 'Understanding MRI: basic MR physics for physicians' by Currie *et al.* (2013). This is followed by a review of the principal approaches that have been adopted within lung MRI literature, focusing on the use of exogenous gas agents to assess pulmonary ventilation properties. The potential clinical application of ^{19}F-MRI of inhaled PFP represents the main focus for the remainder of this thesis.

1.5.1 Principles of MRI

MRI is fundamentally based upon the detection of nuclear spins (also known as angular momentum) of MR-sensitive atomic nuclei when placed in an external magnetic field. Nuclear spin is an intrinsic property shared by all nuclei (akin to atomic mass or charge), which describes the direction of rotation around an arbitrary axis. Through this rotation, positively charged nuclei exhibit an intrinsic magnetic field (known as a magnetic moment), analogous to what is observed with a small bar magnet.

The normally random orientation of nuclear magnetic moments can be influenced by applying an external magnetic field (known as B_0), which has the effect of aligning nuclei in the same (parallel) or opposite (anti-parallel) direction as the external field. Typically, a very slight excess of nuclei will be aligned in the parallel direction at any given time, reflecting its lower energy state. However, by applying an additional oscillating magnetic field – known as a radiofrequency (RF) pulse – it is possible for nuclei to transition between these two energy states (i.e. change from a low energy to a high energy state). The RF excitation pulse has the effect of orientating the magnetic moments of the nuclei such that they combine (are 'in phase') to produce a measurable rotating magnetic field that can be detected as an MR signal. This is achieved when the frequency of the RF pulse matches the Larmor frequency (the frequency at which nuclear spins rotate in the magnetic field), which is determined by the strength of B_0 (measured in units of Tesla, T) and the gyromagnetic ratio (a constant for individual nuclei). Crudely, the gyromagnetic ratio reflects the propensity with which particular nuclei will generate an MR signal: this is greatest for hydrogen nuclei (^{1}H, or protons). Coupled with the high water and/or fat content of most body tissues (which exhibit a high proton density), this underpins the central role of ^{1}H nuclei in conventional MRI.

Upon completion of the RF pulse, the stimulated nuclei return to their resting (equilibrium) state, emitting energy as part of this process. This can be detected using a receiver coil, generating an electrical current that is ultimately transformed into a signal for image formation. The process of MR image formation is complex and uses magnetic field gradients to encode spatial information into the MR signal; this is subsequently transformed into images by a process known as Fourier transformation. Specific RF coils can be used both to transmit energy to the tissue of interest (i.e. to initiate the RF pulse at the Larmor frequency) as well as to receive the resultant signal that is generated. For conventional ^{1}H-MRI, this is

often performed using the scanner's integral body-coil; however, a wide variety of MR-sensitive nuclei can be studied using additional coils that are tuned to the frequency of the specific nuclei under consideration. A description of the RF coils used in this thesis is provided in Chapter 2 (Section 2.5.2).

The signal decay that occurs following RF pulse excitation is governed by two independent but related MRI relaxation properties: these are known as the longitudinal relaxation time (T_1) and the transverse relaxation time (T_2), respectively. T_1 describes the time taken for excited nuclei to return to their resting state, during which energy is transferred to the surrounding environment as small amounts of heat. In contrast, T_2 describes the time taken for the aligned nuclei to 'de-phase', a process which starts immediately upon cessation of the RF pulse. In practice, the T_2 is also heavily influenced by local magnetic field inhomogeneity (stemming from the varying magnetic properties of individual tissue components of the body) which contributes to the de-phasing of nuclei: this is denoted by T_2^* and provides a more accurate description of the *in vivo* rate of signal decay for certain types of MR scan (such as the gradient echo imaging methods employed in this thesis).

The respective lengths of T_1 and T_2^* are important factors that determine the amplitude of MR signal that can be achieved in a scan and are critical in developing appropriate scan protocols (including the timing of RF excitation pulses) that maximise the available signal during a given MRI acquisition. This is especially relevant for pulmonary MRI, since both the T_1 and T_2^* of lung tissue are inherently short (discussed in the following sub-sections). The particular acquisition sequences employed in this thesis – known as spoiled gradient echo (SPGR) scans – were influenced by the specific requirements determined by these relaxation times. This is outlined further in Chapter 3 (Section 3.2).

1.5.2   *^{1}H-MRI of the lungs*

As indicated in Section 1.5.1, conventional MRI relies upon the detection of magnetic properties of hydrogen nuclei within water or fat molecules to generate a signal for image production. Given the relatively low proton density of the lungs – approximately 10% of most body tissues (Wild *et al.*, 2012) – pulmonary imaging by this method remains technically challenging: the paucity of ^{1}H nuclei results in a considerably diminished signal compared to other proton-rich tissues (Mills *et al.*, 2003). In addition, numerous air-tissue

interfaces exist within the lungs, creating significant local magnetic field inhomogeneities. These stem from the differing magnetic properties of air and water (or blood) within the lung when subjected to a magnetic field, termed magnetic susceptibility (Vignaud *et al.*, 2005). Specifically, water is slightly diamagnetic, meaning molecules tend to diminish the local magnetic field; conversely, O_2 within the air is slightly paramagnetic, tending to strengthen the local magnetic field. These differences in magnetic susceptibility give rise to multiple local magnetic field gradients within the lung, causing rapid signal decay through the dephasing of protons. This is characterised by the short T_2^* of lung tissue which, depending on lung inflation levels, is in the region of 1–2 ms (Theilmann *et al.*, 2009). Coupled with motion artefacts arising from cardiac and respiratory cycles, conventional MRI of the lungs presents difficulties for diagnostic use.

To overcome these barriers, a number of techniques have been developed which aim to optimise the innate ^1H signal from the lungs. In particular, the use of ultrashort echo time (UTE) scan sequences – where the echo time, TE, is defined as the time between applying an RF pulse and attaining the peak signal – can partially compensate for the inherently short T_2^* of lung tissue (Bianchi *et al.*, 2013; Johnson *et al.*, 2013). UTE signal intensity has previously shown to correlate well with CT measures of lung tissue density in patients with asthma (Sheikh *et al.*, 2017), as well as spirometric assessment in patients with COPD (Ma *et al.*, 2015). Consequently, it has potential to provide important information on lung morphology and its relation to pulmonary function. Respiratory gating techniques, combined with breath-hold image acquisitions, can improve image quality further by alleviating motion artefacts (Wild *et al.*, 2012). Nonetheless, while the structural integrity of ^1H-based images can be improved by such methods, direct functional assessment of the lungs (such as evaluation of regional ventilation properties) remains lacking.

An alternative technique, known as oxygen-enhanced MRI (OE-MRI), exploits the paramagnetic effects of O_2 in the lungs to augment the innate ^1H signal, based on a shortening of T_1 following inhalation of 100% oxygen (Kruger *et al.*, 2016). This reduces the time taken for protons to return to equilibrium following an RF excitation pulse, increasing the overall parenchymal signal intensity in oxygen-containing tissue by up to 10% (Ebner *et al.*, 2017a). By registering conventional ^1H- and OE-MRI images, it is possible to determine the distribution of ventilation in the lungs: this technique has been used to successfully identify regional ventilation defects (characterised as areas of reduced, or absent, signal

enhancement) in patients with emphysema (Edelman *et al.*, 1996) and lung cancer (Ohno *et al.*, 2001). The degree of change in signal intensity has previously shown to correlate well with $T_L CO$ measurements in emphysema (Müller *et al.*, 2002; Ohno *et al.*, 2002), in addition to offering improved staging of COPD severity compared to CT (Ohno *et al.*, 2008). More recently, Zhang *et al.* (2015) have demonstrated the capacity for OE-MRI to characterise disease severity in asthma compared to spirometry. However, there are several drawbacks that may limit its adoption in clinical practice. Notably, scan time is typically in excess of 10 minutes (Kruger *et al.*, 2016), owing to the requirement to perform image acquisitions on multiple occasions (known as signal averaging) to produce a sufficient and detectable change in signal by this method. In general, the signal-to-noise ratio (SNR) of MR images can be improved by increasing the number of signal averages (NSA) – i.e. the number of times an acquisition sequence is repeated during an MRI scan – but results in a prolonged total scan duration (e.g. if a single acquisition takes 5 s, two acquisitions will take 10 s, and so on). This is relevant for images that require breath-holding (such as the lungs) and is discussed further in Chapter 3 (Section 3.2.2). Moreover, as O_2 readily diffuses within lung tissue, the ensuing signal obtained by OE-MRI is influenced not only by oxygen in the airways, but also within the surrounding parenchyma. As such, this technique provides only an indirect measure of pulmonary ventilation.

Fourier decomposition MRI (FD-MRI) represents an additional approach to proton-based lung imaging that has potential to report on both ventilation and perfusion properties (Bauman *et al.*, 2009). The technique is based upon the detection of subtle changes in ^{1}H signal intensity that occur naturally throughout the respiratory and cardiac cycles; namely, a slight increase in parenchymal signal amplitude during expiration, and a slight reduction in signal amplitude during maximal (i.e. systolic) blood flow through the lungs (Bauman and Eichinger, 2012). By performing repeated acquisitions over the course of several breathing cycles, it is possible to separate the respective respiratory and cardiac frequencies (via a process known as Fourier decomposition analysis) to generate 'ventilation weighted' and 'perfusion weighted' images. Previous studies have highlighted the ability of this technique to map regional ventilation and perfusion defects in patients with COPD (Kaireit *et al.*, 2018; Voskrebenzev *et al.*, 2018) and pulmonary embolic disease (Schönfeld *et al.*, 2015; Johns *et al.*, 2017b), as well as identify response to BD therapy in patients with severe asthma (Capaldi *et al.*, 2017). The procedure holds particular clinical appeal, since images can be acquired during relaxed breathing without the requirement for exogenous contrast agents.

Nonetheless, as with OE-MRI, FD-MRI is limited to providing only an indirect assessment of pulmonary ventilation and perfusion. Moreover, the requirement for extensive post-processing capabilities has, to date, restricted this technique to specialist research centres.

Although not yet employed clinically in the assessment of lung disease, dynamic contrast enhanced MRI (DCE-MRI) is a well-established imaging modality for *in vivo* perfusion measurement (Gordon *et al.*, 2014). The approach draws on the T_1-shortening effect of paramagnetic gadolinium-based contrast agents (GBCAs) during bolus passage through the microvasculature, strengthening the intrinsic ^1H signal arising from the tissue of interest. Various studies have demonstrated the utility of DCE-MRI to identify perfusion defects in patients with acute PE (Kluge *et al.*, 2006; Hosch *et al.*, 2014), as well as improved sensitivity to detect chronic thromboembolic disease compared to SPECT (Johns *et al.*, 2017b). Moreover, the technique has been utilised in the identification of impaired microvascular perfusion in patients with mild to severe COPD (Hueper *et al.*, 2015). Robust post-processing is necessary to facilitate quantitative measurement of regional contrast agent kinetics, such as mean transit time and pulmonary blood flow (Johns *et al.*, 2017a). Nonetheless, given the widespread use of GBCAs in current MRI practice (American College of Radiology, 2020), the technique represents a promising modality for future clinical adoption.

The use of DCE-MRI is revisited in Chapter 6 to explore the feasibility of performing combined ventilation and perfusion imaging alongside ^{19}F-MRI of inhaled PFP.

1.5.3   Hyperpolarised-gas MRI

In contrast to ^1H-based ventilation imaging, hyperpolarised-gas MRI (HP-MRI) is capable of providing high quality images of lung structure and function by direct visualisation of the airways, predominantly via inhalation of the inert noble gases helium-3 (^3He) and xenon-129 (^{129}Xe) (Mugler and Altes, 2013). This approach has been a major focus for pulmonary MRI development over the past two decades, generating a considerable body of research concerning the application of novel biomarkers of disease.

The strength of signal produced by MRI depends on the magnitude of the magnetic polarisation of MR sensitive nuclei (e.g. ^1H) when placed in an external magnetic field. For

conventional MRI (at thermal polarisation) this is normally extremely small though varies proportionally with B_0, such that stronger fields produce larger polarisations and therefore greater MR signals. For example, ^1H has a thermal polarisation of approximately 4.9 x 10^{-6} at a field strength of 1.5 T and 9.9 x 10^{-6} at 3.0 T, respectively (Couch *et al.*, 2015). Hyperpolarisation is a process that involves vastly amplifying the natural polarisation of selected nuclei (e.g. ^3He and ^{129}Xe) before they enter a magnetic field, which can increase their signal magnitude by up to 100000 times (Kruger *et al.*, 2016). This process is achieved through the use of optical pumping techniques, such as spin-exchange optical pumping (Walker and Happer, 1997), whereby a polarised light source is used to excite electrons of an alkali metal – typically Rubidium (Rb) – within a sealed container. The angular momentum (spin) of Rb is subsequently transferred to the nuclear spins of the desired nuclei via nuclear collisions. As a result, the normally modest thermal polarisation of ^3He and ^{129}Xe can be increased to approximately 0.5 (i.e. 50%) (Mugler and Altes, 2013), enabling acquisition of high signal MR images of hyperpolarised gas following inhalation.

HP-MRI of the lungs was first reported by Albert *et al.* (1994) who generated 2D images of excised mouse lungs employing hyperpolarised ^{129}Xe. Since then, the technique has been investigated extensively in *in vivo* human lung imaging, focusing predominantly on the identification of ventilation abnormalities associated with obstructive airways diseases (Kirby *et al.*, 2013; O'Sullivan *et al.*, 2014; Ebner *et al.*, 2017b). Such studies have enabled characterisation of regional gas distribution within the lungs during single breath-holds, where the signal reflects the volume of gas present within each voxel of the acquired image. Notably, while gas distribution is largely homogeneous within the lungs of healthy individuals, conditions such as asthma and COPD show increased signal heterogeneity, relating to regions of poor ventilation and reduced gas uptake (Virgincar *et al.*, 2013; Svenningsen *et al.*, 2014).

Figure 1.5 shows example HP-MRI ventilation images acquired in patients with respiratory disease, illustrating the variation in gas distribution associated with underlying pathology.
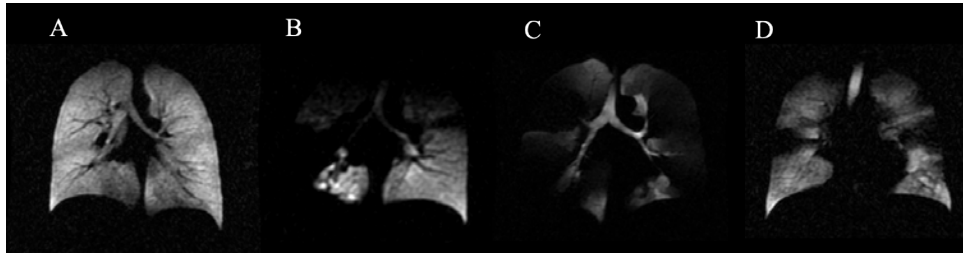
Figure 1.5: Example HP-MRI ventilation images acquired using hyperpolarised ^{129}Xe. **(A)** healthy volunteer; **(B)** patient with CF; **(C)** patient with COPD; **(D)** patient with asthma. Images courtesy of Prof Jim Wild, University of Sheffield.

By combining HP-MR ventilation images with anatomical images acquired by conventional ^{1}H-MRI, it is possible to derive quantitative measures of lung function which can provide important information regarding underlying disease. In particular, the percentage ventilated lung volume (%VV) and its counterpart, the ventilation defect percentage (VDP = 100 – %VV), have been reported widely in HP-MRI studies (Mathew *et al.*, 2012; Virgincar *et al.*, 2013; Horn *et al.*, 2014a), representing functional imaging biomarkers that correlate strongly with conventional spirometric indices, e.g. FEV$_1$ (Kirby *et al.*, 2012a; Ebner *et al.*, 2017b). Previous work has established their use against existing clinically-based imaging modalities like CT (van Beek *et al.*, 2009) and with broader tests of lung function, such as inert gas wash-out (Marshall *et al.*, 2017). Importantly, both %VV and VDP have shown to be effective in distinguishing ventilation properties between healthy volunteers and patients with respiratory disease (Ebner *et al.*, 2017b; Stewart *et al.*, 2018), as well as characterising response to BD therapy in both asthma and COPD (e.g. Kirby *et al.*, 2011; Svenningsen *et al.*, 2013). Moreover, previous studies have reported improved sensitivity to changes in regional airflow obstruction compared to spirometry (de Lange *et al.*, 2009; Pike *et al.*, 2015), in addition to detecting emphysema in asymptomatic smokers (Fain *et al.*, 2006), suggesting ability to identify early sub-clinical disease.

Beyond global ventilated lung volume measurements, HP-MRI offers potential to provide additional regional functional information compared to standard imaging techniques. In particular, the apparent diffusion co-efficient (ADC) provides a measure of gas movement within the alveoli and may be used to characterise microstructural pathology (Yablonskiy *et al.*, 2017). For instance, previous studies have demonstrated significantly elevated ADC values in emphysematous lung regions compared to healthy volunteers (Diaz *et al.*, 2008; Kaushik *et al.*, 2011), as well as corresponding to fibrotic changes observed on CT in patients with pulmonary fibrosis (Chan *et al.*, 2019). Of note, the ADC is governed by the Brownian

motion of molecules (e.g. inhaled gases) within a particular compartment size (e.g. the alveoli of the lungs) and is not to be confused with the diffusion of gas across the respiratory membrane, quantified by the T_LCO. As an example, the ADC is increased in emphysema, whereas the T_LCO is reduced. The sensitivity of HP-MRI to oxygen within the lung has also been exploited in assessing regional partial pressures of O_2 (Deninger $et\ al.$, 1999; Marshall $et\ al.$, 2014a), based on variation in the longitudinal relaxation time in well ventilated (reduced T_1) and poorly ventilated (elevated T_1) lung regions. The clinical utility of HP-MRI methods is further apparent in its potential to predict important disease-related outcomes, such as exacerbation frequency and quality-of-life measures in COPD (Kirby $et\ al.$, 2014; Kirby $et\ al.$, 2017), and symptom control in asthma (Svenningsen $et\ al.$, 2016).

Despite the apparent high sensitivity of HP-MRI to detect airway pathophysiology, several challenges exist in relation to pulmonary imaging with ^{3}He and ^{129}Xe. In particular, the cost of polarising equipment and required technical expertise represents a significant barrier to widespread use and has largely restricted this technique to specialised research settings. Moreover, the hyperpolarised state is finite and heavily influenced by contact with O_2: while the level of polarisation can persist for several hours under appropriate conditions, the T_1 of both ^{3}He and ^{129}Xe is considerably reduced to ~20–30 s following inhalation (Ebner $et\ al.$, 2017b), inducing rapid signal decay. This typically limits the ability to perform imaging of gas distribution within the lungs beyond a single breath-hold duration, although previous studies have demonstrated the feasibility of performing multi-breath imaging (Horn $et\ al.$, 2014b; Hamedani $et\ al.$, 2016).

Early pulmonary HP-MRI research focused predominantly on the use of inhaled ^{3}He. However, its relative expense and scarce supply (sourced primarily from tritium decay of nuclear warheads) has resulted in the increasing use of ^{129}Xe in recent years, benefiting from a high natural abundance which avoids the need for an enriched isotope (Lilburn $et\ al.$, 2013). The inherently lower gyromagnetic ratio of ^{129}Xe compared to ^{3}He typically gives rise to images with slightly lower SNR, though this is now largely offset by advances in polarising technology. Importantly, ^{129}Xe readily diffuses into the pulmonary circulation following inhalation and exhibits mild anaesthetic properties at alveolar concentrations greater than 70% (Goto $et\ al.$, 2000), warranting some caution. On the other hand, this characteristic 'dissolved-phase' presents an additional opportunity to assess gas uptake in the pulmonary circulation, enabling assessment of regional gas transfer properties (Qing $et\ al.$, 2014). This

effect has recently been exploited in the investigation of patients with pulmonary fibrosis (Weatherley *et al.*, 2019), where it has shown potential as an imaging biomarker for monitoring disease progression over time. Nonetheless, the overriding requirement for hyperpolarisation remains a significant barrier to widespread clinical application of this technique.

1.5.4 *Fluorinated-gas MRI*

Fluorinated-gas MRI (^{19}F-MRI) is a relatively novel approach to lung imaging that offers an alternative technical approach to hyperpolarisation, with potential to provide comparable functional information (Couch *et al.*, 2014). Currently, this method remains in development as a research tool for the investigation of pulmonary ventilation properties. However, the relatively low cost compared to HP-MRI, alongside recent successful use in patients with respiratory disease (Halaweish *et al.*, 2013a; Gutberlet *et al.*, 2018; McCallister *et al.*, 2021), make this a promising modality for future clinical application.

One of the principal advantages of ^{19}F-MRI is the lack of requirement for hyperpolarisation, thus avoiding the expense and technical demands associated with HP-MRI. Whereas hyperpolarised gas imaging relies on a large – but rapidly decaying – signal generated by inhaling a small amount of tracer gas (typically ~250 mL ^{3}He or ^{129}Xe), ^{19}F-MRI is based upon repeated averaging of the innate signal generated by thermally polarised ^{19}F nuclei within an inert, inhalable gas. Although this signal is orders of magnitude weaker than that generated using hyperpolarised methods, the high gyromagnetic ratio of ^{19}F nuclei – 94% that of ^{1}H (Couch *et al.*, 2019a) – makes it well suited to MR imaging. Importantly, the negligible innate fluorine content *in vivo* minimises potential for background signal interference during MR acquisitions. Moreover, the intrinsically short T_1 of perfluorinated gas molecules (typically ranging from 2–20 ms) permits rapid RF pulse repetition times (TR), favouring a greater degree of signal averaging (Kruger *et al.*, 2016). These properties facilitate ^{19}F-MR image acquisitions with acceptable SNR over a short period of time – for example, a single breath-hold – which is particularly relevant for use in patient studies. The ability to concurrently inhale O_2 without significant degradation of image quality offers an additional benefit over HP-MRI; namely, the ability to perform sustained breathing maneuvers and potential for dynamic imaging of gas wash-in and wash-out kinetics (e.g. Gutberlet *et al.*, 2018; Goralski *et al.*, 2020). This property is examined further in Chapter 6.

Despite these advantages, significant challenges exist with regards to pulmonary ^{19}F-MRI, largely arising from the short T_2^* of inhaled fluorinated gases. This has been reported in the region of 1–3 ms (Fox *et al.*, 2015), although varies according to which ^{19}F compound is used and the external magnetic field strength employed. In common with [1]H-MRI, the rate of signal decay (namely, T_2^*) can be minimised through use of MR acquisition sequences that employ short echo times, directing much of ^{19}F-MRI development in recent years (Halaweish *et al.*, 2013a; Couch *et al.*, 2013; Ouriadov *et al.*, 2015). Signal strength is further influenced by spin density, which is intrinsically linked to the number of fluorine atoms present within the inhaled gas (Kruger *et al.*, 2016). The use of gas compounds with multiple equivalent ^{19}F nuclei – such as SF_6 and PFP (C_3F_8) – may therefore increase the available signal compared to gases which have a lower fluorine concentration (e.g. tetrafluoromethane, CF_4,).

Perhaps arising from the technical challenges associated with ^{19}F-MRI, human ventilation imaging with inhaled fluorinated gases has, until recently, received relatively little attention. Initial work performed by Rinck *et al.* (1984) employed CF_4 to produce rather crude 2D images of canine lungs at low magnetic field strength (3.76 MHz, roughly equivalent to 0.1 T), but the technique was quickly overshadowed by the development of hyperpolarised gas MRI. Subsequently, Kuethe *et al.* (1998) demonstrated the potential for static ventilation imaging in rat lungs, using an 80% hexafluoroethane (C_2F_6) / 20% O_2 gas mixture. 3D images were acquired during a continuous breathing protocol, showing high spatial resolution (700 µm) at 1.9 T. However, the reported time for image acquisition was in excess of four hours and clearly impractical for clinical application. Since then, a number of pre-clinical and *ex-vivo* studies have been performed (predominantly using SF_6), utilising advances in ^{19}F-MRI technology to investigate various lung parameters (Jacob *et al.*, 2005; Pérez-Sánchez *et al.*, 2005; Wolf *et al.*, 2006). This has included assessment of lung volumes throughout the respiratory cycle (Kuethe *et al.*, 2002), as well as dynamic imaging of gas wash-in and wash-out kinetics (Schreiber *et al.*, 2001; Wolf *et al.*, 2010). Notably, Scholz *et al.* (2009) revealed a strong correlation between SF_6 signal intensity following multi-breath wash-in and the end-expiratory gas fraction in anaesthetised pigs, highlighting the potential role of ^{19}F-MR imaging as a functional biomarker of disease. Additionally, ^{19}F-MRI has effectively demonstrated differences in calculated ADC values in healthy and emphysematous excised lungs (Jacob *et al.*, 2005) and rat models of emphysema (Carrero-González *et al.*, 2013), suggesting the ability to characterise microstructural defects arising from respiratory disease in a similar manner to HP-MRI.

The first human ^{19}F-MRI experiment was performed by Wolf *et al.* (2008), who successfully acquired 2D images in a healthy volunteer following 3–5 deep breaths of a 78% SF_6 / 22% O_2 gas mixture. Although the image acquisition was of a relatively low resolution, this study was pivotal in highlighting the potential for safe *in vivo* measurements of pulmonary ventilation using fluorinated gas compounds. More recently, a number of independent research groups have assessed the feasibility of using ^{19}F-MRI of inhaled PFP to measure ventilation properties in healthy volunteers and patients with respiratory disease. PFP has several characteristics that make it suitable for human ventilation imaging. In particular, its short T_1 (approximately 12 ms at 3.0 T) (Couch *et al.*, 2013) facilitates a short TR and a high degree of signal averaging, meaning 3D scans can be acquired within a single breath-hold. Additionally, it has six magnetically equivalent ^{19}F nuclei per molecule (located on two -CF_3 moieties), enabling imaging with acceptable SNR at thermal polarisation. The SNR is, however, substantially reduced compared to HP-MRI of inhaled [3]He or [129]Xe (Kruger *et al.*, 2016) and represents a fundamental challenge for ventilation imaging by this method. Moreover, fluorinated gases – including PFP – are known to be potent greenhouse gases (Mühle *et al.*, 2010), which has important implications for their future clinical use. Specifically, the 100-year global warming potential (GWP) of PFP has been reported as 8900 times that of CO_2 (IPCC, 2013), such that efforts to collect and recycle the exhaled gas (e.g. Halaweish and Charles, 2014) will be necessary in establishing ^{19}F-MRI as an environmentally sustainable approach.

In an early feasibility study, Couch et al. (2013) performed ^{19}F-MRI in ten healthy volunteers to compare the SNR of breath-hold acquisitions following inhalation of a 79% PFP / 21% O_2 gas mixture. This was initiated according to one of two different inhalation schemes, comprising either a single 1 litre (L) breath of gas (Inhalation scheme 1), or continuous breathing of 5 L of the gas mixture followed by a 1 L inhalation and breath-hold (Inhalation scheme 2). A significant increase in SNR was observed following application of Inhalation scheme 2 (SNR = 32 ± 6) compared to Inhalation scheme 1 (SNR = 18 ± 6). While the number of participants was small (with only three participants undergoing the continuous breathing protocol), these findings demonstrated the potential to acquire ^{19}F-MR ventilation images of sufficient quality to visualise regional gas distribution (Figure 1.6), utilising the ability to 'wash-in' the gas mixture to the lungs prior to image acquisition.
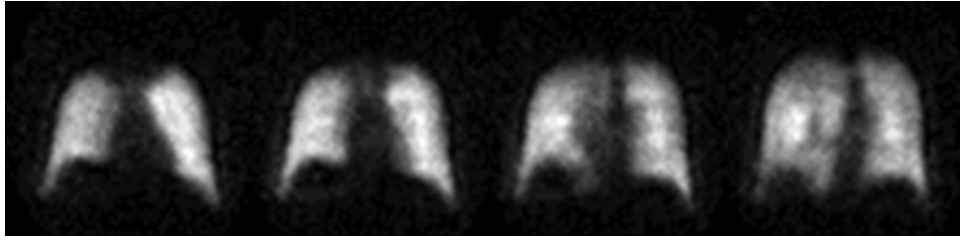
Figure 1.6: Example ^{19}F-MR ventilation images acquired in one healthy volunteer, represented by four coronal slices. Images were acquired during a 15 s breath-hold following 5 L continuous inhalation of a 79% PFP / 21% O$_2$ gas mixture, then a 1 L inhalation. Adapted from Couch *et al.* (2013).

In parallel with this work, Halaweish *et al.* (2013a) examined the use of ^{19}F-MRI to differentiate patterns of ventilation between healthy volunteers and patients with respiratory disease, including asthma, COPD, and single-lung transplant recipients. Using the same 79% PFP / 21% O$_2$ gas mixture and a multi-breath wash-in period, ventilation defects were readily identified in each of the patient groups (characterised as heterogeneous gas distribution), similar to what has been previously described with HP-MRI (see Figure 1.7).

A
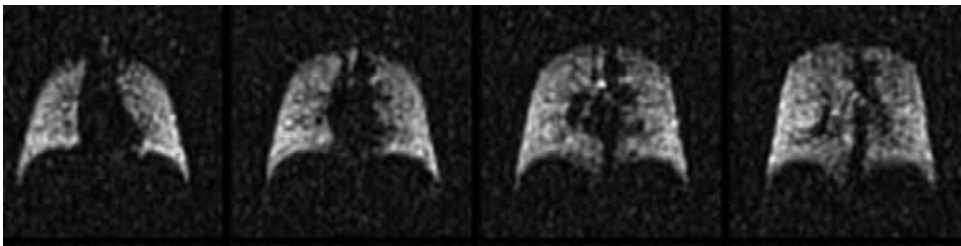
B
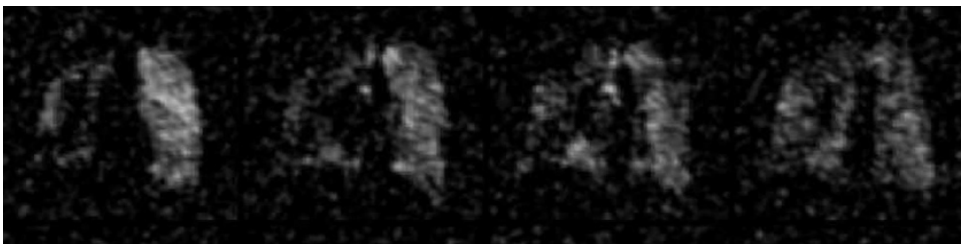
Figure 1.7: Example ^{19}F-MR ventilation images (coronal views) in **(A)** a healthy volunteer, and **(B)** a patient with COPD. Heterogeneous gas distribution can be visualised in the patient, reflecting underlying airways disease and emphysema. Adapted from Halaweish *et al.* (2013a).

Although the 3D image acquisitions demonstrated SNR values approximately half that reported by Couch *et al.* (2013), the resultant images revealed a clear disparity between the homogeneous gas distribution achieved in healthy volunteers and the inhomogeneity present in patients with respiratory disease. Importantly, neither of these studies reported any adverse events relating to PFP gas inhalation and all ^{19}F-MR images were acquired within a 15 s breath-hold duration.

More recently, the ability to breathe PFP concurrently with O_2 over the course of several respiratory cycles has been exploited to investigate regional gas wash-in and wash-out dynamics, building on previous preclinical work which established the technical feasibility of this approach (Schreiber *et al.*, 2001; Ouriadov *et al.*, 2015; Couch *et al.*, 2016). Specifically, Gutberlet *et al.* (2018) performed a combination of wash-in imaging using 79% PFP / 21% O_2 during successive breath-hold acquisitions (~17 s duration), and wash-out imaging during continuous free-breathing of 100% O_2 in patients with COPD. Delayed gas filling (i.e. wash-in) was observed in all patients, with a reduction in late-phase VDP values compared to early-phase VDP values, highlighting the ability to quantify gas distribution even in initially poorly ventilated lung regions. Notably, both early-phase VDP and gas wash-out parameters – namely, the number of breathing cycles and regional gas wash-out time – were shown to correlate well with FEV_1 measurements, indicating the potential to report on clinically-relevant biomarkers. In support of this work, Goralski *et al.* (2020) recently demonstrated the capacity for wash-out time constants to distinguish regional ventilation properties in healthy volunteers and patients with mild to moderate CF, including patients with normal spirometry (i.e. $FEV_1 > 80\%$ predicted).

^{19}F-MRI of inhaled PFP thus represents a nascent field for pulmonary ventilation imaging, offering significant advantages over HP-MRI stemming from the lack of requirement for expensive polarising equipment and expertise (see Table 1.2 for a summary of the relative strengths and challenges of these approaches). The ability to perform dynamic imaging without loss of signal through RF- and T_1-mediated effects provides additional scope to assess ventilation properties beyond conventional breath-hold imaging. Nonetheless, the technique remains in relative infancy and, to date, has not been validated against existing clinical imaging modalities. Importantly, while the repeatability of dynamic wash-out parameters has recently been reported (Gutberlet *et al.*, 2019), the capacity to acquire reproducible measurements relating to static ventilation imaging – such as %VV – has not been evaluated. Moreover, it remains unclear whether ^{19}F-MRI of inhaled PFP is capable of detecting changes in regional gas distribution – for example, in response to BD therapy – in a similar manner to HP-MRI. These represent important avenues to consider in developing the technique as a viable alternative to current established methods. The inert nature of inhaled PFP offers further opportunities to examine ^{19}F-MR ventilation imaging in conjunction with other MR imaging agents, including intravenous GBCAs; this forms the basis of the experimental work presented in later chapters of this thesis.

Gas imaging technique	Strengths	Challenges
^{19}F-MRI of inhaled PFP	100% naturally abundant Multiple ^{19}F nuclei Imaging at thermal polarisation - does not require hyperpolarisation - capacity for dynamic imaging Relatively low cost	Low SNR/spatial resolution Greenhouse gas - capture and recycling strategies needed Technique not yet fully established - lack of standardised approach to imaging/analysis
HP-MRI (^{3}He and ^{129}Xe)	High SNR/spatial resolution Well-established technique Quantitative measurements of pulmonary ventilation - %VV/VDP, ADC, pO$_2$, gas exchange (^{129}Xe)	Requirement for polarisation - high cost - technical demands Limitations for dynamic imaging
OE-MRI	No additional hardware requirements Inexpensive	Low SNR/spatial resolution Unable to provide static breath-hold imaging Long scan times Indirect assessment of ventilation

Table 1.2: Summary of the relative strengths and challenges associated with different gas imaging techniques; namely, ^{19}F-MRI, HP-MRI and OE-MRI.

1.6   Aims and hypotheses

The overarching aim of this research is to develop novel methods for assessing pulmonary ventilation properties using ^{19}F-MRI of inhaled PFP, with potential for translating this technique to clinical practice. Primary objectives are to determine the reproducibility of %VV measurements acquired by ^{19}F-MRI in a group of healthy volunteers, and to demonstrate differences in %VV values between healthy volunteers and patients with respiratory disease; namely, asthma and COPD. A secondary objective is to assess the utility of %VV measurements acquired by ^{19}F-MRI to detect changes in regional gas distribution in response to BD therapy. Additionally, this thesis intends to explore the feasibility of performing combined ventilation and perfusion imaging within a single MRI scan session, utilising novel ^{19}F-MRI methods in conjunction with an established intravenous GBCA.

The primary research hypotheses are that:

1.   %VV of the lungs, as measured by ^{19}F-MRI of inhaled PFP,
    a)   is reproducible in a group of healthy volunteers
    b)   is reduced in patients with asthma and patients with COPD compared to healthy volunteers
    c)   improves in patients with asthma and patients with COPD following administration of BD therapy

These hypotheses are examined in Chapter 4 (1a) and Chapter 5 (1b and 1c), respectively.

2.   Regional wash-in and wash-out times for inhaled PFP and intravenously administered GBCA
    a)   can be assessed concurrently within a single MRI scan session
    b)   differ in patients with respiratory disease (namely, COPD) compared to healthy volunteers

These hypotheses are examined in Chapter 6.

3. Administration of GBCA leads to enhanced T_2^* and MR signal intensity of inhaled PFP, owing to magnetic susceptibility matching in well-perfused and well-ventilated regions of the lung.

This hypothesis is examined in Chapter 7.

1.7   Outline of chapters

The work presented in this thesis was conducted within the framework of three ethically approved studies: a large dual-centre study (LIFT), and two smaller feasibility studies (VQ MRI and LungGas). The first part of this thesis focusses on material arising directly from the LIFT study (Chapters 3, 4 and 5). The second part of this thesis contains material arising from the VQ MRI and LungGas studies (Chapters 6 and 7, respectively).

Chapter 2 begins by outlining the design of the three studies, including a description of the common materials used to perform the experimental work. This is followed by a discussion of the LIFT study development phase (Chapter 3), highlighting key methodological considerations and approaches to performing static ^{19}F-MR ventilation imaging that are subsequently adopted in studies involving healthy volunteers (Chapter 4) and patients with respiratory disease (Chapter 5). The %VV represents a primary outcome measure for this section of the thesis. Chapter 6 extends this work by exploring the feasibility of performing dynamic measurements of pulmonary ventilation and perfusion in healthy volunteers and patients with COPD, employing DCE-MRI in combination with ^{19}F-MRI. Chapter 7 outlines a 'proof of concept' study in healthy volunteers, detailing a novel approach to combined ventilation/perfusion imaging within a single breath-hold. The thesis concludes by providing a general discussion of the work presented (Chapter 8), including an acknowledgement of important study limitations and potential avenues for future research.

Chapter 2.
Materials and Methods

2.1   Introduction

This chapter provides an overview of the experimental studies underpinning this body of research, including a description of the common materials and methods employed. A more detailed description of the specific methods (including statistical analyses) applied to individual studies involving healthy volunteers and patients with respiratory disease is contained within the relevant chapters of this thesis.

The chapter begins by outlining the design of the LIFT study: this study forms a central component of the work presented, upon which subsequent conclusions are drawn regarding the utility of static ventilation imaging using ^{19}F-MRI of inhaled PFP. This is followed by a description of the VQ MRI and LungGas studies, both of which explore the potential for combined ventilation and perfusion imaging using inhaled PFP alongside an intravenously administered GBCA. The chapter concludes by detailing the materials used to perform these experimental studies.

2.2   Overview of LIFT study

The LIFT study – 'Lung magnetic resonance Imaging with Fluorocarbon Tracer gases' – is a prospective, dual-centre study between Newcastle University and the University of Sheffield, funded by the Medical Research Council (MRC) (reference MR/N018915/1). Ethical approval was granted by the Newcastle and North Tyneside 1 Research Ethics Committee (REC) (reference 16/NE/0282) on 7th October 2016 and the NHS Health Research Authority (HRA) on 2nd December 2016. Study sponsorship was agreed by The Newcastle upon Tyne Hospitals NHS Foundation Trust (NUTH) on 5th December 2016.

2.2.1   Study design

The study comprises three consecutive phases, reflecting the developmental nature of the research and the need to establish reproducible MR imaging protocols prior to implementation in patient cohorts.

Phase 1: Method development

The first phase of the LIFT study was designed to enable the development and optimisation of ^{19}F-MRI scan protocols for successful measurement of the %VV in healthy volunteers and patients with respiratory disease. This work was performed in close collaboration with MR physicists based in Newcastle upon Tyne (Newcastle Magnetic Resonance Centre (NMRC), Newcastle University) and Sheffield (Academic Unit of Radiology, University of Sheffield), involving the testing of MRI scan procedures in up to 40 healthy volunteers and 10 patients with asthma or COPD.

The anticipated number of participants required to complete Phase 1 of the LIFT study was based on previous experience with lung imaging and scan protocol development work conducted in Newcastle upon Tyne and Sheffield: in total, 31 healthy volunteers and 4 patients with respiratory disease (2 patients with asthma and 2 patients with COPD) were considered sufficient to fulfil the initial developmental aims.

Material stemming from Phase 1 of the LIFT study is presented in the next chapter of this thesis (Chapter 3).

Phase 2: Healthy volunteer reproducibility study

The second phase of the LIFT study was designed to assess the same-day reproducibility of %VV measurements acquired by ^{19}F-MRI of inhaled PFP. Methods established during study Phase 1 were applied to a planned cohort of healthy volunteers (20 participants in Newcastle upon Tyne and 20 participants in Sheffield), enabling acquisition of four successive ^{19}F-MR ventilation images per participant, from which %VV measurements were calculated.

The sample size was determined during the design phase of the study by Prof Debra Stocken (former Senior Lecturer in Biostatistics and Clinical Trials, Newcastle University), based on

existing data from the University of Sheffield concerning the reproducibility of %VV measurements derived from hyperpolarised ^{129}Xe studies.

Phase 2 of the LIFT study forms the basis of Chapter 4.

Phase 3: Patient study

The third phase of the LIFT study was designed to test the ability of ^{19}F-MRI to distinguish ventilation properties between healthy volunteers and patients with respiratory disease (40 patients with asthma and 40 patients with COPD, split between the two study sites) using the %VV as the primary outcome measure. Patient data were compared with healthy volunteer data acquired during Phase 2 of the study to determine if any differences in %VV measurements were present between the respective groups. Additionally, for patients with respiratory disease, %VV measurements were acquired before and after administration of nebulised salbutamol (2.5 mg), enabling assessment of the ability to detect response to BD therapy using ^{19}F-MRI.

The sample size was determined during the design phase of the study by Prof Debra Stocken; power calculations were informed by data derived from previous HP-MRI studies, based on the ability to detect a 10% difference in %VV values between patient groups and healthy volunteers. A minimum of 34 participants per patient group was considered sufficient to achieve this effect (where alpha = 0.025 and beta = 0.2), inflated to 40 per group to cover the potential for withdrawal or non-compliance with study procedures.

At the time of writing, recruitment to Phase 3 of the LIFT study has been suspended as a result of the novel coronavirus (COVID-19) pandemic and, as such, the planned target of 40 patients at each study site has not yet been achieved. For the purpose of completing and submitting this thesis within the available timeframe, only those patients who have been successfully recruited and scanned in Newcastle upon Tyne ($n = 29$) are included for analysis and discussion.

Phase 3 of the LIFT study forms the basis of Chapter 5.

2.2.2   Recruitment and screening procedures

Healthy volunteers

Healthy volunteers attending either Phase 1 or Phase 2 of the LIFT study were recruited by email and/or poster advertisements distributed to local University and NHS organisations at each of the two respective study sites. Interested volunteers were asked to contact a member of the local research team, who provided them with a copy of the relevant Participant Information Sheet (PIS). Volunteers were contacted by a member of the study team after a period of at least 24 hours to confirm that they had read the PIS and would still like to participate in the study.

Volunteers who expressed an interest in continuing with the study were subsequently invited to attend their local research centre for a single study visit. During this visit, volunteers were asked to provide written informed consent before undergoing screening procedures to confirm that all study eligibility requirements were met. This included performing pulse oximetry, height and weight measurements, spirometric measurements (namely, FEV_1 and FVC), and a brief cardio-respiratory examination. All participants completed an MRI safety questionnaire as part of the screening process to ensure that there were no contraindications to performing MRI scans. Additionally, as the study was not recruiting pregnant females, women of childbearing age were asked to perform a pregnancy test as part of the screening process.

A summary of healthy volunteer inclusion and exclusion criteria is outlined in Table 2.1.

Inclusion criteria	Exclusion criteria
Aged 18 or over	History of respiratory disease and/or current evidence of respiratory tract infection
Normal spirometric lung function[*]	
	Cardiac or cerebrovascular disease, anaemia, or other serious medical condition
Body weight 50-100 kg[†]	
	Current prescribed medication (excluding oral contraceptives)
	History of smoking in past 2 years, ex-smoker with greater than 2 pack year history[‡] and/or ex-smoker who has smoked for more than 2 years in total
	Contraindications to performing MRI, including incompatible body habitus (body mass index (BMI) greater than 35; chest circumference greater than ~130 cm) and/or claustrophobia
	Inability to perform spirometry in a reproducible manner
	Pregnant or breastfeeding

Table 2.1: Summary of eligibility criteria for healthy volunteers participating in the LIFT study. [*]FEV_1 greater than or equal to 80% predicted; FEV_1/FVC greater than or equal to 0.7. [†]In accordance with coil manufacturer guidelines and Specific Absorption Rate (SAR) limits – see Section 2.5.3. [‡]1 pack year = smoking 20 cigarettes per day for one year.

Patients with respiratory disease

Patients with asthma and patients with COPD attending either Phase 1 or Phase 3 of the LIFT study were recruited from secondary care outpatient clinics in adult respiratory medicine at NUTH and The Sheffield Teaching Hospitals NHS Foundation Trust (STH). Patients were identified by a clinically qualified member of the study team and/or local clinicians aware of the study and potential suitability for participation according to inclusion and exclusion requirements outlined in Table 2.2. The diagnosis of asthma was made clinically by the relevant member of the study team and/or referring clinician, based on the combination of compatible symptoms and supportive investigations (e.g. historical evidence of reversible airways obstruction, or FeNO results). There was no requirement for patients to undergo BD reversibility testing prior to participation in the study. Previous smoking history was not a specific exclusion criterion for patients with asthma and therefore did not preclude study participation; however, recruitment was primarily focussed on patients with no or little smoking history (typically less than 15 pack years) to minimise the possibility of co-existent smoking-related small airways disease. All patients with COPD had severe disease ($FEV_1 <$ 50% predicted) according to GOLD criteria (GOLD, 2020), with evidence of emphysema on previous CT imaging.

Inclusion criteria	Exclusion criteria
Aged 18 or over	Resting average O_2 saturations breathing room air (sitting) of < 92% measured over a 2-minute period
Body weight 50-100 kg	
Physician diagnosis of asthma[*]	Resting average O_2 saturations breathing room air (lying supine) of < 90% measured over a 2-minute period
OR	Angina in previous 48 hours
COPD with evidence of emphysema on previous CT, and $FEV_1/FVC <$ 0.7, and $FEV_1 < 50\%$ predicted	Cardiac arrhythmias (except sinus arrhythmia, ectopic beats, or chronic and stable atrial fibrillation)
	Neurological symptoms or signs in the previous 48 hours
	Contraindications to MRI, including incompatible body habitus (BMI greater than 35; chest circumference greater than ~130 cm) and/or claustrophobia
	Inability to perform spirometry in a reproducible manner
	Pregnant or breastfeeding
	History of hypersensitivity to salbutamol
	History of seizure in the previous 12 months
	History of significant renal impairment requiring dialysis
	History of hepatic cirrhosis
	Other significant respiratory disease, such as bronchiectasis or chest wall disease

Table 2.2: Summary of eligibility criteria for patients with respiratory disease participating in the LIFT study. [*]Step 3 or above (i.e. at least a moderate dose inhaled corticosteroid and a long-acting bronchodilator), in accordance with the British Thoracic Society (BTS)/Scottish Intercollegiate Guidelines Network (SIGN) guideline on the management of asthma (2014).

The study was discussed with suitably identified patients, who were provided with a copy of the relevant PIS. Patients were contacted by a member of the study team after a period of at least 24 hours to confirm that they had read the PIS and would still like to participate in the study.

Patients who expressed an interest in continuing with the study were subsequently invited to attend their local research centre for an initial screening visit. During this visit, patients provided written informed consent to participate in the study before undergoing screening procedures to confirm that all study eligibility requirements were met. These mirrored the screening procedures conducted in healthy volunteers. Upon completion of the screening visit, eligible patients were invited to attend the research centre for a second study visit,

during which MRI scanning was performed (see Section 2.2.3). The second study visit typically occurred within 1–2 weeks of the first study visit.

Prior to attending the second study visit, patients were instructed to withhold long-acting BD medication (including combination corticosteroid inhalers where relevant) for a duration of greater than 12 hours, and short-acting BD medication for a duration of greater than 4 hours. All patients were provided with a written medication withdrawal document as a reminder of when specific medications should be withheld prior to the second study visit, and this was confirmed with participants prior to leaving respective study centres on their first study visit. No medication was withheld for more than 24 hours from the usual administration time, and patients were advised to take their medication if this was felt necessary for clinical reasons (e.g. significant breathlessness); in these circumstances, the second study visit was postponed to another day, or cancelled. In the event that the second visit was postponed as a result of patients not withholding their BD medication, rescheduling was performed on no more than two occasions, and patients were withdrawn from the study if withholding BD medication was not considered feasible.

2.2.3   MRI scan procedures

Healthy volunteers

Healthy volunteers who remained eligible to continue with the study underwent a single MRI scan session immediately following initial screening procedures. The MRI scan session lasted approximately 1 hour, comprising conventional ^{1}H-MRI scans whilst breathing room air, and up to five ^{19}F-MRI scans whilst breathing a 79% PFP / 21% O_2 gas mixture (see Section 2.5.4). Each of the five gas inhalation sessions involved breathing up to 25 L of the gas mixture for a period of up to one minute followed by a breath-hold, during which ^{19}F-MRI scans were acquired.

The nature of the scans performed during each gas inhalation session, as well as the specific breathing instructions provided to participants, was refined during Phase 1 of the LIFT study, such that final inhalation procedures and ^{19}F-MRI scan protocols were determined prior to commencing Phase 2 of the study. The process of testing and optimising these scan procedures is described in further detail in Chapter 3.

The timeline for healthy volunteer involvement in the LIFT study is illustrated in Figure 2.1. Participant involvement in the study was terminated upon completion of the MRI scan session.
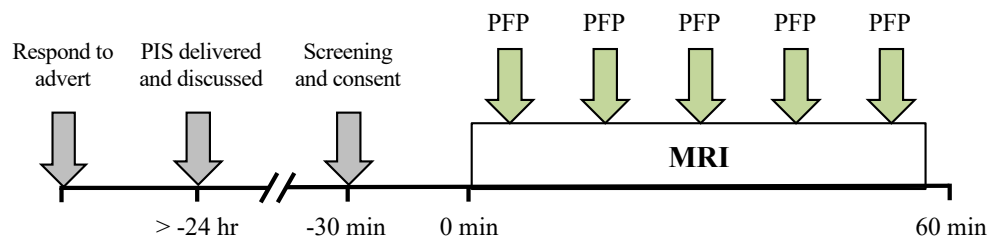
Figure 2.1: Timeline for healthy volunteers participating in Phase 1 or Phase 2 of the LIFT study.

Patients with respiratory disease

Eligible patients attending the second study visit were briefly re-screened (including further spirometric assessment) to confirm that there had been no significant alteration in clinical status since their initial screening visit (such as recent changes to medication, or illness) and that relevant BD medication had been withheld appropriately as instructed. Women of childbearing age were asked to perform a pregnancy test at the time of their second visit to confirm ongoing study eligibility.

The MRI scan session was split into two parts, lasting approximately 1.5 hours in total. The first part included performing conventional ^{1}H-MRI scans whilst breathing room air, and up to three ^{19}F-MRI scans whilst breathing the same 79% PFP / 21% O_2 gas mixture used during healthy volunteer studies. Patients then left the scanner to receive nebulised salbutamol (2.5 mg), administered by a member of the study team (see Section 2.5.8). Spirometry measurements were subsequently repeated 20 minutes after completion of the nebuliser, following which patients re-entered the MRI scanner for the second part of the scan session. This involved repeating conventional ^{1}H-MRI scans whilst breathing room air and performing up to two further (post-BD) ^{19}F-MRI scans whilst breathing the 79% PFP / 21% O_2 gas mixture. In common with healthy volunteers, each of the five gas inhalation sessions involved breathing up to 25 L of the gas mixture for a period of up to one minute followed by a breath-hold, during which ^{19}F-MRI scans were acquired.

The timeline for patient involvement in the LIFT study is illustrated in Figure 2.2. Patient involvement in the study was terminated upon completion of the MRI scan session.
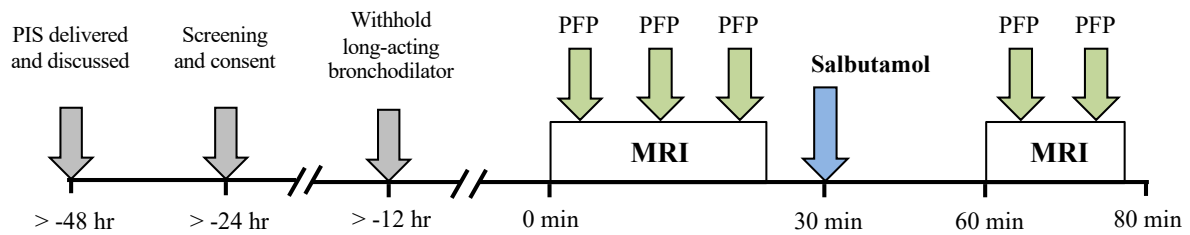
Figure 2.2: Timeline for patients with respiratory disease participating in Phase 1 or Phase 3 of the LIFT study.

2.3 Overview of VQ MRI study

The VQ MRI study – 'Assessing pulmonary ventilation and perfusion properties with MRI' – is a small feasibility study at Newcastle University, funded by the MRC (Confidence in Concept (CiC) award: MC/PC/18057). Ethical approval was granted by the Newcastle and North Tyneside 2 REC (Reference 18/NE/0297) on 25th October 2018 and the NHS HRA on 26th October 2018. Study sponsorship was agreed by NUTH on 17th January 2019.

2.3.1 Study design

The study was initially conceived with four distinct study groups, enabling the development and application of dynamic ventilation and perfusion imaging protocols in heathy volunteers and patients with respiratory disease.

Group 1: Healthy volunteers (method development)
The first study group was designed to test and optimise DCE-MRI scan procedures in up to five healthy volunteers, for the purpose of assessing lung perfusion properties in subsequent study groups.

Group 2: Patients with COPD
The second study group was designed to assess the feasibility of performing combined ventilation and perfusion imaging in five patients with COPD, employing ^{19}F-MRI of inhaled PFP in conjunction with DCE-MRI scan procedures established in study Group 1.

Group 3: Patients with PE

The third study group was designed to assess the feasibility of performing combined ventilation and perfusion imaging in five patients with PE, employing the same procedures adopted for study Group 2.

Group 4: Healthy volunteers (control group)

The fourth study group was designed to provide control data in five healthy volunteers for comparison with DCE-MRI perfusion measurements and ^{19}F-MRI ventilation measurements acquired in Study Groups 2 and 3.

The sample size for each of the respective study groups was informed by previous DCE-MRI and ^{19}F-MRI literature regarding the ability to detect overt ventilation and/or perfusion defects in these patient populations, and local experience with scan protocol development work. The study was not statistically powered, however, since its primary purpose was to determine the technical feasibility of applying these two MRI techniques in combination, rather than specific hypothesis testing.

Unfortunately, the VQ MRI study was halted prematurely owing to the emergence of the COVID-19 pandemic in March 2020 and it was not possible to proceed with recruitment to study Group 3 (patients with PE). As such, the following description of study procedures relates only to study Groups 1, 2 and 4.

2.3.2   Recruitment and screening procedures

Healthy volunteers

Healthy volunteers (Group 1 and Group 4) were recruited by email advertisements distributed to staff and students working at Newcastle University, Newcastle upon Tyne. Subsequent recruitment and screening procedures were conducted in an identical manner as described for healthy volunteers attending Phase 1 or Phase 2 of the LIFT study (see Section 2.2.2, above).

A summary of the healthy volunteer inclusion and exclusion criteria is outlined in Table 2.3.

Inclusion criteria	Exclusion criteria
Aged 18 or over	History of respiratory disease and/or current evidence of respiratory tract infection
Normal spirometric lung function[*]	
	Cardiac or cerebrovascular disease, anaemia, or other serious medical condition
Body weight 50-100 kg[†]	
	History of smoking in past 2 years and/or ex-smoker with greater than 10 pack year history[‡]
	Contraindications to performing MRI, including incompatible body habitus (BMI greater than 35; chest circumference greater than ~130 cm) and/or claustrophobia
	Inability to perform spirometry in a reproducible manner
	Pregnant or breastfeeding
	Known or suspected renal disease
	Previous allergic reaction to GBCAs

Table 2.3: Summary of eligibility criteria for healthy volunteers participating in the VQ MRI study. [*]FEV_1 greater than or equal to 80% predicted; FEV_1/FVC greater than or equal to 0.7. [†]In accordance with coil manufacturer guidelines and SAR limits (see Section 2.5.3). [‡]1 pack year = smoking 20 cigarettes per day for one year.

Patients with COPD

Patients with COPD (Group 2) were recruited from secondary care outpatient clinics in adult respiratory medicine at NUTH, in accordance with inclusion and exclusion requirements outlined in Table 2.4. The study was discussed with suitably identified patients, who were provided with a copy of the relevant PIS. Patients were contacted after a period of at least 24 hours to confirm that they had read the PIS and would still like to participate in the study. Patients who expressed an interest in continuing with the study were subsequently invited to attend the NMRC for a single study visit. During this visit, patients provided written informed consent to participate in the study before undergoing screening procedures to confirm that all study eligibility requirements were met. These mirrored the screening procedures conducted in healthy volunteers (outlined in Section 2.2.2).

Inclusion criteria	Exclusion criteria
Aged 18 or over	Resting average O_2 saturations breathing room air (lying supine) of < 90% measured over a 2-minute period
COPD with evidence of emphysema on previous CT and $FEV_1/FVC < 0.7$	Known or suspected cardiac disease
Body weight 50-100 kg[†]	Other significant respiratory or chest wall disease
	Known or suspected renal disease
	Previous allergic reaction to GBCAs
	History of seizure or cerebrovascular disease
	Contraindications to MRI, including incompatible body habitus (BMI greater than 35; chest circumference greater than ~130 cm) and/or claustrophobia
	Inability to perform spirometry in a reproducible manner
	Pregnant or breastfeeding

Table 2.4: Summary of eligibility criteria for patients with COPD participating in the VQ MRI study. [†]In accordance with coil manufacturer guidelines and SAR limits (see Section 2.5.3).

2.3.3 MRI scan procedures

Healthy volunteers (Group 1)

Healthy volunteers who remained eligible to continue with the study underwent a single MRI scan session directly following initial screening procedures. The MRI scan session lasted approximately 30 minutes, comprising conventional [1]H-MRI scans whilst breathing room air and up to two DCE-MRI scans. Each DCE-MRI scan was commenced immediately prior to administration of a single dose of intravenous GBCA (Gadobutrol), allowing acquisition of MRI data before, during and after contrast agent passage through the lungs.

The DCE-MRI scan procedures were refined following the first participant, enabling determination of the most suitable acquisition parameters, breathing procedures, and dose of contrast agent for implementation in subsequent study groups. The final adopted scan procedures are outlined in Chapter 6 (Section 6.2.2).

The timeline for healthy volunteer (Group 1) involvement in the VQ MRI study is illustrated in Figure 2.3. Participant involvement in the study was terminated upon completion of the MRI scan session.
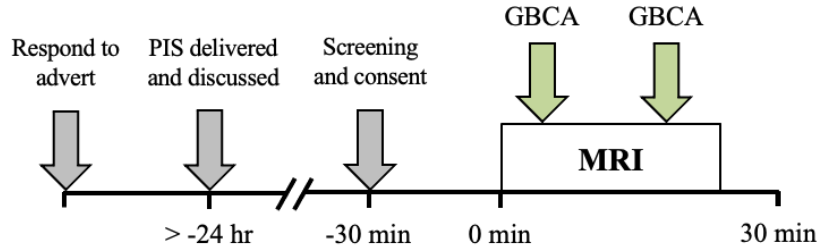
Figure 2.3: Timeline for healthy volunteers (Group 1) participating in the VQ MRI study.

Patients with COPD (Group 2) and healthy volunteers (Group 4)

Healthy volunteers and patients with COPD who remained eligible to continue with the study underwent a single MRI scan session immediately following initial screening procedures. The MRI scan session was split into two parts, lasting approximately 1.5 hours in total. The first part included performing conventional ^{1}H-MRI scans whilst breathing room air, and a single DCE-MRI scan following administration of intravenous GBCA. This was performed in accordance with scan procedures established in study Group 1. Participants then left the MRI scanner briefly to enable substitution of relevant RF coils (see Section 2.5.2), following which they re-entered the scanner for the second part of the scan session. This involved repeating conventional ^{1}H-MRI scans whilst breathing room air, and subsequently performing up to four ^{19}F-MRI scans whilst breathing the same 79% PFP / 21% O_2 gas mixture employed in the LIFT study. Each of the four gas inhalation sessions involved breathing up to 25 L of the gas mixture – either continuously or punctuated by breath-holds – during which ^{19}F-MRI scans were acquired. The nature of the scans performed during each gas inhalation session, as well as the specific breathing instructions provided to participants, is outlined in Chapter 6 (Section 6.2.2).

The timeline for healthy volunteer (Group 2) and patient (Group 4) involvement in the VQ MRI study is illustrated in Figure 2.4. Participant involvement in the study was terminated upon completion of the MRI scan session.
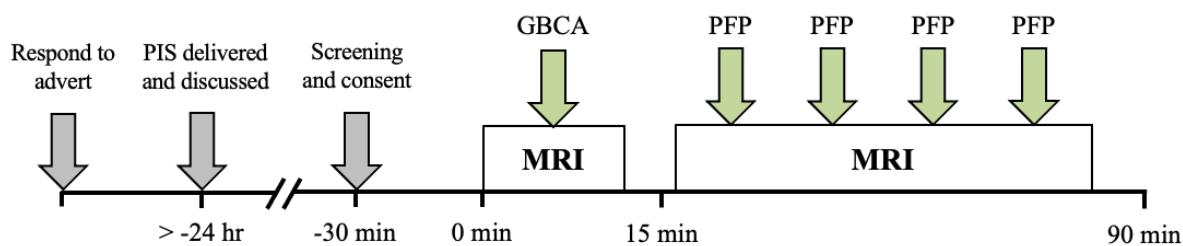
Figure 2.4: Timeline for patients with COPD (Group 2) and healthy volunteers (Group 4) participating in the VQ MRI study.

2.4 Overview of LungGas study

The LungGas study – 'Imaging lung ventilation by MRI of fluorocarbon gases' – was a small pilot study at Newcastle University, funded by the MRC (CiC award: MC/PC/16054). Ethical approval was granted by the Newcastle and North Tyneside 1 REC (Reference 14/NE/0135) on 1st July 2014. Study sponsorship was agreed by NUTH on 7th August 2014.

A substantial amendment was approved by the NHS HRA on 19th April 2017 to enable testing of the specific study hypothesis outlined in Chapter 1 (Section 1.6).

2.4.1 Study design

The study comprised four groups of healthy volunteers, each involving the testing and optimisation of scan procedures relating to human ^{19}F-MR ventilation imaging.

Group 1:
Five participants were recruited for the purpose of determining optimal MRI sequence parameters for conducting ^{19}F-MRI of inhaled PFP, utilising the 2D surface coil outlined later in this chapter (Section 2.5.2).

Group 2:
Seven participants were recruited for the purpose of demonstrating repeatability of ^{19}F-MRI scan procedures developed in study Group 1.

Group 3:

Eight participants were recruited to enable further optimisation of ^{19}F-MRI scan protocols for the purpose of conducting human ventilation imaging using the 3D birdcage coil outlined in Section 2.5.2.

Group 4:

Four participants were recruited to assess the impact of administering an intravenous GBCA (Gadobutrol) on the quality of ^{19}F-MRI acquisitions, enabling testing of a novel approach to combined pulmonary ventilation and perfusion imaging.

The first three study groups lie outside the scope of this thesis and were concerned with the initial establishment of ^{19}F-MRI scanning capabilities at the NMRC; these experiments formed the basis of the developmental work conducted by Dr Mary Neal during her PhD at Newcastle University (Neal, 2017).

The final study group represents the focus for the experimental work presented in Chapter 7 of this thesis. A sample size of four healthy volunteers was considered appropriate to demonstrate proof of principle of the technique and to confirm initial feasibility in human participants.

2.4.2   Recruitment and screening procedures

Healthy volunteers (study Group 4) were recruited by email advertisements distributed to staff and students working at Newcastle University, Newcastle upon Tyne. Subsequent recruitment and screening procedures were conducted in an identical manner as described for healthy volunteers attending Phase 1 or Phase 2 of the LIFT study (see Section 2.2.2).

A summary of the study inclusion and exclusion criteria is outlined in Table 2.5.

Inclusion criteria	Exclusion criteria
Aged 18-65	History of respiratory disease and/or current evidence of respiratory tract infection
Normal spirometric lung function[*]	
	Cardiac or cerebrovascular disease, anaemia, or other serious medical condition
Body weight 50-100kg	
	History of smoking in past 2 years and/or ex-smoker with greater than 10 pack year history
	Contraindications to performing MRI, including incompatible body habitus (BMI greater than 35) and/or claustrophobia
	Inability to perform spirometry in a reproducible manner
	Pregnant or breastfeeding
	Known or suspected renal disease
	Previous allergic reaction to GBCAs

Table 2.5: Summary of eligibility criteria for healthy volunteers participating in the LungGas study.
[*]FEV_1 greater than or equal to 80% predicted; FEV_1/FVC greater than or equal to 0.7.

2.4.3   MRI scan procedures

Healthy volunteers who remained eligible to continue with the study underwent a single MRI scan session immediately following initial screening procedures. The MRI scan session lasted approximately 30 minutes, comprising conventional ^{1}H-MRI scans whilst breathing air, and up to three ^{19}F-MRI scans whilst breathing the same 79% PFP / 21% O_2 gas mixture employed in the LIFT study. Each gas inhalation session involved breathing up to 25 L of the gas mixture for a period of up to 1 minute followed by a breath-hold, during which ^{19}F-MRI scans were acquired. During one of the gas inhalation sessions, participants were administered a single dose of intravenous GBCA (Gadobutrol), enabling MRI scans of pulmonary ventilation to be acquired concurrently with contrast agent passage through the lungs.

The timeline for healthy volunteer involvement in the LungGas study is illustrated in Figure 2.5. Participant involvement in the study was terminated upon completion of the MRI scan session.
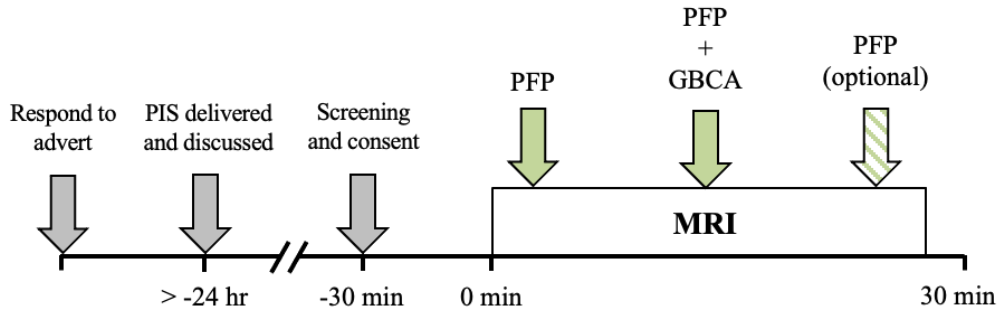
Figure 2.5: Timeline for healthy volunteers (Group 4) participating in the LungGas study.

2.5 Study materials and practical considerations

The preceding sections of this chapter outlined the design of the LIFT study, the VQ MRI study and the LungGas study, providing the context for the work presented in this thesis. The following section outlines the specific materials used to conduct these experimental studies, including the main practical considerations with respect to performing human ^{19}F-MR ventilation imaging.

2.5.1 MRI scanners

All MRI scans were performed supine on designated 3.0 T research scanners located at the NMRC, Newcastle University (Philips Achieva, Philips Healthcare, Best, The Netherlands) or the Academic Unit of Radiology, University of Sheffield (Philips Ingenia, Philips Healthcare, Best, The Netherlands).

2.5.2 RF coils

LIFT study

^{1}H- (anatomical) and ^{19}F- (ventilation) MRI acquisitions were performed using one of two custom built 50 cm long ^{19}F/^{1}H elliptical birdcage coils (Rapid Biomedical, Rimpar, Germany) interfaced to the MRI scanner at respective study sites (see Figure 2.6). This permitted 3D imaging with full lung coverage, enabling %VV measurements to be acquired in accordance with the study aims. Contraindications relating to participant body mass index (BMI), chest circumference, and a maximum body weight of 100 kg (specified by the coil manufacturer) are reflected in the study eligibility criteria (see Tables 2.1 and 2.2).

Figure 2.6: ^{19}F/^{1}H elliptical birdcage coil (Rapid Biomedical, Rimpar, Germany) used in the LIFT study, shown *in situ* on the MRI scanner bed at the NMRC, Newcastle University.

VQ MRI study

DCE-MRI acquisitions were performed using an 8-element ^{1}H receive array torso coil (Philips Healthcare, Best, The Netherlands) (see Figure 2.7). This permitted improved signal compared to the scanner's integral body coil, due to the closer proximity of the coil to participants and the ability to accelerate scans through parallel imaging (see Chapter 6, Table 6.2). ^{19}F-MRI acquisitions were performed using the same ^{19}F/^{1}H elliptical birdcage coil employed in the LIFT study.

Figure 2.7: 8-element ^{1}H receive array coil (Philips Healthcare, Best, The Netherlands) used in the VQ MRI study, shown with a study participant *in situ.*

LungGas study

^{19}F-MRI acquisitions were performed using a 20 cm diameter ^{19}F surface coil (PulseTeq Ltd., Woking, UK), as shown in Figure 2.8. The surface coil was chosen based on its immediate availability (at the time of conducting the LungGas study, the ^{19}F/^{1}H elliptical birdcage coil was with the manufacturer in Germany undergoing repair and was subsequently not available to use for several months), in addition to its capacity to produce 2D images with higher signal

intensity and temporal resolution compared to the 3D elliptical birdcage coil. This provided an appropriate means of testing the proposed study hypothesis and to determine initial feasibility of the technique.

Figure 2.8: [19]F surface coil (PulseTeq Ltd., Woking, UK) used in the LungGas study.

2.5.3   *Specific absorption rate and power limits*

In common with all MRI scan procedures, imaging for the respective studies was performed within the framework of specific power limits stipulated by the scanner manufacturer and respective coil manufacturers. This was necessary to avoid the theoretical risk of local tissue damage (namely, heating) secondary to energy transfer that occurs during all MRI acquisitions. This energy transfer is known as the Specific Absorption Rate (SAR), which describes the amount of energy that is potentially absorbed by a participant during MRI scanning (measured in Watts per kilogram, W/kg). To reduce the possibility of adverse heating effects, a minimum weight limit of 50 kg was implemented during the design phase of the studies (guided by specialist MR Physics expertise in Newcastle upon Tyne and Sheffield), underpinning the minimum weight requirements specified by the study inclusion criteria.

MRI scanner operation is further governed by international safety regulations (the International Electrotechnical Commission, IEC) documented in IEC 60601-2-33 (2010), which outlines acceptable SAR limits over the whole body, as well as localised areas (such as the torso), during MRI scanning. This is particularly relevant for the ^{19}F/^{1}H birdcage coil, since its field of view (FOV) encompasses the entire torso (unlike the ^{19}F surface coil). Both the LIFT study and VQ MRI study were designed to ensure that both whole body and local

torso SARs delivered to participants were well below the IEC 60601-2-33 'first controlled operating mode' limits for energy transfer used in clinical MRI scans. For the LIFT study, this was achieved by restricting MRI acquisitions to no more than one minute, with a duration of at least five minutes between acquisitions, such that the average SAR over a 6-minute period was maintained within acceptable limits. For the VQ MRI study (which employed different scan protocols to the LIFT study) this was achieved by restricting continuous operation of the coil to a maximum of 90 s in a 6-minute period, with a duration of 10 minutes between respective acquisitions.

Safety testing was performed by Prof Pete Thelwall and Dr Mary Neal using phantom models prior to implementation of scan protocols in human participants.

2.5.4   Choice of inhaled gas agent

A 79% PFP / 21% O_2 gas mixture (BOC Special Products, Guildford, UK) was used for all ^{19}F-MRI studies presented in this thesis.

The choice of inhaled gas agent stemmed largely from the favourable properties of PFP (C_3F_8); specifically, it is a chemically and physiologically inert gas which can be purchased from appropriate gas manufacturers as 'patient consumption grade', pre-mixed with 21% O_2 (i.e. avoiding the potential risk of asphyxiation relating to inhalation of pure PFP). Moreover, the high number of chemically equivalent ^{19}F nuclei – located on two -CF_3 groups – provides an acceptable source for MR image production. While a number of fluorinated-gas compounds have been utilised in ^{19}F-MR ventilation imaging (see Chapter 1, Section 1.5.4), to date the vast majority of human studies have employed 79% PFP / 21% O_2 as the inhaled contrast agent of choice. As such, there is a clear precedent for adopting PFP within the context of the LIFT study, as well as the two smaller feasibility studies outlined in this thesis.

2.5.5 Gas administration

The 79% PFP / 21% O_2 gas mixture was supplied to each of the two study sites in metallic gas cylinders (Figure 2.9A). Each cylinder contained approximately 300 L of the PFP/oxygen gas mixture. For the purpose of administering PFP to participants during experimental studies, a 25 L MR-safe Douglas bag (Figure 2.9B) was filled with the 79% PFP / 21% O_2 gas mixture immediately prior to conducting MRI scan sessions. This was performed by Dr Mary Neal in Newcastle upon Tyne and by Dr Adam Maunder in Sheffield. Typically, the 25 L Douglas bag was filled once per participant during the LungGas study, twice per participant during the LIFT study, and three to four times per participant during the VQ MRI study, reflecting the different imaging protocols explored.
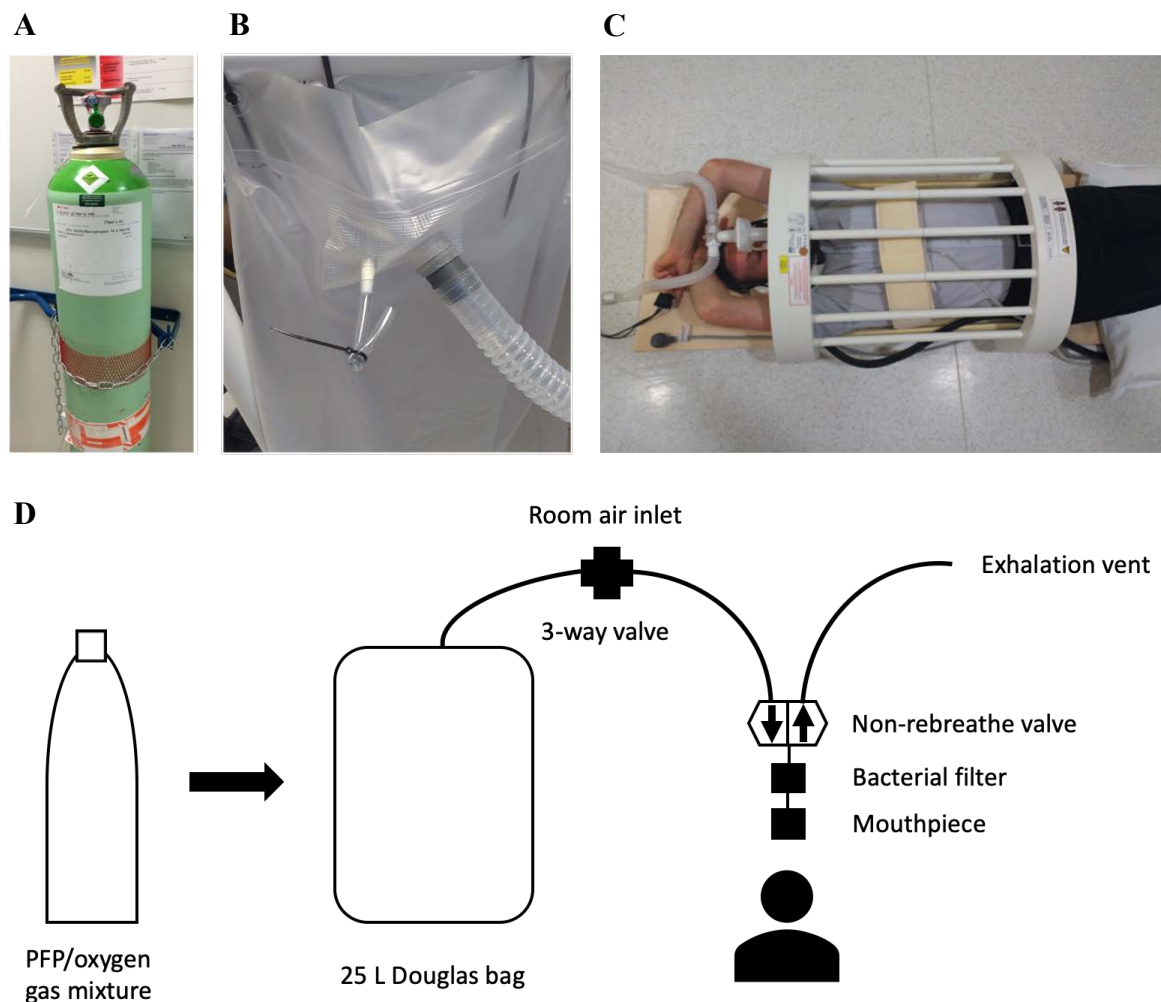
Figure 2.9: Study materials and process of gas administration. (**A**) Metallic gas cylinder. (**B**) 25 L Douglas bag. (**C**) Participant *in situ*, connected to gas tubing and mouthpiece. (**D**) Schematic representation of the gas administration set-up, illustrating the process of transferring the PFP/O_2 mixture from the metallic gas cylinder to study participants.

Each 25 L Douglas bag was connected to a 3-way valve (2500 Series, Hans Rudolph, Shawnee KS, USA) via a single 35 mm internal diameter smooth bore plastic tube (length = 30 cm), allowing the supply of gas mixture or room air to be controlled manually by a member of the study team whilst in the MRI scanner room (Figure 2.9D). 22 mm internal diameter plastic tubing (length = 40 cm) was subsequently used to deliver the inspired gas (or room air) between the 3-way valve and a separate 2-way non-rebreathe valve (1410 Series, Hans Rudolph, Shawnee KS, USA) and to direct exhaled gas away from the magnet bore (Figure 2.9C and 2.9D). Each non-rebreathe valve was connected to an antibacterial filter and single-use disposable mouthpiece. All participants wore non-magnetic nose clips during gas inhalation sessions to ensure consistency of breathing manoeuvres via the mouth throughout.

A separate supply of O_2 was available at each study site (located in the scanner control room), which could be delivered to participants using MR-compatible tubing in the event of significant desaturation and/or clinical concern. A significant desaturation (constituting an adverse event) was defined as a sustained O_2 saturation below 88% over the course of 1 minute with a good trace. All participants were provided with a handheld alarm which could be used to alert scanner radiographers if needed (for example, if they experienced any discomfort during MRI scan procedures).

For the majority of the MRI scan session, participants breathed room air freely and were only required to breathe through the study inhalation equipment at the point of performing respective gas inhalation sessions. During these times, the nose clip was applied to participants and the mouthpiece positioned and held securely in place by a member of the study team located in the MRI scanner room (me in Newcastle upon Tyne; Dr Adam Maunder in Sheffield). The gas mixture was subsequently administered to participants by manually switching the 3-way valve between the room air inlet and the gas mixture inlet. This was timed according to verbal breathing instructions provided by radiographer colleagues from within the scanner control room via MR-compatible headphones; these were worn by participants and the researcher present within the MRI scanner room, both to enable communication whilst inside the scanner bore and to protect hearing during MRI acquisitions. The specific breathing instructions provided to participants was refined during Phase 1 of the LIFT study, such that a standardised approach to the timing of PFP/O_2 gas administration was established prior to commencing Phase 2 of the study (see Chapter 3,

Section 3.3.3); this approach to gas administration was also adopted for the LungGas study, but differed for the VQ MRI study (see Chapter 7, Section 7.2.2).

2.5.6   GBCA administration

Intravenous Gadobutrol (Gadovist 1.0 mmol/mL, Bayer Shering Pharma) was administered to study participants attending the VQ MRI and LungGas studies via an 18-gauge cannula sited in a central antecubital fossa vein of the right arm. The contrast agent was delivered by the study radiographer using a power injector (MEDRAD Spectris Solaris EP, Bayer Ltd., Reading, UK) at a rate of no more than 5 ml/s and a dose of no greater than 0.2 mmol/kg, in accordance with product manufacturer guidelines (Bayer, 2020). Each GBCA bolus was followed immediately by a 20 mL saline flush (0.9% NaCl) at the same injection rate. Administration was performed in line with local NHS Trust guidelines, with dose and delivery equipment checked by two members of the research team prior to administration. Gadobutrol was procured from the pharmacy department at NUTH and subsequently delivered to the NMRC for use in the study.

Specific procedures relating to contrast agent administration during the VQ MRI and LungGas studies are outlined in Chapters 6 and 7, respectively.

2.5.7   Spirometry

Pulmonary function tests were performed using a Vyntus Spiro spirometer (CareFusion, Basingstoke, UK) at the NMRC (Newcastle University) and a PFT Pro spirometer (CareFusion, Basingstoke, UK) at the Academic Unit of Radiology (University of Sheffield). Each spirometer was interfaced to a pre-configured computer running the same pulmonary function test software (SentrySuite, Version 2.19, Carefusion, Basingstoke, UK).

Spirometry assessments were conducted in an upright seated position in accordance with established American Thoracic Society (ATS)/European Respiratory Society (ERS) guidelines (Miller *et al.*, 2005). All breathing manoeuvres were performed using a Jaeger pneumotachometer (Carefusion, Basingstoke, UK) in combination with a single-use disposable bacterial filter and mouthpiece (MicroGard II, Carefusion, Basingstoke, UK). Participants wore a nose clip during all spirometric breathing manoeuvres. Prior to

performing spirometry, each participant was coached in the correct technique by a suitably qualified member of the study team (me in Newcastle upon Tyne; Matt Austin, Respiratory Physiologist, in Sheffield) and testing was continued until at least three acceptable manoeuvres (determined by the relevant member of the study team) had been performed.

Conventional spirometric measurements – namely, FEV_1, FVC and FEV_1/FVC – were acquired by recording the highest achieved value for each parameter from a minimum of three technically acceptable trials (where the highest FEV_1 and FVC were not necessarily obtained from the same trial). Corresponding predicted values for FEV_1 and FVC were calculated automatically by the spirometry software using GLI-2012 reference equations (derived from the Global Lung Function Initiative study by Quanjer *et al.* (2012)), based on relevant participant characteristics; namely, participant age, weight, sex, and ethnicity.

For patients with asthma and COPD attending Phase 3 of the LIFT study, BD response was calculated according to BTS/SIGN guidelines (BTS, 2019) (defined as an increase in FEV_1 of $\geq 12\%$ and ≥ 200 ml as an absolute value compared to pre-BD measurements) and ERS/ATS guidelines (Pellegrino *et al.*, 2005) (defined as an increase in **either** FEV_1 **or** FVC of $\geq 12\%$ and ≥ 200 ml as an absolute value compared to pre-BD measurements).

To ensure consistency of recorded values, spirometry equipment was calibrated on the morning of all planned study visits (performed by me in Newcastle upon Tyne, and Matt Austin in Sheffield) using a manual 3 L syringe pump (Carefusion, Basingstoke, UK) at varying flow rates (e.g. slow, medium and fast).

2.5.8 Nebulised salbutamol administration

Patients with asthma and patients with COPD attending either Phase 1 or Phase 3 of the LIFT study were administered 2.5 mg (equivalent to 2.5 ml) nebulised salbutamol during the course of the MRI scan session (study visit 2). This was administered by me in Newcastle upon Tyne and Matt Austin in Sheffield, using an InnoSpire Deluxe compressor nebuliser in conjunction with a single-use disposable SideStream chamber and mouthpiece (Philips Healthcare, Best, The Netherlands). All patients were instructed to sit in an upright position and to breathe through the mouthpiece until the nebule was complete (typically after a

duration of approximately 10 minutes), supervised by the relevant researcher at respective study sites.

Salbutamol nebules were procured from local pharmacy departments at NUTH and STH, and were subsequently delivered to respective research centres for use in the study. Salbutamol was prescribed by a clinically qualified member of the study team (me in Newcastle upon Tyne; Dr Rod Lawson, Consultant Respiratory Physician, in Sheffield) using a written drug prescription form, which was subsequently filed in the patient's medical notes.

2.5.9 Pulse oximetry

Participant heart rate and oxygen saturation readings were monitored continuously throughout all MRI scan sessions using an MR-compatible pulse oximeter (Nonin 7500FO, Nonin Medical Inc., Plymouth, MA). The sensor was positioned securely on each volunteer's finger prior to entering the MRI scanner bore. The same equipment was used to perform pulse oximetry screening assessments for potential study participants.

2.5.10 Anthropometry

Height and weight measurements were performed for each participant as part of the initial screening procedures and, for patients attending the LIFT study, prior to repeating spirometry tests during study visit 2. Height measurements (in metres, m) were documented to two decimal places; weight measurements (in kilograms, kg) were documented to one decimal place. Participant BMI was calculated automatically to one decimal place upon entering height and weight measurements into the spirometry software (SentrySuite, Version 2.19, Carefusion, Basingstoke, UK) by applying the following equation:

$$BMI = \frac{Weight\ (kg)}{Height\ (m)^2}$$

2.5.11 Pregnancy testing

All female participants of childbearing age were asked to perform a pregnancy test as part of study screening procedures. For the LIFT study, this was performed at the time of the first

study visit for healthy volunteers, and at the time of the second study visit for patients with respiratory disease. Participants were provided with a urine pregnancy test kit and specimen pot and asked to carry out the test on their own. The result of the pregnancy test was subsequently confirmed by a member of the study team before appropriate disposal of the test kit and urine sample.

2.5.12 Clinical examination

All participants underwent a brief cardio-respiratory examination (performed by me in Newcastle upon Tyne, and by Dr Rod Lawson or a member of the clinical radiology team in Sheffield) as part of the study screening procedures. This involved auscultation of participants' heart and lungs to confirm that there was no evidence of acute abnormality and/or signs that were inconsistent with the diagnosis (in the case of patients with asthma and COPD).

Chapter 3.
Development of LIFT study methodology

3.1 Introduction

The previous chapter introduced the structure and design of the LIFT study (Chapter 2, Section 2.2), in addition to providing a summary of the materials and methods used to conduct experimental studies in human participants. In this chapter, key aspects of initial development work conducted within Phase 1 of the LIFT study are presented, leading to the establishment of methods suitable for performing static ^{19}F-MR ventilation imaging in healthy volunteers and patients with respiratory disease.

The primary purpose of Phase 1 of the LIFT study was to develop and refine scan protocols and procedures, rather than the testing of specific study hypotheses. As such, the following discussion represents a descriptive analysis of the principal findings arising from the optimisation process which directly informed progression to Phase 2 of the study. A more detailed analysis of the study hypotheses pertaining to Phase 2 and Phase 3 of the LIFT study is presented in Chapter 4 and Chapter 5, respectively.

3.2 Development of ^{19}F-MRI scan protocols

MRI scan protocols were developed by, and tested in close collaboration with, MR Physicists based in Newcastle upon Tyne (Prof Pete Thelwall and Dr Mary Neal) and Sheffield (Prof Jim Wild and Dr Adam Maunder), building upon previous work conducted by Mary Neal during her PhD studies (Neal, 2017). Central to this phase was the translation of optimised scan protocols derived from simulated models to human participants, with particular application to the ^{19}F birdcage coil described in Chapter 2 (Section 2.5.2).

3.2.1 Choice of scan parameters

In common with all MR imaging techniques, the scan acquisition parameters adopted during ^{19}F-MRI are interdependent, such that alteration of one parameter can directly influence the performance of other parameters. For instance, the minimum scan repetition time (TR) is

dependent on the scan echo time (TE), which in turn is determined by the selected acquisition bandwidth (BW), matrix size (or image resolution), flip angle (°), and other scan parameters. Table 3.1 provides a brief description of the principal scan parameters employed in this thesis.

Parameter	Description
Longitudinal relaxation time (T_1)	Time taken for nuclei to return to equilibrium following an RF excitation pulse
Transverse relaxation time (T_2)	Time taken for nuclei to de-phase following an RF excitation pulse
Reduced transverse relaxation time (T_2^*)	Rate of signal decay (de-phasing of nuclei) following an RF excitation pulse, influenced by the *in-vivo* magnetic environment
Echo time (TE)	Time interval between applying an RF excitation pulse and acquiring the peak signal (middle of acquisition period)
Repetition time (TR)	Time interval between applying one RF excitation pulse and the next excitation pulse
Flip angle (°)	Amount of rotation from the B_0 direction that is induced by applying an RF excitation pulse at the Larmor frequency
Bandwidth (BW)	Frequency range sampled when the signal is acquired following an RF excitation pulse
Field of view (FOV)	Dimensions of image (i.e. body region) over which MRI data are acquired
Matrix size (resolution)	Number of data points acquired over the FOV
Sampling frequency	Rate at which MRI data are recorded during the data acquisition period
Number of samples	Number of datapoints recorded during the data acquisition period
Acquisition time	Duration of the MRI data acquisition period

Table 3.1: Description of the principal scan parameters employed in this thesis.

The inherent relationship that exists between these scan parameters ultimately impacts the efficiency of MRI acquisitions, including the resultant SNR that can be achieved for a given acquisition sequence. Based on this understanding, research led by Dr Mary Neal (Neal *et al.*, 2019) applied computer simulations to derive optimised ^{19}F-MRI acquisition parameters for a modified SPGR sequence, in preparation for performing human ^{19}F-MR ventilation imaging studies. SPGR sequences are well suited to human lung imaging, since they permit the use of

rapid repetition times that are possible when T_1 is short, enabling full 3D acquisitions within seconds. Moreover, SAR is generally lower for gradient echo scans compared to other MRI sequences, since fewer RF excitation pulses are required during image acquisition.

Twenty healthy participants were subsequently recruited to the Newcastle upon Tyne study site to assess the ability to apply these critical scan parameters *in vivo*, taking into consideration the restrictions imposed by scanner SAR limits outlined in Chapter 2 (Section 2.5.3). Additionally, in a small number of these participants ($n = 7$) the optimised SPGR sequence was compared with an alternative sequence previously utilised by colleagues at the University of Sheffield (known as Steady State Free Procession, or SSFP) to determine the most appropriate scan protocol to implement in subsequent phases of the LIFT study. The developmental nature of Phase 1 of the LIFT study permitted significant flexibility in the type of acquisition performed during each of the five PFP/O_2 gas inhalation sessions. It was therefore possible to test more than one scan protocol and/or breathing manoeuvre per participant. Initial testing in three healthy volunteers revealed negligible alteration of simulated parameters was necessary in order to perform *in vivo* ^{19}F-MRI acquisitions using the ^{19}F birdcage coil (see Table 3.2).

Parameter	Simulated SPGR	*In vivo* SPGR
TE (ms)	1.7	1.7
TR (ms)	7.5	7.5
Flip angle (°)	50	45
FOV (mm^3)	$400 \times 400 \times 250$	$400 \times (310\text{-}360) \times 250$
Resolution (mm^3)	$10 \times 10 \times 10$	$10 \times 10 \times 10$
BW (Hz/pixel)	500	500

Table 3.2: Comparison of the optimised simulated SPGR parameters and their application *in vivo*. Negligible changes to the FOV and requested flip angle were required to conduct human ^{19}F-MRI acquisitions.

Figure 3.1A illustrates a full 3D ^{19}F-MRI dataset acquired in one healthy participant using the optimised SPGR scan protocol. Images were acquired during a 13.4 s breath-hold, performed at maximal inspiration following three deep breaths of the 79% PFP / 21% O_2 gas mixture (see Section 3.3 for a description of the specific breathing strategy employed). Figure 3.1B shows a comparable 3D ^{19}F-MRI dataset acquired in the same participant using the

alternative SSFP scan protocol with identical resolution and a similar breath-hold duration (14 s).
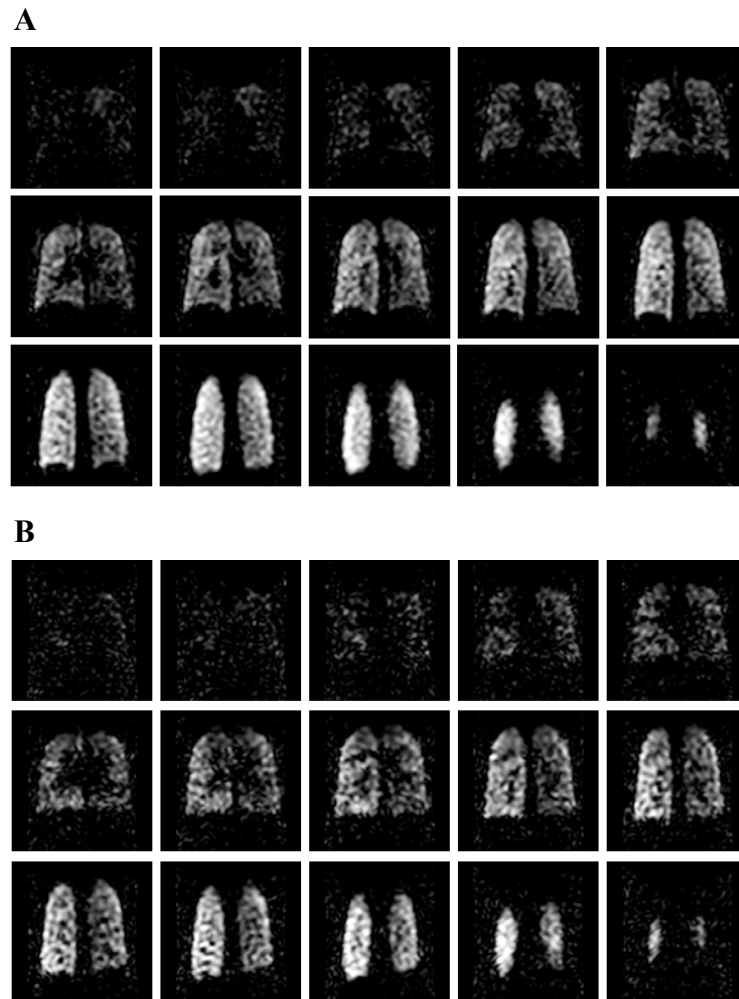
Figure 3.1: Comparison of ^{19}F-MRI datasets acquired in one healthy volunteer using **(A)** the optimised SPGR sequence and **(B)** an equivalent SSFP sequence.

Both images are characterised by the presence of background noise, particularly evident towards the anterior lung slices (top rows) where there is a general reduction in PFP signal. This signal 'drop-off' was thought to relate to a coil fault identified during the initial development phase of the LIFT study, which prompted a return of the coil to the manufacturer for repair. Nonetheless, differences in image quality can still be appreciated between the two acquisitions, with the SPGR sequence (Figure 3.1A) revealing greater signal homogeneity and delineation of lung boundaries compared to the SSFP sequence (Figure 3.1B). This finding was replicated in the remaining participants, most likely reflecting the requirement to use a sub-optimal flip angle during SSFP imaging at 3.0 T in order to comply with scan SAR limits (Maunder *et al.*, 2019). As a consequence, the optimised SPGR

sequence was considered most appropriate for adoption in subsequent phases of the LIFT study.

Figure 3.2 illustrates a full 3D dataset in a different participant, acquired using the optimised SPGR sequence following return of the birdcage coil from the manufacturer. A global improvement in image quality can be observed compared to Figure 3.1A, with homogeneous gas distribution visualised throughout the lung fields.
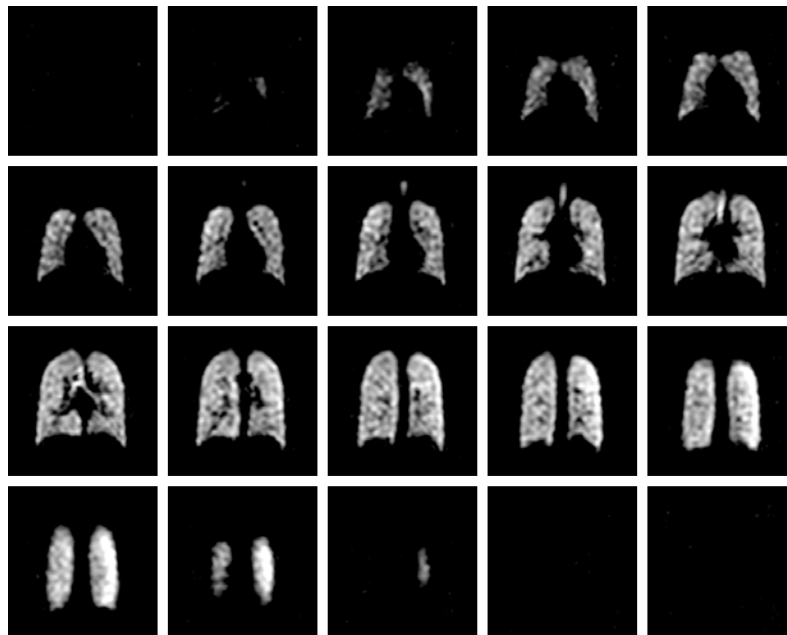
Figure 3.2: Example ^{19}F-MR ventilation images (coronal slices) acquired in one healthy volunteer using the optimised SPGR sequence, showing homogeneous gas distribution throughout the lung fields. Acquisition time = 13.4 s.

Importantly, a number of ^{19}F-MRI scans performed towards the start of the developmental phase were impacted by significant blurring effects (see Figure 3.3), occurring in nine participants in total (seven healthy volunteers; one patient with asthma; and one patient with COPD). Subsequent testing conducted in a small number of healthy participants ($n = 3$) confirmed that this related primarily to a specific scan setting applied during the initial preparation of ^{19}F-MRI acquisitions ('prep steps'). Notably, when these preparatory steps were set to run automatically ('auto'), a marked improvement in image quality was observed compared to when these preparatory steps were set to 'skip' (see Figure 3.4).
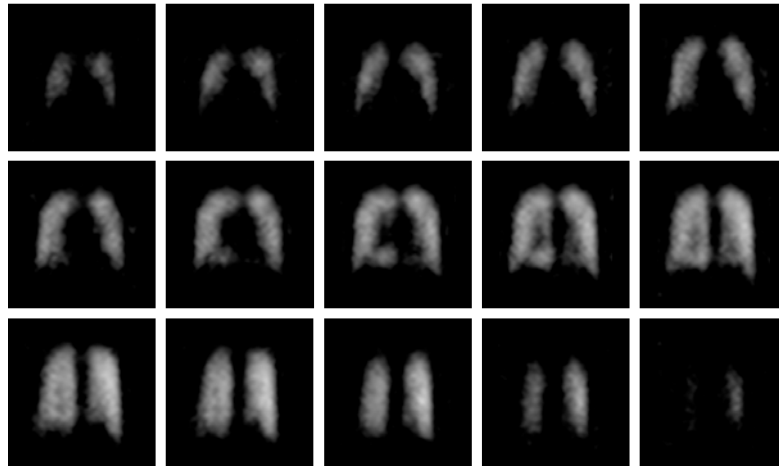
Figure 3.3: Example ^{19}F-MR ventilation images (coronal slices) from an early study participant, demonstrating marked blurring effects with indistinct lung borders.
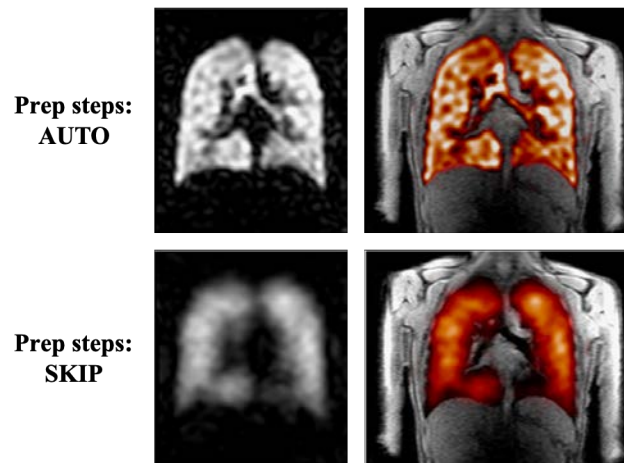
Figure 3.4: Comparison of ^{19}F-MR ventilation images (single coronal slices) acquired in one healthy participant with preparatory steps set to 'auto' (top row) and 'skip' (bottom row). Combined ^{1}H (greyscale) and ^{19}F (coloured) images are presented in the upper and lower right hand image panes. Both sets of images were acquired using the same inhalation scheme and identical scan parameters, such that the only difference related to the use of preparatory step settings.

Input from the scanner manufacturer (Dr Matthew Clemence, Senior Clinical Scientist, Philips Healthcare) suggested that the failure to include these initial preparatory steps within the acquisition sequence (i.e. set to 'skip') was likely to result in misconfiguration of critical scanner calibrations necessary for performing ^{19}F-MRI (but not conventional ^{1}H imaging). Given the substantial impact on image quality, all subsequent scans were performed with this parameter set to 'auto'. In parallel with this finding, it was recognised that the scanner's automatic calibration steps were susceptible to incorrect calculation of PFP's -CF$_3$ resonant frequency, leading to a further reduction in the quality of ^{19}F-MR image acquisitions

(manifest as a lower ^{19}F flip angle than requested). Consequently, the first gas inhalation session was preserved for manual measurement of PFP's resonant frequency (rather than acquisition of ventilation images), permitting correct application within the remaining ^{19}F-MRI acquisitions. This was achieved by performing a free-induction decay (FID) spectroscopy scan, whereby a non-localised (i.e. whole-lungs) ^{19}F-MRI measurement (containing no imaging information) is collected and Fourier transformed by the scanner to produce a ^{19}F spectrum. PFP's -CF$_3$ resonant frequency was manually measured from this spectrum by Dr Mary Neal. ^{19}F-MR images were subsequently acquired using this measured resonant frequency in place of the scanners automatically (and incorrectly) calculated ^{19}F resonant frequency.

3.2.2 Number of signal averages

The SNR and resulting image quality may be further improved by increasing the breath-hold duration within which ^{19}F-MR images are acquired, thereby increasing the number of signal averages (NSA) that can be performed during a given scan. As indicated in Chapter 1 (Section 1.5.2), the NSA represents the number of times a scan sequence is repeated within an individual MRI acquisition. Increasing the NSA has the effect of amplifying the SNR by combining ('averaging') the signal generated with each successive acquisition, but with the result of extending the total acquisition period. For the SPGR sequence adopted in this study, a single ^{19}F-MRI acquisition (i.e. NSA = 1) lasted ~4.5 s, determined by the combination of parameter settings outlined in Table 3.1. Several scans performed during Phase 1 of the LIFT study (including those used to evaluate the use of compressed sensing, outlined in Section 3.2.3 below) were acquired with NSA = 4 (i.e. four repetitions, corresponding to an 18 s breath-hold duration). However, the potential gains in SNR arising from increasing the NSA must be balanced by the need to maintain breathing strategies that can be achieved by all participants; this is especially relevant for patients with respiratory disease, who may not be able to tolerate prolonged breath-hold manoeuvres. Consequently, a 13.5 s acquisition (where NSA = 3) was felt to represent an acceptable trade-off by providing adequate SNR within an achievable breath-hold duration (i.e. < 15 s), comparable with previously published studies (Kirby *et al.*, 2012a; Halaweish *et al.*, 2013a; Couch *et al.*, 2013).

3.2.3 Compressed sensing

Compressed sensing (CS) is a well-established approach in MR imaging (Hollingsworth, 2015) which offers further scope to reduce breath-hold duration by limiting the amount of raw data acquired during a given scan, enabling potential acceleration of MRI acquisition times. While this method has shown utility in HP-MRI studies (Ajraoui *et al.*, 2010; Chan *et al.*, 2017), the application of CS to ^{19}F-MR ventilation imaging has not previously been evaluated. Consequently, an important aspect of Phase 1 of the LIFT study was to explore the potential use of CS in a small number of healthy volunteers ($n = 11$).

Three different acceleration (or under-sampling) schemes were developed by Dr Kieren Hollingsworth (Reader in MR Physics, Newcastle University), allowing a comparison of retrospectively applied CS ($n = 8$) and prospectively applied CS ($n = 3$) with corresponding fully sampled ^{19}F-MRI acquisitions.

Figure 3.5 shows equivalent coronal image slices from a ^{19}F-MRI dataset acquired in one healthy volunteer using the fully sampled (i.e. optimised SPGR) sequence (top image), alongside retrospectively applied CS employing three different acceleration schemes (1.8×, 2.4× and 3.0×, respectively). Each of the under-sampling acceleration schemes (represented in the left-hand column) demonstrated comparable image quality to the fully sampled acquisition (NSA = 4; breath-hold duration = 18 s). However, as expected, the 1.8× acceleration scheme showed the most similarity, reflected in the small root mean square error (RMSE), which indicates the magnitude of differences between fully sampled and 1.8× scans; this revealed greater variation between fully sampled and under-sampled acquisitions as the acceleration factor increased, confirmed by amplifying the difference images 5-fold (see right-hand column).

Similar results were observed in the remaining healthy participants (see Figure 3.6), such that the 1.8× under-sampling scheme was considered most appropriate for the purpose of applying CS to subsequent prospective ^{19}F-MRI acquisitions.
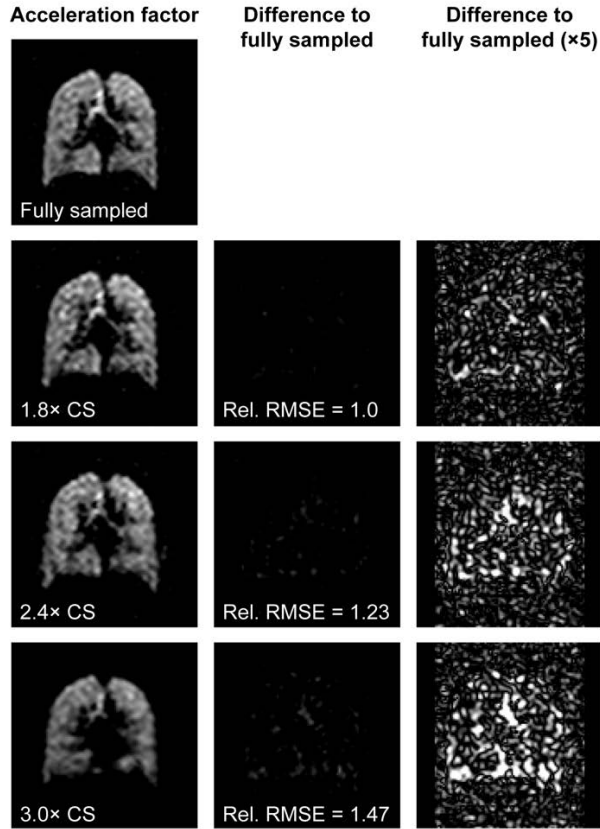
Figure 3.5: ^{19}F-MR ventilation images (single coronal slices), showing a fully sampled dataset alongside under-sampled reconstructions of the same dataset (under-sampling ratios of 1.8×, 2.4×, and 3.0×). The difference images represent the change in image content between fully sampled and under-sampled images.
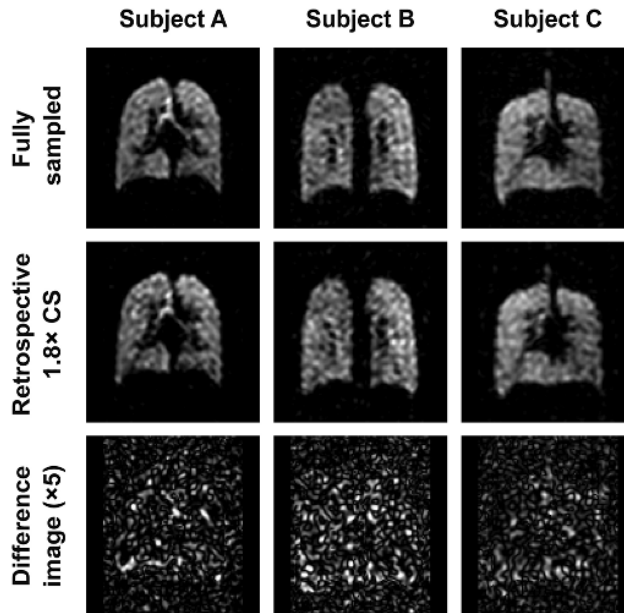
Figure 3.6: Example ^{19}F-MR ventilation images (single coronal slices) acquired in three healthy volunteers, revealing minimal differences between fully sampled and 1.8× retrospectively under-sampled datasets.

In agreement with the findings presented in Figures 3.5 and 3.6, prospective application of the 1.8× acceleration scheme in three healthy participants (NSA = 4; breath-hold duration = 7.5 s) revealed minimal variation in image quality compared to corresponding fully sampled acquisitions (Figure 3.7). Subtraction (i.e. difference) images were not generated for these prospective data, since fully sampled and under-sampled ^{19}F-MRI scans were acquired during separate breath-holds, which may have produced slight differences in achieved lung volume. Nonetheless, a comparison of SNR values (calculated by Dr Mary Neal, based on methods outlined in Chapter 4, Section 4.2.3) revealed similar results for 1.8× under-sampled (mean = 13.4, standard deviation (SD) = 4.0) and fully sampled (mean = 14.1, SD = 5.0) datasets in these participants.
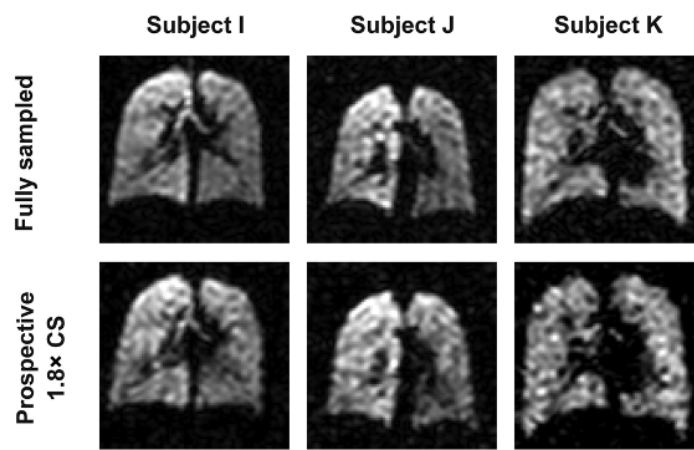
Figure 3.7: Comparison of fully sampled (top row) and 1.8× prospectively under-sampled (bottom row) ^{19}F-MRI datasets in three healthy volunteers.

Given the overriding goal of the LIFT study – to demonstrate the reproducibility and potential clinical applicability of ^{19}F-MR ventilation imaging across different study sites – use of a conventional fully sampled acquisition protocol was ultimately considered most appropriate for adoption in subsequent phases of the study. Nevertheless, these findings support the ability to apply CS to ^{19}F-MRI of inhaled PFP with minimal impact on image quality, offering scope to reduce scan times (for example, from 13.5 s to 7.5 s) that could benefit future studies in patients with respiratory disease.

The use of CS is revisited in Chapter 6, where its capacity to diminish ^{19}F-MRI acquisition times is exploited in determining the ability to perform dynamic ventilation imaging with inhaled PFP.

3.3 Development of gas inhalation scheme

Effective ^{19}F-MR ventilation imaging is dependent not only on the implementation of appropriate scan acquisition protocols but also the adoption of inhalation schemes and breathing manoeuvres that can be readily applied to patient cohorts. This relates to the duration of breath-hold that can be achieved, as well as the depth of inhalation and number of respiratory cycles performed prior to ^{19}F-MRI acquisition.

Several different approaches to PFP gas inhalation have been reported in the literature, ranging from a single, fixed volume (1 L) breath-hold (Couch *et al.*, 2013) to two or more continuous breaths punctuated by breath-hold acquisitions (e.g. Halaweish *et al.*, 2013a; Gutberlet *et al.*, 2018; Goralski *et al.*, 2020). However, given the relative infancy of pulmonary ^{19}F-MRI, there is currently no consensus regarding the most appropriate method for performing PFP ventilation imaging in humans. The techniques described in this chapter were largely influenced by existing HP-MRI literature concerning static ventilation imaging. Alternative approaches to dynamic ventilation imaging are explored in Chapter 6.

3.3.1 Number of wash-in breaths

Previous work conducted by Dr Mary Neal (Neal, 2017) highlighted the impact of performing successive breaths of a 79% PFP / 21% O_2 gas mixture on the SNR of ^{19}F-MR ventilation images in twelve healthy volunteers, using the ^{19}F surface coil introduced in Chapter 2 (Section 2.5.2). Notably, an increase in mean SNR was observed after one, two, and three deep breaths of gas respectively, but with diminishing returns in SNR following each successive breath (Figure 3.8).
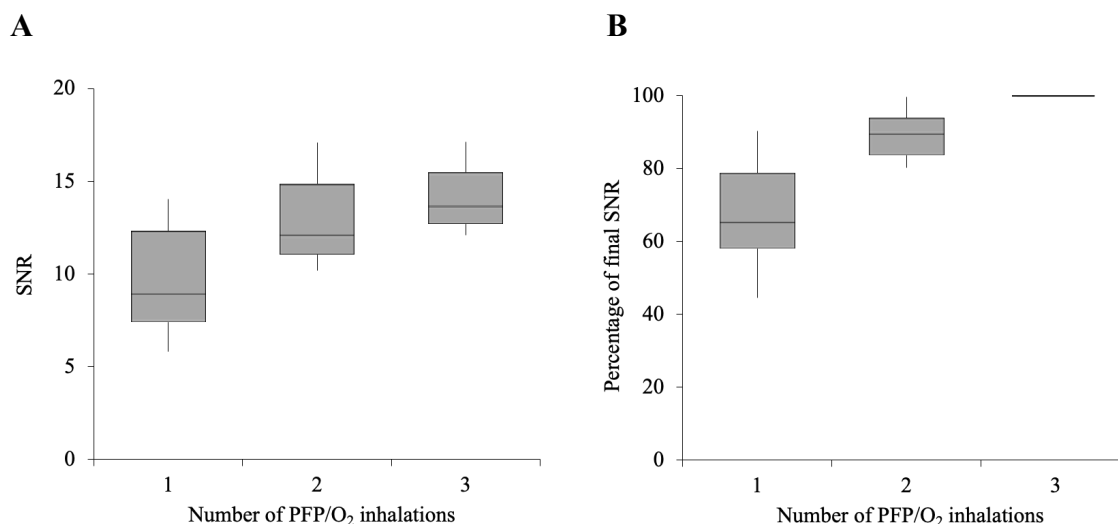
Figure 3.8: Illustration of **(A)** the absolute SNR, and **(B)** the percentage of final SNR achieved following three successive breaths of the PFP/O_2 gas mixture in twelve healthy volunteers. Box plots demonstrate the mean SNR (horizontal line) and interquartile range, with error bars indicating the maximum and minimum SNR values obtained. Adapted from Neal (2017) with permission.

This work was extended during Phase 1 of the LIFT study to determine the optimum number and depth of gas inhalations required to perform static ^{19}F-MR ventilation imaging using the ^{19}F/^{1}H elliptical birdcage coil presented in Chapter 2 (Section 2.5.2).

Figure 3.9 depicts unlocalised spectroscopy scans acquired in two healthy participants, showing the relative change in PFP signal intensity following successive wash-in breaths of the 79% PFP / 21% O_2 gas mixture. Participants were instructed to perform deep breaths (i.e. approximating TLC) throughout the acquisition sequence, which ran continuously over a 60 s period. Spectroscopy scans were acquired using a FID sequence (TR = 200 ms, flip angle = 90°, BW = 8000 Hz, number of datapoints = 256), where the amplitude of PFP's -CF$_3$ signal was determined by measuring the area under the peak of the ^{19}F spectra, using in-house software developed in Matlab (Mathworks Inc., Natick MA, USA) by Prof Pete Thelwall. The -CF$_3$ peak area is directly proportional to the amount of PFP present within the volume of the RF coil. The generated plots show the resultant change in PFP signal amplitude with time (i.e. following successive breaths of the gas mixture).
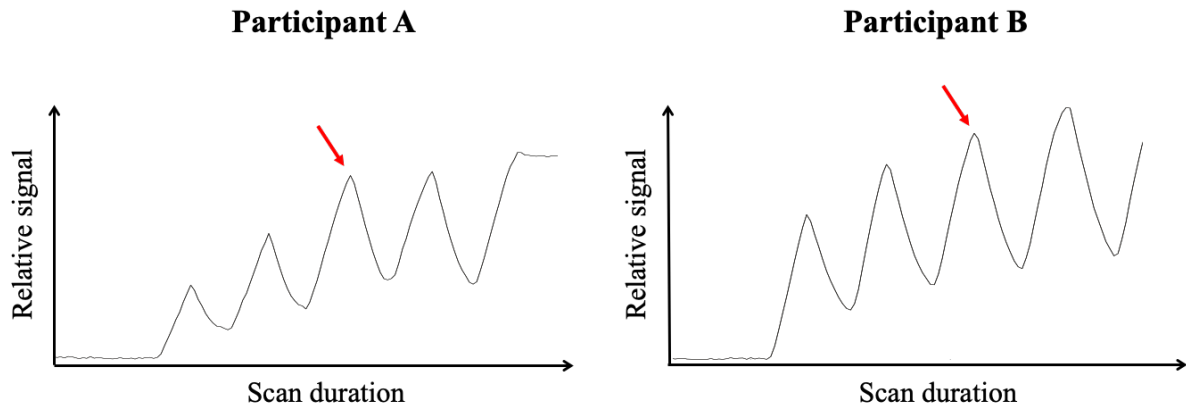
Figure 3.9: Unlocalised spectroscopy scans in two participants, showing relative PFP signal following successive deep wash-in breaths of the 79% PFP / 21% O_2 gas mixture. Arrows (red) indicate the timing of the third gas inhalation within the acquisition sequence.

As with the SNR values obtained by Neal (2017), the relative PFP signal intensity in these two participants began to plateau after approximately three deep breaths of gas (indicated by red arrows), such that further gains in signal were marginal beyond this point (though some increase in signal can still be appreciated, particularly for Participant B). This global effect on lung signal intensity corresponded to a visually evident change in regional gas distribution in response to repeated breaths (Figure 3.10). Specifically, when ^{19}F-MRI scans were acquired after just one deep gas inhalation, images revealed marked degradation and ventilation heterogeneity with weak or absent signal representing regions of poor gas uptake (Figure 3.10A). Conversely, when images were acquired after three deep breaths of the gas mixture, greater homogeneity of gas distribution was observed, reflecting the pattern of ventilation expected in healthy volunteers (Figure 3.10C).
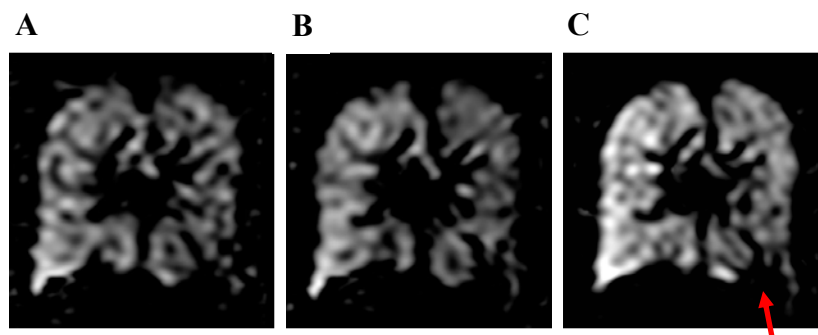
Figure 3.10: ^{19}F-MR images (represented by single coronal slices) acquired in one healthy volunteer, showing PFP gas distribution after **(A)** one, **(B)** two, and **(C)** three deep breaths of the 79% PFP / 21% O_2 gas mixture. Increased homogeneity of gas distribution was observed following each successive breath. The red arrow in **(C)** indicates a region of persisting signal deficit; this stemmed from an intrinsic fault with the birdcage coil, prompting a return to the manufacturer for repair.

Of note, a number of ^{19}F-MRI scans acquired at Newcastle University during the early stages of development revealed an apparent 'fixed' ventilation defect to the base of the left lung (illustrated in Figure 3.10C). Following discussion with the coil manufacturer, it was determined that this related to an intrinsic fault associated with the ^{19}F/^{1}H birdcage coil; subsequent testing by specialist MR coil engineers in Germany confirmed the presence of a loose solder joint which, once repaired, resolved this issue.

Further evaluation in a small number of healthy volunteers ($n = 4$) revealed that the difference in ^{19}F-MR image quality between two and three deep wash-in breaths was less apparent, although a degree of ventilation heterogeneity could often still be appreciated towards the lung peripheries in particular (see Figure 3.11). Increasing the number of wash-in breaths beyond three deep gas inhalations did not substantially alter the appearance of ^{19}F-MR ventilation images in healthy volunteers. As such, an inhalation scheme comprising three deep breaths of the 79% PFP / 21 % O_2 gas mixture was considered most appropriate to provide a benchmark for comparison with patient populations (see Section 3.5, below).
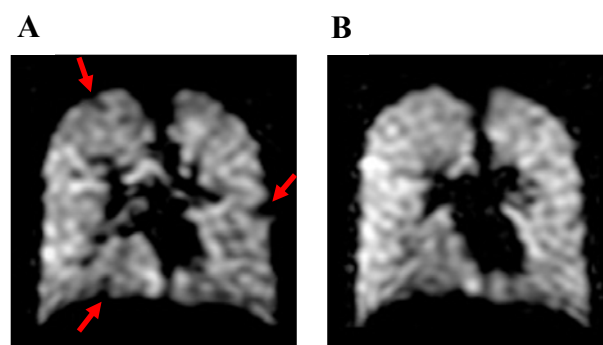
Figure 3.11: Example ^{19}F-MR ventilation images (represented by single coronal slices), illustrating the difference in gas distribution following **(A)** two, and **(B)** three deep wash-in breaths of the 79% PFP / 21% O_2 gas mixture in one healthy volunteer. Apparent ventilation defects (illustrated by red arrows) are present in **(A)** but not in **(B)**.

3.3.2   Depth of inhalation

The depth of gas inhalation and subsequent breath-hold performed were found to have a substantial impact on the quality of ^{19}F-MR images acquired and appear fundamental to ensuring the efficacy of the adopted technique. Figure 3.12 illustrates the effect of acquiring breath-hold images at different lung volumes in one healthy volunteer; namely, a breath-hold following maximal inspiration (i.e. at TLC) and a breath-hold following a relaxed inspiration.

Both sets of images were acquired after performing two preceding deep wash-in breaths of gas, such that the only difference in procedure related to the depth of the final breath and subsequent breath-hold. A marked reduction in image quality was observed at the reduced level of inflation (Figure 3.12A), associated with an apparent heterogeneity of gas distribution similar to that observed with fewer wash-in breaths (see Figure 3.10, above). This likely stems from a reduction in the T_2^* of inhaled PFP at lower lung volumes (Maunder *et al.*, 2021), giving rise to an increasing loss of PFP signal with diminishing inspiratory levels.

A

B
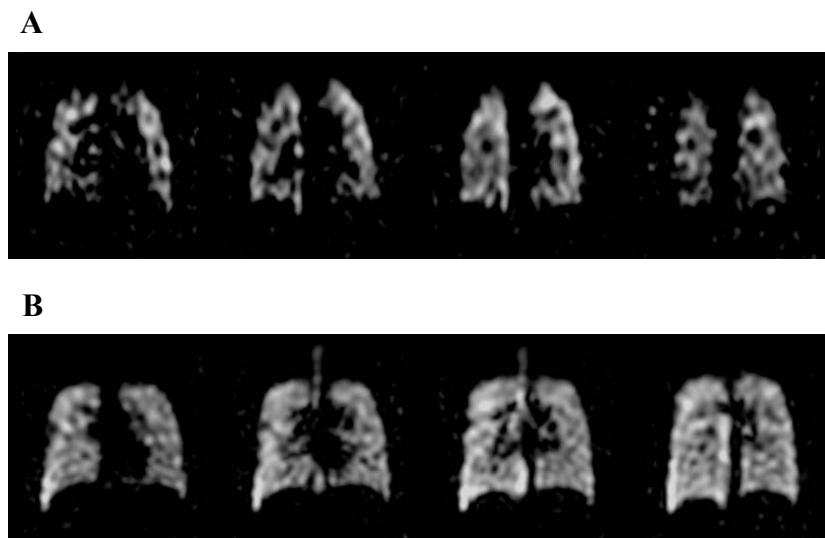
Figure 3.12: Example ^{19}F-MR ventilation images (coronal slices) acquired in one participant after three deep gas inhalations, demonstrating the change in image quality with breath-holds performed following **(A)** a relaxed inspiration, and **(B)** a deep inspiration.

Similar effects were observed when participant effort was reduced during the initial wash-in phase, even if the final gas inhalation was performed at maximal inspiration. Specifically, the participant represented in Figure 3.13 was instructed to perform sub-maximal inspiratory efforts (Figure 3.13A) or maximal inspiratory breaths (Figure 3.13B) prior to the final gas inhalation and subsequent breath-hold at TLC. The resultant impact on image quality was substantial, emphasising the need to perform maximal inspiratory manoeuvres throughout all gas inhalations, as well as the subsequent breath-hold, to ensure consistency of the approach.

A

B
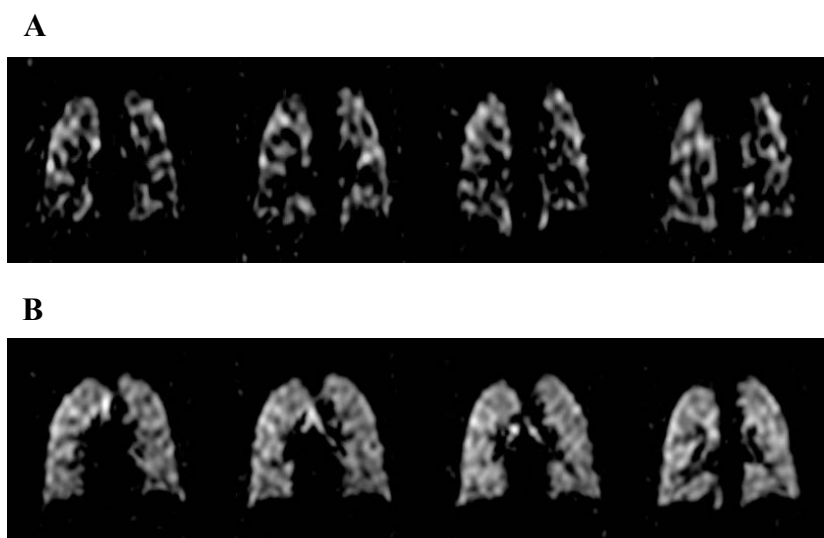
Figure 3.13: Example ^{19}F-MR ventilation images (coronal slices) acquired in one healthy volunteer, showing the impact of **(A)** poor (i.e. sub-maximal) initial inspiratory breaths, and **(B)** maximal inspiratory breaths on the quality of images acquired.

Based on these observations, all ^{19}F-MRI scans were subsequently acquired at maximal inspiration (i.e. at TLC) after instructing participants to perform three deep breaths of gas from a starting point of relaxed end-expiration (i.e. FRC). It should be noted, however, that the number and depth of breaths necessary to achieve homogeneous gas distribution in healthy volunteers was influenced by the particular equipment used in this study (see Chapter 2, Section 2.5.5); for a different set-up (e.g. gas tubing of different lengths or diameter), the number and/or depth of inhalation required may vary slightly. It is also important to recognise that the use of maximal inspiratory efforts has potential to mask the true extent of ventilation heterogeneity that exists, reducing the magnitude of acquired ventilation defect measurements (Smith *et al.*, 2018; Hughes *et al.*, 2019). On the other hand, the primary purpose of Phase 1 of the LIFT study was to establish an imaging protocol in healthy volunteers that would provide a suitable baseline for comparison with patient groups (see Section 3.5 below, and Chapter 5); this was guided by existing HP-MRI literature, where the pattern of gas distribution observed in healthy volunteers is typically homogeneous in nature (e.g. Mugler and Altes, 2013). Alternative approaches to PFP gas wash-in may be more efficient than the adopted protocol in achieving this goal – for example, asking participants to fully exhale to RV, followed by a maximal inhalation. Nonetheless, any approach must be balanced by the need to perform practicable and reproducible breathing manoeuvres in a supine position within the confines of an MRI scanner. The chosen approach was considered appropriate for these purposes.

3.3.3 Delivery of breathing instructions

The timing of breathing manoeuvres is integral to ensuring optimal gas delivery to participants prior to performing ^{19}F-MRI acquisitions. To facilitate this, study radiographers were asked to provide breathing instructions slowly and steadily (typically leaving 4–5 seconds between inspiratory and expiratory manoeuvres), allowing sufficient time for participants to fully inhale (to TLC) and exhale (to FRC). Compliance with breathing instructions was confirmed visually by radiographers situated in the scanner control room, as well as by the member of the study team controlling the gas delivery system from within the scanner room. The inhalation scheme was explained to participants and practised by them prior to entering the MRI scanner, and all volunteers were reminded to breathe as deeply as possible before each of the five gas inhalation sessions.

For simplicity, the breathing instructions relating to anatomical ^{1}H scans (performed prior to any gas inhalation) were kept identical to those relating to ^{19}F-MRI scans, providing an opportunity for participants to rehearse the inhalation scheme within the MRI scanner before breathing the 79% PFP / 21% O_2 gas mixture. This also served as a guide to establish the time required for individual participants to achieve full inspiration and return to FRC: the timing of breathing instructions could therefore be tailored accordingly (though, as indicated above, for the vast majority of participants a 4–5 s interval was appropriate). If participants were observed not to have performed the breathing manoeuvres as instructed (e.g. poor inspiratory effort, or poor adherence to radiographer commands) the ^{1}H scans were repeated until this was deemed satisfactory.

Instructions regarding the finalised gas inhalation scheme are presented in Table 3.2: this framework was used for all subsequent inhalation sessions conducted during Phase 2 and Phase 3 of the LIFT study, as well as the 'proof of concept' study outlined in Chapter 7 (the breathing instructions delivered to participants during the dynamic imaging study presented in Chapter 6 differed from the instructions provided here and are outlined further in Section 6.2.2). For all PFP/O_2 gas inhalation sessions, the first instruction to 'breathe-in' and 'breathe-out' served as a dummy inhalation, allowing the relevant member of the study team to switch the 3-way valve from the room air inlet to the gas inlet. Thus, a total of four inhalations were performed prior to starting the ^{19}F-MRI acquisition, comprising an initial dummy inhalation and three PFP/O_2 gas inhalations. All ^{19}F-MRI scans (duration = 13.4 s)

were commenced immediately after initiation of the breath-hold, such that the total breath-hold duration was less then 15 s. A visual representation of the final inhalation scheme is illustrated in Figure 3.14.

	Radiographer instructions	Participant response	Action taken by inhalation rig controller
Pre-inhalation	-	-	Apply participant mouthpiece and nose clip
			Ensure 3-way valve set to room air inlet
Inhalation 1	'Breathe-in' (wait 4–5 s)	Deep inhalation	-
	'Breathe-out' (wait 4–5 s)	Exhale	Switch 3-way valve from room air to gas mixture
Inhalation 2	'Breath-in' (wait 4–5 s)	Deep inhalation	-
	'Breath-out' (wait 4–5 s)	Exhale	-
Inhalation 3	'Breath-in' (wait 4–5 s)	Deep inhalation	-
	'Breath-out' (wait 4–5 s)	Exhale	-
Inhalation 4	'Breath-in' (wait 4–5 s)	Deep inhalation	-
^{19}F-MRI scan	'Hold your breath' (<15 s)	Maintain breath-hold at maximal inspiration	Switch 3-way valve from gas to room air
Post-inhalation	'Breathe normally'	Exhale	Remove mouthpiece and nose clip

Table 3.3: Sequence of breathing instructions provided to participants during gas inhalation sessions performed as part of the LIFT study.
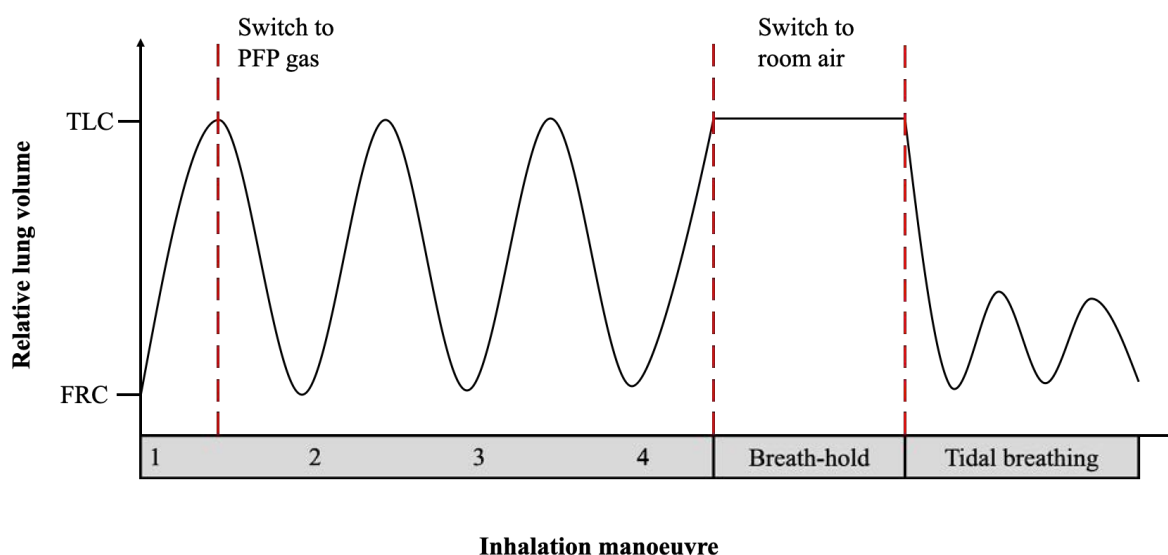
Figure 3.14: Diagrammatic representation of the gas inhalation scheme adopted during the LIFT study. Participants were instructed to perform four deep breaths (three of which involved inhalation of the 79% PFP / 21% O_2 mixture) from a starting point of relaxed end-expiration (i.e. FRC), followed by a breath-hold at TLC.

3.4 Application of scan procedures to different study sites

The majority of initial LIFT study method development work was conducted at the NMRC in partnership with Dr Mary Neal and Prof Pete Thelwall. However, MR Physics colleagues based at the University of Sheffield (Dr Adam Maunder and Prof Jim Wild) played a central role in testing the suitability of scan procedures established during Phase 1 of the study. This work was fundamental in demonstrating parity of approach between the two study sites and enabling successful progression to Phase 2 of the study (i.e. to assess the feasibility of acquiring reproducible data across different study sites).

Eleven healthy volunteers were recruited to the Sheffield study site for the purpose of confirming appropriate implementation of optimised scan protocols and inhalation procedures, as outlined in Section 3.2 and Section 3.3 of this chapter. Figure 3.15 shows an example full 3D dataset acquired using the optimised SPGR sequence in one healthy volunteer, following the inhalation scheme described above (Section 3.3.3). Homogeneous gas distribution can be visualised throughout the lung fields, demonstrating comparable image quality to scans acquired in Newcastle upon Tyne (see Figure 3.2). Similar results were obtained in the remaining participants, confirming the ability to successfully apply the established scan procedures across both study sites.

Figure 3.15: Example of a full 3D ^{19}F-MRI dataset in a healthy volunteer attending the Sheffield study site, employing the optimised SPGR sequence (acquisition time = 13.4 s).

A quantitative analysis of the healthy volunteer datasets subsequently acquired using these methods as part of Phase 2 of the LIFT study is presented in the next chapter of this thesis.

3.5   Application of scan procedures to patients with respiratory disease

A central goal of the LIFT study design was to determine the ability of ^{19}F-MRI of inhaled PFP to distinguish ventilation properties between healthy volunteers and patients with respiratory disease; namely, asthma and COPD. As such, an important consideration for the initial phase of the study was to confirm the suitability of applying scan procedures developed in healthy volunteers to a small number of patients, in preparation for performing Phase 3 of the study. Two patients with asthma and two patients with COPD were subsequently recruited to the Newcastle upon Tyne study site for this purpose.

As previously indicated (Section 3.2.1), ^{19}F-MRI scans performed in two of these patients (one patient with asthma and one patient with COPD) were adversely impacted by incorrect application of ^{19}F-MRI preparatory scan settings, resulting in suboptimal image acquisitions. However, ventilation images of acceptable quality were acquired in the remaining two patients (where preparatory steps were set to 'auto'). Figure 3.16 shows a comparison of ^{19}F-MR ventilation images (represented by single coronal slices) acquired in these two patients, alongside images acquired in one healthy participant. Ventilation images (coloured) are overlaid on corresponding ^{1}H-MRI acquisitions (greyscale), enabling a direct visual comparison of the volume of lung that is ventilated by the PFP/O_2 gas mixture. Homogeneous gas distribution can be visualised throughout the lung fields of the healthy volunteer (Figure 3.16A). In contrast, both the patient with asthma (Figure 3.16B) and the patient with COPD (Figure 3.16C) demonstrate heterogeneous gas distribution, reflecting impaired regional ventilation that mirrors the degree of airflow limitation observed by spirometric measurements.

A	B	C
Healthy volunteer (28y. F)	Patient with asthma (43y. M)	Patient with COPD (66y. F)
FEV_1 = 95% predicted	FEV_1 = 47% predicted	FEV_1 = 18% predicted
FEV_1/FVC = 88%	FEV_1/FVC = 58%	FEV_1/FVC = 33%
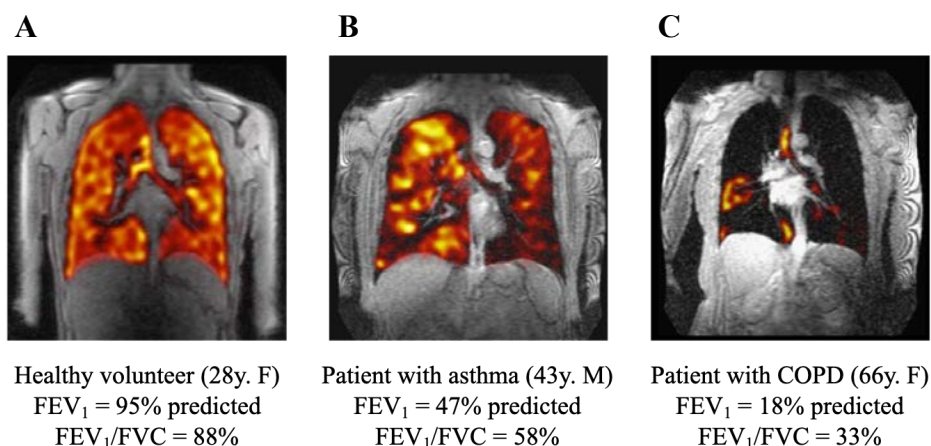
Figure 3.16: Example ^{19}F-MR ventilation images (single coronal slices) showing PFP distribution (coloured) overlaid on conventional ^{1}H-MRI scans (greyscale) in **(A)** one healthy volunteer, **(B)** one patient with asthma, and **(C)** one patient with COPD. (y = age in years; F = female; M = male).

All three ^{19}F-MR ventilation images were acquired using the same inhalation scheme and optimised scan protocol, providing confidence that the adopted technique was capable of detecting compromised ventilation in patients with respiratory disease compared to healthy volunteers. Importantly, the scan procedures were extremely well tolerated by each of the four patients, as well as by participants later attending Phase 3 of the LIFT study; while a formal evaluation of patient experience was beyond the scope of this research, several patients specifically commented that they found the procedures more comfortable to perform than conventional spirometry. These preliminary data provided a firm foundation upon which to progress to Phase 3 of the LIFT study, which intends to quantify potential differences in ventilation between healthy volunteers, patients with asthma, and patients with COPD, including response to BD therapy. A detailed analysis of this patient study is presented in Chapter 5.

3.6   Conclusion

The aim of this chapter was to outline the principal methodological considerations relating to static ^{19}F-MR ventilation imaging within the context of the LIFT study (Phase 1), focussing on the establishment of optimised scan protocols and gas inhalation strategies. MRI scan procedures were evaluated in healthy volunteers at two different study sites, and further tested in a small number of patients at one study site (Newcastle upon Tyne) in preparation for conducting subsequent phases of the LIFT study. The successful implementation of these finalised scan procedures paved the way to test the experimental hypotheses outlined in

Chapter 1 (Section 1.6), which relate directly to Phase 2 and Phase 3 of the study. This work is discussed in detail in the following two chapters of this thesis.

Chapter 4.

Reproducibility of static ^{19}F-MR ventilation imaging in healthy volunteers

4.1 Introduction

Chapter 3 provided an overview of the work conducted during Phase 1 of the LIFT study, focussing on key aspects of method development necessary for performing static ^{19}F-MR ventilation imaging in healthy volunteers and patients with respiratory disease. The present chapter intends to build upon this preliminary work by evaluating the reproducibility of established ^{19}F-MRI scan procedures in a cohort of healthy volunteers (study Phase 2), employing the %VV as a primary outcome measure.

As outlined in Chapter 1 (Section 1.5.3), the %VV and related VDP have been reported widely in the HP-MRI literature (e.g. Mathew *et al.*, 2012; Horn *et al.*, 2014a), providing clinically useful metrics of ventilatory function which correlate strongly with spirometric indices, e.g. FEV_1 (Kirby *et al.*, 2012a; Ebner *et al.*, 2017b). Previous studies have established the reproducibility of these HP-MRI measurements in healthy volunteers (Mathew *et al.*, 2008; Horn *et al.*, 2014a; Ebner *et al.*, 2017b) and patients with respiratory disease (Mathew *et al.*, 2008; Kirby *et al.*, 2012b; O'Sullivan *et al.*, 2014; Stewart *et al.*, 2018). However, to date, no studies have evaluated the utility of %VV measurements acquired by ^{19}F-MRI of inhaled PFP, reflecting the relative infancy of this technique. Determining the capability of pulmonary ^{19}F-MRI to accurately report on such lung biomarkers is vital in progressing the field towards clinical implementation, and to lay the foundation for performing future clinical trials.

The purpose of this study was to test the hypothesis that %VV measurements acquired by ^{19}F-MRI of inhaled PFP are reproducible in healthy volunteers, in preparation for conducting Phase 3 of the LIFT study. Study reproducibility was defined as the ability to acquire comparable ^{19}F-MR image datasets (assessed by SNR measurements) across two different study sites (Newcastle upon Tyne and Sheffield), using the adopted scan procedures. The same-day repeatability of %VV measurements (i.e. the consistency of repeated measurements acquired in individual participants attending one of the two study sites) was evaluated using a

components of variance model, intraclass correlation co-efficients (ICC) and coefficients of variation (CoV), based upon analysis of data performed by two different assessors.

4.2   Methods

The work presented in this chapter was conducted within the framework of Phase 2 of the LIFT study, as outlined in Chapter 2 (Section 2.2).

4.2.1   Study population

A planned sample size of forty healthy volunteers was chosen (see Chapter 2, Section 2.2.1). In total, 59 participants provided written informed consent and were screened for study eligibility at one of the two study sites (35 participants in Newcastle upon Tyne; 24 participants in Sheffield) between May 2018 and June 2019. Seven participants were deemed ineligible for continuation in the study following completion of initial screening tests (two participants did not fulfil the required spirometric criteria; two participants were receiving regular medication; one participant had a previous diagnosis of asthma; one participant was an ex-smoker with > 2 pack year history; one participant was unable to undertake MRI scanning). A further twelve participants attending the Newcastle upon Tyne study site (the first twelve participants recruited to Phase 2 of the LIFT study) were subsequently withdrawn after completing the MRI scan session, following identification of an intermittent coil fault affecting ^{19}F-MRI acquisitions in these participants, prompting a return of the coil to the manufacturer for repair. It is likely this fault stemmed from a recurring loose solder joint within the birdcage coil, impacting the quality of ^{19}F-MRI acquisitions in these participants. A substantial amendment was approved by the NHS HRA on 1st March 2019 to enable replacement of these participants with an additional twelve volunteers.

Accordingly, 40 healthy participants (21 male, 19 female; aged 23–67, mean = 41 years) were considered to have satisfactorily completed the study, as illustrated in Figure 4.1. All participants were non-smokers in good health with normal lung function as assessed by spirometry, in agreement with study inclusion and exclusion criteria outlined in Chapter 2 (Section 2.2.2).

```
┌─────────────────────────────┐
│ Assessed for study eligibility │
│  • Newcastle (n = 35)        │
│  • Sheffield (n = 24)        │
└─────────────────────────────┘
                                      ┌─────────────────────────┐
                                      │ Failed screening         │
                                      │  • Newcastle (n = 3)     │
                                      │  • Sheffield (n = 4)     │
                                      └─────────────────────────┘
┌─────────────────────────────┐
│ Recruited to study           │
│  • Newcastle (n = 32)        │
│  • Sheffield (n = 20)        │
└─────────────────────────────┘
                                ┌──────────────────────────────────────┐
                                │ Withdrawn after completing MRI scan    │
                                │  • Newcastle (n = 12)                  │
                                └──────────────────────────────────────┘
┌─────────────────────────────┐
│ Completed study              │
│  • Newcastle (n = 20)        │
│  • Sheffield (n = 20)        │
└─────────────────────────────┘
```
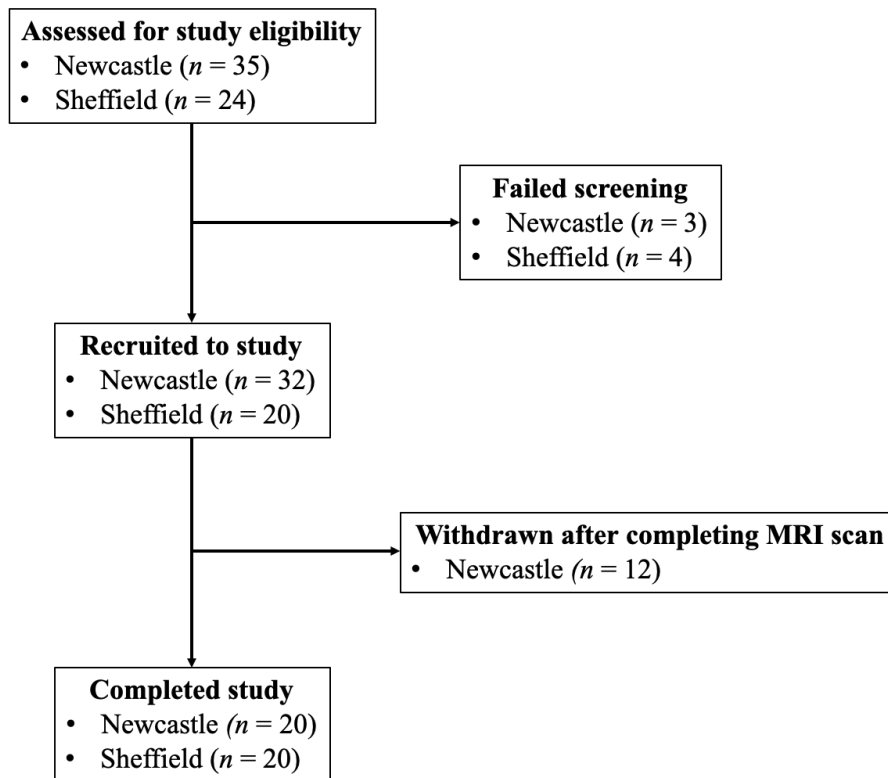
Figure 4.1: Flow diagram summarising recruitment to Phase 2 of the LIFT study. A total of 59 healthy volunteers were assessed for study eligibility. Seven participants were excluded after failing screening procedures (two participants did not fulfil the required spirometric criteria; two participants were receiving regular medication; one participant had a previous diagnosis of asthma; one participant was an ex-smoker with > 2 pack year history; one participant was unable to undertake MRI scanning). A further twelve participants were withdrawn from the Newcastle upon Tyne study site following identification of an intermittent coil fault after completing the MRI scan.

4.2.2   MRI scan procedures

Following completion of initial screening procedures, eligible participants underwent a single MRI scan session at one of the two study sites. All scans were performed supine on a 3.0 T scanner interfaced to a ^{19}F/^{1}H elliptical birdcage coil, as outlined in Chapter 2 (Section 2.5). Participants were positioned on the scanner bed with the assistance of radiographer colleagues, such that the entire lung fields were maintained centrally within the birdcage coil. Arms were positioned to rest comfortably on participants' legs, maintaining as much distance as possible from the side of the coil. The upper and lower components of the coil were secured in place using integrated plastic clips at either end.

Initial scout ^{1}H-MR images (coronal views) were acquired with the scanner's integral body coil using a conventional multi-slice 2D gradient echo sequence (see Table 4.1), in order to confirm correct positioning within the scanner bore. Participants were repositioned if

necessary and scans repeated to ensure full lung coverage was achieved. Anatomical ^{1}H scans were subsequently acquired after instructing participants to perform a breath-hold at maximal inspiration (i.e. TLC), using a conventional 3D SPGR sequence previously employed by colleagues at the University of Sheffield (Table 4.1).

Parameter	Scan			
	[1]H Scout	[1]H anatomical	[19]F FID	[19]F SPGR
TE (ms)	1.44	0.49	-	1.7
TR (ms)	4.0	4.0	200	7.5
Flip angle (°)	10	6	90	45
FOV (mm^3)	$440 \times 440 \times 262$	$440 \times 440 \times 247.5$	-	$400 \times (310\text{-}360) \times 250$
Resolution (mm^3)	$6.1 \times 6.1 \times 7.3$	$3 \times 3 \times 7.5$	-	$10 \times 10 \times 10$
BW (Hz / pixel)	500	3400	-	500
Number of averages	1	1	50	3
Acquisition time (s)	11.4	14.6	10	13.4
Number of samples	-	-	256	-
Sampling frequency (Hz)	-	-	8000	-

Table 4.1: Summary of the scan acquisition parameters employed during the LIFT study.

Following successful acquisition of anatomical ^{1}H scans, participants were instructed to inhale the 79% PFP / 21% O_2 gas mixture on five occasions during the MRI scan session. The sequence of gas inhalation sessions within the framework of the entire MRI scan session is illustrated in Figure 4.2.
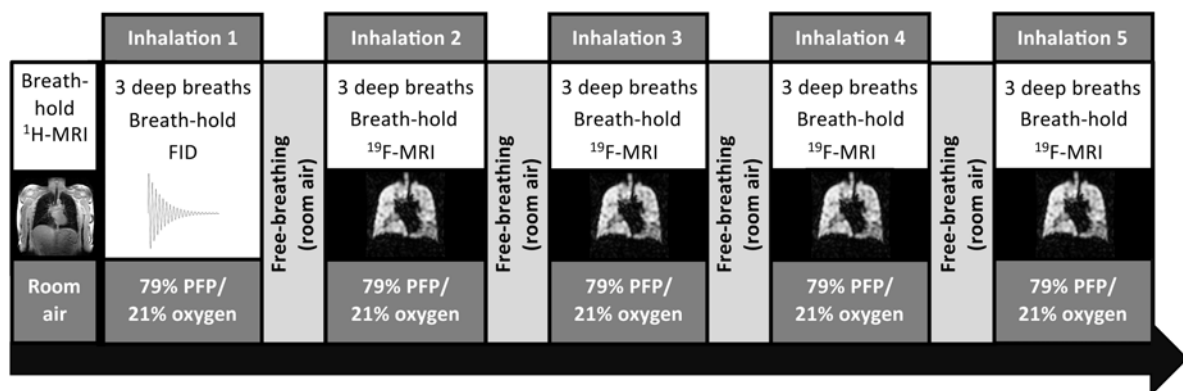
Figure 4.2: MR imaging protocol employed during Phase 2 of the LIFT study, comprising an initial anatomical [1]H-MRI breath-hold acquisition followed by five ^{19}F-MRI breath-hold acquisitions. The first PFP gas inhalation session was used for a whole-lungs spectroscopy (FID) scan; the remaining 4 inhalation sessions were used to acquire ^{19}F-MR ventilation images, each separated by an interval of approximately 6 minutes.

Each gas inhalation session lasted approximately 30 s, comprising three deep breaths of gas from a starting point of relaxed end-expiration (i.e. FRC) followed by a breath-hold (~13.5 s) at maximal inspiration (i.e. TLC). Breathing instructions were relayed to study participants and a member of the study team within the MRI scanner room (me in Newcastle upon Tyne; Dr Adam Maunder in Sheffield) via headphones, enabling appropriate timing of gas delivery according to the finalised inhalation scheme outlined in Chapter 3 (Section 3.3.3). All participants were coached in the inhalation scheme prior to entering the MRI scanner, and instructions were reiterated before each gas inhalation session to ensure compliance with breathing manoeuvres. The PFP/O_2 gas mixture was administered by the relevant member of the study team inside the MRI scanner room, using the inhalation equipment described in Chapter 2 (Section 2.5.5).

A whole-lungs unlocalised spectroscopy (FID) scan (see Table 4.1) was acquired at the onset of breath-hold during the first gas inhalation session, allowing measurement of PFP's -CF_3 ^{19}F resonant frequency (see Chapter 3, Section 3.2.1). A 3D SPGR sequence (see Table 4.1, comprising the optimised ^{19}F-MRI scan protocol developed during Phase 1 of the LIFT study) was acquired at the onset of breath-hold for the remaining four gas inhalation sessions, enabling acquisition of four 3D ^{19}F-MR ventilation images per participant. Each ^{19}F-MRI acquisition was separated by an interval of at least 5 minutes (mean (SD) = 358 (74) s), in accordance with scan SAR limits outlined in Chapter 2 (Section 2.5.3). During this time, participants breathed room air freely until the start of the next gas inhalation session.

Following completion of the final gas inhalation session, participants were removed from the MRI scanner and observed for a period of 10 minutes to ensure heart rate and O_2 saturations remained at baseline (i.e. pre-gas inhalation) levels, prior to leaving the study centre.

4.2.3   *Image analysis and measurement of %VV values*

All ^1H- and ^{19}F-MR images were analysed independently by two assessors at Newcastle University (me; and Dr Mary Neal), with each assessor performing %VV measurements according to two different analysis methods. The image analysis tools adopted in this study are described in further detail below.

Image analysis method 1: 'VV Tool'

VV Tool image analysis software was developed in-house in Matlab (Mathworks Inc., Natick MA, USA) by researchers at the University of Sheffield, in conjunction with open-source 3D image segmentation functionality in ITK-SNAP (Yushkevich *et al.*, 2006). The software was originally designed to enable semi-automated calculation of %VV values obtained using HP-MRI (namely, inhaled ³He and ¹²⁹Xe) and was subsequently adapted by Dr Alberto Biancardi (Image Computing Staff Scientist, University of Sheffield) for use in the LIFT study.

¹H- and ¹⁹F-MR image masks (depicting the anatomical boundaries of the lungs and PFP gas signal, respectively) were initially generated by each assessor using a semi-automated region-growing algorithm, permitting registration of ¹H images to each of the four corresponding ¹⁹F-MR ventilation images. Image masks relating to individual lung slices were adjusted manually where the algorithm failed to provide accurate coverage of the lung fields. Registered image pairs were subsequently segmented independently by each assessor to calculate total lung volumes (from ¹H images) and ventilated lung volumes for each ¹⁹F-MR image (see Figure 4.3). This was achieved using a semi-automated clustering approach developed at the University of Sheffield (Hughes *et al.*, 2018), employing a threshold-based algorithm to identify ventilated regions from ¹⁹F-MR images. The distinction between ventilated and non-ventilated lung regions was assessed qualitatively (i.e. by visual inspection) by each assessor and corrected manually where necessary, e.g. in instances where the automatic segmentation process was judged to have mis-assigned ventilated/non-ventilated regions. This included removal of signal from the trachea, main bronchi and major vessels at the level of the hilum. Importantly, the semi-automated VV Tool software frequently mis-assigned ventilated and non-ventilated regions of the 3D dataset, requiring significant manual segmentation of individual image slices to be performed by each assessor. This is discussed further in Section 4.4.

%VV values were subsequently calculated by the software for each segmented image pair by dividing the ventilated volume (VV) of each ¹⁹F-MR ventilation image by the total lung volume (TLV) of the corresponding ¹H image, using the following equation:

$$\%VV = \frac{VV}{TLV} \times 100$$

A Registration of
^{1}H and ^{19}F images

B Segmentation and exclusion of airways
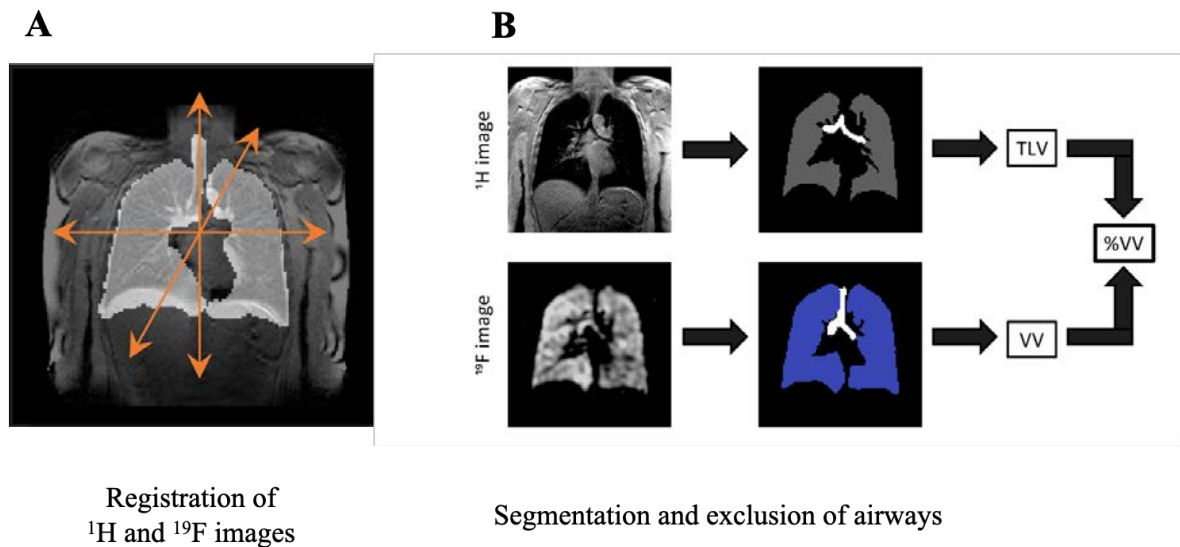
Figure 4.3: Examples of **(A)** registration of ^{1}H and ^{19}F images, enabling correction of potential differences in lung inflation level between scans, and **(B)** semi-automated segmentation of individual ^{1}H and ^{19}F image slices, performed independently by each assessor. The %VV was calculated for each of the four ventilation images per participant by dividing the ventilated lung volume (VV) by the total lung volume (TLV).

Image analysis method 2: 'RegSeg'

RegSeg (i.e. *Reg*istration and *Seg*mentation) image analysis software was developed in-house in Matlab (Mathworks Inc., Natick MA, USA) by Dr Mary Neal at Newcastle University. The software was designed for the specific purpose of evaluating ^{19}F-MR ventilation images, such as those acquired during the course of the LIFT study.

All participant datasets were analysed by applying a semi-automated script in Matlab, enabling each of the four acquired ^{19}F-MR ventilation images to be selected in turn, alongside the corresponding anatomical ^{1}H image. An initial signal threshold was applied to the ^{1}H dataset (set at the mean image signal) to remove any extra-pulmonary (i.e. non-lung) regions containing high signal. Individual ^{1}H slices were subsequently segmented using a clustering-based method (Ester *et al.*, 1996), which divided each image slice into distinct regions based on the relative distribution of pixel densities present in that image. Regions were classified automatically as either 'lung' or 'not lung' according to the 3D region size, voxel intensity, and spatial location. In cases where the semi-automated algorithm failed to accurately segment ^{1}H image slices (e.g. through poor identification of lung boundaries), the software permitted manual input from assessors in order to delineate the lung borders, including removal of central airways where necessary (see Figure 4.4). The process was then repeated until appropriate ^{1}H image segmentation was achieved.
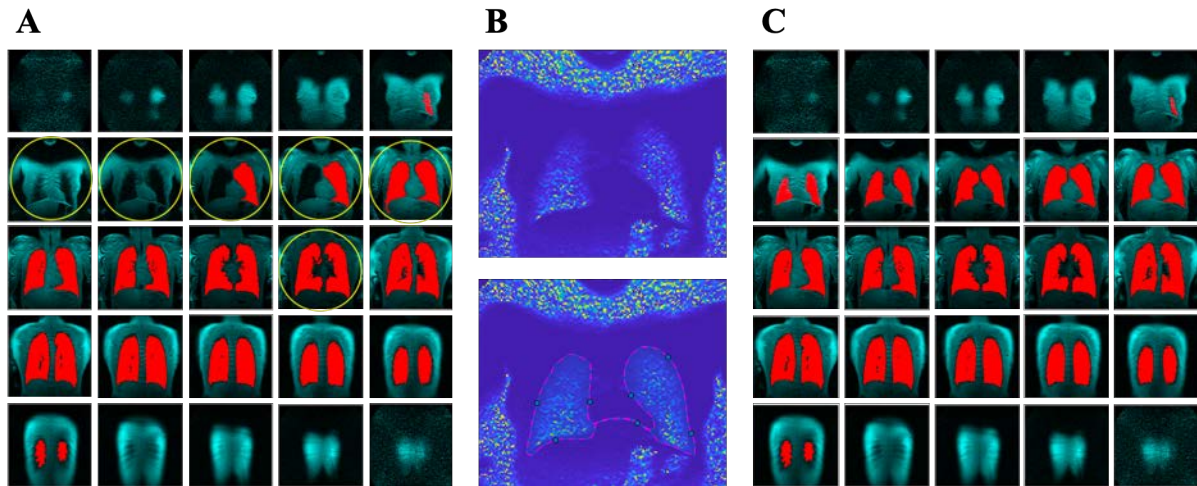
Figure 4.4: Semi-automated segmentation of a healthy volunteer ^{1}H dataset (Participant N1) using RegSeg image analysis software. **(A)** shows an example of inaccurate automated segmentation, where yellow circles indicate the individual slices requiring manual correction. **(B)** shows an example of manual adjustment for one slice that was incorrectly segmented (top image), with correct manual delineation of lung borders (bottom image). **(C)** shows the complete ^{1}H segmentation following manual adjustment of the selected slices.

Binary segmentation of ^{19}F-MR ventilation images was subsequently performed by applying a fixed signal threshold at the 99th percentile above a noise region of interest (ROI), which was manually selected by each assessor from a single image slice located 1–2 slices after the last visible PFP signal. Registration of ^{1}H/^{19}F image pairs was achieved by aligning the bronchi of anatomical (^{1}H) and ventilation (^{19}F) images through manual selection of corresponding central image slices, using the original non-segmented images as a point of reference. Each ^{1}H image was scaled to the corresponding ^{19}F image, accounting for potential differences in the depth of breath-hold achieved between respective acquisitions. The use of registered or non-registered image slices was determined manually by each assessor (see Figure 4.5) prior to automated calculation of %VV values using the same equation as indicated above.
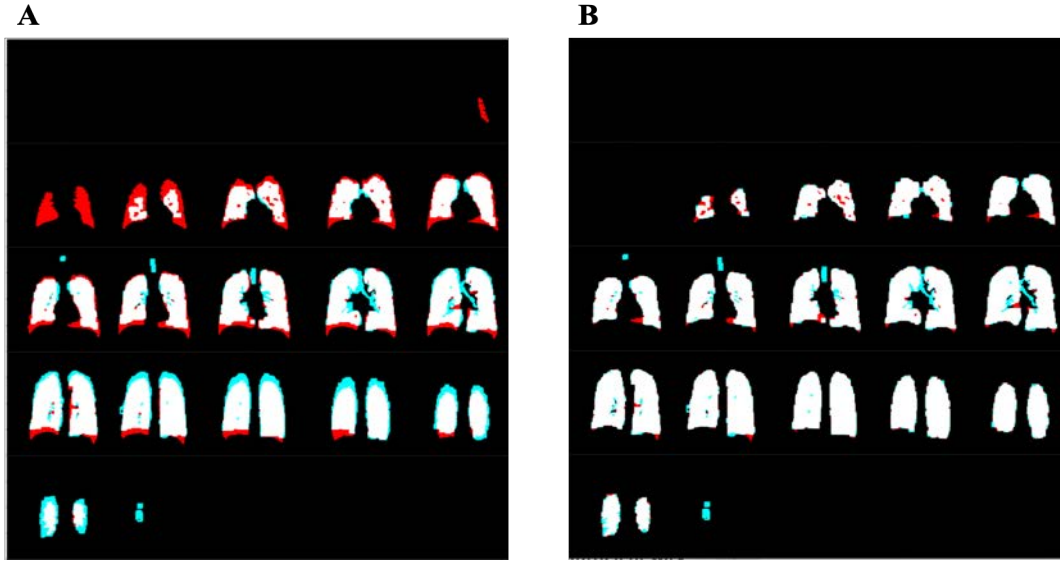
Figure 4.5: Example of **(A)** non-registered and **(B)** registered ^{1}H and ^{19}F image slices generated by RegSeg image analysis software. Lung regions containing both [1]H (red) and [19]F (blue) signal are shown in white. The combination of registered or non-registered slices, from which %VV calculations were derived, was selected manually by each assessor.

SNR

The SNR was measured for each ^{19}F-MR ventilation image by placing a 4×4 cm^2 ROI in the apex of the right lung (signal) and a 100 cm^2 ROI below the lung (noise) in a central image slice where the trachea was seen to bifurcate. SNR was calculated by applying the following expression in Matlab, where the constant ($\sqrt{2 - \frac{\pi}{2}}$) accounts for the Rayleigh distribution (i.e. variance) of background noise in MR images (Edelstein *et al.*, 1984):

$$\left(\frac{\text{mean signal - mean noise}}{\text{standard deviation of noise}} \right) \sqrt{2 - \frac{\pi}{2}}$$

4.2.4 Statistical analysis

Principal data analysis was performed by Prof John Matthews (Professor of Medical Statistics and LIFT study statistician, Newcastle University) by fitting linear random-effects models with three independent components of variance: namely, differences in %VV values between participants; differences in %VV values between the four acquisitions for each participant; and differences in %VV values calculated by the two assessors for each acquisition. This permitted an estimation of the contribution of each of the three individual variance components to the total variation from the true %VV value. The models were fitted in R (R Core Team, 2015) using the package lme4 (Bates *et al.*, 2014) and applied to each of

the two analysis methods described in Section 4.2.3. Estimates obtained from these fits were also used to compute ICC values as a measure of intra-participant repeatability of %VV measurements; 95% confidence intervals (CI) were found using the bootstrap.

Additional analyses were performed by me, with statistical advice provided by Prof John Matthews and Dr Holly Fisher (Biostatistician and LIFT study co-investigator, Newcastle University). The consistency of intra-participant %VV measurements was assessed by computing coefficients of variation (CoV) in Excel (Version 16, Microsoft Corporation, Redmond WA, USA); in common with previous HP-MRI literature (Parraga *et al.*, 2008; Horn *et al.*, 2014a; Stewart *et al.*, 2018), this was defined as the standard deviation divided by the mean over all repeated %VV measurements, expressed as a percentage. Inter-assessor agreement in calculated %VV values was further evaluated using the Dice similarity coefficient as a measure of spatial overlap between segmented image pairs. This was calculated in Matlab using a script implemented by Dr Mary Neal (Newcastle University). Mann Whitney *U* tests were performed using GraphPad Prism (Version 9, GraphPad software, San Diego, California, USA) to assess for potential differences in %VV measurements between assessors, and to compare %VV measurements between the two study sites; independent samples *t*-tests were used to compare SNR measurements between the two study sites. Tests of normality were performed using the Shapiro-Wilk and Kolmogorov-Smirnov tests. A *p*-value of < 0.05 was considered to represent a significant difference in all cases. Associations between %VV measurements and spirometric measurements were assessed using the Pearson correlation coefficient, *r*.

4.3   Results

Participant demographic information is summarised in Table 4.2. ^{19}F-MRI scans were well tolerated throughout by all participants, with no adverse events. Of the 40 participants who successfully completed the study, a total of 38 were included for image analysis: two participants attending the Sheffield study site were excluded from analysis as a result of poor compliance with breathing instructions during one or more PFP gas inhalation sessions, which impacted the ability to make a true assessment of ventilated lung volumes in these participants.

90

Parameter	Newcastle upon Tyne (n = 20)	Sheffield (n = 18)	Combined (n = 38)
Sex			
Male	11	9	20
Female	9	9	18
Age (years)			
Male	35 (23–58)	43 (28–64)	39 (23–64)
Female	43 (27–67)	42 (26–56)	43 (26–67)
Total	39 (23–67)	43 (26–64)	41 (23–67)
Body mass index (kg/m^2)	24.4 (18.3–32.3)	23.3 (17–34.9)	23.9 (17–34.9)
Spirometry[*]			
FEV$_1$ (% pred.)	105 (88–120)	100 (83–114)	103 (83–120)
FVC (% pred.)	108 (86–125)	100 (79–117)	104 (79–125)
FEV$_1$/FVC (%)	80 (71–93)	81 (71–96)	80 (701–96)
Mean heart rate (bpm)[†]			
Pre-inhalation	70 (42–104)	65 (48–107)	68 (42–107)
Post-inhalation	72 (44–103)	67 (48–108)	70 (44–108)
Mean oxygen saturation (%)			
Pre-inhalation	98 (96–100)	98 (96–100)	98 (96–100)
Post-inhalation	98 (95–100)	98 (93–99)	98 (93–100)

Table 4.2: Summary of participant demographics relating to Phase 2 of the LIFT study (n = 38). Data are presented as mean values with range in parenthesis. [*]FEV$_1$ = forced expiratory volume in 1 second; FVC = forced vital capacity; % pred. = percentage of predicted value. [†]bpm = beats per minute.

4.3.1 Repeatability of %VV measurements

Image analysis method 1: VV Tool

Calculated %VV measurements for the remaining 38 participants, acquired using the VV Tool image analysis software, are presented in Table 4.3. The mean %VV value calculated per participant by each of the two assessors was uniformly above 94% (range = 94.0% – 99.5%; median = 98.2%).

The CoV in %VV measurements was calculated as $CoV_{assessor1} = 0.43\%$ and $CoV_{assessor2} = 0.63\%$. Separate analyses by the two assessors revealed ICCs (95% CI) of 0.683 (0.578, 0.837) for assessor 1 and 0.614 (0.493, 0.784) for assessor 2. The combined analysis of both assessors (performed by Prof John Matthews) gave components of variance for differences between participants, differences between acquisitions for each participant, and differences between assessor for each acquisition of 0.90, 0.18 and 0.54, respectively. For an individual participant, the variation about the true value has two components: the image-to-image

variation (0.18) and the assessor-to-assessor variation (0.54). Consequently, for a given participant, the SD of the error in a single image would be $\sqrt{(0.18 + 0.54)} = 0.85$, such that 95% of single image estimates would be within ± 1.7% (i.e. 2 SD) of the true value.

Participant		Assessor 1					Assessor 2				
		%VV 1	%VV 2	%VV 3	%VV 4	Mean %VV	%VV 1	%VV 2	%VV 3	%VV 4	Mean %VV
Newcastle	**N1**	98.0	96.9	98.6	97.4	97.7	98.9	97.2	98.9	97.8	98.2
	N2	97.3	96.6	98.4	96.7	97.2	97.8	97.0	96.9	96.2	97.0
	N3	98.9	98.8	98.9	98.9	98.9	98.9	98.7	97.7	98.6	98.5
	N4	97.9	97.5	97.8	97.9	97.8	97.4	96.5	96.7	96.9	96.9
	N5	98.6	98.2	98.8	98.8	98.6	99.7	99.2	99.1	99.1	99.2
	N6	97.7	97.9	97.6	98.2	97.8	97.5	97.4	97.3	98.9	97.8
	N7	98.8	99.1	98.5	98.3	98.7	98.6	98.3	98.9	97.9	98.4
	N8	98.2	98.0	97.5	98.7	98.1	98.9	99.6	98.8	99.1	99.1
	N9	98.1	97.8	97.7	98.1	97.9	97.9	97.4	97.1	98.1	97.6
	N10	98.3	98.6	98.8	98.8	98.6	99.3	99.1	99.5	99.3	99.3
	N11	97.8	97.8	98.1	98.5	98.1	97.8	97.4	98.0	97.7	97.7
	N12	98.5	98.6	98.9	99.0	98.7	99.0	98.9	98.6	98.8	98.8
	N13	98.5	98.7	99.1	98.9	98.8	98.9	99.2	99.0	98.9	99.0
	N14	98.8	98.9	98.7	99.0	98.9	99.4	99.6	99.6	99.3	99.5
	N15	97.6	97.8	98.3	98.3	98.0	97.7	97.9	97.9	97.6	97.8
	N16	99.2	99.3	99.4	99.2	99.3	99.4	99.2	99.2	99.1	99.2
	N17	98.9	98.9	99.1	99.1	99.0	98.3	98.5	97.3	98.4	98.1
	N18	97.9	97.6	97.9	97.5	97.7	98.6	97.6	97.7	97.3	97.8
	N19	98.7	97.3	97.8	99.2	98.3	97.8	96.4	97.6	97.7	97.4
	N20	99.1	99.3	99.3	98.7	99.1	97.3	98.6	98.2	98.3	98.1
Sheffield	**S1**	96.4	96.6	96.3	95.4	96.2	94.3	94.1	96.1	97.1	95.4
	S2	99.8	99.1	99.1	99.2	99.3	99.5	99.5	99.6	99.5	99.5
	S3	98.1	98.5	98.2	98.5	98.3	97.6	98.3	97.6	97.2	97.7
	S4	97.0	96.6	97.6	96.3	96.9	96.6	95.9	97.2	95.5	96.3
	S5	98.4	98.1	98.4	98.7	98.4	98.2	97.6	98.2	97.8	97.9
	S6	98.3	98.4	97.8	97.7	98.0	98.3	96.9	97.5	97.9	97.7
	S7	99.4	99.2	99.6	99.8	99.5	98.5	98.5	98.3	98.9	98.5
	S8	99.4	99.2	99.3	99.2	99.3	97.1	98.7	98.4	97.6	97.9
	S9	99.3	98.4	99.0	97.6	98.6	96.9	97.0	96.1	96.4	96.6
	S10	99.3	99.1	99.1	99.4	99.2	99.0	98.2	98.6	98.2	98.5
	S11	98.0	98.0	97.7	98.0	97.9	97.6	97.2	97.2	97.3	97.3
	S12	98.9	98.8	99.1	99.2	99.0	98.7	97.3	98.6	97.8	98.1
	S13	93.8	97.3	97.0	98.4	96.6	90.4	93.2	95.3	96.9	94.0
	S14	97.8	97.6	93.6	95.3	96.1	96.3	97.8	90.2	95.8	95.0
	S15	97.6	98.7	99.1	98.9	98.5	98.1	98.7	98.0	99.0	98.4
	S16	98.9	99.1	98.9	99.0	99.0	98.9	97.7	98.1	98.4	98.3
	S17	99.3	99.4	99.4	99.2	99.3	98.2	97.7	98.3	98.6	98.2
	S18	96.1	95.7	95.4	97.1	96.1	98.6	97.3	95.6	97.2	97.2

Table 4.3: Calculated %VV values for healthy volunteers ($n = 38$) using VV Tool image analysis software.

Image analysis method 2: RegSeg

Equivalent %VV measurements acquired using the RegSeg image analysis software are presented in Table 4.4. The mean %VV value calculated per participant by each of the two assessors was consistently above 89% (range = 89.4% – 98.0%; median = 96.7%).

The CoV in %VV measurements was calculated as 0.71% for both assessor 1 and assessor 2. Separate analyses by assessor revealed ICCs (95% CI) of 0.609 (0.490, 0.778) for assessor 1 and 0.618 (0.496, 0.789) for assessor 2. The analysis combining both assessors gave components of variance for differences between participants, differences between acquisitions for each participant, and differences between assessors for each acquisition of 2.63, 1.59 and 0.09, respectively. Thus, the SD of the error in a single image would be √(1.59 + 0.09) = 1.3, such that 95% of single image estimates would be within ± 2.6% (i.e. 2 SD) of the true value.

The increased range of %VV values obtained using the RegSeg analysis software compared to VV Tool analysis software was influenced by one dataset in particular (S14). Exclusion of this dataset revealed mean %VV values with a range of 92.1% – 98.0%; CoV values of 0.53% for assessor 1 and 0.54% for assessor 2; ICC values of 0.746 (0.658, 0.885) for assessor 1 and 0.755 (0.672, 0.896) for assessor 2; and single image %VV estimates within ± 1.8% of the true value.

Participant		Assessor 1					Assessor 2				
		%VV 1	%VV 2	%VV 3	%VV 4	Mean %VV	%VV 1	%VV 2	%VV 3	%VV 4	Mean %VV
Newcastle	**N1**	96.3	96.5	97.0	95.5	96.3	96.4	96.0	96.9	95.0	96.1
	N2	96.4	96.4	95.4	89.4	94.4	95.7	95.3	94.9	89.3	93.8
	N3	96.4	96.7	96.0	96.1	96.3	95.8	96.4	96.0	96.8	96.3
	N4	96.8	96.9	96.4	97.1	96.8	96.9	97.3	96.8	97.6	97.2
	N5	97.9	97.9	97.8	97.9	97.9	97.9	98.0	97.7	98.2	98.0
	N6	95.3	95.9	95.2	96.3	95.7	94.9	95.7	95.1	96.2	95.5
	N7	96.4	96.7	96.7	97.3	96.8	96.9	97.0	96.4	96.8	96.8
	N8	96.1	96.8	96.4	96.3	96.4	96.4	97.3	96.4	96.6	96.7
	N9	96.6	96.9	96.7	96.4	96.7	97.0	97.3	96.7	96.8	97.0
	N10	97.3	97.1	96.7	97.6	97.2	96.7	96.4	96.8	97.1	96.8
	N11	95.7	96.4	96.4	96.2	96.2	95.9	96.8	96.9	96.9	96.6
	N12	97.3	97.1	97.1	96.3	97.0	96.9	97.2	97.1	96.8	97.0
	N13	97.2	97.1	97.0	97.4	97.2	97.4	97.0	97.0	97.0	97.1
	N14	97.1	97.1	97.4	97.2	97.2	97.1	97.4	96.9	97.3	97.2
	N15	97.5	97.0	95.6	96.7	96.7	97.2	96.8	96.1	96.7	96.7
	N16	97.8	98.0	98.1	97.9	98.0	97.7	97.6	97.8	97.6	97.7
	N17	97.4	97.6	97.6	97.6	97.6	97.4	97.0	97.6	97.7	97.4
	N18	95.9	95.5	96.7	96.3	96.1	96.0	96.0	96.6	96.4	96.3
	N19	96.8	95.6	95.7	96.2	96.1	96.6	95.1	95.1	96.1	95.7
	N20	96.4	97.5	96.9	97.7	97.1	97.0	97.3	96.8	97.5	97.2
Sheffield	**S1**	94.1	93.8	94.3	93.7	94.0	94.6	94.5	94.8	94.2	94.5
	S2	97.1	97.4	97.5	97.6	97.4	97.2	97.4	97.4	97.7	97.4
	S3	96.3	96.0	96.1	96.1	96.1	95.7	95.8	95.2	95.8	95.6
	S4	93.5	91.9	94.3	91.9	92.9	94.8	91.7	94.6	92.6	93.4
	S5	96.3	95.9	96.6	97.2	96.5	96.4	96.0	96.2	96.7	96.3
	S6	95.3	95.7	95.7	95.7	95.6	95.0	95.6	95.5	95.6	95.4
	S7	97.3	97.4	97.8	97.9	97.6	97.2	97.3	97.8	97.9	97.6
	S8	96.1	96.5	96.3	96.7	96.4	96.7	96.8	96.6	97.2	96.8
	S9	96.1	95.0	95.1	93.9	95.0	95.9	94.8	94.4	92.3	94.4
	S10	97.1	97.2	96.9	97.4	97.2	97.2	97.0	97.0	97.5	97.2
	S11	96.9	96.7	96.6	96.6	96.7	96.5	96.6	96.7	96.7	96.6
	S12	97.8	97.4	97.5	97.8	97.6	97.2	97.0	97.3	97.5	97.3
	S13	91.8	92.4	92.5	95.1	93.0	91.8	92.7	92.5	95.0	93.0
	S14	94.3	95.0	81.1	87.2	89.4	94.2	95.2	81.7	87.2	89.6
	S15	96.5	96.5	96.6	97.1	96.7	96.6	96.6	96.6	97.1	96.7
	S16	96.0	96.9	96.9	96.6	96.6	96.2	97.0	97.1	96.4	96.7
	S17	96.7	96.9	97.1	97.0	96.9	96.7	96.5	96.9	96.8	96.7
	S18	93.9	92.8	90.5	91.2	92.1	92.5	93.3	90.6	91.9	92.1

Table 4.4: Calculated %VV values for healthy volunteers ($n = 38$) using RegSeg image analysis software.

4.3.2 *Inter-assessor agreement in %VV measurements*

Figure 4.6A shows single coronal slices (top row = anterior; bottom row = posterior) from a representative 3D ^{19}F-MRI dataset in one healthy participant (S2: 26 year-old female; FEV_1 = 102% predicted, FVC = 104% predicted, FEV_1/FVC = 83%) acquired during a 13.4 s breath-hold at maximal inspiration. Figure 4.6B demonstrates orthogonal views from the same participant, with ^{19}F-MR ventilation images (coloured) superimposed on the corresponding

anatomical ^{1}H MR images (greyscale). Homogeneous gas distribution can be visualised throughout the entire lung fields, with only minor apparent ventilation heterogeneity observed towards the most peripheral anterior-posterior lung slices.

%VV measurements derived from the VV Tool and RegSeg analysis software for this participant were 99.1% and 97.4% (assessor 1), and 99.5% and 97.4% (assessor 2), respectively.
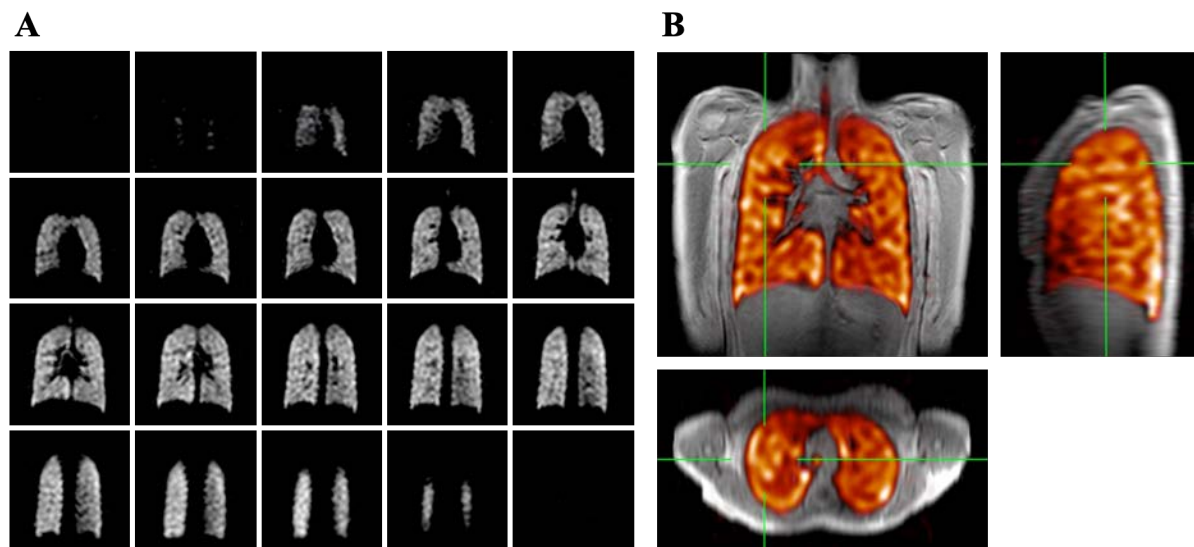
Figure 4.6: (A) Representative ^{19}F-MR ventilation images (coronal views) from a healthy participant (S2), acquired during a 13.4 s breath-hold scan following three deep breaths of the 79% PFP / 21% O_2 gas mixture. **(B)** Combined ^{1}H and ^{19}F-MR ventilation images (coloured) in the same participant, showing homogeneous gas distribution throughout the lung fields.

Figure 4.7 shows analogous images from a different participant (S14: 64 year-old male; FEV_1 = 91% predicted, FVC = 98% predicted, FEV_1/FVC = 71.5%), also acquired during a 13.4 s breath-hold at maximal inspiration. In this dataset, images were characterised by increased background noise and ventilation heterogeneity, particularly evident towards the anterior of the lungs (Figure 4.7A, top row).

%VV measurements derived from the VV Tool and RegSeg analysis software for this participant were 95.3% and 87.2% (assessor 1), and 95.8% and 87.2% (assessor 2), respectively.
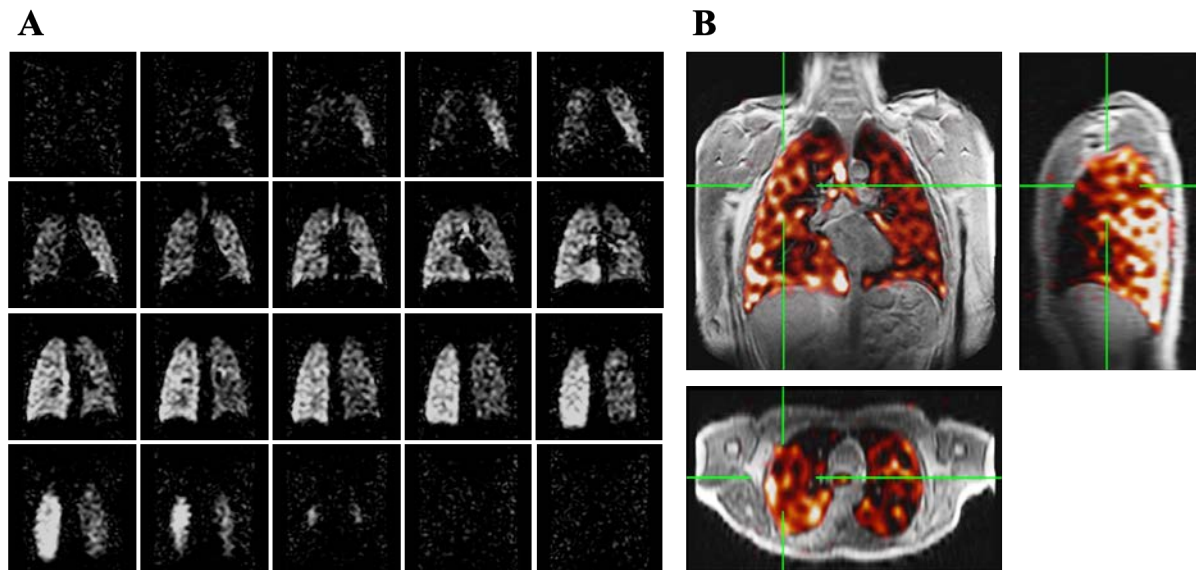
Figure 4.7: (A) ^{19}F-MR ventilation images (coronal views) from a healthy participant (S14), acquired during a 13.4 s breath-hold scan following three deep breaths of the 79% PFP / 21% O_2 gas mixture. **(B)** Combined ^{1}H- and ^{19}F-MR ventilation images (coloured) in the same participant, showing heterogeneous gas distribution within the lungs. The image quality in this participant was considerably reduced compared to other datasets.

The mean (SD) and median (IQR, interquartile range) calculated %VV values across all analysed participant datasets ($n = 38$) were similar between assessors for both VV Tool (98.2 (0.9)% and 98.5 (97.8–99.0)% for assessor 1; 97.8 (1.2)% and 98.0 (97.4–98.5)% for assessor 2) and RegSeg (96.1 (1.8)% and 96.7 (96.0–97.2)% for assessor 1; 96.1 (1.7)% and 96.7 (95.6–97.2)% for assessor 2). Mann Whitney U tests revealed no evidence of a difference in %VV values calculated between assessors using VV Tool ($p = 0.09$) or RegSeg analysis software ($p = 0.96$). The estimated variance in %VV measurements arising from differences between assessors for each acquisition was computed as 0.54 (VV Tool) and 0.09 (RegSeg), respectively.

Figure 4.8A shows an example of a combined ^{19}F-MR image segmentation performed by the two assessors for one healthy participant (N7: 37 year-old male; $FEV_1 = 113$% predicted, FVC = 120% predicted, FEV_1/FVC = 76%) using the VV Tool image analysis software. Figure 4.8C shows the equivalent combined ^{19}F-MR image segmentation performed using the RegSeg image analysis software. Inter-assessor agreement for each of the respective image segmentations is shown in white (VV Tool) and yellow (RegSeg), while disagreement between assessors is shown in red (VV Tool) and green (RegSeg), respectively. There was a high degree of spatial overlap between individual assessor segmentations using both VV Tool and RegSeg analysis software, with disagreement most prominent towards the peripheral anterior-posterior lung slices (more evident in segmentations performed using VV Tool).

Figure 4.8B and 4.8D show combined assessor segmentations from a different participant (N6: 34 year-old male; FEV_1 = 113% predicted, FVC = 118% predicted, FEV_1/FVC = 79%). In this participant, the discrepancy between assessors was more apparent using VV Tool (red) compared to RegSeg (green).

The Dice similarity coefficient, calculated as a measure of inter-assessor agreement across all ^{19}F-MR image segmentations, demonstrated a high mean (SD) value of 0.97 (0.02) for VV Tool and 0.98 (0.01) for RegSeg, respectively.
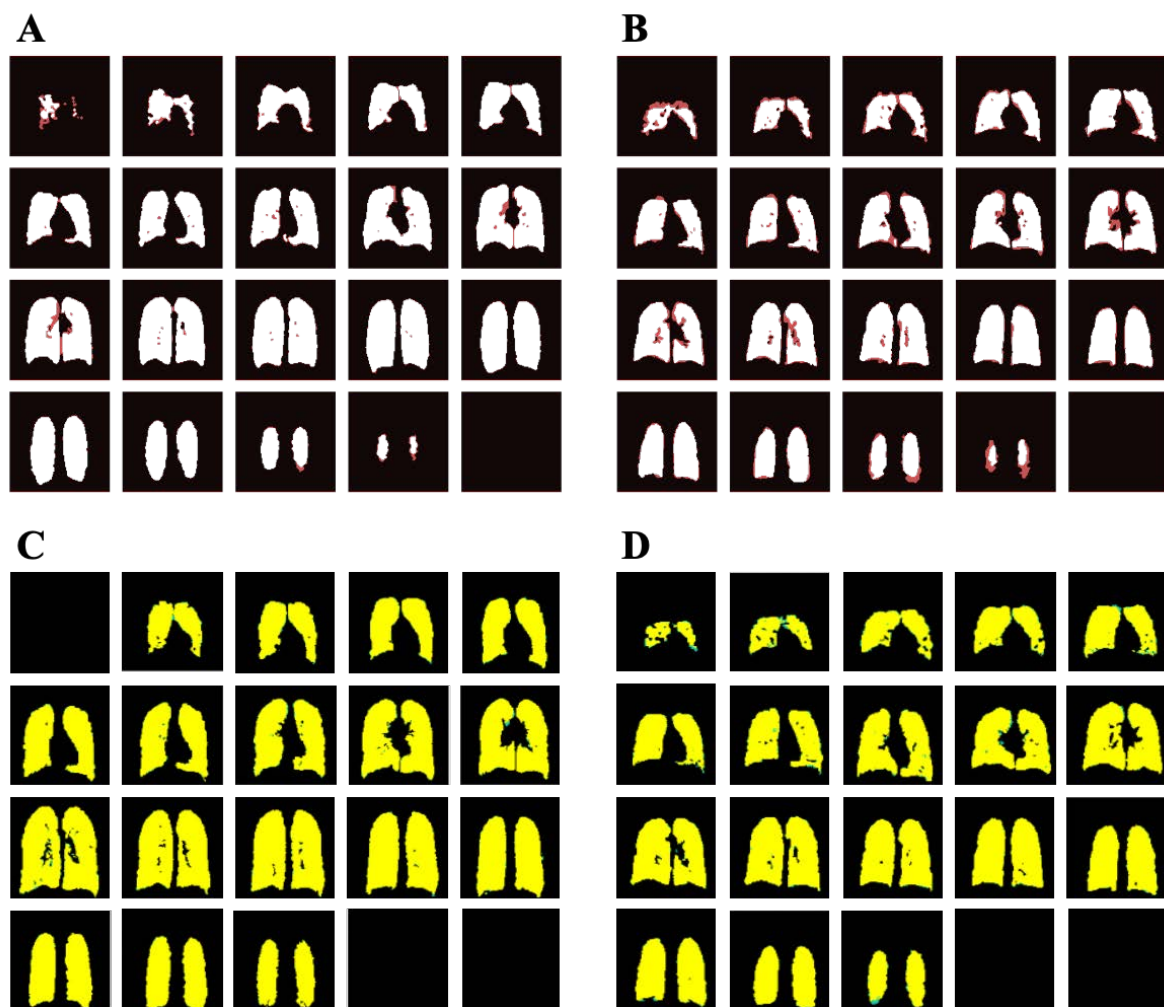
Figure 4.8: Combined ^{19}F-MR image segmentations performed independently by the two assessors. Segmentations performed using the VV Tool are shown in **(A)** and **(B)**; equivalent segmentations performed using RegSeg are shown in **(C)** and **(D)**. There was close agreement between assessor segmentations in participant N7 (**A** and **C**, respectively), with Dice similarity coefficients of 0.98 (VV Tool) and 0.99 (RegSeg). Segmentations performed in participant N6 (**B** and **D**, respectively) demonstrated slight differences between the Dice similarity coefficients acquired using VV Tool (0.92) and RegSeg (0.98).

4.3.3 Comparison between study sites

Image quality was of a sufficient standard across the two study sites to determine %VV values using the two different semi-automated segmentation tools, with comparable SNR achieved between the respective study sites (mean $SNR_{Newcastle}$ = 14.8 (2.5), range = 8.4–19.8; mean $SNR_{Sheffield}$ = 13.9 (4.0), range = 6.5–25.4). An independent-samples t-test revealed no evidence of a difference in SNR values between study sites (p = 0.11).

%VV values, averaged across both assessors, were compared between the two study sites. A summary of the mean, median, and range of %VV values according to study site and analysis method is presented in Table 4.5. Mann Whitney U tests revealed no evidence of a difference in %VV values between participants attending the two study sites as calculated by VV Tool (p = 0.25) or RegSeg image analysis software (p = 0.094).

%VV values	VV Tool		RegSeg	
	Newcastle upon Tyne (n = 20)	Sheffield (n = 18)	Newcastle upon Tyne (n = 20)	Sheffield (n = 18)
Minimum	97.1	95.3	94.1	89.5
Maximum	99.3	99.4	98.0	97.6
Mean (SD)	98.3 (0.6)	97.7 (1.3)	96.7 (0.9)	95.4 (2.2)
Median	98.6	98.1	96.9	96.5

Table 4.5: Comparison of %VV values across the two study sites, as acquired by VV Tool and RegSeg analysis software.

4.3.4 Comparison with spirometric measurements

Figure 4.9A shows the relationship between %VV measurements (averaged across both assessors) and % predicted FEV_1 measurements acquired in the 38 study participants. %VV values acquired using VV Tool are shown in orange, while values acquired using RegSeg are shown in blue. A corresponding relationship between %VV and % predicted FVC, and between %VV and FEV_1/FVC is illustrated in Figure 4.9B and 4.9C, respectively.

Pearson correlation analysis revealed a slight positive association between %VV and % predicted FEV_1 (r = 0.39, p = 0.01_{VVTool}; r = 0.32, p = 0.05_{RegSeg}) and between %VV and % predicted FVC (r = 0. 34, p = 0.04_{VVTool}; r = 0.28, p = 0.09_{RegSeg}), reflecting the clustering of

values towards 100%. %VV poorly correlated with FEV_1/FVC ($r = 0.12$, $p = 0.48$ for values acquired using both VV Tool and RegSeg).
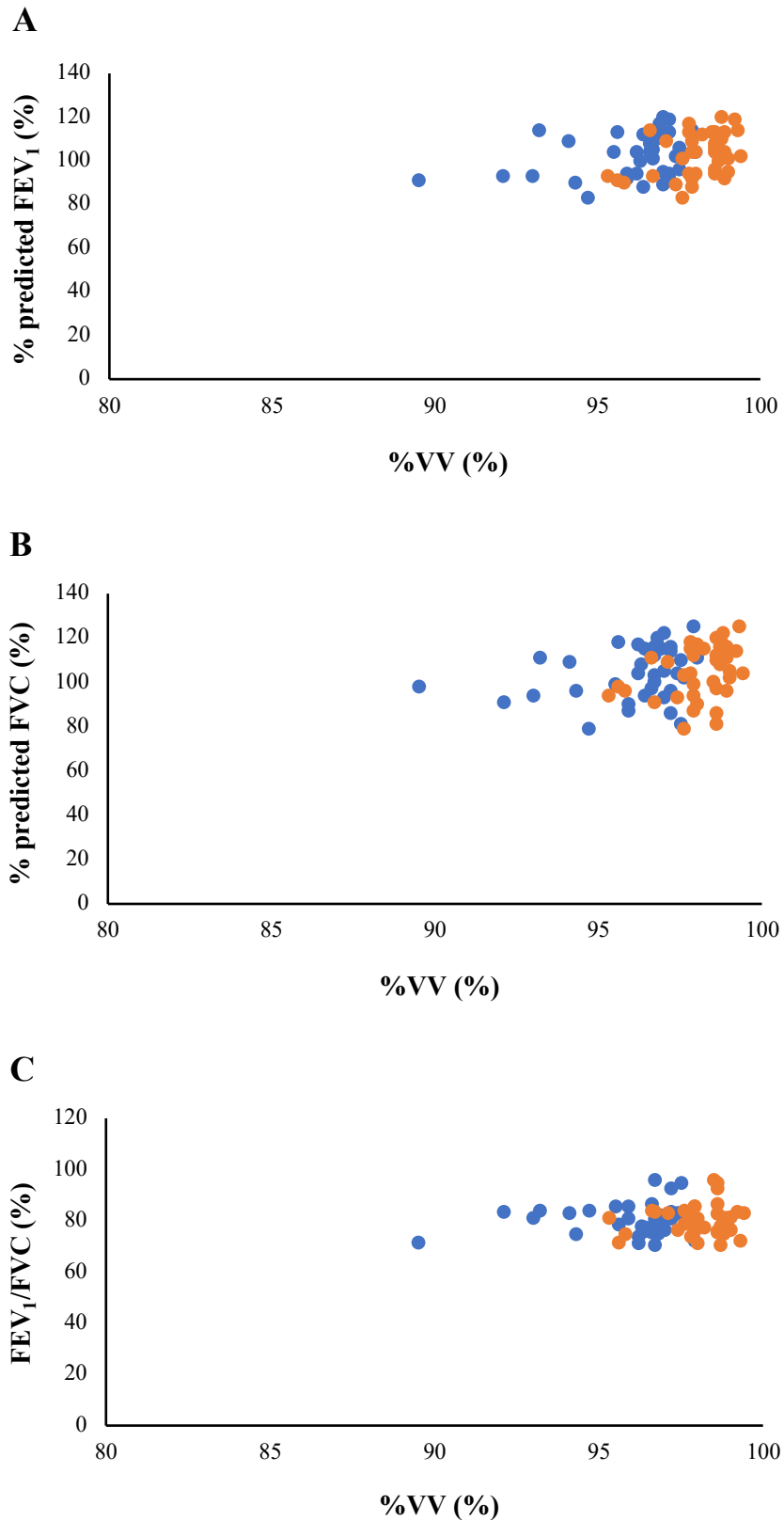
Figure 4.9: Associations between calculated %VV values and **(A)** % predicted FEV$_1$, **(B)** % predicted FVC, and **(C)** FEV$_1$/FVC for healthy volunteers attending Phase 2 of the LIFT study. %VV values acquired using VV Tool are shown in orange; %VV values acquired using RegSeg are shown in blue. The majority of values are clustered between 95% and 100%, reflecting the population of healthy volunteers included in the study.

4.4   Discussion

A central goal of Phase 2 of the LIFT study was to establish the technical feasibility of performing ^{19}F-MR ventilation imaging across different study sites whilst maintaining reproducibility of data acquisition. In this study, ^{19}F-MRI scan procedures were successfully implemented at two different research centres with sufficient image quality and SNR to determine %VV measurements in 38 healthy volunteers.

The findings presented in Section 4.3 indicate a high degree of consistency in calculated %VV values across all study participants, with a low CoV (< 1%) between respective ^{19}F-MR acquisitions. These values compare favourably to values reported in the HP-MRI literature: e.g. 1.8% (Parraga *et al.*, 2008); 5% (Kirby *et al.*, 2012b); 1.21% (Horn *et al.*, 2014a); 4% (Stewart *et al.*, 2018). However, it should be noted that the CoV reported in this study was heavily influenced by the clustering of %VV measurements towards the upper end of the scale (i.e. approaching 100%), reflecting the particular population of healthy volunteers included. This selection bias also likely underpins the relatively weak correlations observed between %VV and spirometric measurements. Inclusion of a broader range of %VV and spirometric values (i.e. from patients with underlying respiratory disease) will enable a more comprehensive analysis of the relationship between spirometric and ^{19}F-MRI based measurements; this is examined further in Chapter 5.

The ICC offers an alternative method of assessing the same-day repeatability of %VV measurements that has been widely adopted in the HP-MRI literature (Kirby *et al.*, 2012b; Niles *et al.*, 2013; Horn *et al.*, 2014a; Stewart *et al.*, 2018). In this study, the reported ICC values (range = 0.609–0.755) were unexpectedly lower than values previously published in relation to healthy volunteers, which are typically in the region of 0.85–1.0 (Parraga *et al.*, 2008; Horn *et al.*, 2014a; Ebner *et al.*, 2017b). While this may at first suggest comparatively reduced reproducibility of %VV measurements by ^{19}F-MRI, it is important to recognise that the ICC is intrinsically determined by the values of the between-acquisition and between-assessor components of variance relative to the between-participant component of variance. As highlighted above, there was little variation in the %VV values measured in the cohort of healthy volunteers recruited to Phase 2 of the LIFT study compared to previously reported HP-MRI studies (e.g. Horn *et al.*, 2014a; Ebner *et al.*, 2017b), with the majority of participants demonstrating %VV values of 97–99% (VV Tool) and 95–97% (RegSeg),

respectively. As such, the relatively modest ICC values observed in this study are likely to reflect the marked homogeneity of this particular cohort, rather than diminished repeatability per se. The high degree of inter-assessor consistency and precision in calculated %VV values (± 1.7% for VV Tool; ± 1.8–2.6% for RegSeg) supports the ability of the adopted study methodology to provide reliable measures of pulmonary ventilation in a large group of healthy participants. Nevertheless, it is important to recognise that these results are based on optimised conditions to maximise the technical reproducibility of the adopted approach; the experimental design, by its nature, largely removes any biological variation that may exist between measurements, given the short time-interval between respective acquisitions. This is likely to be more relevant for patients with respiratory disease than healthy volunteers, though should be considered as part of future study development (see also Chapter 8, Section 8.2).

The %VV values reported in this study were calculated according to two different image analysis tools; namely, VV Tool and RegSeg. Variants of these semi-automated approaches to image segmentation have been well documented in the HP-MRI literature (Kirby *et al.*, 2012b; He *et al.*, 2014). However, to date, no image analysis tools have been established for use with ^{19}F-MRI datasets. Importantly, the range of %VV values achieved by ^{19}F-MRI of inhaled PFP were comparable to values previously reported in healthy volunteers using ^{129}Xe and ^{3}He (Stewart *et al.*, 2018; Hughes *et al.*, 2019). Nonetheless, it is notable that calculations performed by VV Tool were typically 1–2% higher than equivalent calculations performed by RegSeg. These differences likely stem from the degree of manual correction applied to image segmentations performed by the two assessors, particularly in datasets affected by low SNR. Specifically, for segmentations undertaken with VV Tool, substantial manual input was required in order to accurately segment respective ^{1}H/^{19}F image pairs, reflecting the inherently lower SNR and spatial resolution of PFP ventilation images compared to HP-MR ventilation images (for which VV Tool was originally developed). By contrast, the binary signal-threshold approach applied to the RegSeg software (which was specifically designed to assess PFP ventilation images) greatly reduced the need for manual correction of segmented image pairs.

The impact of the two different semi-automated segmentation approaches on resultant %VV calculations was particularly apparent in one participant (S14), where the SNR of acquired ventilation images was especially low (see Figure 4.7). As with other datasets, the manual

correction applied by each assessor in this case likely led to a relative overestimation of %VV values calculated by VV Tool, secondary to poor discrimination between true PFP signal and background noise: it is possible that assessors were intrinsically biased towards including poorly differentiated regions of background noise as regions of PFP signal, based on an assumption that ventilated lung volumes would be high in this particular cohort of healthy volunteers. Conversely, the %VV values obtained using RegSeg (requiring substantially less manual segmentation) are more representative of the reduced quality of images acquired in this participant, which were characterised by regions of low signal similar to what might be anticipated in patients with underlying respiratory pathology (e.g. Halaweish *et al.*, 2013a). The cause of the reduced SNR observed in participant S14 is not entirely clear. However, it is possible this represents an example of poorly performed gas inhalation manoeuvres, as previously outlined in Chapter 3 (Section 3.3.2).

Despite the element of subjectivity inherent in %VV calculations that require a degree of manual input, the inter-assessor agreement between respective measurements was high for both VV Tool and RegSeg analyses. This may reflect the relative efficacy of the chosen tools, although it is likely these results are also heavily influenced by the careful standardisation of segmentation procedures between the two assessors involved in this study. In particular, for analyses performed using VV Tool, both assessors endeavoured to follow a pre-defined process for visual determination of lung boundaries, manual signal thresholding (i.e. image contrast settings) and removal of airways and pulmonary vasculature. While this facilitated a consistent approach to manual segmentation, the resulting time required to analyse each of the four ^{1}H/^{19}F image pairs was substantial, typically in the region of 1–1.5 hours. In contrast, the time taken to perform an equivalent analysis using RegSeg was approximately 5–10 minutes, reflecting the significant reduction in manual input required when using this particular software. The efficiency of image analysis is clearly relevant when processing a large number of datasets, such as those generated as part of the LIFT study. Moreover, the ability to limit assessor input has important implications for ensuring parity of approach in future clinical studies, where multiple assessors may be involved across several different research sites. Although not yet achieved, the avoidance of subjectivity entirely in image processing (e.g. through fully-automated image segmentation software) represents a clear goal for future optimisation and development in this area. For these reasons, the RegSeg image analysis tool was considered most appropriate for application to Phase 3 of the LIFT study (Chapter 5), as well as the smaller feasibility study (VQ MRI) presented in Chapter 6.

As outlined in Chapter 3 (Section 3.3), correct adherence to breathing instructions is central to maintaining reproducibility of image acquisitions and highlights a key methodological difference compared to HP-MRI ventilation imaging, which typically involves a single inhalation of a small, fixed volume of gas (Ebner *et al.*, 2017a). The sensitivity of inhaled PFP to changes in lung inflation level has previously been reported (Maunder *et al.*, 2019, 2021) and underpins the specific breathing protocol adopted in this study (i.e. three deep wash-in breaths of gas, followed by a breath-hold at maximum inspiration). This contrasts the fixed (1 L) inhalation protocol reported by Couch *et al.* (2013). Nonetheless, by adopting this approach, the PFP wash-in volume may be standardised relative to the volume of maximal inhalation achievable by each participant, rather than adopting a fixed wash-in volume irrespective of lung capacity. Importantly, in the 38 participants who performed breathing manoeuvres as instructed, good reproducibility of %VV measurements was demonstrated. It is notable, however, that two participants were excluded from image analysis owing to poor compliance with breathing instructions, which impacted the quality of acquired ventilation images; it is possible this was also responsible for the reduced image quality observed in Participant S14, with resultant impact on calculated %VV measurements. This represents an important consideration for future study design involving patients with underlying respiratory disease, where variability in performance may be more apparent. The utility of the adopted ^{19}F-MRI scan procedures in patients with asthma and patients with COPD is assessed in detail in Chapter 5.

4.5   Conclusion

This study reports, for the first time, an evaluation of %VV measurements acquired by ^{19}F-MRI of inhaled PFP, demonstrating good same-day repeatability in a large number of healthy participants. The successful implementation of ^{19}F-MRI scan protocols and inhalation schemes across two different research sites provides a firm foundation on which to compare image quality and %VV values acquired in patients with respiratory disease as part of Phase 3 of the LIFT study. This represents the focus for the next chapter of this thesis.

Chapter 5.

Assessment of static ^{19}F-MR ventilation imaging in patients with asthma and patients with COPD

5.1 Introduction

The previous chapter demonstrated the feasibility of acquiring reproducible %VV measurements in a cohort of healthy volunteers, employing ^{19}F-MRI scan procedures developed during Phase 1 of the LIFT study. This work was fundamental in determining the suitable application of an established outcome measure to human ^{19}F-MR ventilation imaging, in preparation for conducting future clinical studies. The present chapter aims to extend this work by assessing the utility of the adopted study procedures to quantify differences in regional ventilation between healthy volunteers and patients with respiratory disease; namely, asthma and COPD.

The regional variation in gas distribution observed in patients with asthma and patients with COPD has been well described in the HP-MRI literature, corresponding to reduced global ventilated lung volume measurements compared to healthy volunteers (Virgincar *et al.*, 2013; Ebner *et al.*, 2017b; Stewart *et al.*, 2018). Previous studies have established the capability of %VV and VDP measurements to report on changes in response to BD therapy (Kirby *et al.*, 2011; Svenningsen *et al.*, 2013; Horn *et al.*, 2017a), in addition to showing improved sensitivity to early smoking-related disease (Pike *et al.*, 2015) and asthma control (Svenningsen *et al.*, 2016) over conventional spirometry. While a growing body of research has demonstrated the feasibility of ^{19}F-MRI to assess regional gas distribution in patients with respiratory disease (Halaweish *et al.*, 2013a; Gutberlet *et al.*, 2018), to date %VV measurements acquired by this technique have not been evaluated. Given the widespread use of %VV as a marker of pulmonary ventilation, this represents an important avenue towards establishing ^{19}F-MR ventilation imaging as a viable alternative to HP-MRI.

The primary aim of this study was to test the hypothesis that %VV measurements, as acquired by ^{19}F-MRI of inhaled PFP, are reduced in patients with asthma and patients with COPD compared to healthy volunteers. Additionally, based on existing HP-MRI literature (e.g. Kirby *et al.*, 2011; Svenningsen *et al.*, 2013), it was hypothesised that calculated %VV

values would improve in patients with asthma and patients with COPD following administration of BD therapy.

5.2   Methods

The work presented in this chapter was conducted within the framework of Phase 3 of the LIFT study, as outlined in Chapter 2 (Section 2.2).

5.2.1   Study population

A planned sample size of forty patients with asthma and forty patients with COPD was chosen, split between the two study sites (see Chapter 2, Section 2.2.1). Unfortunately, recruitment to Phase 3 of the LIFT study was heavily impacted by the emergence of the COVID-19 pandemic in March 2020, resulting in a suspension to the study; at the time of writing, only one patient has been recruited to the Sheffield study site. Consequently, for the purpose of completing and submitting this thesis within the available timeframe, the remainder of this chapter will focus solely on those patients who have been successfully recruited to the Newcastle upon Tyne study site.

In total, 34 patients provided written informed consent and were screened for study eligibility at the NMRC between July 2019 and February 2020, in accordance with study recruitment criteria outlined in Chapter 2 (Section 2.2.2). Two patients were deemed ineligible to continue with the study following completion of initial screening tests (one patient with COPD did not meet spirometric requirements; one patient with COPD did not meet resting O_2 saturation requirements). A further three patients were withdrawn from the study prior to completion of the MRI scan session (two patients with asthma were unable to participate due to claustrophobia; one patient with COPD was unable to attend the scan visit on more than two occasions).

Twenty-nine participants, comprising 16 patients with asthma (9 male, 7 female; aged 20–73, mean = 52 years) and 13 patients with COPD (8 male, 5 female; aged 60–78, mean = 69 years) subsequently completed the study, as illustrated in Figure 5.1. Patients were identified as described in Chapter 2 (Section 2.2.2). All except for one (with COPD) were non-smokers at the time of study participation (see Table 5.2).
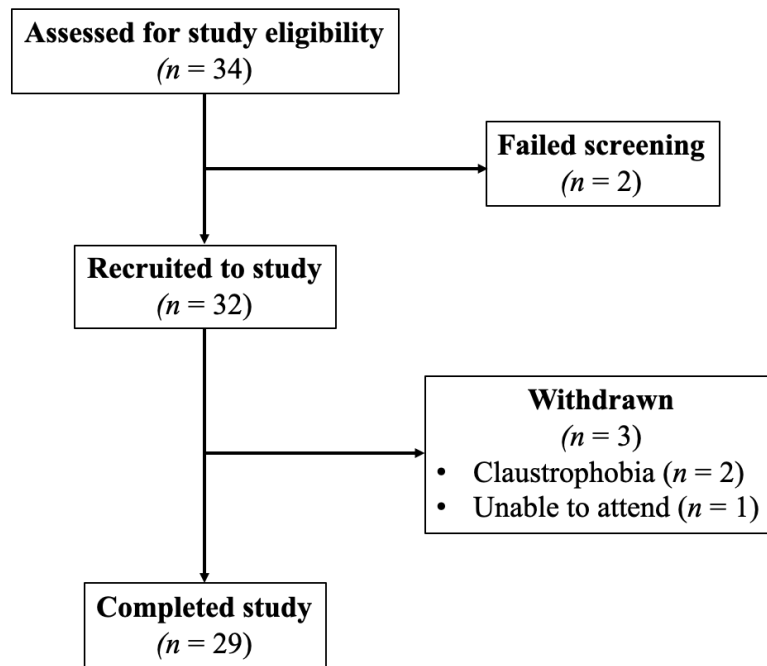
Figure 5.1: Flow diagram summarising recruitment to Phase 3 of the LIFT study. A total of 34 patients were assessed for study eligibility. Two patients were excluded after failing initial screening procedures (one patient with COPD did not meet spirometric requirements; one patient with COPD did not meet resting oxygen saturation requirements). A further three patients were withdrawn prior to completing the MRI scan visit (two patients with asthma were unable to participate due to claustrophobia; one patient with COPD was unable to attend the scan visit on more than two occasions).

5.2.2   MRI scan procedures

Following completion of initial screening procedures (study visit 1), eligible patients underwent a single MRI scan session at the NMRC (study visit 2). The mean time interval between the two study visits was 8 days (range 1–39 days; median = 5 days). Prior to attending the second study visit, all patients were instructed to withhold regular long- and short-acting BD medication, as outlined in Chapter 2 (Section 2.2.2). A summary of the timings for withholding relevant BD medication is provided in Table 5.1.

Usual frequency	Example bronchodilator	Last dose
As required	Ventolin (SABA[*])	At least 4 hours before study visit time, if needed
Once daily (morning)	Spiriva (LAMA[†]) Relvar (LABA[‡]/ICS[§]) Trelegy (ICS/LAMA/LABA)	Morning of day prior to study visit (i.e. omit on morning of study visit)
Once daily (evening)	Montelukast (LRA[**])	Evening two days prior to study visit (i.e. omit on evening prior to study visit)
≥ Twice daily (e.g. morning/evening)	DuoResp (ICS/LABA) Symbicort (ICS/LABA) Eklira Genuair (LABA/LAMA) Theophylline (PDE-I[††])	Evening prior to study visit (at least 12 hours before study visit time)

Table 5.1: Timings for withholding bronchodilator medication during Phase 3 of the LIFT study. [*]SABA = short-acting β_2 agonist; [†]LAMA = long-acting muscarinic antagonist; [‡]LABA = long-acting β_2 agonist; [§]ICS = inhaled corticosteroid; [**]LRA = leukotriene receptor antagonist; [††]PDE-I = phosphodiesterase inhibitor

Pre-bronchodilator MRI scans

Initial scout [1]H-MR images (coronal views) were acquired with the scanner's body coil using the same multi-slice 2D gradient echo sequence adopted for healthy volunteers attending Phase 2 of the LIFT study (see Table 4.1, Chapter 4). Patients were repositioned if necessary and scans repeated to ensure full lung coverage was achieved. Anatomical ^{1}H scans were subsequently acquired after instructing patients to perform a breath-hold at maximal inspiration (i.e. TLC), using the same 3D SPGR sequence adopted for healthy volunteers.

Following successful acquisition of anatomical ^{1}H scans, patients were instructed to inhale the 79% PFP / 21% O_2 gas mixture on up to three occasions (where the third pre-BD gas inhalation session provided a 'failsafe' in the event of a problem arising during either the first or second gas inhalation sessions; it was not mandatory to complete the third inhalation session providing the preceding acquisitions were performed satisfactorily). Each gas inhalation session was conducted in an identical manner to that performed by healthy volunteers attending Phase 2 of the LIFT study, as outlined in Chapter 4 (Section 4.2.2).

Bronchodilator administration

Upon completion of pre-BD MRI scans, patients left the MRI scanner to receive nebulised salbutamol (2.5 mg). This was administered by a member of the study team as outlined in Chapter 2 (Section 2.5.7). Post-BD spirometry was subsequently performed in all patients at an interval of 20 minutes after the nebuliser was complete.

Post-bronchodilator MRI scans

Following post-BD spirometry testing, patients immediately returned to the MRI scanner for the second part of the MRI scan session. This involved repeating initial scout and anatomical ^{1}H MRI scans, in addition to performing two further 79% PFP / 21% O$_2$ gas inhalation sessions. These were performed in an identical manner to the pre-BD inhalation sessions outlined above.

The sequence of gas inhalation sessions within the framework of the entire MRI scan is illustrated in Figure 5.2.
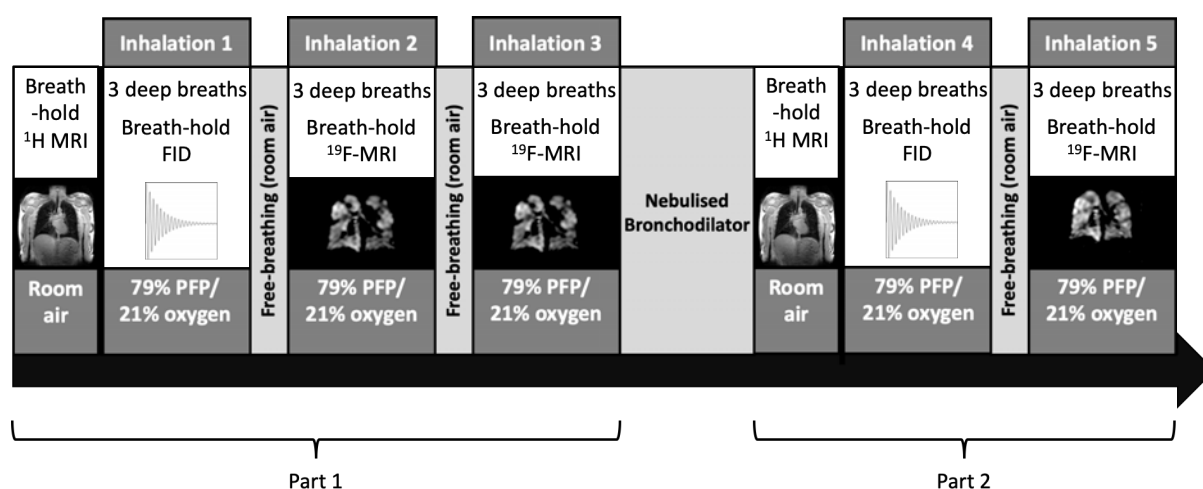
Figure 5.2: Summary of the MR imaging protocol employed during Phase 3 of the LIFT study. The first pre-BD (Part 1) and post-BD (Part 2) ^{19}F-MRI acquisition was used to perform a whole-lungs spectroscopy (FID) scan; the remaining ^{19}F-MRI acquisitions were used to perform static ventilation imaging. Each ^{19}F-MRI scan was separated by an interval of approximately 6 minutes.

^{19}F-MRI acquisitions

An unlocalised spectroscopy scan (FID) was acquired at the onset of breath-hold during the first pre-BD and first post-BD gas inhalation session (Inhalation 1 and Inhalation 4, respectively), permitting measurement of PFP's -CF$_3$ ^{19}F resonant frequency (see Chapter 3,

Section 3.2.1.). A 3D SPGR sequence was acquired at the onset of breath-hold for the remaining gas inhalation sessions (Inhalation 2, 3 and 5), enabling acquisition of at least one pre-BD ^{19}F-MR ventilation image and one post-BD ^{19}F-MR ventilation image per patient. Each pre-BD and post-BD ^{19}F-MRI acquisition was separated by an interval of at least 5 minutes (mean (SD) = 401 (87) s; median = 360 s), in accordance with scanner SAR limits outlined in Chapter 2 (Section 2.5.3). During this time, patients breathed room air freely until the start of the next gas inhalation session.

The scan parameters relating to ^{19}F FID and 3D SPGR acquisitions were identical to those adopted during Phase 2 of the LIFT study, as summarised in Table 4.1 (Chapter 4, Section 4.2.2).

Following completion of the final post-BD gas inhalation session, patients were removed from the MRI scanner and observed for a period of 10 minutes to ensure heart rate and oxygen saturations remained at baseline (i.e. pre-gas inhalation) levels, prior to leaving the study centre.

5.2.3   *Image analysis and measurement of %VV values*

All ^{1}H- and ^{19}F-MR images were analysed independently by two assessors at Newcastle University (me; and Dr Mary Neal). Pre-and post-BD %VV values were calculated using the same RegSeg image analysis software adopted during Phase 2 of the LIFT study, enabling a direct comparison of %VV measurements acquired in healthy volunteers, patients with asthma, and patients with COPD. A detailed description of the image analysis software is provided in Chapter 4 (Section 4.2.3).

The SNR was calculated for each pre- and post-BD ^{19}F-MR ventilation image, using the same approach as outlined in Chapter 4 (Section 4.2.3). However, for patient datasets, SNR measurements were performed using a slightly larger signal ROI (6×6 cm^2), allowing for the increased signal heterogeneity encountered in patient images compared to healthy volunteers.

5.2.4   Statistical analysis

Unless otherwise stated, all analyses were performed using GraphPad Prism (Version 9, GraphPad software, San Diego, California, USA), with a *p*-value less than 0.05 considered statistically significant where relevant.

Tests of normality were performed using the Shapiro-Wilk and Kolmogorov-Smirnov tests. Potential differences in %VV values between healthy volunteers (attending Phase 2 of the LIFT study), patients with asthma and patients with COPD were assessed using Mann-Whitney *U* tests. SNR values acquired in patients with asthma and patients with COPD were evaluated using independent samples *t*-tests; a comparison of pre- and post-BD SNR measurements was performed using paired *t*-tests. Pre- and post-BD %VV values in patients with asthma were assessed using the Wilcoxon signed-rank test; pre- and post-BD %VV measurements in patients with COPD were evaluated using paired *t*-tests. Inter-assessor agreement in calculated %VV values was assessed using the Mann-Whitney *U* test for patients with asthma, and independent samples *t*-test for patients with COPD. The Dice similarity coefficient was calculated in Matlab (Mathworks Inc., Natick MA, USA) as a further measure of spatial overlap between assessors for each segmented image pair, using the same approach adopted during Phase 2 of the LIFT study (see Chapter 3, Section 3.2.4). Associations between calculated %VV measurements and spirometric parameters were assessed using the Pearson correlation coefficient.

5.3   Results

Patient demographic and clinical information are summarised in Table 5.2. ^{19}F-MRI scans were well tolerated throughout by all patients, with no adverse events. Of the 29 patients who successfully completed the study, a total of 26 (14 with asthma and 12 with COPD) were subsequently included for image analysis: three patients (one with asthma and two with COPD) were excluded from analysis as a result of poorly functioning RF coil performance during MRI scanning, which impacted the quality of ^{19}F-MR ventilation images acquired in these patients (see Figure 5.3).

Example pre- and post-BD images (represented as single coronal slices) for the remaining 26 study participants are presented in Figure 5.4. The mean time interval between completion of

nebulised salbutamol and acquisition of post-BD ^{19}F-MR ventilation images was 34 minutes (range = 28–40 minutes; median = 34.5 minutes).

Parameter	Asthma (*n* = 14)	COPD (*n* = 12)	Combined (*n* = 26)
Sex			
Male	8	7	15
Female	6	5	11
Age (years)			
Male	53 (20–73)	68 (60–78)	60 (20–78)
Female	52 (22–66)	69 (66–71)	59 (22–71)
Total	52 (20–73)	69 (60–78)	60 (20–78)
BMI (kg/m^2)	26.4 (19.4–31.3)	25.8 (20.3–30.7)	26.1 (19.4–31.3)
Smoking status			
Current	0	1	1
Previous	6	11	17
Never	8	0	8
Pack years	8 (1–15)	50 (30–70)	36 (1–70)
Pre-BD Spirometry			
FEV$_1$ (% pred.)	71 (40–109)	36 (16–49)	55 (16–109)
FVC (% pred.)	86 (55–111)	76 (44–96)	81 (44–111)
FEV$_1$/FVC (%)	64 (42–82)	36 (27–45)	51 (27–82)
Post-BD Spirometry			
FEV$_1$ (% pred.)	85 (48–117)	40 (18–58)	64 (18–117)
FVC (% pred.)	98 (66–116)	86 (55–111)	92 (55–116)
FEV$_1$/FVC (%)	69 (44–86)	35 (26–44)	53 (26–86)
Heart rate (bpm)†			
Pre-inhalation	76 (53–106)	81 (61–103)	79 (53–106)
Post-inhalation	77 (50–105)	82 (61–101)	79 (50–105)
Oxygen saturation (%)			
Pre-inhalation	96 (89–99)	95 (90–98)	96 (89–99)
Post-inhalation	97 (90–99)	95 (90–98)	96 (90–99)

Table 5.2: Summary of patient clinical and demographic information relating to Phase 3 of the LIFT study (*n* = 26). Data are presented as mean values with range in parenthesis. *FEV$_1$ = forced expiratory volume in 1 second; FVC = forced vital capacity; % pred. = percentage of predicted value. †bpm = beats per minute.
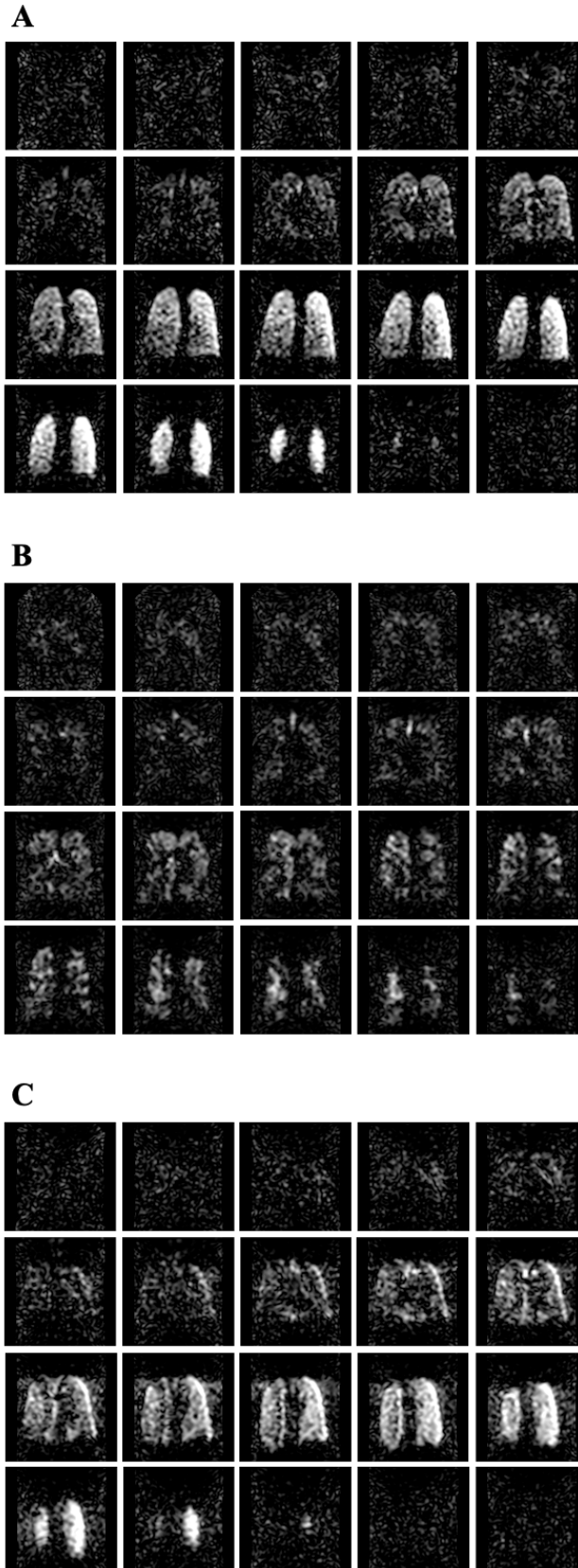
Figure 5.3: Example sub-optimal ^{19}F-MRI datasets from **(A)** a patient with asthma, and **(B and C)** two patients with COPD. All acquisitions performed in these patients were characterised by poor image quality and significant background noise, likely stemming from a recurrent coil fault. All three patients were subsequently excluded from further image analysis.
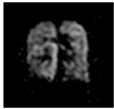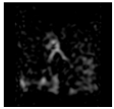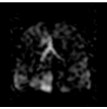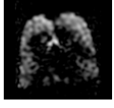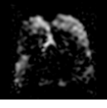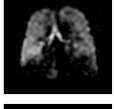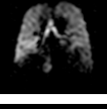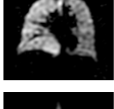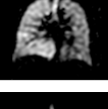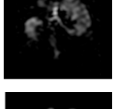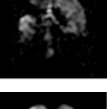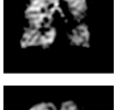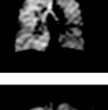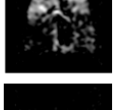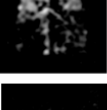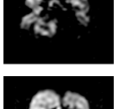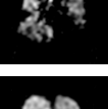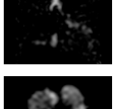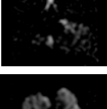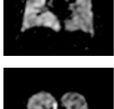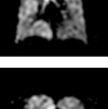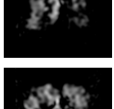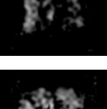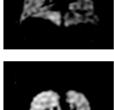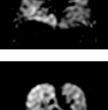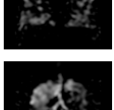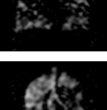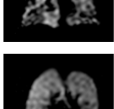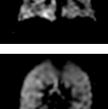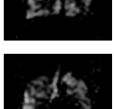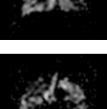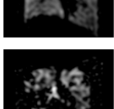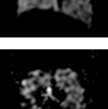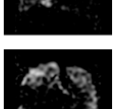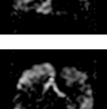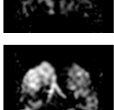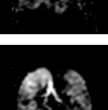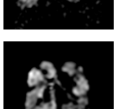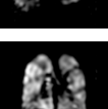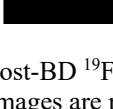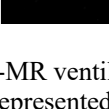
Figure 5.4: Example pre-and post-BD ^{19}F-MR ventilation images, acquired before and after administration of 2.5 mg nebulised salbutamol. Images are represented as single coronal views from an equivalent central image slice where the trachea was seen to bifurcate.

5.3.1 Global %VV measurements

%VV measurements for the 26 study patients, as calculated by each assessor, are presented in Table 5.3.

Patient		Assessor 1		Assessor 2	
		Pre-BD	Post-BD	Pre-BD	Post-BD
Asthma	1	81.7	84.6	83.5	83.9
	2	86.3	89.2	83.2	87.6
	3	96.6	97.0	95.8	96.0
	4	69.1	89.7	78.0	89.8
	5	93.4	94.1	93.9	94.9
	6	87.5	92.7	89.7	94.0
	7	75.3	77.3	75.8	77.3
	8	95.8	95.0	96.8	96.4
	9	85.9	87.7	89.6	89.8
	10	91.2	92.4	91.7	92.8
	11	95.2	95.3	95.1	95.1
	12	41.5	58.2	42.7	58.6
	13	59.3	78.5	60.6	79.5
	14	85.6	91.7	90.0	94.2
COPD	15	44.6	65.9	43.6	64.9
	16	64.7	60.3	64.0	61.5
	17	90.0	86.9	86.6	82.8
	18	89.2	85.5	91.1	88.0
	19	58.8	58.0	59.1	59.1
	20	69.2	68.2	67.9	67.7
	21	24.6	30.0	24.2	28.7
	22	78.2	70.9	74.4	69.2
	23	67.3	65.6	68.1	67.3
	24	77.6	83.8	80.4	83.5
	25	74.8	82.8	71.0	77.5
	26	37.9	44.8	40.4	45.8

Table 5.3: Calculated %VV values for patients attending Phase 3 of the LIFT study ($n = 26$).

Patients with asthma

The range of %VV values calculated across both assessors was 41.5% – 96.6% (pre-BD) and 58.2% – 97.0% (post-BD). Mean (SD) and median (IQR) pre-BD %VV values were 81.7 (15.8)% and 86.1 (73.8–93.9)% for assessor 1, and 83.3 (15.3)% and 89.7 (77.5–94.2)% for assessor 2; mean (SD) and median (IQR) post-BD %VV values were 87.4 (10.3)% and 90.7 (83.1–94.3)% for assessor 1, and 87.9 (10.4)% and 91.3 (82.8–95.0)% for assessor 2, respectively.

Patients with COPD

The range of %VV values calculated across both assessors was 24.2% – 91.1% (pre-BD) and 28.7% – 88.0% (post-BD). Mean (SD) and median pre-BD %VV values were 64.7 (20.2)% and 68.3 (48.2–78.1)% for assessor 1, and 64.2 (19.7)% and 68.0 (47.5–78.9)% for assessor 2; mean (SD) and median (IQR) post-BD %VV values were 66.9 (17.3)% and 67.1 (58.6–83.6)% for assessor 1, and 66.3 (16.8)% and 67.5 (59.7–81.5)% for assessor 2, respectively.

5.3.2   *Inter-assessor agreement*

There was no evidence of a difference in calculated %VV values between assessors for patients with asthma ($p = 0.71_{pre-BD}$; $p = 0.71_{post-BD}$) or for patients with COPD ($p = 0.95_{pre-BD}$; $p = 0.94_{post-BD}$).

Examples of combined pre- and post-BD ^{19}F-MR image segmentations for two patients with asthma (Patients 4 and 12) and two patients with COPD (Patients 19 and 21) are presented in Figures 5.5–5.8, respectively. Inter-assessor agreement for each of the respective image segmentations is shown in yellow, while disagreement between assessors is shown in green. A high degree of spatial overlap was observed between individual assessor segmentations using the RegSeg image analysis software, with a mean (SD) Dice similarity coefficient of 0.95 (0.04) calculated across all 26 patient datasets. There was no evidence of a difference in Dice similarity coefficients for pre- and post-BD image segmentations ($Dice_{pre-BD} = 0.95$ (0.05); $Dice_{post-BD} = 0.96$ (0.02); $p = 0.29$). However, inter-assessor agreement in image segmentations was significantly improved for patients with asthma compared to patients with COPD ($Dice_{asthma} = 0.97$ (0.01); $Dice_{COPD} = 0.94$ (0.05); $p = 0.01$).
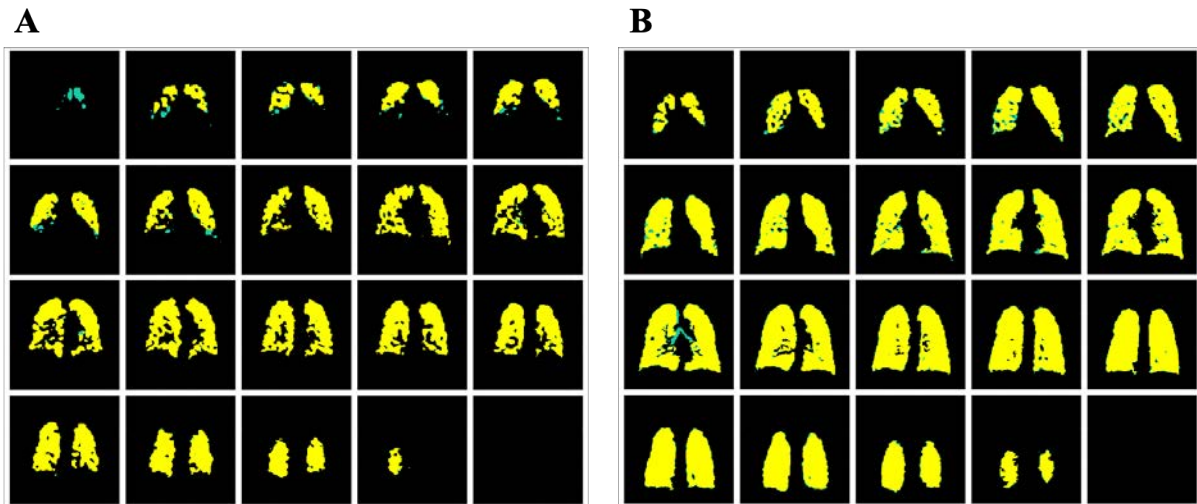
Figure 5.5: Combined ^{19}F-MR image segmentations performed independently by the two assessors in a patient with asthma (Patient 4: 64 year old female, $FEV_1/FVC_{pre-BD} = 2.00/2.94$; $FEV_1/FVC_{post-BD} = 2.45/3.57$). Pre-BD image segmentations are shown in **(A)**; post-BD image segmentations are shown in **(B)**. Agreement between assessors is shown in yellow; disagreement is shown in green. There was close agreement between the assessors for both pre-BD and post-BD segmentations in this patient (Dice similarity coefficient = 0.98_{pre-BD} and $0.97_{post-BD}$). SNR measurements in this patient were 6.9 (pre-BD) and 10.7 (post-BD), respectively.
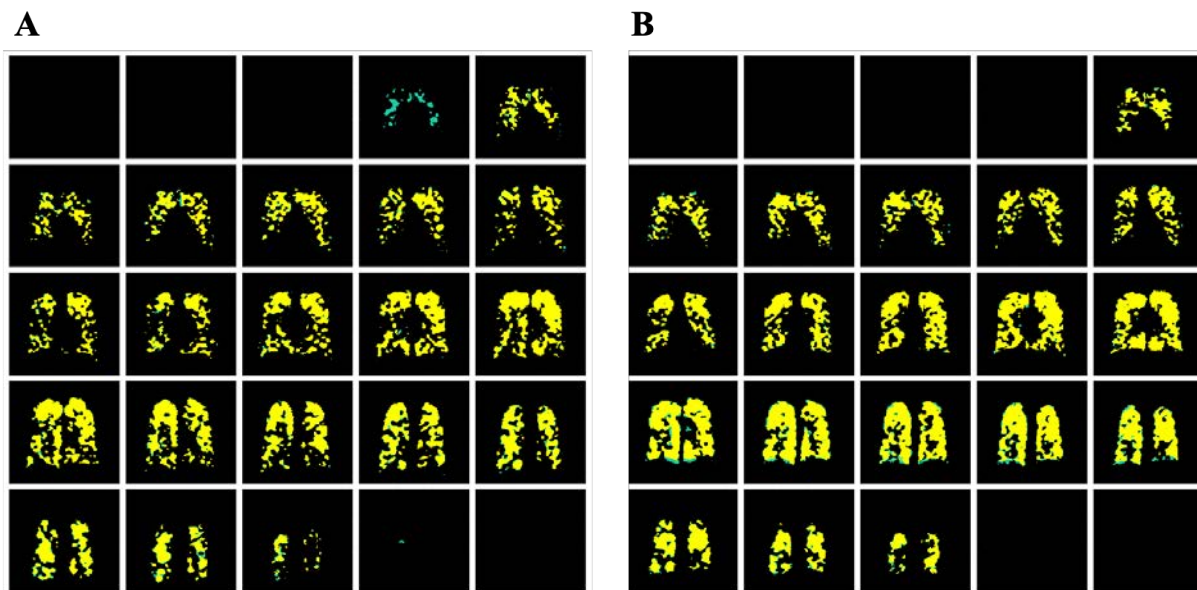
Figure 5.6: Combined ^{19}F-MR image segmentations performed independently by the two assessors in a different patient with asthma (Patient 12: 56 year old male, $FEV_1/FVC_{pre-BD} = 1.84/3.64$; $FEV_1/FVC_{post-BD} = 2.71/5.12$). Pre-BD image segmentations are shown in **(A)**; post-BD image segmentations are shown in **(B)**. Agreement between assessors is shown in yellow; disagreement is shown in green. There was slightly reduced but still close agreement between the assessors for both pre- and post-BD segmentations in this patient (Dice similarity coefficient = 0.95_{pre-BD} and $0.96_{post-BD}$). SNR measurements in this patient were 4.5 (pre-BD) and 5.6 (post-BD), respectively.

A

B
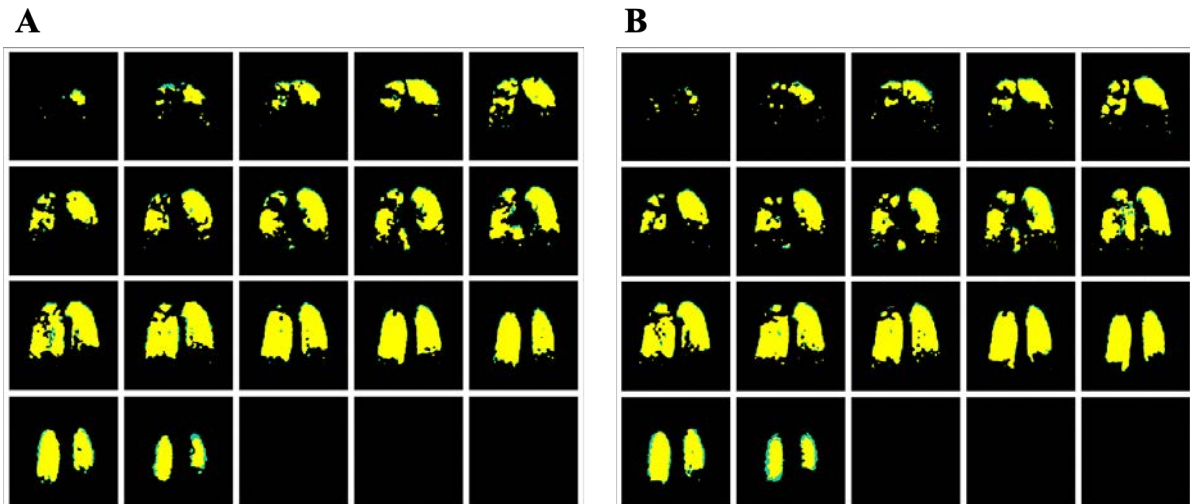
Figure 5.7: Combined ^{19}F-MR image segmentations performed independently by the two assessors in a patient with COPD (Patient 19: 66 year old female, $FEV_1/FVC_{pre-BD} = 0.63/1.84$; $FEV_1/FVC_{post-BD} = 0.68/1.96$). Pre-BD image segmentations are shown in **(A)**; post-BD image segmentations are shown in **(B)**. Agreement between assessors is shown in yellow; disagreement is shown in green. There was good agreement between the assessors for both pre-BD and post-BD segmentations in this patient (Dice similarity coefficient = 0.95_{pre-BD} and $0.95_{post-BD}$). SNR measurements in this patient were 6.5 (pre-BD) and 5.0 (post-BD), respectively.

A

B
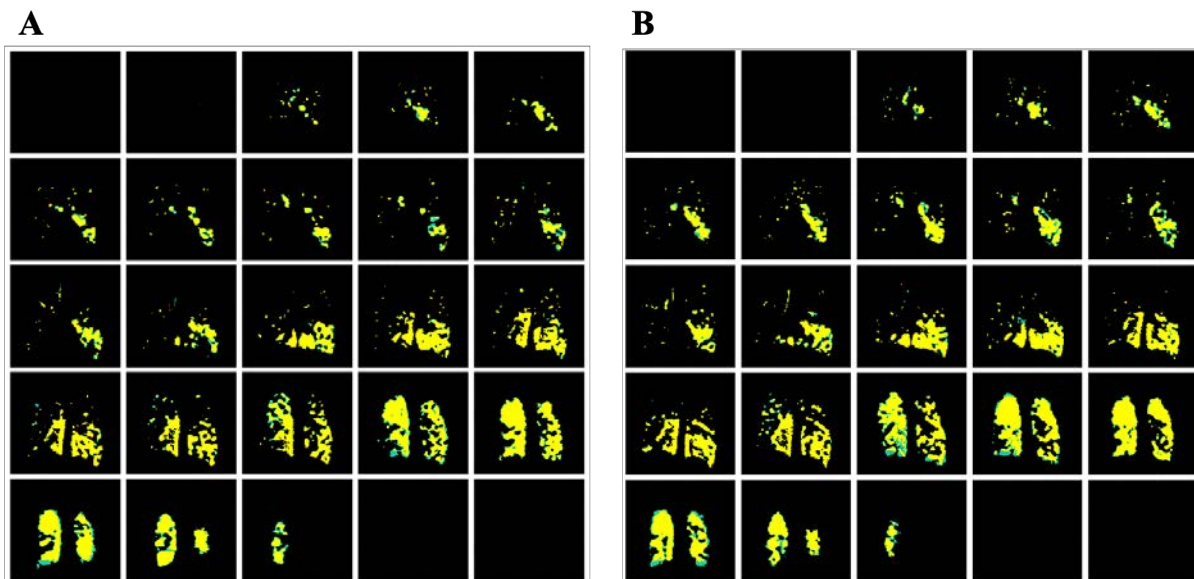
Figure 5.8: Combined ^{19}F-MR image segmentations performed independently by the two assessors in a different patient with COPD (Patient 21: 60 year old male, $FEV_1/FVC_{pre-BD} = 0.54/1.95$; $FEV_1/FVC_{post-BD} = 0.62/2.44$). Pre-BD image segmentations are shown in **(A)**; post-BD image segmentations are shown in **(B)**. Agreement between assessors is shown in yellow; disagreement is shown in green. There was increased discrepancy between the assessors for both pre- and post-BD segmentations in this patient (Dice similarity coefficient = 0.91_{pre-BD} and $0.92_{post-BD}$), likely reflecting the reduced SNR in this patient compared to other images ($SNR_{pre-BD} = 1.2$; $SNR_{post-BD} = 1.4$).

5.3.3 Comparison of %VV measurements between patients and healthy volunteers

Figure 5.9 shows a comparison of pre-BD %VV measurements acquired in patients with asthma ($n = 14$) and patients with COPD ($n = 12$), alongside %VV measurements acquired in healthy volunteers during Phase 2 of the LIFT study ($n = 38$). Calculated %VV values were averaged across both assessors to provide a single value per study participant. Results are presented as box and whisker plots, with individual values (where visible) represented by (●). Boxes indicate the IQR with group medians represented by horizontal lines; whiskers indicate the maximum and minimum values recorded, respectively.
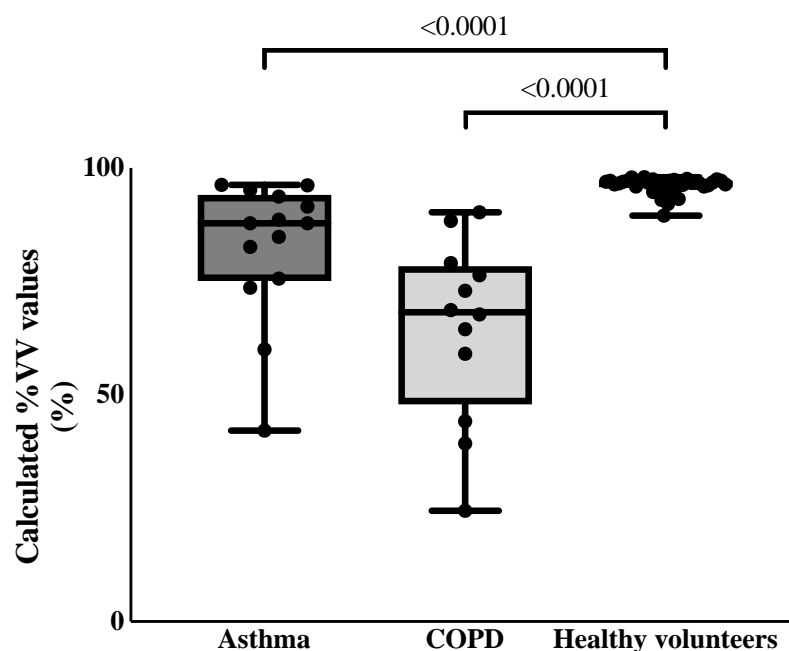
Figure 5.9: Comparison of pre-BD %VV values acquired in patients with asthma and patients with COPD, alongside %VV values acquired in healthy volunteers during Phase 2 of the LIFT study. Box plots show the IQR with group medians represented by horizontal lines. Individual values, where visible, are represented by (●). Whiskers indicate the maximum and minimum values recorded, respectively. *P*-values, reflecting differences between healthy volunteer and patient %VV values, are included.

Mean (SD) and median (IQR) pre-BD %VV values, averaged across both assessors, were 82.5 (15.5)% and 87.8 (75.1–94.1)% for patients with asthma, and 64.5 (19.9)% and 68.2 (47.8–78.3)% for patients with COPD, respectively. %VV values acquired in healthy volunteers (mean (SD) = 96.1 (1.8)%; median (IQR) = 96.7 (95.8–97.2)%) differed significantly from pre-BD %VV values acquired in patients with asthma ($p < 0.0001$) and in patients with COPD ($p < 0.0001$). Pre-BD %VV values acquired in patients with asthma also differed significantly from %VV values acquired in patients with COPD ($p = 0.01$).

5.3.4   Comparison of pre- and post-BD ^{19}F-MRI measurements

%VV values

Figure 5.10 shows a comparison of paired pre- and post-BD %VV measurements, averaged across both assessors, acquired in patients with asthma (Figure 5.10A) and patients with COPD (Figure 5.10B), respectively.
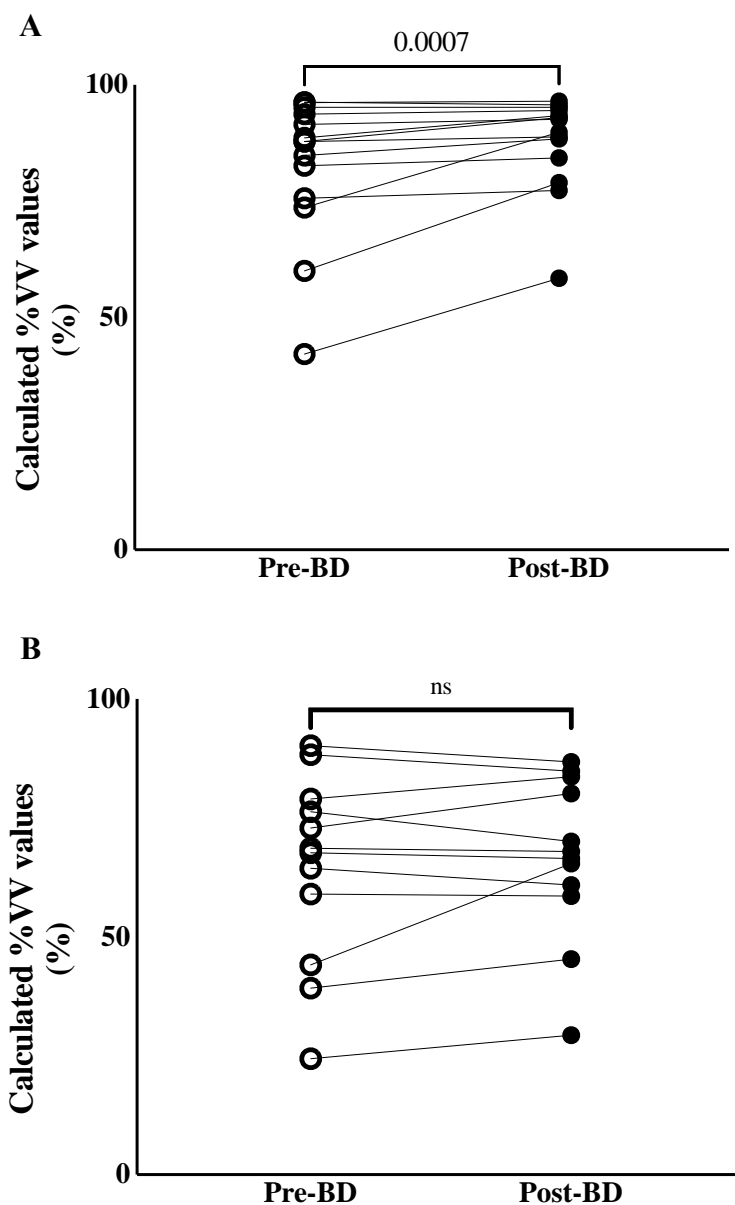
Figure 5.10: Comparison of pre- and post-BD %VV measurements acquired in (**A**) patients with asthma and (**B**) patients with COPD. A significant difference between pre- and post-BD values was observed for patients with asthma ($p = 0.0007$), but not for patients with COPD (ns = not significant).

Mean (SD) and median (IQR) post-BD values, averaged across both assessors, were 87.6 (10.3)% and 91.2 (82.9–94.7)% for patients with asthma, and 66.7 (17.0)% and 67.2 (59.1–

82.8)% for patients with COPD, respectively. A significant difference between pre- and post-BD %VV values was observed for patients with asthma ($p = 0.0007$); however, there was no evidence of a difference between pre- and post-BD %VV values for patients with COPD ($p = 0.35$).

SNR values

Figure 5.11 shows a comparison of SNR values calculated from pre- and post-BD ^{19}F-MR ventilation images acquired in patients with asthma (Figure 5.11A) and patients with COPD (Figure 5.11B), respectively.
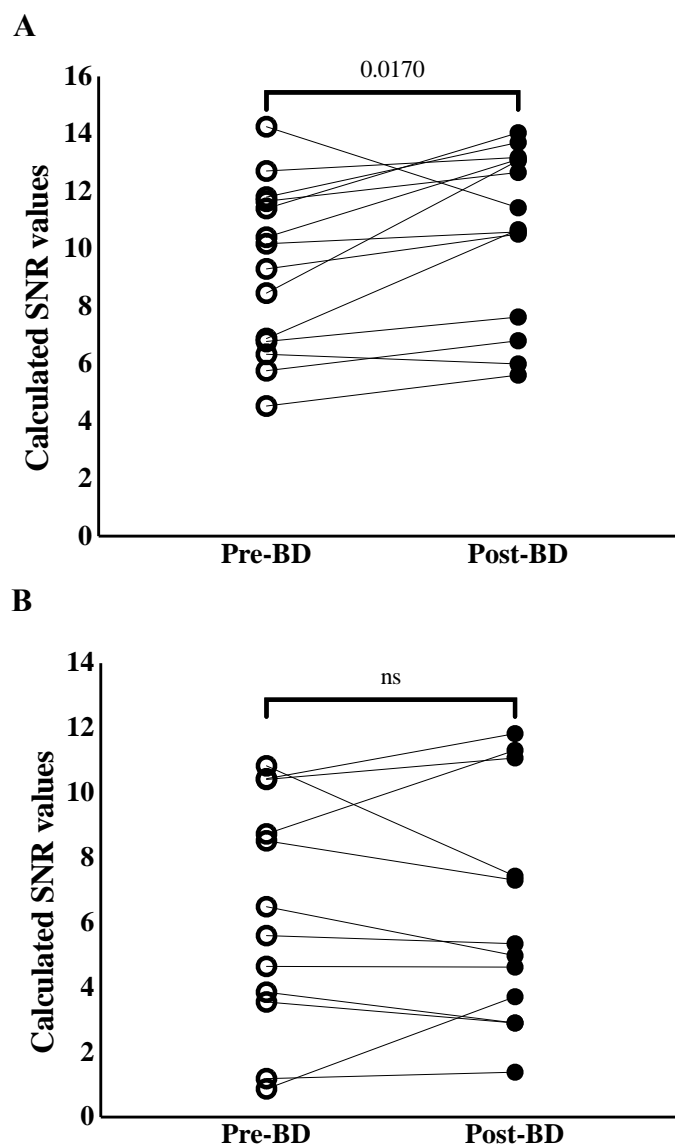
Figure 5.11: Comparison of pre- and post-BD SNR measurements acquired in (**A**) patients with asthma and (**B**) patients with COPD. A significant difference between pre- and post-BD values was observed for patients with asthma ($p = 0.017$), but not for patients with COPD (ns = not significant).

Mean (SD) pre-BD SNR values were 9.3 (2.9) for patients with asthma (range = 4.5–14.3) and 6.3 (3.5) for patients with COPD (range = 0.9–10.8). Mean (SD) post-BD SNR values were 10.7 (2.9) for patients with asthma (range = 5.6–13.7) and 6.2 (3.6) for patients with COPD (range = 1.4–11.8). Independent samples t-tests revealed a significant difference between the SNR values acquired in patients with asthma and patients with COPD ($p = 0.024_{pre-BD}$ and $p = 0.002_{post-BD}$, respectively). Paired samples t-tests revealed a significant difference between pre- and post-BD SNR values acquired in patients with asthma ($p = 0.017$), but no evidence of a difference between pre- and post-BD SNR values acquired in patients with COPD ($p = 0.96$).

^{19}F-MR ventilation images

Figures 5.12A and 5.12C show single coronal slices from representative pre- and post-BD 3D ^{19}F-MRI datasets in one patient with asthma (Patient 14; 21 year-old female), acquired during 13.4 s breath-holds at maximal inspiration. Figures 5.12B and 5.12D demonstrate orthogonal views from the same patient, with pre-and post-BD ^{19}F-MR ventilation images (coloured) superimposed on the corresponding anatomical ^{1}H-MR images (greyscale). Improvement in regional PFP gas distribution can be visualised throughout the lung fields following administration of 2.5 mg nebulised salbutamol, corresponding to observed changes in spirometry and global %VV values.
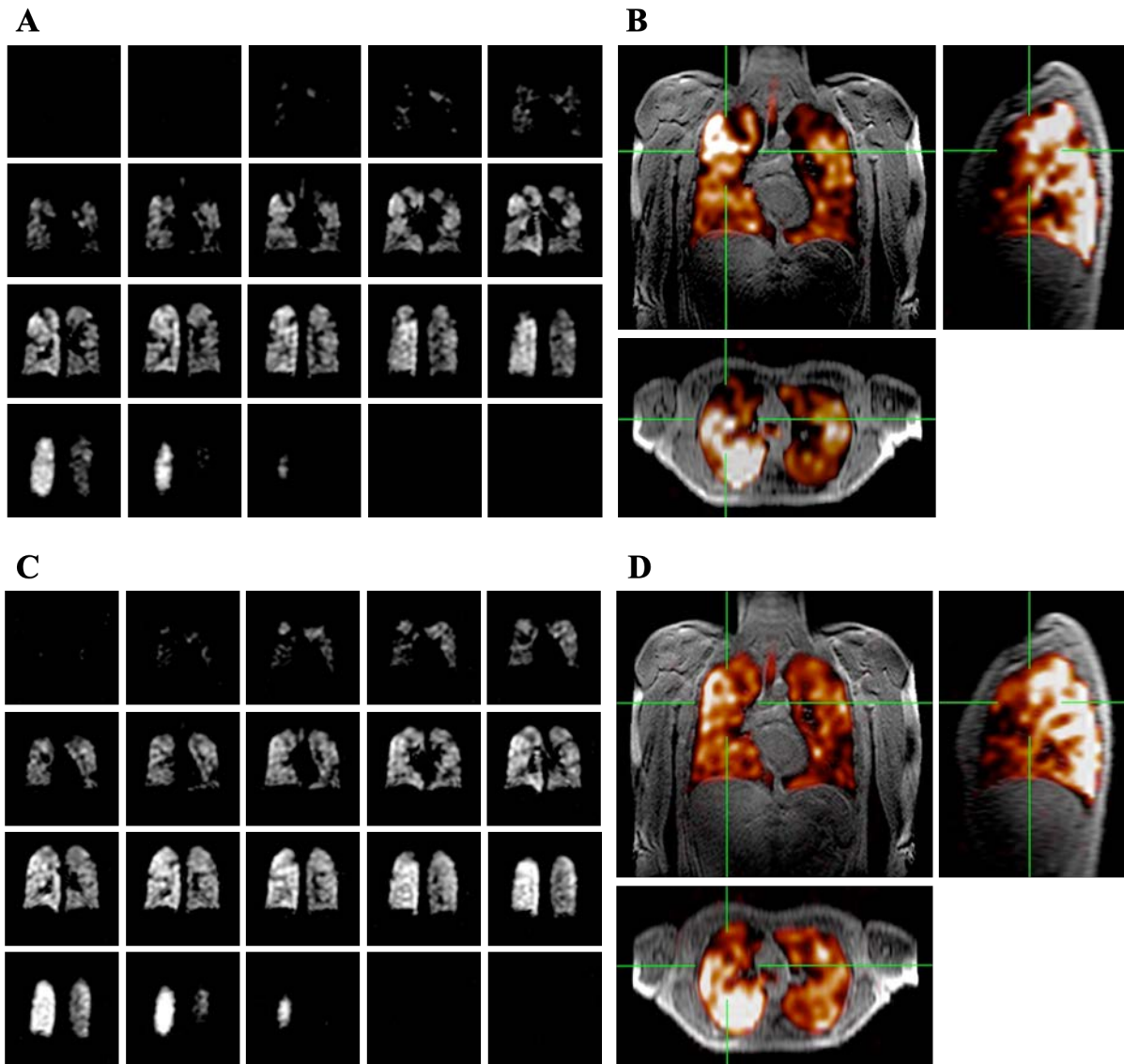
Figure 5.12: Representative pre- and post-BD ^{19}F-MR ventilation images from a patient with asthma (Patient 14), acquired during a 13.4 s breath-hold scan following three deep breaths of the 79% PFP / 21% O_2 gas mixture. **(A)** and **(C)** show full 3D datasets (coronal views) for pre- and post-BD acquisitions, respectively; **(B)** and **(D)** show orthogonal views for combined ^{1}H (greyscale) and ^{19}F ventilation images (coloured) from the same patient, demonstrating improved gas distribution following 2.5 mg nebulised salbutamol. A corresponding improvement in spirometry ($FEV_1/FVC_{pre-BD} = 1.92/3.13$; $FEV_1/FVC_{post-BD} = 3.21/4.10$) and mean calculated %VV values (%VV$_{pre-BD}$ = 87.8%; %VV$_{post-BD}$ = 93.0) was also observed.

Figure 5.13A-D illustrates analogous pre- and post-BD 3D ^{19}F-MRI datasets acquired in one patient with COPD (Patient 19; 66 year-old female). There was little apparent change in regional PFP gas distribution in this patient following administration of 2.5 mg nebulised salbutamol, reflecting the relative lack of change in global %VV and spirometric measurements.
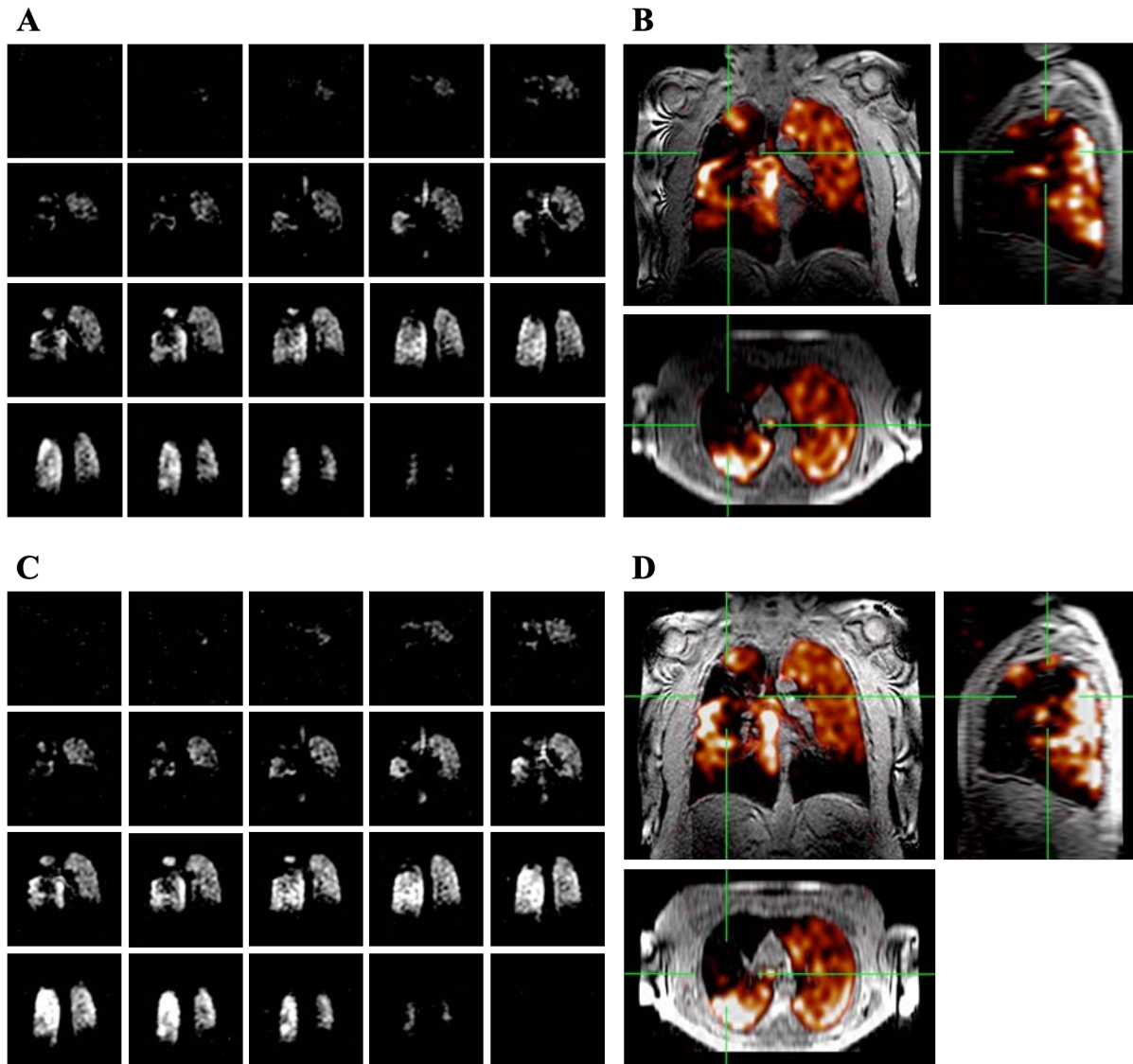
Figure 5.13: Representative pre- and post-BD ^{19}F-MR ventilation images from a patient with COPD (Patient 19), acquired during a 13.4 s breath-hold scan following three deep breaths of the 79% PFP / 21% O_2 gas mixture. **(A)** and **(C)** show full 3D datasets (coronal views) for pre- and post-BD acquisitions, respectively; **(B)** and **(D)** show orthogonal views for combined ^{1}H (greyscale) and ^{19}F ventilation images (coloured) from the same patient. There was little variation in regional gas distribution following 2.5 mg nebulised salbutamol in this patient, corresponding to the relative lack of change in spirometry ($FEV_1/FVC_{pre-BD} = 0.63/1.84$; $FEV_1/FVC_{post-BD} = 0.68/1.96$) and mean calculated %VV values (%$VV_{pre-BD} = 58.4\%$; %$VV_{post-BD} = 59.1\%$).

5.3.5 Comparison of %VV and spirometric measurements

Pre- and post-BD spirometric measurements (namely, FEV_1, FVC, and FEV_1/FVC) for each of the 26 study patients are presented in Table 5.4. All post-BD measurements were performed at an interval of 20 minutes following completion of nebulised salbutamol (2.5 mg).

Patient		FEV₁		FVC		FEV₁/FVC (%)	
		Pre-BD	Post-BD	Pre-BD	Post-BD	Pre-BD	Post-BD
Asthma	1	2.49 (102)	2.63 (108)	3.14 (101)	3.09 (100)	79.2	85.3
	2	2.21 (76)	2.42 (83)	2.70 (72)	2.82 (75)	81.9	85.9
	3*	3.79 (74)	4.24 (83)	5.45 (90)	5.45 (90)	69.6	77.7
	4*†	2.00 (80)	2.45 (98)	2.94 (91)	3.57 (111)	67.9	68.7
	5	2.56 (109)	2.75 (117)	3.29 (109)	3.50 (116)	77.7	78.6
	6	1.14 (48)	1.23 (52)	2.72 (91)	2.83 (95)	41.9	43.5
	7*†	0.91 (40)	1.10 (48)	1.63 (55)	1.96 (66)	56.0	56.1
	8*	2.23 (79)	2.51 (89)	2.88 (81)	3.07 (87)	77.5	81.6
	9	3.40 (109)	3.56 (114)	4.53 (111)	4.50 (111)	76.7	79.1
	10*†	1.50 (47)	1.93 (61)	3.14 (78)	3.56 (88)	47.8	54.3
	11*	3.33 (73)	4.13 (91)	5.75 (107)	6.01 (112)	58.0	68.7
	12*†	1.84 (49)	2.71 (72)	3.64 (75)	5.12 (105)	50.7	53.0
	13*†	1.39 (45)	2.13 (68)	3.21 (78)	4.24 (102)	43.2	50.1
	14*†	1.92 (59)	3.21 (99)	3.13 (62)	4.10 (110)	61.5	78.4
COPD	15†	0.66 (22)	0.76 (25)	2.14 (54)	2.81 (71)	30.9	27.2
	16†	0.93 (28)	1.12 (34)	3.47 (82)	4.20 (99)	26.8	26.6
	17	0.87 (33)	0.89 (34)	2.77 (78)	2.96 (84)	31.5	29.9
	18	1.45 (48)	1.60 (52)	3.50 (87)	3.63 (90)	41.3	43.9
	19	0.63 (31)	0.68 (34)	1.84 (72)	1.96 (77)	34.2	34.5
	20†	0.61 (32)	0.63 (33)	1.51 (62)	1.77 (72)	40.0	35.9
	21†	0.54 (16)	0.62 (18)	1.95 (44)	2.44 (55)	27.8	25.5
	22†	0.74 (39)	0.86 (45)	1.63 (67)	2.20 (90)	45.4	38.9
	23	1.59 (49)	1.63 (51)	3.81 (90)	3.71 (87)	41.7	43.9
	24*†	1.01 (48)	1.23 (58)	2.56 (94)	3.02 (111)	39.4	40.6
	25	0.92 (43)	1.04 (49)	2.62 (96)	2.66 (98)	35.2	39.1
	26†	1.19 (41)	1.21 (42)	3.26 (85)	3.71 (96)	36.4	32.5

Table 5.4: Pre- and post-BD spirometric measurements acquired in patients attending Phase 3 of the LIFT study (n = 26). FEV_1 and FVC measurements are presented as absolute values (in L) with % predicted values shown in parentheses.
[*] Patients demonstrating a clinically significant BD response according to BTS/SIGN guidelines (BTS, 2019), defined as an increase in FEV_1 of ≥ 12% and ≥ 200 ml as an absolute value compared to pre-BD measurements.
[†] Patients demonstrating a clinically significant BD response according to ERS/ATS guidelines (Pellegrino *et al.*, 2005), defined as an increase in **either** FEV_1 **or** FVC of ≥ 12% and ≥ 200 ml as an absolute value compared to pre-BD measurements.

%VV values were averaged across both assessors to provide a single pre- and post-BD value, allowing comparison of %VV measurements with pre- and post-BD spirometric measurements across the 26 study patients.

Patients with asthma (*n* = 14)

Pearson correlation analysis revealed moderate associations between pre-BD %VV values and % predicted FEV_1 ($r = 0.42$; $p = 0.14$), % predicted FVC ($r = 0.35$; $p = 0.21$) and FEV_1/FVC ($r = 0.42$; $p = 0.14$). Slightly weaker associations were observed between post-BD %VV values and % predicted FEV_1 ($r = 0.32$; $p = 0.27$), % predicted FVC ($r = 0.09$; $p = 0.77$) and FEV_1/FVC ($r = 0.42$; $p = 0.14$).

Patients with COPD (*n* = 12)

Pearson correlation analysis revealed stronger associations between pre-BD %VV values and % predicted FEV_1 ($r = 0.65$; $p = 0.02$), % predicted FVC ($r = 0.60$; $p = 0.04$) and FEV_1/FVC ($r = 0.51$; $p = 0.09$). Similar associations were observed between post-BD %VV values and % predicted FEV_1 ($r = 0.65$; $p = 0.02$), % predicted FVC ($r = 0.56$; $p = 0.06$) and FEV_1/FVC ($r = 0.58$; $p = 0.05$).

Patients (*n* = 26) and healthy volunteers (*n* = 38)

Pre-BD %VV values were combined with %VV values acquired in healthy volunteers during Phase 2 of the LIFT study (averaged across both assessors to provide a single value per participant), enabling a comparison of the wider range of %VV measurements with corresponding spirometric measurements. Pearson correlation analysis revealed a strong positive association between %VV and % predicted FEV_1 ($r = 0.78$; $p < 0.0001$), % predicted FVC ($r = 0.66$; $p < 0.0001$) and FEV_1/FVC ($r = 0.77$; $p < 0.0001$).

The relationship between these parameters is illustrated in Figure 5.14.
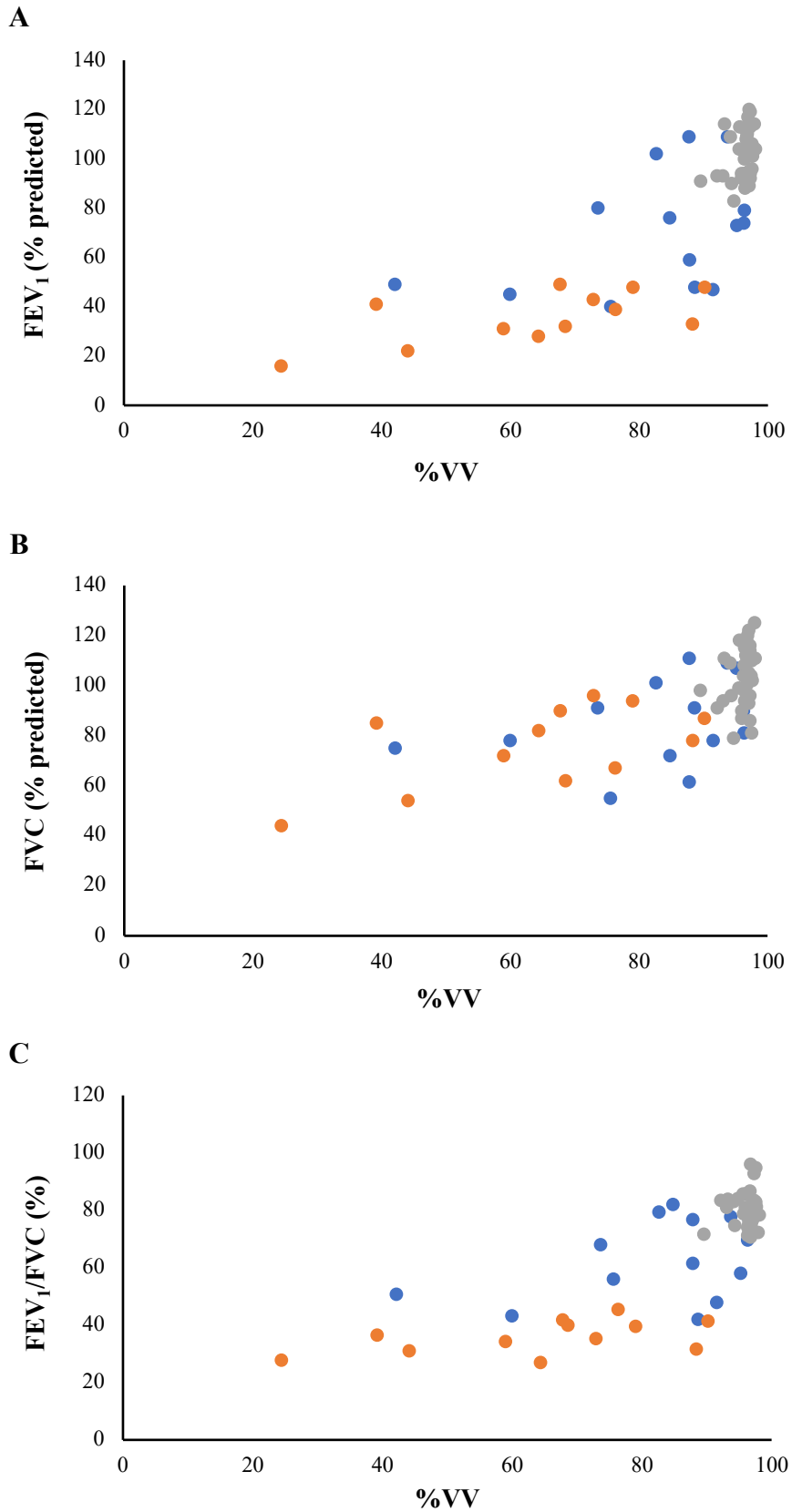
Figure 5.14: Associations between calculated %VV values (pre-BD) and **(A)** % predicted FEV$_1$, **(B)** % predicted FVC, and **(C)** FEV$_1$/FVC. Orange markers represent patients with COPD; blue markers represent patients with asthma. Grey markers represent healthy volunteers attending Phase 2 of the LIFT study (see Chapter 4) and are included for comparison.

The mean difference between pre- and post-BD %VV values was 5.1% (range = 0.3% – 19.1%; median = 1.7%) for patients with asthma and 2.1% (range = -0.6% – 21.3%; median = -0.5%) for patients with COPD. The percentage change (%Δ) in %VV measurements was calculated as 8.2% (range = 0.3% – 38.7%; median = 2.2%) for patients with asthma and 6.3% (range = -0.9% – 48.3%; median = -0.8%) for patients with COPD, respectively.

A visual representation of the %Δ in pre- and post-BD %VV values compared to corresponding changes in spirometric indices (namely, %Δ in FEV_1, %Δ in FVC and %Δ in FEV_1/FVC) is shown in Figure 5.15. Box and whisker plots illustrate the mean (×) and median (horizonal lines) percentage change within the interquartile range; individual values beyond 1.5 times the interquartile range are represented by single points (•).

Pearson correlation analysis across all 26 study patients revealed moderately strong associations between %Δ in %VV and %Δ in FEV_1 ($r = 0.4$; $p = 0.04$) and %Δ in FVC ($r = 0.58$; $p = 0.002$), but not with %Δ in FEV_1/FVC ($r = -0.09$; $p = 0.63$). For patients with asthma, the associations between %Δ in %VV and %Δ in FEV_1 ($r = 0.59$; $p = 0.03$) and %Δ in FVC ($r = 0.81$; $p = 0.0005$) were stronger. Weaker associations were observed between %Δ in %VV and %Δ in FEV_1 ($r = 0.16$; $p = 0.63$), %Δ in FVC ($r = 0.38$; $p = 0.23$) and %Δ in FEV_1/FVC ($r = -0.31$; $p = 0.33$) for patients with COPD.

The relationship between these parameters is illustrated in Figure 5.16.

A

B
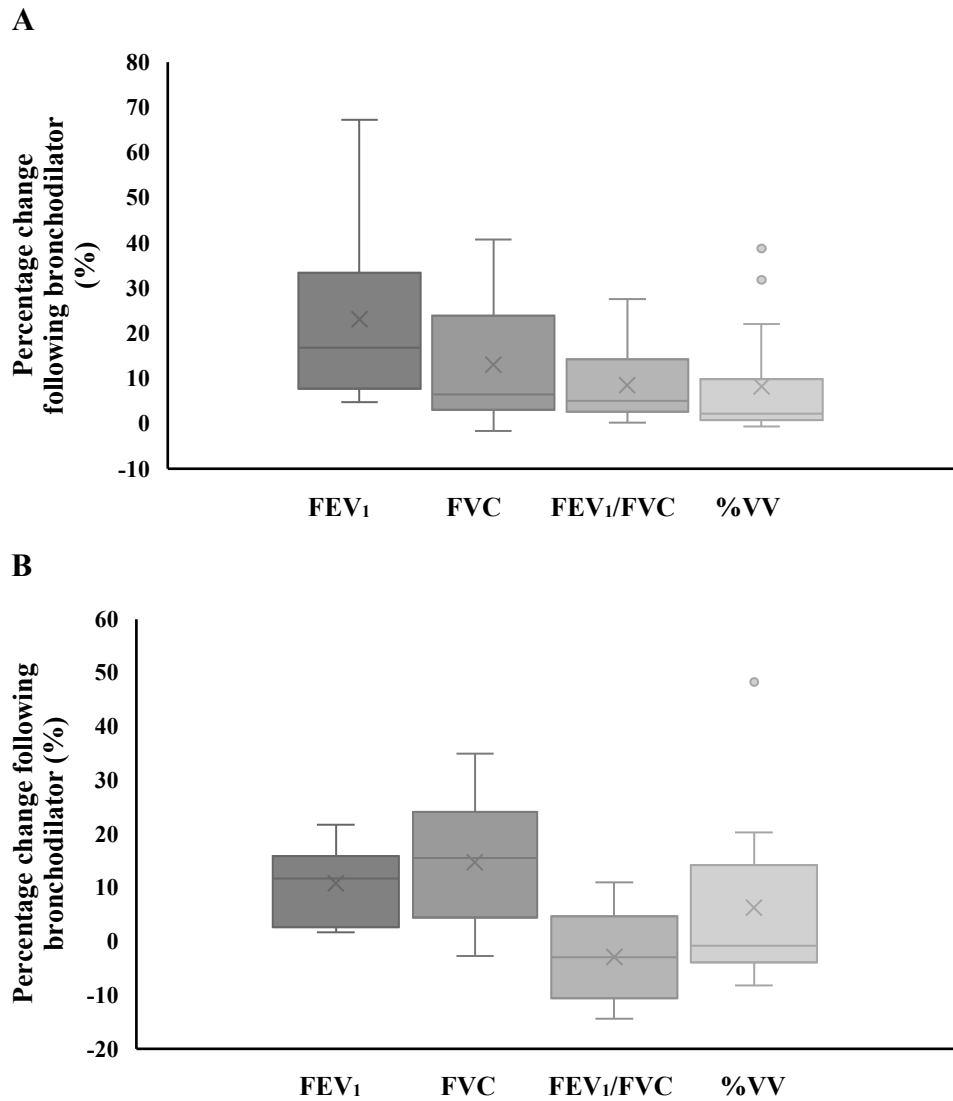
Figure 5.15: Visual representation of the percentage change (%Δ) in %VV and spirometric indices following BD administration (2.5 mg nebulised salbutamol) in **(A)** patients with asthma and **(B)** patients with COPD. The mean %Δ for patients with asthma was: %VV = 8.2%; FEV_1 = 23.1%; FVC = 13.0%; FEV_1/FVC = 8.5%. The mean %Δ for patients with COPD was: %VV = 6.3%; FEV_1 = 10.8%; FVC = 14.8%; FEV_1/FVC = -2.9%.
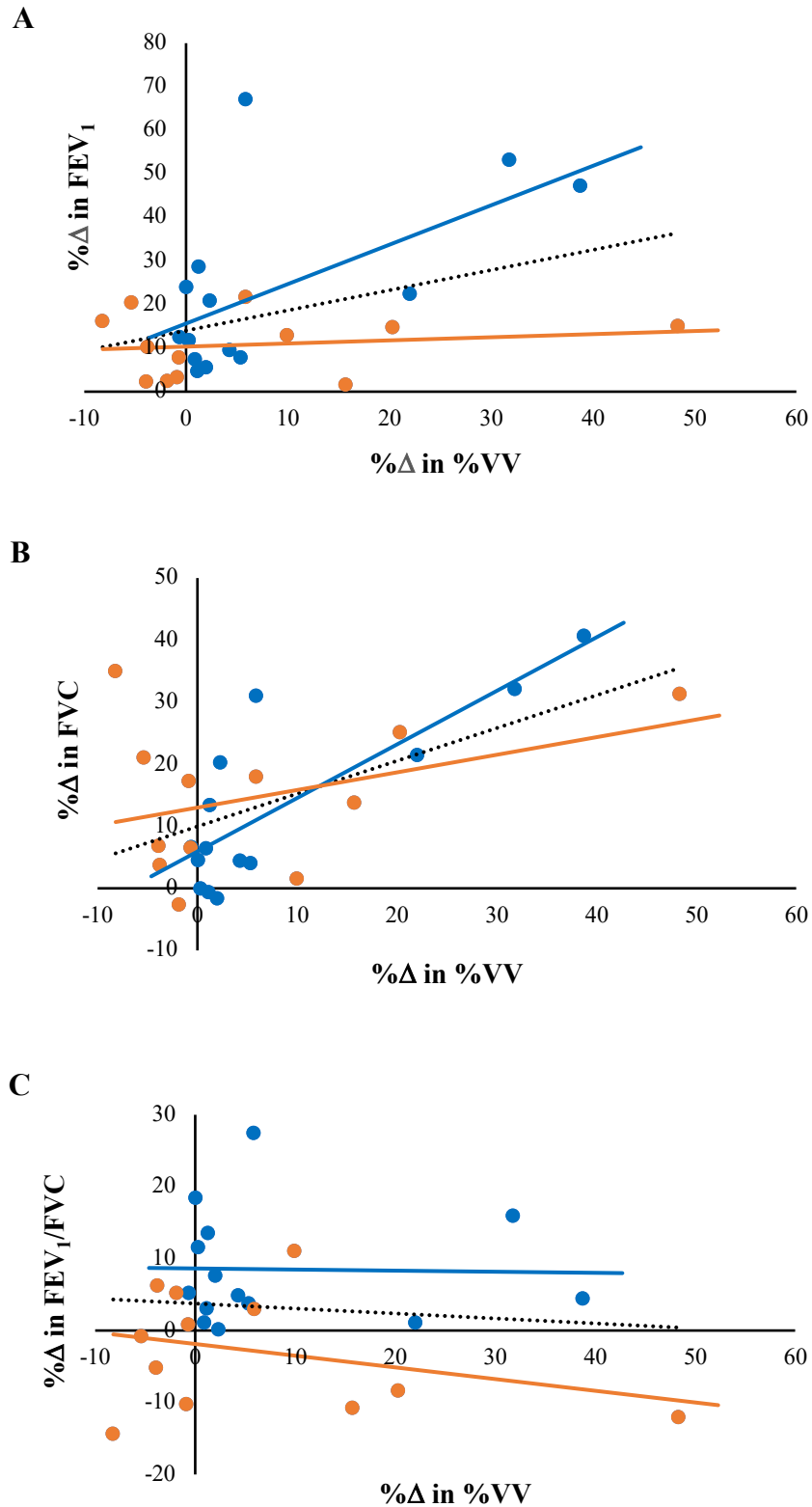
Figure 5.16: Associations between the percentage change (%Δ) in %VV and %Δ in spirometric indices: **(A)** %Δ in FEV_1; **(B)** %Δ in FVC; **(C)** %Δ in FEV_1/FVC. Orange markers represent patients with COPD; blue markers represent patients with asthma. Lines of best fit illustrate the relationships that exist for each patient group separately (orange = COPD; blue = asthma) and combined (dotted black line).

5.4   Discussion

The primary purpose of Phase 3 of the LIFT study was to assess the utility of static ^{19}F-MR ventilation imaging to provide quantitative measures of pulmonary ventilation in patients with respiratory disease. The work presented in this chapter has demonstrated the ability to apply ^{19}F-MRI scan procedures to detect regional gas distribution in patients with asthma and patients with COPD, and to quantify potential differences using %VV measurements. To date, this represents the first study to report on %VV measurements acquired by ^{19}F-MRI of inhaled PFP in a patient population.

In agreement with previous HP-MRI studies (e.g. Ebner *et al.*, 2017b; Stewart *et al.*, 2018), the findings presented in Section 5.3.2 support the hypothesis that %VV values, as acquired by ^{19}F-MRI of inhaled PFP, are reduced in patients with asthma and patients with COPD compared to healthy volunteers. Specifically, the pre-BD %VV values calculated in patients with asthma (mean = 82.5%) and patients with COPD (mean = 64.5%) differed significantly from equivalent %VV values acquired in healthy volunteers during Phase 2 of the LIFT study (mean = 96.1%). Crucially, the same MRI scan procedures and approach to semi-automated image segmentation were implemented for each of the three study groups, confirming the suitability of the adopted study methods to identify impaired ventilation (i.e. gas distribution) associated with underlying pathology. It is important to recognise, however, that the observed differences in %VV measurements are likely to be influenced by the particular characteristics of the participants recruited to this study, including the older age of patients compared with healthy volunteers. Notably, all patients with COPD had severe disease as determined by spirometry ($FEV_1 < 50\%$ predicted) (GOLD, 2020) with evidence of emphysema on previous CT imaging. Similarly, all patients with asthma required regular therapy comprising *at least* a moderate dose inhaled corticosteroid and a long-acting bronchodilator; the majority of patients ($n = 11$) were taking two or more long-acting bronchodilators, with several ($n = 4$) also receiving biologic agents (1 omalizumab; 3 mepolizumab), indicating severe disease (BTS, 2019). The range of FEV_1 values reported for patients with asthma (see Table 5.4) likely reflects the differences in severity between participants. By comparison, the healthy volunteers recruited to Phase 2 of the LIFT study all had well-preserved lung function (see Chapter 4, Table 4.2). As such, it is unsurprising that differences in %VV measurements were identified between the respective study groups, building on preliminary work conducted during Phase 1 of the study (Chapter 3, Section 3.5).

The ability of the adopted scan procedures to detect differences in regional gas distribution in patients with less overt disease (e.g. mild or moderate COPD) is less certain and was beyond the scope of this study. Nonetheless, a review of data acquired in patients with asthma suggests that in cases where spirometric measurements were relatively preserved, %VV values may still point towards underlying disease. In particular, the %VV values acquired in Patients 1, 5 and 9 were all reduced compared to equivalent values reported in healthy volunteers, despite the observation of supra-normal spirometric indices in these patients. This finding is in agreement with previous work involving HP-MRI, where it has been suggested ventilated lung volume measurements offer improved sensitivity to detect subclinical disease compared to conventional spirometry (Pike *et al.*, 2015; Marshall *et al.*, 2017). Conversely, the %VV values acquired in Patients 3, 8 and 11 (which were all comparable to values acquired in healthy volunteers) failed to identify the slightly reduced spirometric measurements observed in these patients.

The relationship between reported %VV measurements and spirometric indices is therefore not entirely straightforward, despite the positive associations demonstrated in Figure 5.14. This may reflect fundamental differences in the physiological measurements being acquired (i.e. air flow during spirometry, compared to lung volumes during ^{19}F-MRI), as well as inherent factors relating to %VV calculation (e.g. use of a pre-determined signal threshold that underpins sensitivity to detect PFP gas distribution). Of note, Ebner *et al.* (2017b) reported similar disparity between FEV_1 measurements and ^{129}Xe ventilation defects in patients with asthma; the authors conclude that, while detection of gas signal relies on distribution throughout the entire bronchial tree, FEV_1 is influenced predominantly by resistance in the larger airways (see Bossé *et al.*, 2009), which may account for some of the apparent discrepancy in identifying airway obstruction. Moreover, as indicated in Chapter 3 (Section 3.3.2), the ability to perform correct breathing manoeuvres (i.e. deep inspiratory breaths) is likely to have a strong bearing on the %VV measurements acquired by ^{19}F-MRI; this is particularly relevant for patients with respiratory disease, where the anticipated increase in ventilation heterogeneity compared to healthy volunteers (see Halaweish *et al.*, 2013a) may be difficult to differentiate from poor PFP gas inhalation.

An additional focus for this study was to examine the capability of ^{19}F-MRI of inhaled PFP to quantify changes in regional gas distribution in response to BD therapy; namely, nebulised salbutamol (2.5 mg). In accordance with the initial study hypothesis, a significant

improvement in post-BD %VV values was observed in patients with asthma compared to pre-BD values, supporting findings involving ^{3}He and ^{129}Xe (Svenningsen *et al.*, 2013; Capaldi *et al.*, 2017; Horn *et al.*, 2017a). By contrast, there was no apparent difference between pre- and post-BD %VV measurements acquired in patients with COPD, despite previous studies reporting a detectable BD response within the HP-MRI literature (Kirby *et al.*, 2011; Kirby *et al.*, 2012c). This may stem from differences in the specific patient populations recruited to respective studies and/or an inherently reduced sensitivity of ^{19}F-MR ventilation imaging to detect changes in gas distribution compared to other techniques: notably, a number of patients with COPD – as well as patients with asthma – demonstrated a positive spirometric response to BD therapy according to ERS/ATS standards (see Table 5.4) but failed to show a corresponding improvement in %VV measurements. However, this effect was not borne out when using BTS criteria (BTS, 2019). It is possible that any observed changes in FEV$_1$ (and %VV) simply reflects a degree of normal biological variability, though the short timeframe between assessments (approximately 1–2 hours) makes this unlikely; a future study examining spirometric and ^{19}F-MRI measurements without BD administration, or over different days, could help to clarify this issue. An alternative explanation is that the apparent discrepancy represents a further example of inconsistent breathing manoeuvres performed by patients between respective image acquisitions. Importantly, in seven of the twelve patients evaluated with COPD, post-BD %VV measurements were *reduced* compared to corresponding pre-BD measurements, suggesting variability in gas inhalation may be a significant and limiting factor in determining true BD response in these patients.

Notwithstanding these differences, the observed changes in post-BD %VV measurements were in broad agreement with changes in spirometric measurements (namely, FEV$_1$ and FVC), as illustrated in Figure 5.16. This was particularly evident for patients with asthma, where an improvement in %VV values was seen in all but one participant (Patient 8). Nonetheless, in some instances, the magnitude of change in spirometric and %VV measurements does not appear to correspond directly. Specifically, in Patient 14 (21 year-old female), a marked improvement in FEV$_1$ was observed following BD administration (1.92 L – 3.21 L) but with a relatively modest increase in %VV measurements (87.8 – 93.0%). This could reflect differences in breathing efficacy between the different measurements, as previously discussed. Alternatively, it is possible that the use of maximal inspiratory efforts masked the true extent of initial ventilation impairment present in this participant (see Hughes *et al.*, 2019), limiting the differences observed between pre- and post-BD %VV

measurements. The criteria underpinning a positive spirometric response to BD has been well documented (Kaminsky, 2019), although there remains some controversy within published guidelines; both the Global Initiative for Asthma (2020) and BTS/SIGN (2019) propose an improvement in FEV_1 of $\geq 12\%$ and ≥ 200 ml compared to baseline, whereas the ERS/ATS adopt a slightly broader definition that includes similar changes in FVC (Pellegrino *et al.*, 2005). By contrast, there is no agreed definition regarding what constitutes a clinically significant change in %VV following BD administration. Of note, the absolute change in pre- and post-BD %VV values acquired in this study showed considerable variability, both for patients with asthma (range = 0.3% – 19.1%) and patients with COPD (range = -0.6% – 21.3%). Determining which of these measurements represents a clinically meaningful response (see Eddy *et al.*, 2018) is therefore challenging, particularly in view of the various factors influencing ^{19}F-MRI acquisitions and resultant %VV calculations; based on findings presented in Chapter 4 (Section 4.3.1), it is unlikely that a difference in %VV of $\pm 2\%$ represents anything other than measurement variability. Indeed, given the increased ventilation heterogeneity observed in patients compared to healthy volunteers, this confidence interval may be considerably wider. A more complete assessment of %VV measurement precision was beyond the scope of Phase 3 of the LIFT study, though reassuringly the inter-assessor agreement in pre-and post-BD image segmentations was high for both groups of patients examined.

The SNR measurements acquired in patients with asthma and patients with COPD were generally lower than equivalent values acquired in healthy volunteers during Phase 2 of the LIFT study (see Chapter 4, Section 4.3.3). This was not wholly unexpected, given the increased variation in gas distribution observed in patient datasets compared to healthy volunteers. For patients with COPD, this reduction in PFP signal was particularly apparent and likely contributed to the slightly increased inter-assessor variability in image segmentations generated for this group of patients; a similar effect has previously been reported in relation to segmentation of ^{129}Xe images in patients with CF exhibiting large ventilation defects (Couch *et al.*, 2019b). In conjunction with changes in %VV outlined in Section 5.3.3, the reported SNR values support an improvement in regional gas distribution (i.e. detected signal) following BD administration in patients with asthma, but not in patients with COPD. However, it is important to note that SNR measurements were calculated from a single lung region of interest, which may not be representative of gas distribution throughout

the lungs as a whole. This is especially relevant for patients with respiratory disease, who may demonstrate marked ventilation heterogeneity characterised by regions of high gas concentration (i.e. increased SNR) and regions of low – or absent – gas concentration (i.e. reduced SNR).

The regional variation in gas distribution underpins one of the central limitations of employing %VV measurements to report on pulmonary ventilation properties. Specifically, by relying on a binary classification across the entire lung (i.e. ventilated versus non-ventilated), the diversity of regional information provided by ^{19}F-MR ventilation images, including response to BD, is essentially lost. This may account for some of the disparity observed between %VV and spirometric measurements – especially in patients with COPD – where it is possible local changes in gas distribution are not reflected by a single global measurement. Efforts to establish more regional-based quantitative measures of pulmonary ventilation (e.g. Horn *et al.*, 2017) offer potential to characterise response to treatment beyond %VV, based on calculation of voxel-wise changes in the ratio of inspired gas to baseline volume. Of note, Kaireit *et al.* (2018) recently employed FD-MRI and ^{19}F-MRI methods to quantify lobar fractional ventilation (i.e. changes in end-inspiratory signal over multiple breaths) in patients with COPD, reporting good correlation with global tests of lung function. Such techniques may provide improved sensitivity to subtle localised differences in gas distribution that remain otherwise undetected, which could be invaluable in assessing the efficacy of novel therapeutic interventions. This represents an area of interest for colleagues at Newcastle University, where work is currently underway (led by Dr Mary Neal) to develop an effective non-binary image segmentation tool that can be utilised in future clinical studies.

The ability to breathe PFP continuously over several respiratory cycles has also recently been exploited as an alternative to static breath-hold imaging (Gutberlet *et al.*, 2019; McCallister *et al.*, 2021), enabling dynamic image acquisition during free breathing. This approach reduces the requirement to follow a rigid inhalation protocol (such as that employed in the LIFT study) and is an attractive option for patients with respiratory disease, or young children, who may not be able to perform effective breath-hold manoeuvres. The application of dynamic imaging to ^{19}F-MRI of inhaled PFP is examined further in the next chapter of this thesis. Nonetheless, given the widespread adoption of %VV measurements within the HP-MRI literature, the present work provides an important benchmark from which to determine the utility of static ^{19}F-MR ventilation imaging in patients with respiratory disease.

5.5   Conclusion

This study has established the capability of applying ^{19}F-MRI scan procedures to identify differences in %VV measurements between healthy volunteers, patients with asthma, and patients with COPD. The response to BD demonstrated in patients with asthma supports the efficacy of this technique to report on changes in regional gas distribution, though for patients with COPD this effect is less clear. Evaluation in a larger cohort of patients (which was reduced in this study through unforeseen circumstances related to the COVID-19 pandemic) will help to clarify the true nature of this response. Ultimately, however, the utility of static ^{19}F-MR ventilation imaging is determined by the ability to follow a specified breathing protocol which, for patients with respiratory disease, may make the distinction between true ventilation impairment and poor gas inhalation challenging. Exploring alternative approaches to assessing pulmonary ventilation properties using ^{19}F-MRI is therefore of considerable interest: this represents the focus for the following section of this thesis (Chapter 6 and Chapter 7).

Chapter 6.

Dynamic ventilation and perfusion imaging using ^{19}F-MRI and DCE-MRI: feasibility in healthy volunteers and patients with COPD

6.1   Introduction

The preceding section of this thesis (Chapters 3, 4 and 5) outlined the development and application of ^{19}F-MRI scan procedures to distinguish ventilation properties in healthy volunteers, patients with asthma, and patients with COPD. This work was conducted within the framework of the LIFT study, employing one particular methodological approach that has been widely reported within the HP-MRI literature – namely, the adoption of single breath-hold acquisitions to evaluate global %VV measurements. In this chapter, an alternative approach to ^{19}F-MR ventilation imaging is explored, utilising the favourable properties of inhaled PFP to assess regional gas wash-in and wash-out dynamics over the course of several respiratory cycles.

Previous studies have investigated the feasibility of performing dynamic measurements of gas distribution using hyperpolarised ^{3}He (Horn *et al.*, 2014b; Hamedani *et al.*, 2016). However, the irrecoverable T_1-mediated loss of hyperpolarised signal that arises from contact with paramagnetic O_2 in the lungs presents challenges for multi-breath acquisitions (Couch *et al.*, 2015), compounded by the unavoidable hardware requirements for hyperpolarisation. Alternative techniques utilising FD-MRI (e.g. Bauman *et al.*, 2009; Voskrebenzev *et al.*, 2018) enable assessment of combined ventilation and perfusion properties during free-breathing, without the need for exogenous contrast agents; yet, these approaches are reliant upon extensive post-processing to provide only an indirect measure of pulmonary function. Recently, the potential for dynamic imaging of inhaled PFP has been reported in patients with COPD (Kaireit *et al.*, 2018; Gutberlet *et al.*, 2019) and CF (Goralski *et al.*, 2020; McCallister *et al.*, 2021), permitting evaluation of a broad range of regional wash-in/wash-out rates that may not be apparent during static breath-hold images. In addition, although not currently used routinely in the assessment of lung disease, DCE-MRI is a well-established technique (see Chapter 1, Section 1.5.2) that has previously demonstrated the capacity to identify perfusion defects in a variety of respiratory pathologies (Kluge *et al.*, 2006; Hueper *et al.*, 2015; Chen *et al.*, 2018). In combination with dynamic ^{19}F-MRI, this offers scope to develop

a novel approach to pulmonary ventilation and perfusion measurement, without recourse to ionising radiation.

The aim of this study was to assess the ability to perform dynamic ^{19}F-MRI of inhaled PFP, permitting evaluation of regional pulmonary ventilation properties in patients with respiratory disease. Specifically, it was hypothesised that PFP gas wash-in and wash-out times differ between healthy volunteers and patients with COPD, and that these differences can be quantified using serial SNR and %VV measurements over the course of several respiratory cycles. Additionally, this study examined the feasibility of applying ^{19}F-MRI methods alongside DCE-MRI to facilitate combined pulmonary ventilation and perfusion imaging within a single scan session.

6.2   Methods

The work presented in this chapter was conducted within the framework of the VQ MRI study, as outlined in Chapter 2 (Section 2.3).

6.2.1   Study population

A planned sample size of ten healthy volunteers and ten patients with respiratory disease (five patients with COPD and five patients with PE) was originally chosen (see Chapter 2, Section 2.3.1). Unfortunately, in common with Phase 3 of the LIFT study, recruitment to the VQ MRI study was heavily impacted by the emergence of the COVID-19 pandemic in March 2020, resulting in a suspension to the study. This was exacerbated by an initial delay in commencing the study, stemming from a technical fault relating to the ^{19}F birdcage coil (a recurring loose solder joint), necessitating return of the coil to the manufacturer for repair. Consequently, at the time of writing, the number of participants available for inclusion in this chapter is substantially lower than originally planned (see Table 6.1).

Study group	Participant type	Planned number of participants	Actual number recruited
1 (DCE-MRI development)	Healthy volunteers	Up to 5	4
2 (^{19}F-MRI and DCE-MRI)	Patients with COPD	5	2
3 (^{19}F-MRI and DCE-MRI)	Patients with PE	5	0
4 (^{19}F-MRI and DCE-MRI)	Healthy volunteers	5	1

Table 6.1: Summary of planned recruitment numbers and actual number of participants recruited to the VQ MRI study.

In total, five healthy volunteers and two patients with COPD provided written informed consent and were screened for study eligibility at the NMRC between November 2019 and March 2020, in accordance with study recruitment criteria outlined in Chapter 2 (Section 2.3.2).

Four healthy volunteers (3 males, aged 21, 25 and 33; 1 female, aged 31) were recruited for the purpose of testing the suitability of DCE-MRI scan protocols for application in subsequent study groups. The remaining three participants (one healthy female volunteer, aged 31; two male patients with COPD, aged 68 and 76) were recruited to determine the feasibility of performing combined ventilation and perfusion imaging using the adopted DCE- and ^{19}F-MRI scan procedures.

6.2.2 MRI scan procedures

Following completion of initial screening procedures, participants had an 18-gauge cannula sited in a central antecubital fossa vein (in accordance with aseptic non-touch technique) for the purpose of administering Gadobutrol during the MRI scan session. Participants subsequently entered the MRI scanner room to undergo a single MRI scan session. All scans were performed at the NMRC on a 3.0 T scanner interfaced to an 8-element ^{1}H receive array torso coil for DCE-MRI acquisitions, and a ^{19}F/^{1}H birdcage coil for ^{19}F-MRI acquisitions (see Chapter 2, Section 2.5.2).

DCE-MRI development phase

Healthy volunteers ($n = 4$) were positioned supine on the scanner bed with the assistance of radiographer colleagues, such that the entire lung fields were contained within the centre of the torso coil (see Chapter 2, Figure 2.7).

Initial scout [1]H-MR images (coronal views) were acquired using the same multi-slice 2D gradient echo sequence applied during the LIFT study (see Chapter 4, Table 4.1), in order to confirm correct positioning within the scanner bore. Two DCE-MRI scans were subsequently performed per participant, whereby each acquisition was initiated immediately prior to administration of an intravenous dose of Gadobutrol (see Chapter 2, Section 2.5.6). This was administered by the study radiographer at a rate of 4 ml/s and a dose of either 0.05 ml/kg or 0.025 ml/kg, in line with previously published DCE-MRI studies (Swift *et al.*, 2014; Kaireit *et al.*, 2019). Participants were instructed by the study radiographer to breathe in a relaxed manner for the duration of the scan (i.e. free tidal breathing), or to perform a breath-hold at maximal inspiration for as long as possible (at least 30 s) throughout the acquisition period. This enabled determination of the most suitable breathing procedures and dose of contrast agent for application to subsequent study groups. DCE-MRI scan parameters (see Table 6.2) were optimised heuristically by qualitative assessment of image quality following the first participant, resulting in a scan protocol with acceptable temporal and spatial resolution to produce a detectable change in signal.

The final adopted DCE-MRI scan procedures are summarised in Table 6.3.

Parameter	DCE-MRI scan protocol	
	A	**B**
TE (ms)	0.58	0.62
TR (ms)	2.55	2.55
Flip angle (º)	12	12
FOV (mm^3)	$420 \times 420 \times 200$	$420 \times 385 \times 200$
Resolution (mm^3)	$5 \times 5 \times 10$	$2.91 \times 2.91 \times 10$
BW (Hz/pixel)	1500	1500
Number of dynamics	30	30
Acquisition time (s)	27	58
SENSE acceleration factor[*]	2×2	1.1×2
Keyhole acceleration factor[†]	50%	35%

Table 6.2: Summary of the scan parameters applied during initial testing of DCE-MRI scan procedures. Protocol B was subsequently considered most suitable for application in the remaining study participants.
[*] Acceleration via parallel imaging (i.e. using multiple signal channels simultaneously to acquire an image).
[†] Acceleration via dynamic partial data sampling (i.e. a sub-sampled dataset is acquired).

Participant	DCE-MRI (Scan 1)			DCE-MRI (Scan 2)		
	Protocol tested	**Dose (mmol/kg)**	**Breathing instruction**	**Protocol tested**	**Dose (mmol/kg)**	**Breathing instruction**
1	A	0.05	Breath-hold	A	0.025	Breath-hold
2	B	0.05	Breath-hold	B	0.05	Free breathing
3	B	0.05	Free breathing	B	0.025	Free breathing
4	B	0.05	Breath-hold	B	0.05	Free breathing

Table 6.3: Summary of the DCE-MRI scan procedures tested in study group 1 (four healthy volunteers). The final adopted scan procedures implemented in the remaining study groups are indicated (shaded in grey).

Following completion of the MRI scan session, participants were removed from the MRI scanner and observed for a period of 30 minutes to ensure that there were no delayed reactions to GBCA administration. The intravenous cannula was subsequently removed, prior to participants leaving the study centre.

Application of DCE-MRI and dynamic ^{19}F-MRI

For the remaining three study participants (one healthy volunteer and two patients with COPD) the MRI scan session was split into two parts. The first part involved positioning participants on the scanner bed and performing initial scout MRI scans as outlined above, followed by a single DCE-MRI scan. This was performed according to the scan procedures

established during the initial development phase (i.e. Protocol B, applied during free-breathing with a dose of 0.05 mmol/kg Gadobutrol). Participants were then briefly removed from the scanner to enable substitution of the torso coil with the ^{19}F/^{1}H birdcage coil, before being re-positioned on the scanner bed for the second part of the scan session (^{19}F-MR ventilation imaging). Scout ^{1}H-MRI scans were repeated to confirm correct positioning within the scanner bore. Anatomical ^{1}H-MRI scans were subsequently acquired after instructing participants to perform a breath-hold at maximal inspiration (i.e. TLC), using the same 3D SPGR sequence adopted during the LIFT study (Chapter 4, Table 4.1). Participants were then instructed to inhale the 79% PFP / 21% O_2 gas mixture on up to four occasions (where the fourth gas inhalation session provided a 'failsafe' in the event of a problem arising during one of the first three gas inhalation sessions). This was administered using the same inhalation equipment as described in Chapter 2 (Section 2.5.5).

During the first gas inhalation session, participants were asked to perform deep, steady breaths of the gas mixture (but not to TLC) at their own pace until the entire contents of the 25 L Douglas bag had been inhaled. A whole-lungs spectroscopy scan (FID, see Table 6.4) was initiated at the onset of the first breath, enabling measurement of PFP's -CF$_3$ resonant frequency. The gas inhalation rig was subsequently switched to the room air inlet, and a dynamic 3D ^{19}F-MR acquisition (see Table 6.4) was initiated as participants continued to breathe steadily via the mouthpiece, enabling assessment of PFP gas wash-out from the lungs. The acquisition was restricted to a duration of 90 s, in accordance with SAR limits and safety tests outlined previously (Chapter 2, Section 2.5.3).

During the second gas inhalation session, participants were again asked to perform deep, steady breaths of the gas mixture at their own pace. This was continued for a period of 90 s, during which time the same dynamic 3D ^{19}F-MRI acquisition was initiated, enabling assessment of PFP gas wash-in to the lungs. The acquisition was commenced at the onset of the first breath, concurrent with switching the gas inhalation rig from room air to PFP gas.

During the third gas inhalation session, participants were instructed to perform two deep breaths of gas from a starting point of relaxed end-expiration (i.e. FRC) followed by a short breath-hold (7.5 s) at maximal inspiration (i.e. TLC). This breathing scheme was continued for at least 5 cycles and up to a maximum of 10 cycles, or until the 25 L Douglas bag was empty; at this point, the gas inlet was switched to room air and the breathing scheme was

continued for up to a further 10 cycles. Breathing instructions were relayed to participants and a member of the study team within the MRI scanner room via headphones, enabling appropriate timing of gas delivery comparable to the inhalation scheme adopted as part of the LIFT study (Chapter 3, Section 3.3.3). A 3D SPGR sequence (see Table 6.4) was initiated at the onset of each breath-hold, utilising the compressed sensing (CS) 1.8× under-sampling scheme developed during Phase 1 of the LIFT study (Chapter 3, Section 3.2.3). This enabled assessment of PFP gas wash-in and wash-out dynamics interleaved with short breath-hold acquisitions.

Parameter	Scan		
	^{19}F FID	Dynamic ^{19}F	^{19}F SPGR (CS)
TE (ms)	-	1.7	1.7
TR (ms)	200	8.5	8.5
Flip angle (°)	90	45	45
FOV (mm^3)	-	$420 \times 405 \times 240$	$400 \times 320 \times 250$
Resolution (mm^3)	-	$15 \times 15 \times 15$	$10 \times 10 \times 10$
BW (Hz/pixel)	-	500	500
NSA	50	-	3
Acquisition time (s)	10	90	7.5
Number of dynamics	256	39	(varied)
Sampling frequency (Hz)	8000	-	-

Table 6.4: Summary of the ^{19}F-MRI acquisition parameters employed during the VQ MRI study.

A summary of the three different inhalation schemes is illustrated in Figure 6.1. Each gas inhalation session was separated by an interval of at least 10 minutes (mean (SD) = 14 (4.7) minutes), in accordance with scanner SAR limits outlined in Chapter 2 (Section 2.5.3). During this time, participants breathed room air freely until the start of the next gas inhalation. Upon completion of the MRI scan session, participants were removed from the MRI scanner and observed for a period of 10 minutes to ensure heart rate and O$_2$ saturations remained at baseline (i.e. pre-inhalation) levels and that there were no delayed reactions to Gadobutrol administered during the first part of the scan session. The intravenous cannula was subsequently removed, prior to participants leaving the study centre.
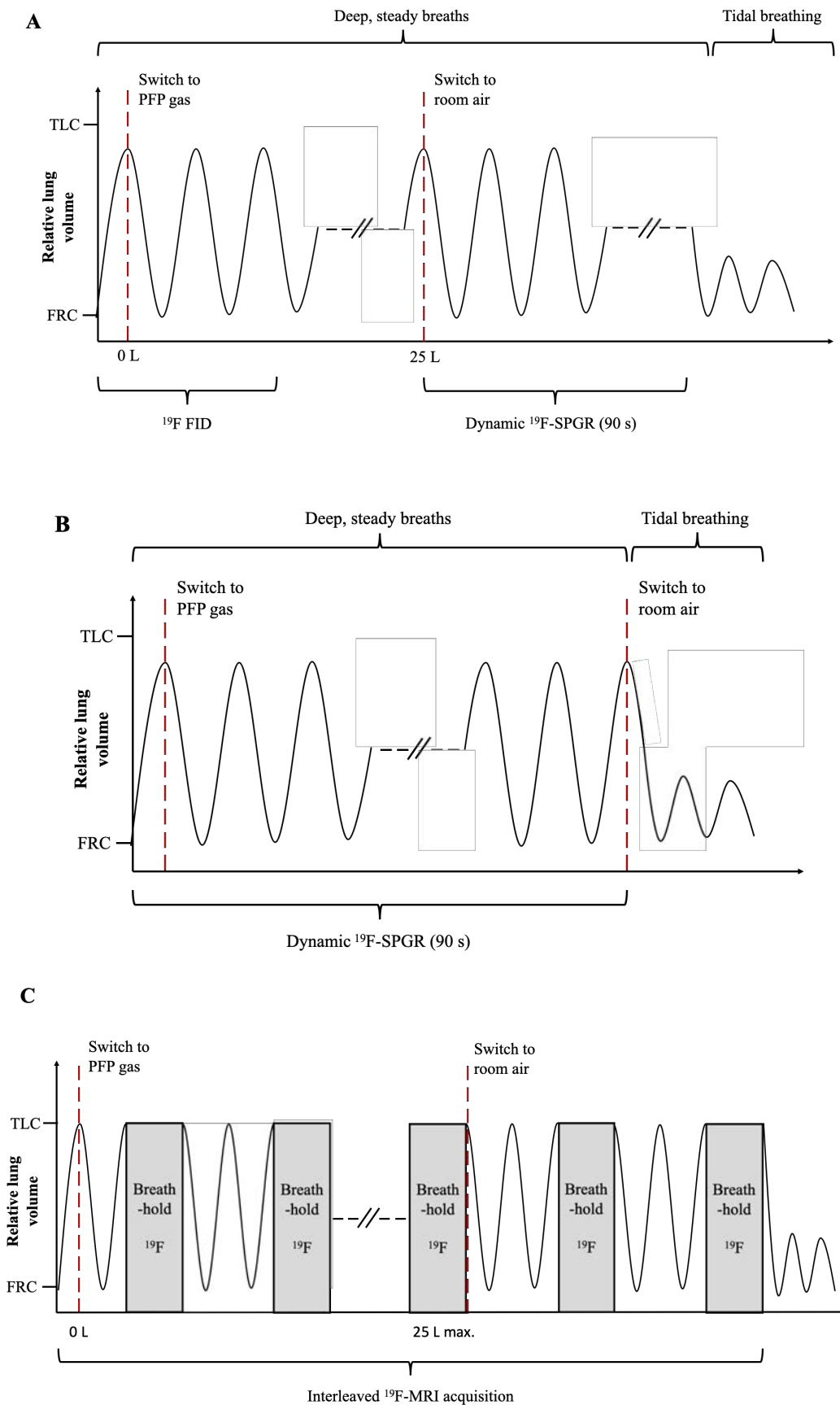
Figure 6.1: Diagrammatic representation of the three different gas inhalation schemes employed in the VQ MRI study. **(A)** Inhalation scheme 1: dynamic ^{19}F-MRI (PFP wash-out); **(B)** Inhalation scheme 2: dynamic ^{19}F-MRI (PFP wash-in); **(C)** Inhalation scheme 3: Interleaved ^{19}F-MRI (PFP wash in/wash-out).

6.2.3 Image analysis

^{19}F-MRI

The SNR was calculated for each time point of the 90 s dynamic ^{19}F acquisition (Inhalation sessions 1 and 2) using the same approach as outlined in Chapter 4 (Section 4.2.3). For interleaved ^{19}F acquisitions (Inhalation session 3), the SNR was calculated at six different lung regions, comprising three different lung slices (anterior, central and posterior) each with two 4 x 4 cm^2 ROIs placed in the apex and base of the right lung, respectively.

The %VV was calculated for all breath-hold ^{19}F images acquired during PFP gas wash-in (Inhalation session 3), enabling a comparison of early-phase and late-phase %VV measurements in all three participants. %VV calculations were performed using the same RegSeg image analysis software adopted during Phase 2 and Phase 3 of the LIFT study (see Chapter 4, Section 4.2.3).

DCE-MRI

All images were assessed qualitatively for the presence of perfusion defects and compared with ventilation defects observed in ^{19}F-MR images. The change in parenchymal signal intensity relative to baseline (i.e. the first dynamic image acquisition) was calculated for each time point in the dynamic DCE-MRI acquisition by placing a 4 x 4 cm^2 ROI in the apex of the right lung of the corresponding image slice. This enabled characterisation of the time to peak signal intensity and contrast agent transit time through the lungs in all three participants.

6.3   Results

Participant demographic information (study Groups 2 and 4) is summarised in Table 6.5. DCE-MRI and ^{19}F-MRI scans were well tolerated by all participants (including the four healthy volunteers attending study Group 1), with no adverse events relating to gas inhalation or Gadobutrol administration.

Participant	Age	Sex	BMI (kg/m^2)	FEV$_1$*	FVC*	FEV$_1$/FVC (%)	HR[†] (pre)	HR[†] (post)	O$_2$ (%) (pre)	O$_2$ (%) (post)
1 (HV)	31	F	25	108	106	85.7	69 (62-74)	64 (60-66)	97 (96-98)	98 (97-99)
2 (COPD)	76	M	26	39	77	38.2	56 (54-58)	56 (53-60)	96 (93-98)	96 (93-98)
3 (COPD)	68	M	24	28	73	29.2	84 (82-85)	85 (82-91)	95 (95-96)	95 (94-95)

Table 6.5: Summary of participant demographic information (VQ MRI study groups 2 and 4).
* reported as % predicted values; [†]HR = heart rate (beats per minute); O$_2$ (%) = peripheral oxygen saturation
HR and O$_2$ measurements are reported as mean values (pre- and post GBCA administration or gas inhalation), with range in parenthesis.

6.3.1   Dynamic ^{19}F-MR ventilation imaging

Free-breathing acquisitions: SNR measurements

Figure 6.2 illustrates the change in SNR with PFP wash-out from the lungs over the course of a 90 s dynamic acquisition (duration of one dynamic = 2.3 s), performed during Inhalation session 1 (i.e. deep, steady breaths of room air following inhalation of 25 L of the 79% PFP / 21% O$_2$ gas mixture). For each participant, the SNR was calculated from a ROI in the apex of the right lung in a central image slice where the trachea was seen to bifurcate. In Participant 1 (healthy volunteer, grey), the SNR declined steadily from a starting point of ~15, reaching a baseline value (i.e. SNR = 0) after approximately 50 s (number of breaths = 7). A slower decline in SNR was observed in Participant 2 (patient with COPD, blue), with PFP wash-out continuing up to the end of the 90 s scan period (number of breaths = 10). For Participant 3 (patient with COPD, orange), the SNR remained relatively static at ~10 throughout the entire duration of the scan (number of breaths = 10), indicating retained gas (i.e. 'gas trapping') within this particular region of the lung.
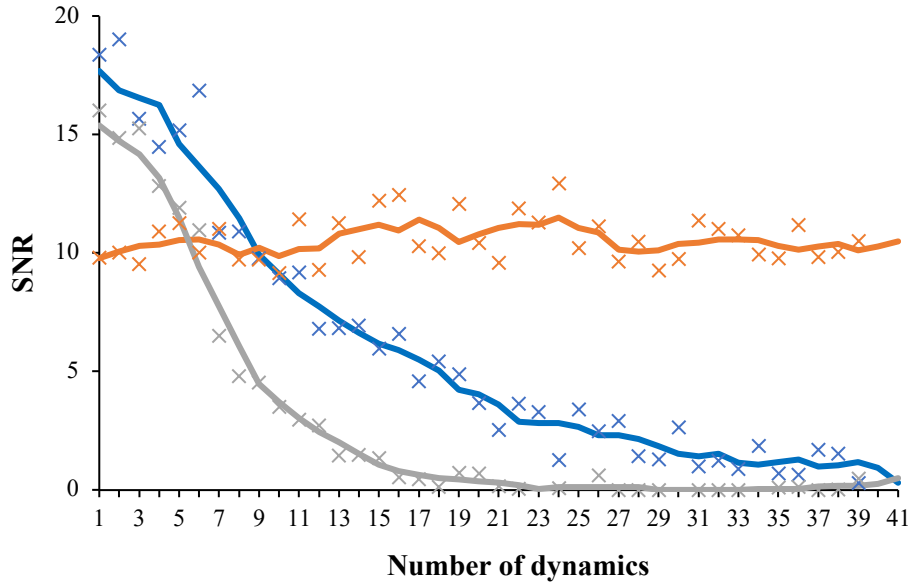
Figure 6.2: Calculated SNR values for the three study participants during a 90 s dynamic wash-out acquisition. Individual dynamic measurements (acquired every 2.33 s) are represented by ×. Trend lines were generated by calculating a 5-point moving average over the entire dataset. Participant 1 (healthy volunteer) = grey; Participant 2 (COPD) = blue; Participant 3 (COPD) = orange.

Figure 6.3 shows a similar representation of change in SNR with PFP gas wash-in to the lungs over the course of a 90 s dynamic acquisition during Inhalation Session 2 (i.e. deep, steady breaths of the 79% PFP / 21% O_2 gas mixture). SNR values were calculated from the same ROI in the apex of the right lung.
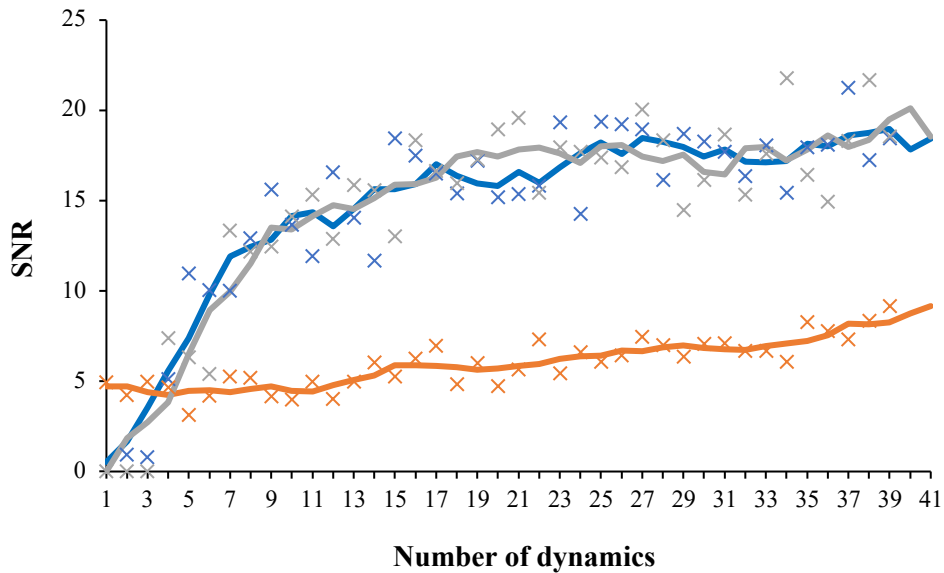
Figure 6.3: Calculated SNR values for the three study participants during a 90 s dynamic wash-in acquisition. Individual dynamic measurements (acquired every 2.33 s) are represented by ×. Trend lines were generated by calculating a 5-point moving average over the entire dataset. Participant 1 (healthy volunteer) = grey; Participant 2 (COPD) = blue; Participant 3 (COPD) = orange.

The wash-in time was similar for Participant 1 (grey) and Participant 2 (blue), with the SNR for both participants reaching a plateau after approximately 50 s (number of breaths = 7). By comparison, Participant 3 demonstrated a much slower PFP gas wash-in period, with SNR measurements continuing to rise towards the end of the 90 s scan (number of breaths = 10). Of note, the SNR value acquired at the start of the ^{19}F-MRI acquisition period for Participant 3 was non-zero (~5), indicating the presence of PFP gas within this lung region *prior* to commencing the inhalation protocol (i.e. persisting from the previous gas inhalation session). This finding is discussed further in Section 6.4.

Interleaved breath-hold acquisitions: SNR measurements

Figure 6.4A shows a comparison of ^{19}F-MR ventilation images (coronal views) from three lung slices in Participant 1, acquired during short breath-hold scans (duration = 7.5 s) following successive breaths of PFP (wash-in phase) or room air (wash-out phase). Figure 6.4B illustrates corresponding SNR measurements calculated from two ROIs placed in the apex and base of the right lung in these three slices, enabling evaluation of SNR across a total of six distinct lung regions.

Serial ^{19}F-MR ventilation images demonstrated substantial wash-in after just one deep breath of the PFP/O_2 gas mixture in Participant 1, with no apparent visible change in gas distribution between 3 and 13 deep breaths of gas (Figure 6.4A). A similarly rapid wash-out of PFP from the lungs was observed, with very little signal remaining after the first two deep breaths of room air. SNR measurements showed a comparable pattern of PFP gas wash-in and wash-out, with a more gradual rise in SNR with successive wash-in breaths for central (red) and anterior (yellow) lung regions compared to posterior (green) regions. The variability in SNR measurements observed in posterior ROIs (green) during gas wash-in may reflect slight differences in lung inflation level between respective breath-hold acquisitions.
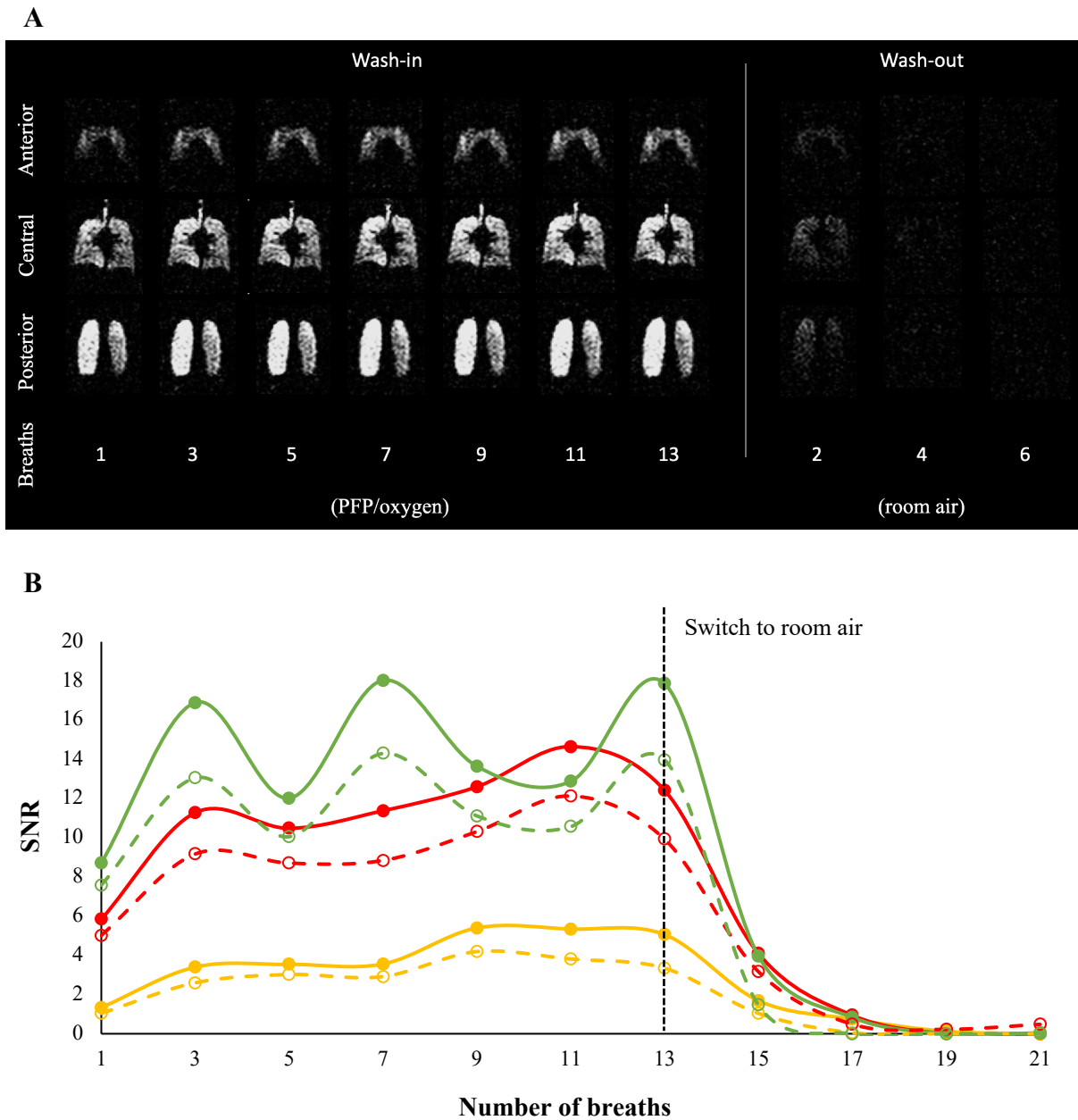
Figure 6.4: **(A)** ^{19}F-MR ventilation images (coronal views) acquired in Participant 1 (healthy volunteer), showing representative anterior, central and posterior lung slices during wash-in and wash-out phases. **(B)** Corresponding SNR measurements from six ROIs: green = posterior slice (solid = apex; broken = base); red = central slice (solid = apex; broken = base); yellow = anterior slice (solid = apex; broken = base).

Equivalent ^{19}F image slices and SNR measurements for Participant 2 are shown in Figure 6.5. Wash-out data were not available for this participant, owing to early termination of the inhalation session secondary to a faulty connection between the finger probe and pulse oximeter monitor. A steady increase in gas distribution and SNR measurements was observed in all regions up to the fifth image acquisition (i.e. following 9 deep breaths of gas), after which point further PFP inhalation appeared to have little impact on ^{19}F-MR acquisitions. An overt ventilation defect was visible to the base of the left lung which remained present after 17 deep breaths of the gas mixture.
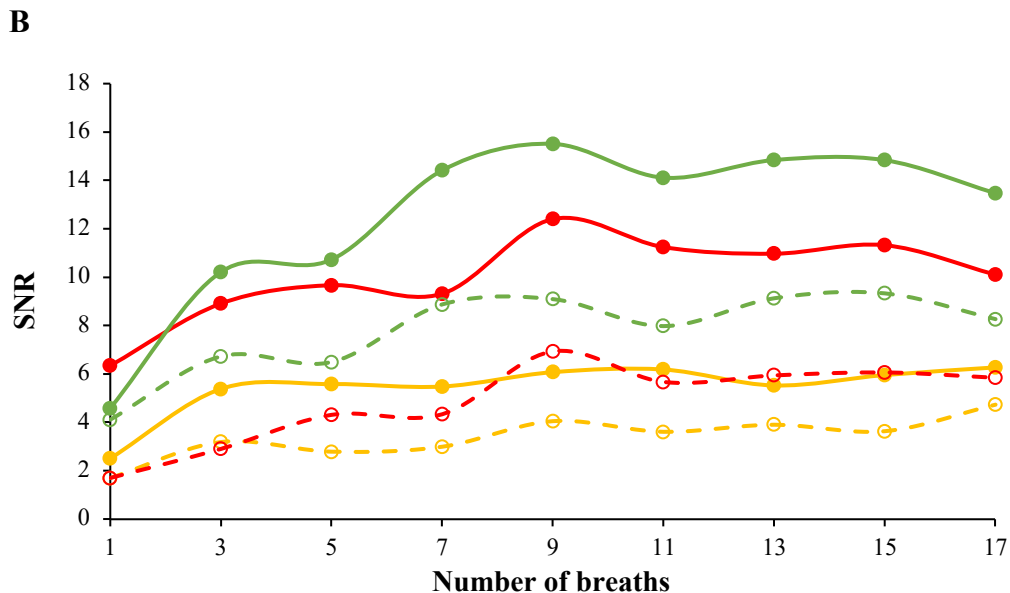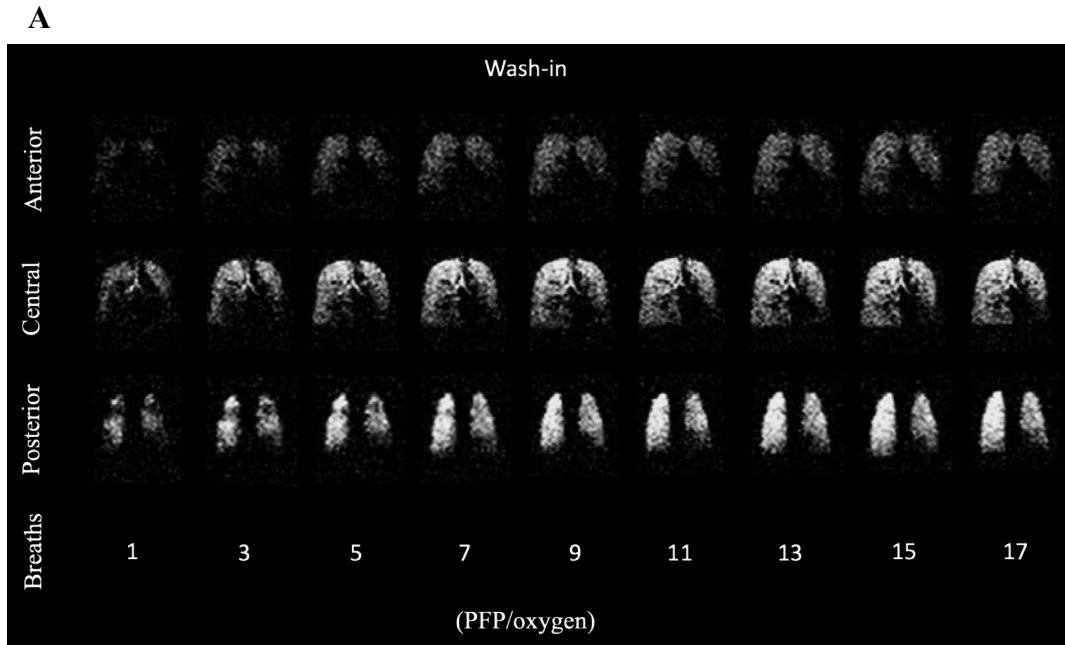
Figure 6.5: (A) ^{19}F-MR ventilation images (coronal views) acquired in Participant 2 (patient with COPD), showing representative anterior, central and posterior lung slices during wash-in and wash-out phases. **(B)** Corresponding SNR measurements from six ROIs: green = posterior slice (solid = apex; broken = base); red = central slice (solid = apex; broken = base); yellow = anterior slice (solid = apex; broken = base).

Ten cycles of PFP wash-in and ten cycles of PFP wash-out (where one cycle comprised 2 deep breaths of gas mixture or room air, followed by a breath-hold) were performed by Participant 3 (see Figure 6.6). Heterogeneous gas distribution was visualised throughout the three lung slices, which improved substantially with successive wash-in breaths. A marked disparity between apical and basal lung regions was observed during gas wash-out, most prominently towards the posterior regions of the lung (Figure 6.6A); this was reflected in regional SNR measurements, where the apical posterior ROI (solid green) indicated

significant gas trapping despite 20 deep breaths of room air (Figure 6.6B). A single 2.3 s dynamic ^{19}F-MRI acquisition was performed after a period of 25 minutes following completion of the interleaved acquisition protocol, revealing persisting PFP gas signal within the lung apices at this time.

A

B
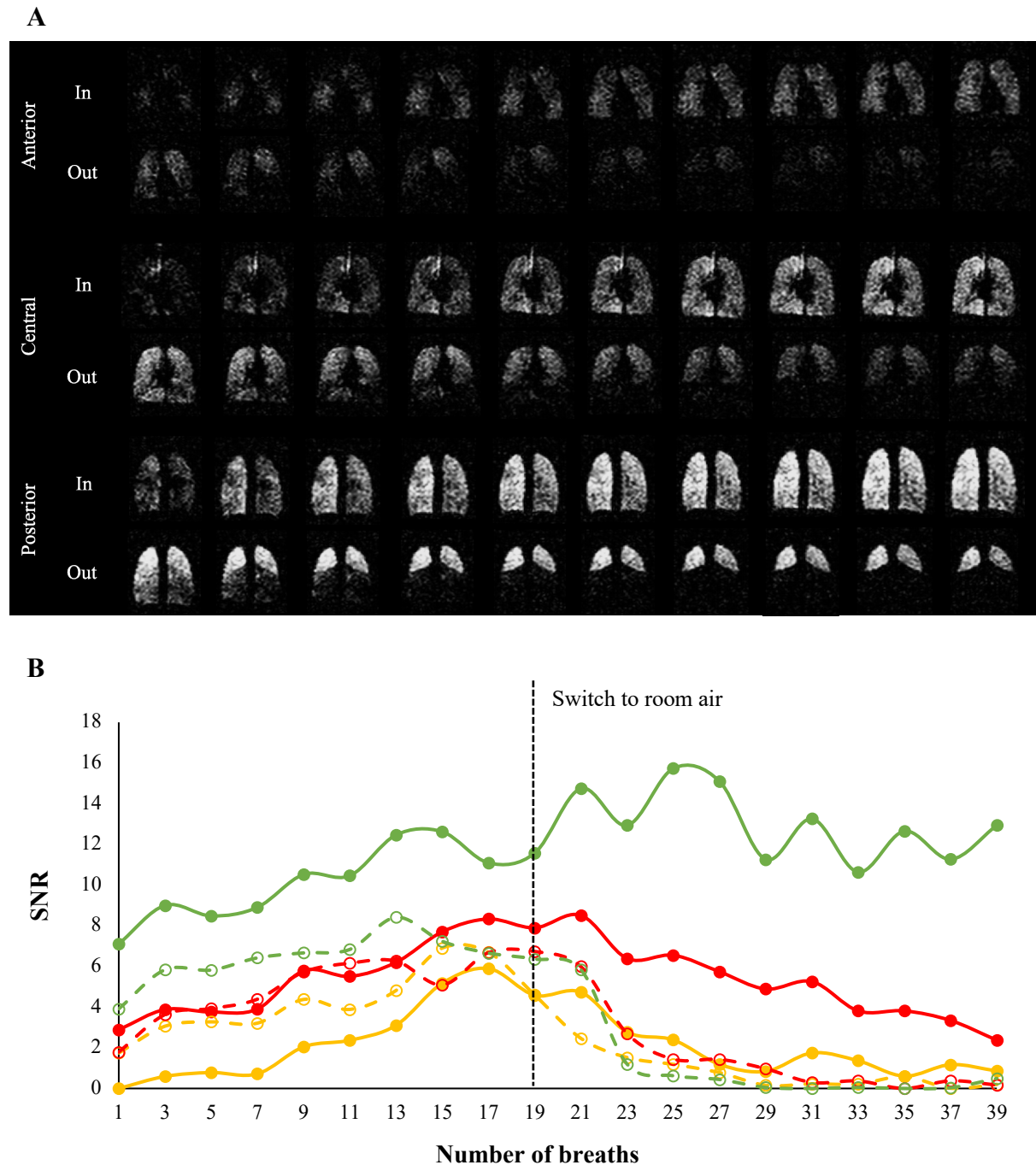
Figure 6.6: (A) ^{19}F-MR ventilation images (coronal views) acquired in Participant 3 (patient with COPD), showing representative anterior, central and posterior lung slices during wash-in and wash-out phases. **(B)** Corresponding SNR measurements from six ROIs: green = posterior slice (solid = apex; broken = base); red = central slice (solid = apex; broken = base); yellow = anterior slice (solid = apex; broken = base).

Interleaved breath-hold acquisitions: %VV measurements

Figure 6.7 shows a comparison of serial %VV measurements acquired in all three participants during the PFP wash-in phase. Baseline %VV values, acquired after 1 deep breath of the PFP/O_2 gas mixture, were 83.0% for Participant 1 (healthy volunteer), 42.9% for Participant 2 (COPD), and 41.1% for Participant 3 (COPD), respectively. Subsequent %VV measurements for Participant 1 were all within the range of 94.3% – 96.2% (peak after 5 wash-in breaths), consistent with values reported in healthy volunteers during Phase 2 of the LIFT study (see Chapter 4, Table 4.4). For both patients with COPD, %VV values continued to rise with successive gas inhalation cycles, reaching a maximum value of 89.0% for Participant 2 (15 wash-in breaths), and 95.3% for Participant 3 (19 wash-in breaths).
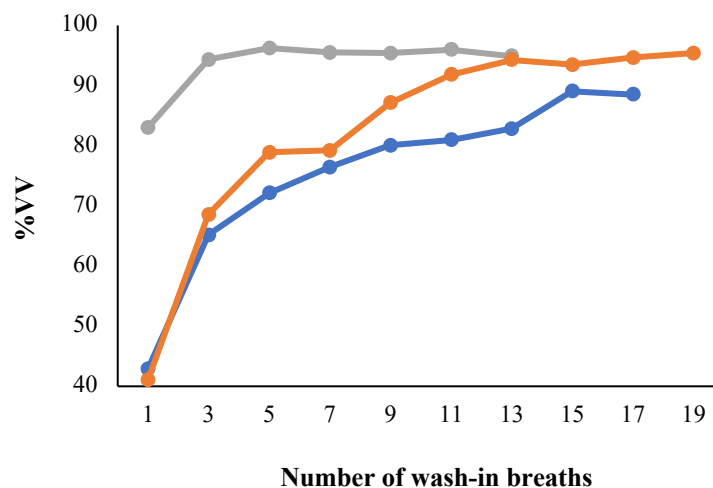
Figure 6.7: Serial %VV measurements acquired in all three study participants following successive PFP wash-in breaths. Participant 1 (healthy volunteer) = grey; Participant 2 (COPD) = blue; Participant 3 (COPD) = orange.

6.3.2   DCE perfusion MRI

The mean volume of Gadobutrol administered was 3.6 mL (range = 3.3–4 mL), determined by participant weight (range = 66–80 kg) and dose (0.05 mL/kg in all participants). Figure 6.8A shows example T_1-weighted DCE-MRI acquisitions (where image intensity is determined by the change in tissue T_1) from a single coronal slice acquired in Participant 1 (healthy volunteer) during first passage of Gadobutrol through the pulmonary circulation. The top row represents the acquired raw image datasets, with corresponding subtraction images (demonstrating the difference between the first and subsequent timepoints) shown in the second row. The relative change in parenchymal signal intensity compared to baseline

(i.e. the first image slice, prior to Gadobutrol arrival in the lungs) over the course of the dynamic acquisition (where one dynamic = 1.93 s) is illustrated in the third row. Equivalent datasets for Participant 2 and Participant 3 are shown in Figures 6.8B and 6.8C, respectively.
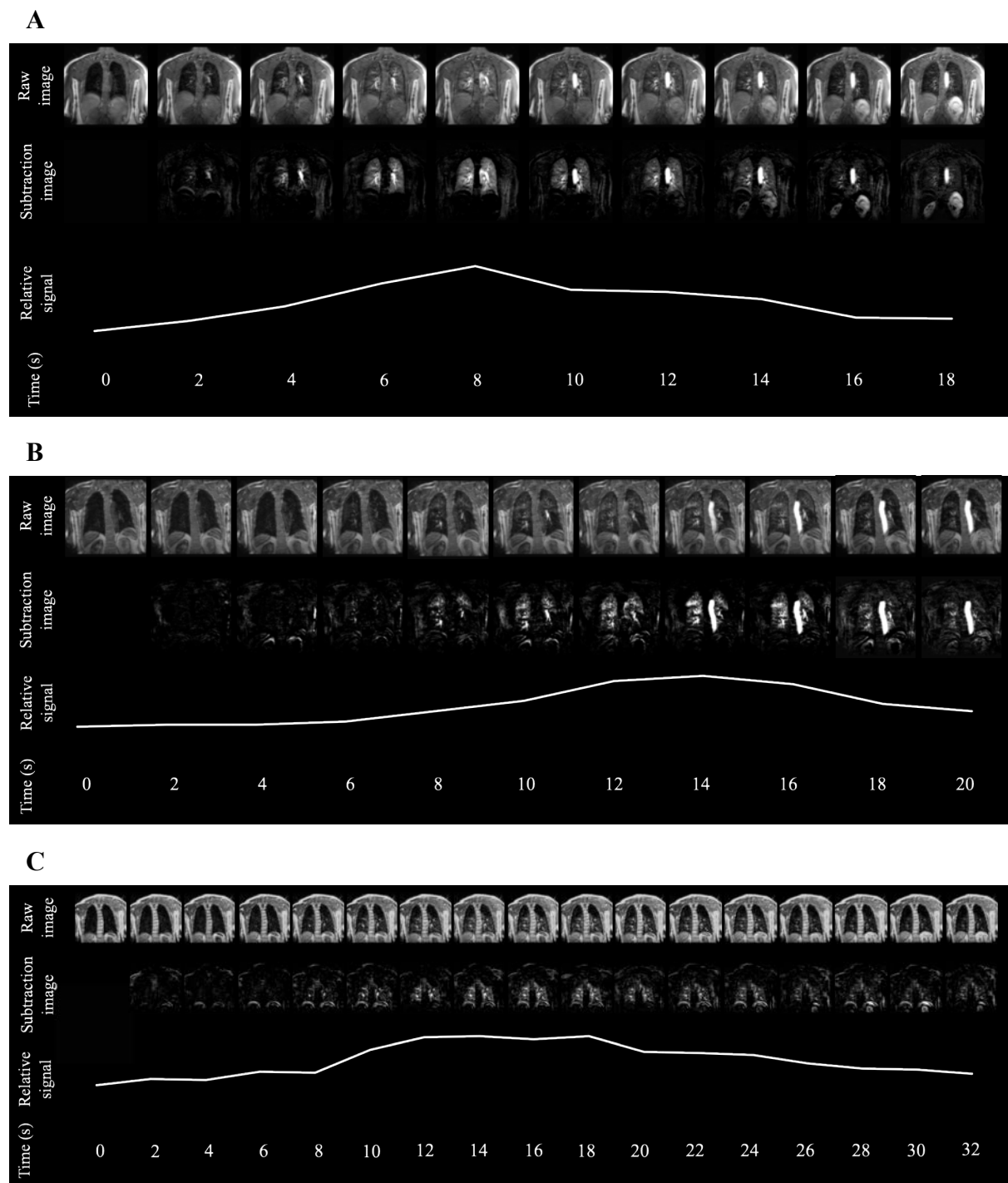
Figure 6.8: DCE perfusion images acquired in **(A)** Participant 1 (healthy volunteer); **(B)** Participant 2 (patient with COPD); and **(C)** Participant 3 (patient with COPD). Regional differences in parenchymal signal intensity and GBCA distribution can be visualised in both patients compared to the healthy volunteer.

Peak signal intensity was observed after approximately 8 s for Participant 1 (healthy volunteer) and after approximately 14 s for Participant 2 and Participant 3. The duration of first passage of Gadobutrol through the lungs was approximately 16 s for Participant 1, 20 s for Participant 2, and 32 s for Participant 3.

Figure 6.9 shows a comparison of DCE-MRI acquisitions (represented by the peak signal intensity images) alongside corresponding ^{19}F-MR ventilation images acquired during Inhalation session 3. Homogeneous GBCA and PFP distribution can be visualised throughout the lungs of Participant 1 (healthy volunteer). By comparison, Participant 2 demonstrated increased heterogeneity of GBCA distribution, with an evident perfusion defect to the left base (red arrow) matching a similar ventilation defect seen on ^{19}F-MRI. In Participant 3, marked perfusion defects were observed to the apices of both lungs (red arrows), corresponding to those regions characterised by gas trapping during PFP wash-out ^{19}F-MRI (i.e. suggesting a ventilation/perfusion mismatch in this participant). Anatomical ^{1}H-MRI scans were not optimised to detect corresponding structural defects in these two patients, though both had evident emphysema on previous CT imaging, most marked in Participant 3.
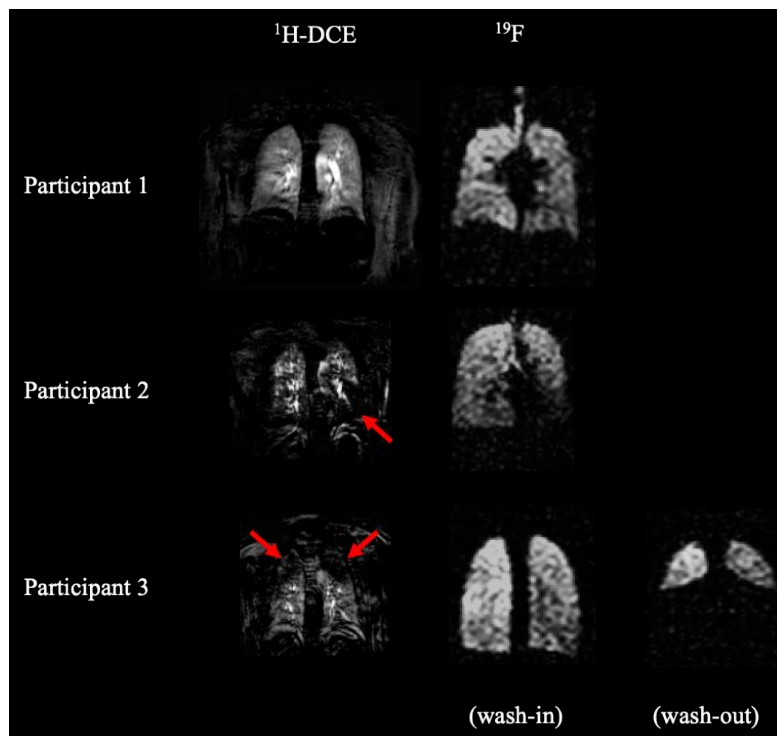
Figure 6.9: Comparison of DCE perfusion MRI and ^{19}F-MR ventilation images in the three study participants. Both perfusion and wash-in ventilation images represent the time of peak signal enhancement relating to GBCA administration or PFP/O_2 gas inhalation. PFP wash-out images were not available for Participant 2; gas wash-out was extremely rapid for Participant 1 and is therefore not displayed.

6.4 Discussion

The aim of this study was to establish the technical feasibility of performing dynamic ^{19}F-MRI of inhaled PFP in combination with DCE-MRI of the lung. This work has demonstrated the capability of adopting the above scan procedures to distinguish regional ventilation and perfusion properties in healthy volunteers and patients with COPD. As far as is known, this represents the first study to employ these two imaging techniques within a single MRI scan session.

PFP is well suited to dynamic ^{19}F-MRI, owing to its thermal polarisation and capacity for inhalation as a normoxic gas mixture (i.e. 79% PFP / 21% O_2), facilitating multiple acquisitions over the course of several breathing cycles (Couch *et al.*, 2019a). This differs from inhalation of hyperpolarised ^{3}He and ^{129}Xe, where irrecoverable loss of signal occurs with repeated breaths secondary to the T_1 shortening effects of paramagnetic O_2 within the lungs and RF pulse-mediated loss of polarisation (Kruger *et al.*, 2016). Consequently, while a small number of studies have demonstrated the potential to perform multi-breath imaging using HP-MRI (Horn *et al.*, 2014b; Hamedani *et al.*, 2016; Horn *et al.*, 2017b), this approach remains challenging in practice. By comparison, dynamic ventilation imaging has been successfully employed in recent human ^{19}F-MRI studies (e.g. Gutberlet *et al.*, 2018; Goralski *et al.*, 2020; McCallister *et al.*, 2021), offering an alternative to single static breath-hold acquisitions.

In agreement with the initial study hypothesis, overt differences in PFP wash-in and wash-out times (represented by dynamic SNR measurements) were observed between the healthy volunteer and two patients with COPD (Figures 6.2 and 6.3). Notably, the wash-in and wash-out times acquired in Participant 1 (healthy volunteer) were roughly equivalent but showed substantial variation for the two patients with COPD, reflecting differences in underlying regional ventilation heterogeneity. This was especially marked for Participant 3, where a sustained gas signal was demonstrated within the lung apices towards the start of Inhalation Session 2 (approximately 13 minutes after completing the first gas inhalation session) and at an interval of 25 minutes following completion of Inhalation Session 3 (Figure 6.6). The delayed wash-out phase observed in this particular ROI likely stems from significant apical-predominant emphysema and gas trapping present in this patient, and supports the findings of

previous ^{19}F-MRI studies involving patients with COPD (Kaireit *et al.*, 2018; Gutberlet *et al.*, 2019).

The non-equivalent rates of PFP wash-in and wash-out (or, alternatively, room air wash-out and wash-in) for each of the two patients with COPD is an important finding and perhaps less intuitive than the global differences observed between healthy and diseased lungs (i.e. wash-in and wash-out might be assumed to be reciprocal in nature). Nonetheless, differences in PFP wash-in and wash-out time constants have previously been described in patients with COPD (Halaweish *et al.*, 2013b), as well as patients with CF (Goralski *et al.*, 2020), suggesting this represents a genuine phenomenon. Of note, Goralski and colleagues adopted a breathing protocol analogous to that employed during Inhalation Session 3, concluding that PFP wash-out rate was a better discriminator between healthy volunteers and patients with mild CF compared to PFP wash-in. Similarly, Gutberlet et al. (2018) reported a strong association between free-breathing PFP wash-out times and FEV_1 in patients with COPD and, more recently, demonstrated potential to use this ^{19}F-MRI measurement to detect changes in response to normal ageing (Gutberlet *et al.*, 2019). A direct comparison of wash-in and wash-out rates was not possible in these studies, however, since different breathing protocols were adopted for the respective wash-in and wash-out phases (namely, interleaved breath-hold acquisitions during wash-in and free-breathing dynamic imaging during wash-out). Moreover, the majority of patients recruited by Gutberlet and colleagues had moderate COPD (GOLD Stage 2; see Chapter 1, Table 1.1), making it difficult to fully compare their findings with results of the present study, where Participants 2 and 3 had severe ($FEV_1 =$ 39% predicted) and very severe ($FEV_1 =$ 28% predicted) COPD, respectively.

The nature of the inhaled gas mixture (i.e. 79% PFP / 21% O_2, versus room air) is likely to have a strong bearing on the pattern of wash-in and wash-out kinetics observed (Couch *et al.*, 2014), which may be exaggerated in patients with underlying pathology. It has previously been proposed that differences in gas density may contribute to the slight discrepancy that exists between static VDP measurements revealed by hyperpolarised [3]He and [129]Xe (Kirby *et al.*, 2013; Svenningsen *et al.*, 2013). Importantly, PFP is approximately six times denser than room air (BOC, 2000), such that airflow through the bronchial tree is likely to differ slightly for these gases. In support of this concept, Chon et al. (2005) previously performed Xe-enhanced CT ventilation imaging in healthy anaesthetised sheep, highlighting a consistently prolonged Xe wash-out time compared to Xe wash-in. The authors largely attribute this

finding to alteration of Rayleigh-Taylor instabilities (i.e. changes in fluid mechanics that occur at the interface between gases of different densities) during respective wash-in and wash-out phases: specifically, during wash-in, it is postulated that the heavier Xe gas is accelerated into the lighter air residing in the lungs, giving rise to a faster wash-in rate; conversely, during wash-out, inhaled room air is thought to decelerate as it encounters the Xe-filled airspaces, leading to a slower wash-out rate. Given the similarity of Xe and 79% PFP / 21% O_2 gas densities (5.75 g/L (Kruger *et al.*, 2016) and 6.07 g/L (Halaweish *et al.*, 2013a), respectively), it is not unreasonable to assume such a mechanism may also be at play during ^{19}F-MR ventilation imaging. Additionally, as outlined in Chapter 1 (Section 1.2.1), both the speed and depth of breath impact airflow through the lungs (Milic-Emili *et al.*, 1966; Hughes *et al.*, 1972) which, in turn, may be influenced by the type of gas inhaled. Anecdotally, a small number of participants (including healthy volunteers and patients with respiratory disease recruited to the LIFT study) reported that breathing the PFP/O_2 gas mixture felt slightly heavier compared to breathing room air, which could contribute to differences in breathing efficacy during wash-in and wash-out phases. On the other hand, many participants failed to notice any difference at all. As such, the determination of PFP wash-in/wash-out kinetics is complex and likely governed by several factors, including the presence of underlying lung pathology (e.g. small airways disease and gas trapping secondary to emphysema), gas properties (e.g. altered density during wash-in and wash-out) and breathing efficiency (e.g. relative tidal volume achieved).

The potential limitations of adopting single global %VV measurements to report on lung ventilation properties was highlighted in Chapter 5 (Section 5.4). By comparison, the interleaved breath-hold scheme employed in this study (Inhalation Session 3) enabled characterisation of both 'fast-' and 'slow-' filling lung compartments, which may otherwise remain categorised as ventilation defects. Recently, this approach has been utilised to report on early-phase and late-phase VDP measurements in patients with CF (McCallister *et al.*, 2021), demonstrating the ability to quantify changes in gas distribution even in those regions with initially poor or absent gas signal. In the present study, a steady improvement in %VV values was observed in the two patients with COPD following successive breaths of PFP/O_2 (Figure 6.7) though, as expected, this was less marked for the healthy volunteer. Notably, %VV measurements were derived from ^{19}F-MRI acquisitions employing CS, facilitating a shorter breath-hold duration (7.5 s) compared to that adopted during the LIFT study (13.4 s). A direct comparison of fully sampled and 1.8× accelerated acquisitions was beyond the scope

of this study. Nonetheless, these data represent the first description of %VV measurements acquired in this manner, building on previous work involving healthy volunteers (Neal *et al.*, 2019).

An additional goal of this study was to assess the capability of performing DCE lung perfusion MRI, drawing on the change in parenchymal signal intensity observed during first passage of Gadobutrol through the pulmonary circulation. In support of previous DCE-MRI studies (Sergiacomi *et al.*, 2014; Hueper *et al.*, 2015; Kaireit *et al.*, 2019), both patients with COPD demonstrated marked heterogeneity of pulmonary blood flow, manifest as a prolonged global GBCA transit time and time to peak signal intensity compared to the healthy volunteer. Importantly, the observed changes to regional perfusion shown in Figure 6.8 corresponded to regions of abnormal ventilation identified on ^{19}F-MRI (Figure 6.9). Specifically, in Participant 2, reduced parenchymal signal enhancement towards the base of the left lung closely matched an area of absent PFP signal, suggesting a physiological adaptation (e.g. hypoxic vasoconstriction) to maintain matched ventilation and perfusion in this patient (Dunham-Snary *et al.*, 2017). Conversely, in Participant 3, reduced parenchymal signal enhancement was visualised towards the lung apices, mirroring those regions characterised by prolonged PFP wash-out (i.e. gas-trapping) although without an overt 'ventilation defect': it is likely this represents a ventilation-perfusion mismatch, whereby the compliant emphysematous lungs are still receiving gas but are poorly functioning and no longer involved in active gas exchange across the disrupted alveolar-capillary membrane (Morris and Sheppard, 2006).

The scan procedures employed by this study enabled DCE-MRI to be performed during relaxed tidal breathing, avoiding the requirement for breath-hold acquisitions. This is particularly relevant for patients with respiratory disease, who may be unable to tolerate prolonged breath-hold manoeuvres. While previous studies have highlighted the ability to employ free-breathing techniques (e.g. Ingrisch *et al.*, 2016; Chen *et al.*, 2018), the vast majority of pulmonary DCE-MRI has been conducted during breath-hold, predominantly at 1.5 T (Swift *et al.*, 2014; Johns *et al.*, 2017b). This likely stems from the improved image quality and relative parenchymal signal enhancement that can be achieved during breath-hold imaging at lower field strengths, owing to reduced artefacts arising from respiratory motion and T_2^* effects (Wild *et al.*, 2012). Despite these challenges, the approach adopted in this study was sufficient to demonstrate the technical feasibility of free-breathing DCE-MRI at

3.0 T, using a dose of Gadobutrol consistent with existing literature (see Johns *et al.*, 2017a) and within recommendations specified by the summary of product characteristics (Bayer, 2020).

Although GBCAs are widely utilised in clinical MRI (American College of Radiology, 2020), it is important to recognise that they are not without risk and have been associated with the development of nephrogenic systemic fibrosis in patients with impaired renal function (Agarwal *et al.*, 2009) and, rarely, allergic reactions (Behzadi *et al.*, 2018). The potential for GBCA deposition within brain tissue has also recently been reported (Guo *et al.*, 2018): while this is not known to have any adverse effects, *linear* GBCAs have subsequently been withdrawn from routine clinical and research use. However, *macrocyclic* agents (including Gadobutrol) are recognised to be more stable than linear counterparts and have been considered appropriate for continued use by the International Society for Magnetic Resonance in Medicine (Gulani *et al.*, 2017). Importantly, Gadobutrol is classified within the low-risk category for adverse events (Royal College of Radiologists, 2015): in a large multi-centre study involving more than 23,000 patients, the incidence of serious reactions (i.e. severe allergic reaction, or death) was less than 0.02% (Prince *et al.*, 2017), underpinning its continued widespread adoption. The use of GBCAs can also be considered within the context of current clinical methods used to assess lung perfusion, namely CTPA and SPECT imaging: both of these techniques incur an ionising radiation dose, whilst CTPA also involves the injection of iodinated contrast, which has been linked to the development of contrast induced nephropathy (Mitchell *et al.*, 2010) and significant allergic reactions (Iyer *et al.*, 2013).

Previous studies have investigated the use of DCE-MRI in combination with HP-MRI (Marshall *et al.*, 2014b; Weatherley *et al.*, 2018), as well as OE-MRI (Nakagawa *et al.*, 2001), offering potential for combined ventilation and perfusion imaging. However, to date, neither of these techniques has emerged as a viable option for routine clinical use: for HP-MRI, the technical demands of hyperpolarisation remain a barrier to widespread implementation, while OE-MRI is reliant on lengthy scan times to provide only an indirect measure of ventilation (Kruger *et al.*, 2016). The application of non-contrast enhanced techniques, such as FD-MRI (Bauman and Eichinger, 2012), represent a promising alternative to methods reliant on exogenous contrast agent administration, yet are currently restricted to centres with specialist image post-processing capabilities. In contrast, the [19]F-

MRI scan procedures outlined in this study enable direct assessment of pulmonary ventilation properties, in combination with a DCE-MRI perfusion technique that has already become established in clinical practice (e.g. Zhang *et al.*, 2016). This offers considerable scope for future clinical application, such as the assessment of severe emphysema and identification of patients suitable for lung volume reduction techniques (e.g. by determining which lung regions remain actively involved in gas exchange). The combined approach to ventilation/perfusion imaging also offers a unique opportunity to investigate pulmonary thromboembolic disease (e.g. acute PE) without recourse to ionising radiation, which may be particularly relevant for higher risk patient groups (such as young, or pregnant females).

6.5 Conclusion

This study outlines the first use of ^{19}F-MRI of inhaled PFP in combination with DCE-MRI within the framework of a single MRI scan session. Importantly, the adopted scan procedures were successfully implemented across all three participants, demonstrating the ability to distinguish regional ventilation and perfusion properties in healthy volunteers and patients with COPD. The dynamic ventilation imaging protocols described offer an alternative to single static breath-hold acquisitions, enabling assessment of gas distribution over the course of several respiratory cycles: this holds potential for characterising both well ventilated and poorly ventilated regions of the lung reflecting underlying pathophysiology. A broader assessment (e.g. in patients with mild to moderate COPD, or patients with thromboembolic disease) is necessary to clarify the suitability of these methods for future clinical application. Nonetheless, this work provides a firm foundation on which to develop dynamic ^{19}F-MRI as a viable tool for both pure ventilation and combined ventilation/perfusion imaging. The use of Gadobutrol as an adjunct to ^{19}F-MR ventilation imaging is explored further in the next chapter of this thesis.

Chapter 7.

Combined ventilation/perfusion imaging using dynamic susceptibility contrast ^{19}F-MRI: a 'proof of concept' study

7.1   Introduction

Chapter 6 outlined the feasibility of performing dynamic measurements of pulmonary ventilation and perfusion within a single MRI scan session, utilising ^{19}F-MRI of inhaled PFP in combination with DCE-MRI of a widely employed intravenous contrast agent (Gadobutrol). In the present chapter, this work is extended to explore a novel approach to combined ventilation/perfusion imaging within a single breath-hold duration, drawing on the T_2^* response of inhaled PFP to the passage of Gadobutrol through the pulmonary circulation.

The chapter begins by recapitulating the inherent relationship that exists between T_2^* and magnetic susceptibility gradients present within the lungs. This is followed by a brief discussion of key preclinical studies that have highlighted the potential to alter the magnetic susceptibility of lung tissue using intravenous paramagnetic contrast agents. Based on this work, an original hypothesis concerning the application of dynamic susceptibility contrast (DSC) ^{19}F-MRI to human ventilation imaging is proposed. This represents the primary focus for the remainder of the chapter.

7.1.1   Magnetic susceptibility and T_2^*

As outlined in Chapter 1 (Section 1.5.2), the T_2^* (transverse relaxation time) is heavily influenced by magnetic field inhomogeneity that exists at ubiquitous air-tissue interfaces throughout the lungs (Bergin *et al.*, 1991). This, in turn, stems from the differing magnetic properties of adjacent gas and aqueous components of the lung when subjected to an external magnetic field – a property known as magnetic susceptibility (χ). Notably, both O_2 and inhaled PFP exert a slight paramagnetic (i.e. strengthening) effect on the local magnetic field (χ_{gas} = +0.4 ppm); conversely, water or blood within the lung parenchyma exert a slight diamagnetic (i.e. weakening) effect on the local magnetic field ($\chi_{aqueous}$ = -9.0 ppm) (Schenck, 1996). This inherent magnetic susceptibility difference ($\Delta\chi$ = 9.4 ppm) underpins the rapid signal decay that is observed in pulmonary MRI in general and in ^{19}F-MR

ventilation imaging in particular, reflected by the short *in vivo* T_2^* of inhaled PFP (approximately 1–2 ms at 3.0 T) (Couch *et al.*, 2013).

The close proximity of respective gas and tissue (capillary) components within a single alveolus is illustrated in Figure 7.1.
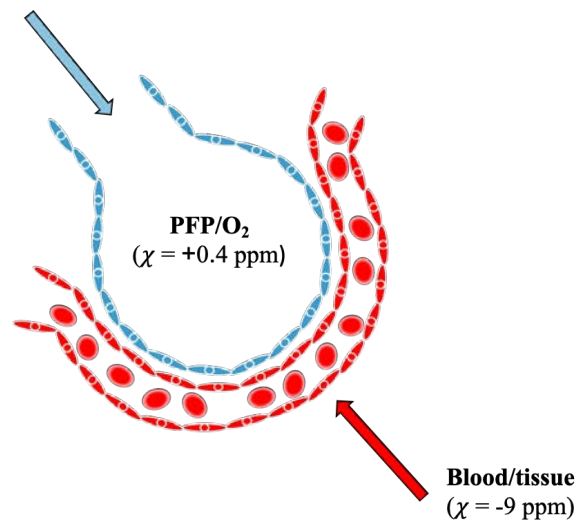
Figure 7.1: Diagrammatic representation of a single alveolus, showing the close proximity of the slightly paramagnetic PFP/O_2 gas mixture (χ_{gas} = +0.4 ppm) and diamagnetic blood within the pulmonary capillary ($\chi_{aqueous}$ = -9.0 ppm). The magnetic susceptibility difference between these two compartments is ~9.4 ppm.

7.1.2 *Reducing susceptibility differences in the lung*

By extending this principle, it can be inferred that overcoming (or reducing) the susceptibility difference between gas and aqueous components of the lung may lead to an improvement in acquired ^{19}F-MR ventilation images, corresponding to a lengthening of PFP T_2^*.

The ability to alter the magnetic susceptibility of body tissues using intravenous contrast agents is well established (Albert *et al.*, 1993) and forms the basis of DSC-MRI. This technique has been utilised widely in the assessment of brain perfusion, where the paramagnetic properties of intravenous GBCAs cause an increase in $\Delta\chi$ in perfused regions, *reducing* the T_2^* (Østergaard, 2005; Shah *et al.*, 2010). By comparison, the presence of paramagnetic contrast within the pulmonary circulation has potential to *elevate* the T_2^* by bringing the magnetic susceptibilities of gas and aqueous components of the lung closer together.

There is a paucity of literature concerning the alteration of magnetic susceptibilities in the lung. However, previous pre-clinical studies have demonstrated the ability to achieve partial or complete susceptibility matching following intravenous injection of paramagnetic contrast agents. Specifically, Vignaud *et al.* (2005) reported a 3-fold increase in the T_2^* of inhaled hyperpolarised ^{3}He following intravenous administration of superparamagnetic iron oxide in rats. Similarly, Dimitrov *et al.* (2005) inferred partial susceptibility matching of the aqueous and gas components of porcine lungs following GBCA administration, represented by a small but detectable difference in the resonant frequency of ^{3}He during contrast passage through the pulmonary circulation.

In support of this work, preliminary studies conducted by Dr Mary Neal and Helena Sexton (BSc undergraduate student at Newcastle University) established the capability of susceptibility-matching aqueous and gas components of PFP-filled foam phantoms, employing the same GBCA (Gadobutrol) adopted in Chapter 6. Notably, an approximate 2-fold elevation in PFP T_2^* was observed at a concentration of 30 mM Gadobutrol (Figure 7.2), where the magnetic susceptibility of the aqueous component matched that of the gas component (i.e. $\Delta\chi = 0$). Increasing the concentration of Gadobutrol beyond this point caused a reduction in PFP T_2^* as the respective susceptibilities of gas and aqueous components diverged.
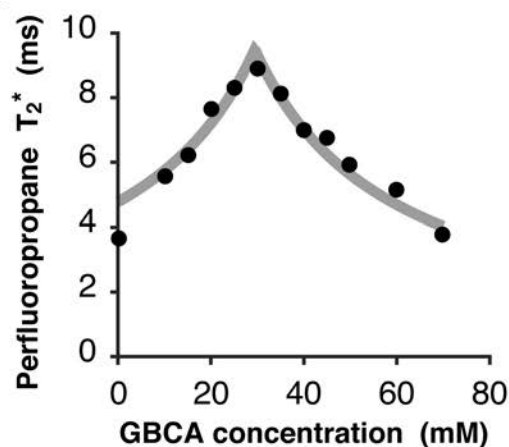
Figure 7.2: Impact of GBCA (Gadobutrol) administration on the T_2^* of PFP in a lung-representative phantom (aqueous foam) with increasing concentration in the aqueous component. The magnetic susceptibilities of aqueous and gas components were matched at a concentration of 30 mM. Adapted from Neal *et al.* (2020).

A similar response to GBCA administration was observed following translation of this effect to a small preclinical murine study, conducted in collaboration with colleagues at Newcastle University (Neal *et al.*, 2020). Specifically, Figure 7.3 demonstrates the change in *in vivo* T_2^* of inhaled PFP in mouse lungs ($n = 4$) following successive administrations of intravenous Gadobutrol. A maximal PFP T_2^* was observed following approximately 400 µL of contrast agent, with further administration leading to a reduction in T_2^* as the susceptibilities of gas and tissue components diverged.
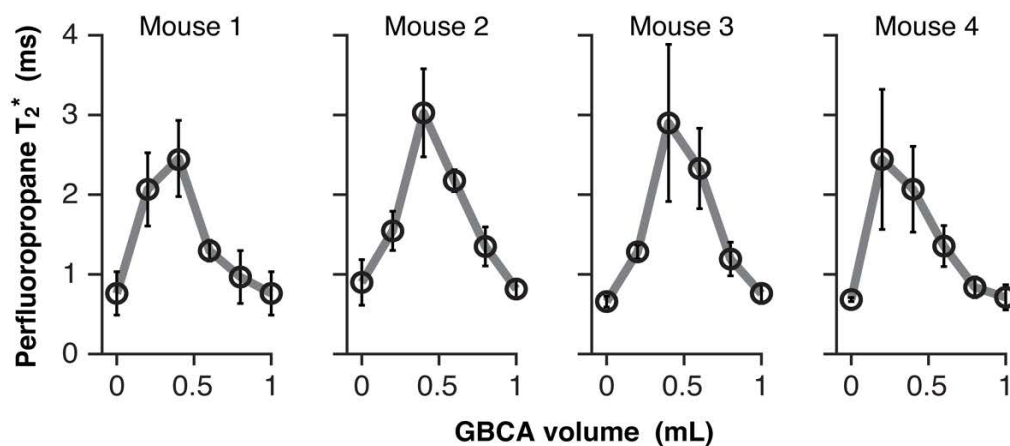
Figure 7.3: Impact of GBCA (Gadobutrol) administration on the T_2^* of inhaled PFP in four mice (error bars indicate 95% CI of exponential fits to the data). PFP T_2^* is maximal where the magnetic susceptibilities of aqueous and gas components of the lungs are matched, following administration and equilibration of approximately 400 µL. Adapted from Neal *et al.* (2020).

7.1.3 Application to human ¹⁹F-MR ventilation imaging

The above studies support the ability to modulate the magnetic susceptibility of lung tissue through intravenous administration of paramagnetic contrast agents, producing a detectable change in the T_2^* of inhaled gases. This has potential to improve the quality of static ¹⁹F-MR ventilation imaging by reducing the rapid signal decay that characterises acquisitions involving inhaled PFP. More importantly, the detection of contrast agent within pulmonary capillaries by changes to gas-phase T_2^* offers a unique ability to concurrently report on lung perfusion during bolus passage through the lungs. To date, no studies have exploited this susceptibility-matching effect in human lung imaging. The widespread clinical use of paramagnetic GBCAs (such as Gadobutrol) presents an opportunity to explore this further.

The purpose of this study was to establish the feasibility of assessing lung perfusion properties through application of DSC ^{19}F-MRI of inhaled PFP. Specifically, it was hypothesised that administration of intravenous paramagnetic Gadobutrol would lead to a transient elevation of PFP T_2^* and signal intensity, owing to susceptibility matching in well-perfused and well-ventilated regions of the lung.

7.2   Methods

Human experiments were conducted within the framework of the LungGas study, as outlined in Chapter 2 (Section 2.4).

7.2.1   Study population

Four healthy volunteers (3 males, aged 24, 28 and 34 years; 1 female, aged 28 years) were recruited to the study between August 2017 and December 2017. All four participants were non-smokers in good health, with no history of respiratory disease, renal impairment, or previous allergic reaction to GBCAs, in accordance with study inclusion and exclusion criteria outlined in Chapter 2 (Section 2.4.2).

7.2.2   MRI scan procedures

Following completion of initial screening procedures, participants had an 18-gauge cannula sited in a central antecubital fossa vein (in accordance with aseptic non-touch technique) for the purpose of administering Gadobutrol during the MRI scan session. Participants subsequently entered the MRI scanner room to undergo a single MRI scan session. All scans were performed at the NMRC on a 3.0 T scanner interfaced to a 20 cm diameter ^{19}F surface coil (see Chapter 2, Section 2.5.2).

Participants were positioned supine on the scanner bed with the assistance of radiographer colleagues. The surface coil was placed centrally below the upper back such that the top of the coil was aligned with the clavicles (see Figure 7.4).
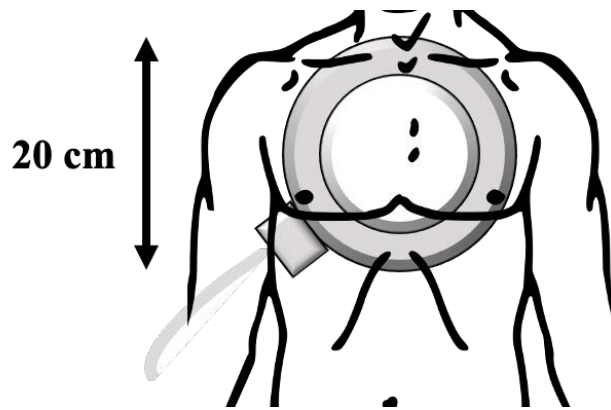
Figure 7.4: Representation of ^{19}F surface coil *in situ*, positioned to cover the apices of both lungs.

Initial scout ^{1}H-MR images (coronal views) were acquired with the scanner's body coil using a conventional multi-slice 2D gradient echo sequence (Table 7.1), in order to confirm correct positioning within the scanner bore.

Parameter	Scan		
	^{1}H Scout	^{19}F FID	^{19}F 2D SPGR
TE (ms)	1.8	-	1.7
TR (ms)	4.0	250	4.2
Flip angle (°)	10	90	50
FOV (mm³)	$450 \times 450 \times 250$	-	$300 \times 300 \times 200$
Resolution (mm³)	$2.3 \times 2.3 \times 3.8$	-	$12.5 \times 12.5 \times 200$
BW (Hz/pixel)	450	-	500
Number of dynamics	1	350	600
Acquisition time (s)	26	88	60
Number of samples	-	256	-
Sampling frequency (Hz)	-	8000	-

Table 7.1: Summary of the scan acquisition parameters employed during the LungGas study.

Participants were subsequently instructed to inhale the 79% PFP / 21% O_2 gas mixture on two occasions (the LungGas study protocol permitted up to three gas inhalation sessions per participant, as outlined in Chapter 2 (Figure 2.5); however, for the purpose of testing the experimental hypothesis, only two gas inhalation sessions were necessary). The PFP/O_2 gas mixture was administered using the same inhalation equipment and set-up as applied to participants recruited to the LIFT study, according to the finalised inhalation scheme outlined in Chapter 3 (Section 3.3.3); specifically, each gas inhalation session lasted approximately

one minute, comprising three deep breaths of gas from a starting point of relaxed expiration (i.e. FRC) followed by a breath-hold at maximal inspiration (i.e. TLC). However, in contrast with the LIFT study, participants were instructed to hold their breath for up to 30 s, or as long as possible. Upon completion of the breath-hold, participants reverted to breathing room air. Participants were coached in the inhalation scheme prior to entering the MRI scanner, and instructions were reiterated before each gas inhalation session to ensure compliance with breathing manoeuvres.

During the second gas inhalation session, participants were administered an intravenous dose of Gadobutrol (Gadovist 1.0 mmol/mL, Bayer Schering Pharma), calculated according to body weight. This was administered by the study radiographer concurrently with the start of breath-hold at a rate of 5 ml/s and a dose of 0.2 ml/kg (0.2 mmol/kg equivalent) in accordance with manufacturer guidelines regarding clinical use (Bayer, 2020) and consistent with doses employed in previous DSC-MRI studies (Thilmann *et al.*, 2005; Alger *et al.*, 2009).

^{19}F-MRI acquisitions

^{19}F-MR data acquisitions were commenced immediately prior to the start of breath-hold for each respective gas inhalation session.

For the first participant (Participant 1), a whole-lungs spectroscopy (FID) scan was acquired on two occasions during the scan session: once without (Inhalation 1), and once with concurrent administration of intravenous Gadobutrol (Inhalation 2). This enabled a comparison of the relative change in PFP T_2^* in response to paramagnetic Gadobutrol administration (see Section 7.3.1 below). For the remaining three participants (Participants 2, 3 and 4), a dynamic ^{19}F 2D SPGR sequence was acquired in place of the spectroscopy scan during the second gas inhalation session, allowing the change in PFP signal in response to Gadobutrol administration to be visually assessed. The temporal resolution of the ^{19}F 2D SPGR sequence was 0.1 s (i.e. one image was acquired every 0.1 s over the course of the entire scan duration). Each ^{19}F-MRI acquisition was separated by an interval of at least 5 minutes (mean (SD) = 463 (96) s), mirroring the procedures implemented for the LIFT study with respect to scanner SAR limits (see Chapter 2, Section 2.5.3).

The scan parameters relating to the ^{19}F FID and 2D SPGR acquisitions are summarised in Table 7.1 above.

Following completion of the MRI scan session, participants were removed from the MRI scanner and observed for a period of 30 minutes to ensure heart rate and O_2 saturations remained at baseline (i.e. pre-inhalation) levels and that there were no delayed reactions to Gadobutrol administration. The intravenous cannula was subsequently removed, prior to participants leaving the study centre.

7.2.3 ^{19}F-MRI data analysis

Dynamic ^{19}F-MR spectroscopy data (acquired in Participant 1) were analysed by Dr Mary Neal in Matlab (Mathworks, Natick WA, USA) by fitting an exponential decay curve (Equation 1) to the amplitude of the ^{19}F FID at each repetition of the dynamic acquisition (number of dynamics = 350; total scan duration = 88 s). This enabled calculation of the T_2^* of inhaled PFP at each time point throughout the acquisition (i.e. every 0.25 s), both with and without concurrent administration of Gadobutrol.

$$S = (S_0 \times e^{-t/T_2^*}) + c$$

(Equation 1)

where S = the measured signal; S_0 = the signal before T_2^* relaxation; t = the time during the FID acquisition; T_2^* = the transverse relaxation time; and c (constant) = the offset from zero equal to the mean noise amplitude.

Baseline PFP R_2^*, denoting the transverse relaxation *rate* (the reciprocal of T_2^*, i.e. $1/T_2^*$), was calculated by averaging the R_2^* over the first 7 s of the dynamic acquisition. The change in R_2^* (i.e. ΔR_2^*) was subsequently calculated for each time point throughout the acquisition, allowing measurement of the magnitude of change in response to Gadobutrol administration. This provided a marker of relative contrast agent concentration within the lung, whereby R_2^* (but not T_2^*) is directly proportional to $\Delta\chi$ following contrast agent administration (Kiselev, 2005; Østergaard, 2005).

168

Dynamic 2D ^{19}F-MR ventilation images (acquired in Participants 2, 3 and 4) were averaged to a temporal resolution of 3 s, such that each image encompassed 30 dynamics (where each dynamic = 0.1 s). The change in PFP signal amplitude over the course of the dynamic acquisition was subsequently calculated using in-house software developed in Matlab by Prof Pete Thelwall on a pixelwise basis relative to the baseline signal amplitude: this was defined as the first 7.5 s of data acquisition, prior to arrival of Gadobutrol in the pulmonary circulation.

7.3 Results

Participant demographic information is summarised in Table 7.2. ^{19}F-MRI scans were well tolerated by all participants, with no adverse events relating to gas-mixture inhalation or intravenous Gadobutrol administration.

Participant	Age	Sex	BMI	FEV$_1$[*]	FVC[*]	FEV$_1$/FVC (%)	HR[†] (pre)	HR[†] (post)	O$_2$ (%) (pre)	O$_2$ (%) (post)
1	28	F	21.6	106	97	92.5	77 (76-77)	79 (76-85)	99 (98-99)	98 (97-99)
2	25	M	27.1	98	103	78	78 (73-84)	87 (81-91)	97 (97)	96 (94-98)
3	34	M	23	121	118	83.5	50 (48-51)	50 (50)	98 (98)	100 (99-100)
4	28	M	25	102	99	86.3	54 (53-55)	55 (54-55)	99 (98-100)	100 (99-100)

Table 7.2: Summary of participant demographic information (LungGas study group 4).
[*] reported as % predicted values; [†]HR = heart rate (beats per minute); O$_2$ (%) = peripheral oxygen saturation HR and O$_2$ measurements are reported as mean values (pre- and post-gas inhalation sessions) with range in parenthesis.

The mean volume of Gadobutrol administered was 14.1 mL (range = 11.6–17.0 mL), determined by participant weight (range = 58–84 kg) and dose (0.2 mL/kg in all participants).

7.3.1 Dynamic PFP T_2^* and R_2^* measurements

Figure 7.5A shows the T_2^* of inhaled PFP acquired in Participant 1 during a ^{19}F-MR spectroscopy scan without concurrent GBCA administration. The mean (SD) calculated T_2^* over the course of the 30 s breath-hold was 1.54 (0.05) ms. Figure 7.5B shows the T_2^* of inhaled PFP in the same participant prior to, during and following bolus passage of GBCA through the pulmonary circulation. The mean (SD) baseline T_2^* prior to Gadobutrol arrival was 1.50 (0.01) ms. A maximum PFP T_2^* value of 1.64 ms was measured at a timepoint of 11.25 s after commencing the dynamic ^{19}F-MRI spectroscopy acquisition, corresponding to a ~9% increase during Gadobutrol bolus passage through the lungs. The magnitude of change in T_2^* contrasts sharply with the low CoV (0.55%) observed in the baseline dataset shown in Figure 7.5A.
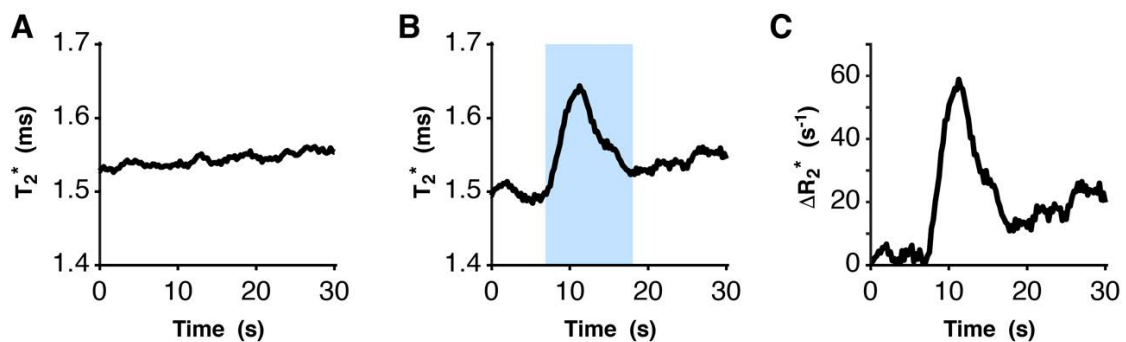
Figure 7.5: Dynamic measurement of the T_2^* of inhaled PFP in Participant 1, acquired during a 30 s breath-hold **(A)** without, and **(B)** with concurrent Gadobutrol administration. The T_2^* of inhaled PFP was transiently elevated to a peak of 1.64 ms as the intravenous bolus of Gadobutrol passed through the pulmonary circulation (highlighted region in **(B)**). **(C)** illustrates the corresponding change in R_2^* of inhaled PFP during Gadobutrol passage through the lungs.

Figure 7.5C illustrates the change in PFP R_2^* (ΔR_2^*) over the experimental time course in response to Gadobutrol administration in the same participant. A transient elevation in ΔR_2^* (approximately 60 s^{-1}) was observed relative to the baseline R_2^* value acquired prior to GBCA arrival in the lungs.

7.3.2 Dynamic ^{19}F-MR ventilation imaging

Figure 7.6A shows example 2D ^{19}F-MR ventilation images (green) superimposed on conventional ^{1}H-MR images for each of the three remaining healthy volunteers (Participants

2, 3 and 4). These images were generated by averaging the first 75 dynamics (i.e. the first 7.5 s, prior to GBCA arrival in the pulmonary circulation) of each respective ^{19}F-MRI acquisition. The position of the ^{19}F surface coil in each participant is represented by blue circles.

Figure 7.6B shows the relative change in PFP signal intensity (colour scale) following Gadobutrol administration in each of the three participants. A mean (SD) transient increase in PFP signal intensity of 8.7 (2.1)% was observed approximately 8–14 s following GBCA administration. The signal acquired in Participant 4 was reduced compared to Participants 2 and 3, secondary to poor coil positioning (as illustrated in Figure 7.6A).
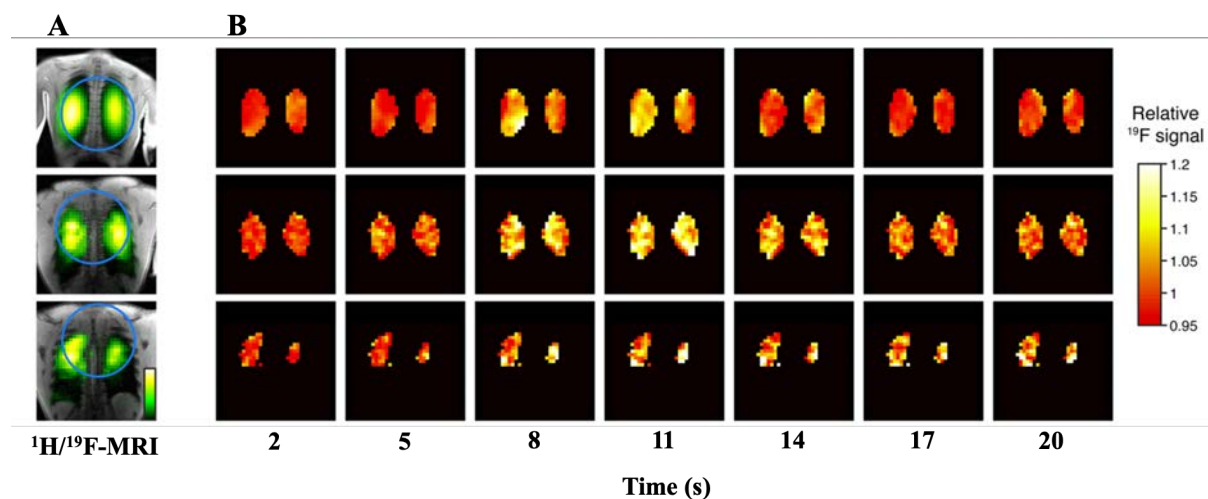
Figure 7.6: Dynamic ^{19}F-MRI of inhaled PFP acquired before, during and after passage of Gadobutrol through the pulmonary circulation. **(A)** shows T_2^*-weighted ^{19}F-MRI images overlaid on ^{1}H anatomical scans, with green circles indicating the position of the ^{19}F surface coil in each of the three participants. **(B)** shows dynamic ^{19}F-MR ventilation images, demonstrating the change in PFP signal relative to baseline (i.e. before arrival of Gadobutrol in the pulmonary circulation). A transient elevation in PFP signal amplitude is observed at approximately 8–14 s following Gadobutrol administration, reflecting partial susceptibility matching of lung water (blood) and gas components.

Plots of relative ^{19}F-MR signal amplitude in response to Gadobutrol administration over the experimental time-course for each of participants 2, 3 and 4 are illustrated in Figure 7.7. A transient elevation in PFP signal amplitude was observed approximately 8–14 s following Gadobutrol administration, reflecting partial susceptibility matching of lung aqueous and gas components.
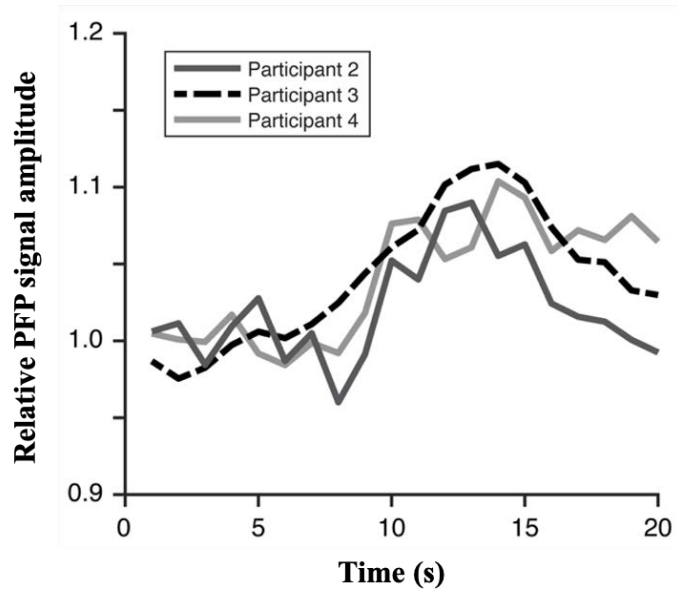
Figure 7.7: Amplitude of lung PFP signal from dynamic T_2^*-weighted ^{19}F-MRI scans acquired in Participants 2, 3 and 4. An elevation of PFP signal amplitude is observed at approximately 8–14 s following Gadobutrol administration, reflecting partial susceptibility matching of lung aqueous and gas components.

7.4   Discussion

The primary aim of this study was to assess the ability to detect paramagnetic contrast agent in the pulmonary circulation through changes to the T_2^* of inhaled PFP within directly adjacent alveoli. In support of the initial hypothesis, an elevation of PFP T_2^* and signal intensity was observed following GBCA administration, indicating transient magnetic susceptibility matching during bolus passage through the lungs. These findings demonstrate the feasibility of performing DSC ^{19}F-MRI of inhaled PFP in a small group of healthy volunteers, utilising an approach that is well suited to concurrent ventilation imaging within a single breath-hold.

The inherently short *in vivo* T_2^* of PFP (~1–2 ms) makes it well suited to observe magnetic susceptibility-matching effects in the lungs, since any changes in T_2^* are likely to have a significant impact on subsequent ^{19}F-MRI acquisitions. However, unlike the diminishing effect on T_2^* that is observed in conventional ^{1}H DSC-MRI (Albert *et al.*, 1993; Shah *et al.*, 2010), DSC ^{19}F-MRI gives rise to an *elevation* of PFP T_2^* following GBCA administration. This positive response to contrast is a direct consequence of the paramagnetic properties of Gadobutrol, leading to a reduction in the magnetic susceptibility difference between adjacent gas and tissue components of the lung. The reported elevation in T_2^* (~10%) supports the findings of previous pre-clinical studies (Dimitrov *et al.*, 2005; Vignaud *et al.*, 2005) (see Section 7.1.2) and extends the concept of magnetic susceptibility matching to human ventilation imaging, drawing on the high sensitivity of PFP T_2^* to lung microstructural properties.

Of note, the baseline T_2^* shown in Figure 7.5A (1.54 ms) was slightly longer than the PFP T_2^* observed during the pre-clinical murine study presented in Section 7.1 (see Figure 7.3). This is likely to reflect differences in the magnetic field strengths applied to respective studies; specifically, a 7.0 T scanner was used for pre-clinical experiments, whereas a 3.0 T scanner was used for all human studies. The impact of field strength may have important implications for demonstrating the efficacy of DSC ^{19}F-MRI of inhaled PFP, since greater magnetic susceptibility differences are likely to occur at higher field strengths (Wild *et al.*, 2012). Importantly, ^{19}F-MR ventilation imaging has previously been performed at 1.5 T (Gutberlet *et al.*, 2018; Maunder *et al.*, 2019, 2021), where PFP T_2^* is lengthened owing to the naturally weaker magnetic field gradients generated within the lung. A future comparison

of DSC ^{19}F-MRI performed at 1.5 T and 3.0 T would be beneficial in establishing the optimal MR scanner configuration and value of this technique.

The depth of inhalation is known to have a substantial impact on the T_2^* of inhaled PFP (Maunder *et al.*, 2021). As such, it is plausible that changes in lung inflation during the course of breath-hold could confound the effect of Gadobutrol administration on acquired T_2^* measurements. This is particularly relevant for patients with respiratory disease, who may not be able to tolerate the slightly longer breath-hold duration adopted in this study (~30 s) compared to the LIFT study (~13.5 s). Crucially, peak PFP signal intensity and T_2^* measurements were achieved within the first ~15 s for all four participants, suggesting that a shorter breath-hold duration may be sufficient to observe this effect. To mitigate the possible variation in lung inflation level during acquisitions, all participants were instructed to perform breath-holds at maximal inspiration, in accordance with the inhalation scheme adopted during Phase 1 of the LIFT study (see Chapter 3, Section 3.3). Nonetheless, slight variation in the depth of breath-hold is largely unavoidable: the difference in pre-GBCA T_2^* observed in Figure 7.5B (1.54 ms) compared to the baseline T_2^* shown in Figure 7.5A (1.50 ms) likely reflects minor alteration in lung inflation level between the two scans. The source of the subtle rise in baseline PFP T_2^* observed in Figure 7.5A (i.e. without GBCA administration) is less clear: one possibility is that this represents progressive deoxygenation of the lung gas-phase during the 30 s breath-hold duration, leading to a relative increase in alveolar PFP concentration; however, this was not corroborated by pulse oximetry measurements over the same time-course. Similarly, the slight increase in T_2^* shown in Figure 7.5B following GBCA passage compared to baseline (pre-GBCA) T_2^* is not fully understood, though this could reflect minor extravasation of Gadobutrol from the pulmonary vasculature into surrounding tissue during passage through the lungs (Cuenod and Balvay, 2013).

The ^{19}F surface coil used in this study was limited to providing low resolution 2D images of the lung apices, such that a detailed assessment of susceptibility matching throughout the lungs was not possible. Nonetheless, this was sufficient to demonstrate technical feasibility of the approach: for all four healthy volunteers, it can be inferred that at least partial susceptibility matching of gas and aqueous components was achieved, based on observed changes in PFP T_2^* and signal intensity that resolved following passage of contrast through the lungs. The ability to acquire 3D imaging of contrast agent distribution on a voxel-by-

voxel basis represents an important focus for future development of this technique, which would open the door to potential clinical application (e.g. the assessment of acute and/or chronic thromboembolic disease). Further optimisation of ^{19}F scan performance through the use of multichannel RF array coils (e.g. Kaireit *et al.*, 2018; Maunder *et al.*, 2021), as well as the adoption of CS acceleration techniques (Hollingsworth, 2015; Neal *et al.*, 2019), offers scope to implement dynamic 3D ^{19}F-MRI acquisitions with higher SNR and/or temporal resolution. This has clear implications for performing combined whole-lung assessment of both ventilation and perfusion, based on observed susceptibility-matching effects demonstrated in this preliminary study.

As discussed in Chapter 6 (Section 6.4), GBCAs represent an essential tool in diagnostic MRI (American College of Radiology, 2020) though are not without risk. Importantly, this study employed a well-established GBCA (Gadobutrol) at a dose consistent with current clinical guidelines (Bayer, 2020). However, it is possible this safety requirement restricted the degree to which susceptibility matching could be achieved within the experimental design. Notably, the doses adopted during the preclinical study outlined in Section 7.1.2 (Figure 7.3) were considerably larger than those applied to healthy volunteers, resulting in complete susceptibility matching of gas and aqueous components of the lung. Increasing the dose of GBCA (e.g. to 0.3 mmol/kg) may therefore improve the efficacy of DSC ^{19}F-MRI in its ability to (indirectly) detect regional changes in microvascular perfusion. On the other hand, it is quite feasible that a *lower* dose of GBCA would be sufficient to demonstrate this effect, given the magnitude of change in R_2^* observed (see Figure 7.5C): this compares favourably with previously reported brain DSC perfusion MRI studies (Alger *et al.*, 2009; Essig *et al.*, 2013). Application of the technique to patients with respiratory disease would enable an evaluation of the impact of pathology on ΔR_2^* over time, as well as the timing of bolus arrival in the lung microvasculature relative to administration.

The ability to assess lung perfusion using DCE-MRI was examined in Chapter 6, employing T_1-weighted imaging to monitor Gadobutrol passage through the lungs. By comparison, the DSC ^{19}F-MRI approach outlined in this chapter facilitates assessment of gas-phase PFP *directly adjacent* to contrast agent within the pulmonary microvasculature. This presents an opportunity to assess lung perfusion properties at the alveolar level, with particular relevance to exploring the efficacy of gas exchange in both health and disease; potential applications

include basic-science studies (for example, assessing the impact of airway inflammation on the pulmonary vasculature), as well as evaluation of the physiological response to therapeutic intervention (for example, the use of O_2 therapy in COPD, or anti-fibrotic medications in pulmonary fibrosis). By its nature, DSC ^{19}F-MRI only permits assessment of lung perfusion in regions of the lung that are adequately ventilated, highlighting a potential limitation of the technique. On the other hand, this also provides a unique ability to report specifically on those regions of the lung that are directly participating in gas exchange (i.e. are both ventilated and perfused), which may be of greater clinical significance. Previous studies employing dynamic ^{19}F-MR ventilation imaging (e.g. Gutberlet *et al.*, 2018; Goralski *et al.*, 2020), including work presented in the previous chapter of this thesis, have demonstrated that even poorly ventilated regions of the lung can exhibit gas wash-in, albeit at slower rates compared to well ventilated regions. As such, with appropriate experimental design, this limitation may be confined to regions of the lung where ventilation is truly absent (for example, complete airway obstruction secondary to an endobronchial mass).

The capacity for simultaneous evaluation of alveolar ventilation and perfusion is of considerable interest, given the central role in facilitating pulmonary gas exchange. Combined ventilation and perfusion imaging has previously been reported in pre-clinical studies employing ^{19}F-MRI of inhaled SF_6 (Adolphi and Kuethe, 2008), based on the accumulation of inhaled gas in lung regions exhibiting a low alveolar ventilation/perfusion ratio. The translation of this approach to human imaging is uncertain, however, given the complex relationship that exists between lung ventilation, perfusion, and the changing concentration of inhaled gas within the lung. The use of FD-MRI represents a promising alternative to techniques reliant on exogenous contrast agent administration, enabling an indirect but entirely non-invasive approach to pulmonary ventilation and perfusion assessment over the course of several respiratory cycles (Bauman *et al.*, 2013; Fischer *et al.*, 2014; Voskrebenzev *et al.*, 2018). However, as indicated previously, the requirement for robust post-processing image capabilities and expertise has currently restricted this approach to specialist research settings. By comparison, the DSC ^{19}F-MRI approach reported in this study offers a rapid (i.e. single breath-hold) assessment that can be readily incorporated into existing ^{19}F-MR ventilation imaging techniques, such as those employed by the LIFT study (outlined in Chapters 3, 4 and 5). This represents a promising avenue for future investigation.

7.5   Conclusion

This study has demonstrated the ability to alter the T_2^* of inhaled PFP following administration of an intravenous paramagnetic contrast agent, reflecting transient susceptibility-matching at the gas-tissue interface. As far as is known, this represents the first *in man* demonstration of DSC ^{19}F-MRI of inhaled PFP. Importantly, these findings offer potential for indirect assessment of pulmonary microvascular perfusion properties through observed changes in gas-phase PFP signal intensity, presenting a novel, radiation-free approach to combined ventilation/perfusion assessment at the alveolar level. Further evaluation against existing MRI methods, as well as conventional imaging modalities and lung function tests, is essential to determine the utility of this technique to provide clinically relevant functional information relating to pulmonary pathophysiology. Nonetheless, in conjunction with work presented in Chapter 6, this study highlights the possibility of extending pulmonary ^{19}F-MRI beyond pure ventilation imaging. The potential clinical applications of this technique, and of ^{19}F-MRI of inhaled PFP in general, are considered further in the final chapter of this thesis (Chapter 8).

Chapter 8.
General Discussion

8.1   Overview

The preceding chapters of this thesis (Chapters 3–7) outlined the development of novel ^{19}F-MRI scan procedures to assess pulmonary ventilation and perfusion properties in healthy volunteers and patients with respiratory disease. This work was conducted within the framework of three independent, but related, studies (LIFT, VQ MRI and LungGas). In this final chapter, a summary of the principal findings stemming from these experimental studies is provided, alongside a discussion of key strengths and limitations relating to this body of research. Potential clinical applications of the methods described, as well as avenues for future research, are also considered.

8.2   Strengths and limitations of this research

The LIFT study forms a major component of the work presented in this thesis, involving a large number of participants across two different research sites. To date, this represents the first study to employ %VV measurements acquired by ^{19}F-MRI of inhaled PFP to distinguish ventilation properties in healthy volunteers and patient populations. The experimental results presented in Chapter 4 and Chapter 5 confirm the ability to acquire reproducible measurements of %VV in a large number of healthy volunteers, and to utilise this approach to identify ventilation defects in patients with asthma and patients with COPD. In addition, this study outlines the first demonstration of changes to regional PFP gas distribution in response to BD therapy, highlighting the potential to quantify treatment response in patients with asthma; for patients with COPD, it is likely a larger number of participants is necessary to determine the true utility of this approach (see Chapter 5). The preliminary data acquired as part of the VQ MRI and LungGas studies (Chapters 6 and 7, respectively) reveal potential advances in scan methodology that may provide richer information regarding lung function applicable to future patient studies. In particular, the ability to combine ^{19}F-MRI scan procedures with established MR perfusion techniques offers the opportunity to perform novel measurements of combined pulmonary ventilation and perfusion properties, with scope for translation to clinical practice.

Despite these findings, a number of challenges exist relating to this work. Specifically, as outlined in Chapter 3 (Section 3.3), static ^{19}F-MR ventilation imaging is intrinsically linked to breathing efficacy, which may limit the ability to accurately distinguish ventilation defects from poor gas inhalation. The breathing protocol employed by the LIFT study (i.e. three deep wash-in breaths of gas, followed by a breath-hold at maximal inspiration) was developed to achieve substantial replacement of air by PFP within the lungs, maximising the SNR in ventilated regions and facilitating reproducibility of scan acquisitions. At the same time, the brevity of this wash-in breathing protocol was designed to preserve the discernibility of poorly ventilated lung regions that is characteristic of patients with obstructive airways disease (Halaweish *et al.*, 2013a; Virgincar *et al.*, 2013; McCallister *et al.*, 2021). This inhalation scheme was fundamental in determining the %VV values reported in Chapter 4 and Chapter 5. However, it is important to recognise that various other factors impact ^{19}F-MRI acquisitions and subsequent %VV measurements: these include the particular scan acquisition parameters employed; inherent participant-coil magnetic field inhomogeneities; and the type of analysis software used (e.g. VVTool or RegSeg). Where one or more of these factors is adversely impacted – for instance, a poorly functioning RF coil, or the use of incorrect scan parameters (see Chapter 3, Section 3.2) – it may be difficult to define true ventilation abnormalities, confounded further by the possibility of poorly performed breathing manoeuvres.

Ensuring correct adherence to study procedures was therefore essential to maintaining reproducibility of the adopted methods. Notably, twelve participants recruited to Phase 2 of the LIFT study were withdrawn following the identification of a recurring intermittent coil fault; a further two participants were excluded from this study as a result of poor compliance with breathing instructions, while three participants were also excluded from Phase 3 of the study secondary to poor coil performance. These cases underscore the highly developmental nature of this work, where the establishment of robust scan procedures and optimal hardware configuration remains very much in infancy. The alternative methods explored in Chapter 6 may offer some benefit in this regard, since dynamic imaging reduces the requirement to follow a rigid inhalation scheme, thereby removing some of the dependence on breathing performance that is critical to static ^{19}F-MR ventilation imaging. This approach also plays to the strengths of ^{19}F-MRI of PFP compared to HP-MRI, where the thermally polarised gas does not exhibit the irrecoverable loss of signal over a dynamic imaging series that is unavoidable with hyperpolarised gases (Kruger *et al.*, 2016). Consequently, while the LIFT

study provides an important benchmark for evaluating ventilated lung volume measurements in line with existing HP-MRI literature (Kirby *et al.*, 2012a; Horn *et al.*, 2014a; Ebner *et al.*, 2017b), it is likely that future ^{19}F-MRI studies will focus on quantifying measures derived from dynamic imaging methods (e.g. Gutberlet *et al.*, 2018; Goralski *et al.*, 2020). Given the emerging nature of human ^{19}F-MR ventilation imaging, it unsurprising that agreed imaging and gas inhalation protocols do not yet exist across different sites. Nonetheless, establishing standardised scan procedures represents an important factor in progressing the field towards clinical implementation; the present work provides an important contribution to this developmental process.

The reproducibility of static ^{19}F-MR ventilation imaging was primarily determined by evaluating the intra-participant and inter-assessor repeatability of same-day %VV measurements in healthy volunteers, based on analysis of images acquired independently in Newcastle upon Tyne and Sheffield. This design was effective in demonstrating the ability to replicate scan procedures across the two study sites, as well as confirming the utility of the adopted methods to quantify gas distribution in a consistent manner. It should be noted, however, that the analysis tools used in this study (VV Tool and RegSeg) were not established methods for analysis of ^{19}F-MRI datasets and, as such, creation of a standardised data processing workflow for the two assessors was required. This has potential to diminish the value of the reported measurements, since both assessors were unblinded to images and trained in an identical manner to analyse these. Nevertheless, this was a necessary step in establishing an acceptable approach to %VV measurement, utilising novel methods as part of a broader developmental pathway. Importantly, this work represents the first evaluation of %VV measurements acquired by ^{19}F-MRI of inhaled PFP, providing a firm basis for future development of a robust, standardised approach to (semi-)automated analysis of participant data.

An alternative approach, involving blinding of assessors to participant details, may add weight to the assessment of %VV measurement reproducibility by removing potential bias stemming from knowledge of the presence or absence of underlying respiratory disease (Kirby *et al.*, 2012b). This would also facilitate an evaluation of *intra*-assessor measurement reproducibility, since multiple %VV values could be generated for the same image dataset presented more than once to individual assessors. Of note, this study was limited to evaluating the same-day reproducibility of %VV measurements in groups of healthy

volunteers attending one of the two study sites. A more detailed analysis of intra-participant %VV reproducibility may benefit from scanning the same participant at both study sites (e.g. Svenningsen *et al.*, 2020), thereby providing a deeper evaluation of the ability to implement procedures consistently across different settings in anticipation of performing larger clinical trials.

Owing to the design of Phase 3 of the LIFT study, it was not possible to perform an analysis of patient %VV reproducibility in the same manner as that performed during Phase 2 of the study; this is likely to be of greater relevance in translating the technique to clinical practice and, as such, represents an important consideration for future study design. Building on this concept, it is salient to recognise that PFP wash-out from the lungs may impact the ability to accurately assess same-day repeatability of %VV measurements in patients using the same procedures adopted for healthy volunteers. This is particularly true for patients with evident gas trapping (e.g. relating to severe emphysema), where the presence of PFP gas within the lungs *prior* to subsequent inhalations will inevitably contribute to successive measures of gas distribution. It is unlikely this was a significant factor during Phase 3 of the LIFT study, since post-BD scans were performed approximately one hour after pre-BD scans, by which time PFP is expected to have been fully expelled from the lungs. Nonetheless, the precise wash-out time for individual patients was not known and may have persisted for *at least* 25 minutes (as highlighted in Chapter 6, Section 6.3.1). Consequently, future assessment of %VV reproducibility should be wary of performing repeated measurements within close temporal proximity: the approximate six-minute interval described in Chapter 4 (Section 4.2.2), whilst suitable for healthy volunteers, is almost certainly too short for patients with respiratory disease who may have a propensity for slow regional gas wash-out.

As indicated in Chapter 5 (Section 5.3.2), the %VV measurements acquired in healthy volunteers differed significantly from measurements acquired in patients with asthma and patients with COPD. This finding is in firm agreement with the original study hypothesis outlined in Chapter 1 (Section 1.6). However, it is well established that lung function varies with age (Lowery *et al.*, 2013) and sex (Lomauro and Aliverti, 2018), both of which may confound observed differences between the respective study groups. This was an unavoidable consequence of the developmental design of the LIFT study, since it was necessary to establish the reproducibility of scan procedures in healthy volunteers *prior* to implementation in patient groups: the availability of a predominantly younger cohort of healthy volunteers

(recruited largely from local University institutions) made it impractical to age-match these participants with subsequent patient groups (who were typically slightly older, especially patients with COPD). On the other hand, the overriding goal of the LIFT study was to demonstrate the utility of the established study methods to quantify differences in ventilation properties using ^{19}F-MRI of inhaled PFP, rather than assessing sensitivity of the technique to detect variations stemming from, for example, age, sex, or severity of disease. This early-phase study provides a robust foundation on which to address these aspects through future experimental design.

Although smaller in scale compared to the LIFT study, the two feasibility studies outlined in Chapter 6 and Chapter 7 were pivotal in exploring alternatives to static ^{19}F-MR ventilation imaging employing single %VV measurements. The reduced number of participants recruited to the VQ MRI study (secondary to the emergence of the COVID-19 pandemic) necessarily impacted the ability to perform a broader analysis of these data, which was restricted to describing individual participants. Nonetheless, these findings highlight the potential to adopt dynamic measurements of gas wash-in/wash-out properties to identify underlying pathology, supporting recent ^{19}F-MRI studies involving patients with COPD (Gutberlet *et al.*, 2018, 2019) and CF (Goralski *et al.*, 2020; McCallister *et al.*, 2021). Importantly, the dynamic imaging protocols employed by the VQ MRI study were restricted to a scan duration of 90 s, determined by a cautious approach to SAR limits relating to use of third-party RF coil hardware. This prevented an assessment of complete gas wash-in and wash-out over a longer acquisition period, underpinning the particular sequence of scans included in this work (see Chapter 6, Section 6.3.2). It is anticipated that, as experience grows, these restrictions on scan duration and power settings will be relaxed, enabling longer acquisition periods and scans with higher RF power, which may help to improve the quality (and resulting information content) of ^{19}F-MRI acquisitions by these methods.

The use of CS (e.g. Ajraoui *et al.*, 2010; Chan *et al.*, 2017; Neal *et al.*, 2019) is likely to benefit dynamic imaging further by facilitating a reduction in scan times and/or an increase in the SNR of acquired ventilation images. This approach was utilised as part of the interleaved protocol outlined in Chapter 6 (see Figure 6.1C), enabling shorter breath-hold durations (~7.5 s) compared to the LIFT study (~13.5 s). Application of CS to the free-breathing protocols explored in this chapter holds potential to improve both the spatial and temporal resolution of individual dynamic acquisitions and represents a promising avenue for future evaluation.

Moreover, by reducing the overall scan time, CS may facilitate combined ^{1}H (anatomical) and ^{19}F (ventilation) imaging within a single breath-hold duration; this approach has previously been reported with hyperpolarised ^{3}He (e.g Horn *et al.*, 2014), alleviating some of the challenges to %VV measurement arising from potential mis-registration of separate breath-hold acquisitions (see Chapter 4, Figure 4.5).

The SNR values reported in this thesis were derived from ^{19}F-MRI acquisitions according to the specific methods outlined in Chapter 4 (Section 4.2.3) and Chapter 6 (Section 6.2.3). As expected, these values are reduced compared to values typically reported in the HP-MRI literature (Kirby *et al.*, 2012a; Hughes *et al.*, 2018), stemming from the thermally polarised nature of inhaled PFP compared to the hyperpolarised state of inhaled ^{3}He and ^{129}Xe. However, it is difficult to directly compare these measurements with previously published ^{19}F-MRI studies (e.g. Halaweish *et al.*, 2013a; Couch *et al.*, 2013), owing to intrinsic differences in the choice of RF coil hardware, scanner field strength, breathing protocols employed, and the relative lack of information regarding adopted scan parameters. As such, what constitutes an 'acceptable' or 'sufficient' SNR remains somewhat nebulous: in this thesis, the absolute value obtained was considered less critical than the ability to visually distinguish gas distribution from background noise, enabling calculation of %VV measurements using one of the two analysis tools (VV Tool and RegSeg). There is a clear element of subjectivity inherent in this approach, which naturally increases with diminishing SNR. An alternative strategy could employ a threshold-based approach (e.g. Couch *et al.*, 2019b), whereby images with an SNR above a pre-determined value are deemed 'acceptable'. However, this runs the risk of excluding datasets where the SNR is appropriately reduced as a manifestation of underlying respiratory disease. Moreover, as discussed in Chapter 5 (Section 5.4), it is possible that SNR measurements may be acquired from a single lung ROI with low or absent signal, despite other lung regions demonstrating substantial gas signal. A pragmatic approach was therefore adopted for this work, whereby images were considered suitable for use provided they were acquired in line with the established scan procedures and inhalation protocols (accepting this would require additional manual interpretation for images with lower SNR).

The use of advanced MR coil hardware, such as multichannel receive array coils (e.g. Kaireit *et al.*, 2018), may help to improve the overall SNR of ^{19}F-MR images, as well as address the spread of SNR values observed between participants (Chapter 4, Section 4.3.3; Chapter 5,

Section 5.3.3): this may, in part, stem from differences in coil loading associated with varying body habitus, in addition to differences in breathing efficiency relating to the gas wash-in protocol used. Moreover, improved coil design may mitigate the tendency for spatially variable signal inhomogeneities, more apparent towards the outermost anterior image slices (e.g. Chapter 4, Figure 4.7; Chapter 5, Figure 5.12); while this potentially reflects a degree of physiological ventilation heterogeneity (e.g. Musch *et al.*, 2002), it is more likely the result of local field inhomogeneity arising from scanner-coil interaction. Notably, previous work conducted by Neal (2017) demonstrated a reduction in SNR with increasing distance from the base of the 3D birdcage coil, highlighting a key limitation of the current set-up (i.e. observed anterior-posterior signal gradients may confound the ability to detect true ventilation defects). This signal gradient was particularly apparent in the VQ MRI study, where measured SNR values were consistently increased in posterior lung regions compared to more anterior lung regions (see Chapter 6, Figures 6.4–6.6). This inhomogeneity in coil performance was not resolved despite multiple interactions with the coil manufacturer, including several coil service returns. Nonetheless, routine clinical and research [1]H-MRI demonstrates that it is technically feasible to build chest RF coil hardware with minimal performance inhomogeneity. Alternative coil designs, such as wrap-around vest coils, have been adopted in previous ^{19}F-MRI studies (Couch *et al.*, 2013; Halaweish and Charles, 2014) and may be appropriate to consider in future study design to minimise such hardware-driven SNR gradients. Importantly, segmentation of these outermost image slices does not appear to have substantial impact on the global %VV measurements reported in the LIFT or VQ MRI studies.

A formal evaluation of the safety profile of inhaled PFP (e.g. through a clinical trial of an investigational medicinal product, or CTIMP) was beyond the scope of this thesis. Nevertheless, the reported studies add weight to the growing body of evidence surrounding the successful use of PFP for human ventilation imaging (Halaweish *et al.*, 2013a; Gutberlet *et al.*, 2018; Goralski *et al.*, 2020). In total, 550 gas inhalation sessions were performed by the 116 participants initially recruited to the LIFT study, with the majority of these sessions comprising three deep breaths of the 79% PFP / 21% O_2 gas mixture. Combined with work conducted as part of the LungGas and VQ MRI studies (which included continuous gas inhalation over the course of several minutes), this represents a substantial dataset (123 participants in total) concerning the tolerability of ^{19}F-MRI of inhaled PFP. Importantly, no adverse events were observed in any of the participants recruited to the respective studies,

providing a robust platform on which to perform larger multi-centre trials, crucial to establishing the suitability of this technique for future clinical adoption.

8.3   Potential clinical applications and future research

A central goal of this thesis was to assess the utility of ^{19}F-MRI of inhaled PFP to quantify ventilation defects in patients with asthma and patients with COPD, including the ability to identify changes in gas distribution in response to BD therapy. Evaluation of treatment response represents an attractive avenue for MR-based pulmonary imaging, since information relating to both lung structure and function can be obtained longitudinally without recourse to ionising radiation. Previous MRI studies have demonstrated the capacity to detect regional changes in ventilation in response to various therapeutic interventions in patients with asthma (Svenningsen *et al.*, 2013; Capaldi *et al.*, 2017; Horn *et al.*, 2017a), COPD (Kirby *et al.*, 2011; Vogel-Claussen *et al.*, 2019) and CF (Altes *et al.*, 2017; Rayment *et al.*, 2019), often with improved sensitivity compared to conventional spirometric measures. Although pulmonary ^{19}F-MRI remains in relative infancy, it is quite feasible that this technique will be used for similar applications in the future: these need not be limited to obstructive lung diseases, since the principles outlined in this thesis can be readily extended to examine other conditions, for example pulmonary fibrosis, where hyperpolarised ^{129}Xe has already shown particular promise (Wild, 2018). Crucially, the lack of requirement for hyperpolarisation equipment and expertise, coupled with the ability to perform dynamic imaging over the course of several respiratory cycles, presents significant advantages for downstream development and application.

Beyond its potential role as an imaging modality for use in clinical trials (e.g. in assessing the efficacy of novel drug therapies), a number of promising applications exist in relation to ^{19}F-MR ventilation imaging. In particular, the ability to characterise 'gas trapping' in the emphysematous lung – both during breath-hold imaging (see Chapter 5), as well as dynamic imaging of PFP wash-in/wash-out (see Chapter 6) – may be valuable in planning for, and assessing response to, lung volume reduction surgery (Adams *et al.*, 2018). The capacity to employ intravenous GBCAs in combination with inhaled PFP (outlined in Chapter 6) offers further benefit, enabling clarification of regional ventilation/perfusion relationships that may help guide targeted intervention. Notably, the combination of ^{19}F-MRI and DCE-MRI presents a novel opportunity to assess pulmonary thromboembolic disease without exposure

to ionising radiation; this is especially appealing for young or pregnant females, in whom the use of conventional CTPA or perfusion scintigraphy is associated with an increased risk of malignancy (Perisinakis *et al.*, 2014). Future studies comparing these scan procedures with existing imaging modalities will be crucial in determining their clinical efficacy; the use of DCE-MRI has already shown promise in this regard (e.g. Johns *et al.*, 2017b), while the concurrent application of ^{19}F-MRI provides an opportunity for complementary evaluation of ventilatory function.

The DSC ^{19}F-MRI technique outlined in Chapter 7 extends the assessment of pulmonary perfusion to the alveolar level, reporting specifically on those areas of the lung that are *both* ventilated *and* perfused. This may be applicable to basic physiology studies concerning gas exchange, as well as to clinical populations that could benefit from the evaluation of regional changes in microvascular perfusion (for example, determining which patients are likely to benefit from initiation and/or continuation of long-term O_2 therapy). Recently, the ability to detect dissolved-phase ^{129}Xe uptake in the capillary blood has been utilised as a potential biomarker of impaired gas transfer (Wang *et al.*, 2018; Qing *et al.*, 2019; Weatherley *et al.*, 2019). Given its inherent dependence on alveolar microstructure, it is possible DSC ^{19}F-MRI could provide similar functional information without the requirement for hyperpolarisation. Future research employing 3D imaging in different patient populations (for example, COPD, PE, and fibrotic lung disease) is necessary to establish the utility of this technique to provide clinically relevant metrics relating to regional gas exchange.

In order to progress the field of pulmonary ^{19}F-MRI towards clinical adoption, it is essential to compare the technique not only with existing clinical modalities (e.g. CT and spirometry), but with other MRI-based methods. Preliminary studies have recently explored the use of dynamic ^{19}F-MRI with FD-MRI in patients with COPD (Kaireit *et al.*, 2018) and with hyperpolarised ^{129}Xe in patients with CF (McCallister *et al.*, 2021), suggesting broad agreement in the ability to detect ventilation defects in these patient groups. Future evaluation of %VV measurements derived from ^{19}F-MRI and HP-MRI (performed at the University of Sheffield alongside the LIFT study) is expected to provide a firm benchmark for this approach to static ventilation imaging. Nonetheless, it is important to recognise that these techniques may not be directly comparable, since the gas inhalation protocols employed differ so considerably; notably, McCallister *et al.* (2021) conclude that VDP measurements stemming from inhaled PFP should not be considered equivalent to VDP measurements

derived from ^{129}Xe, reflecting these inherent differences. Future research is likely to benefit from examining the relationship between early-phase and late-phase %VV (or VDP) measurements in characterising airways disease beyond a single value (Gutberlet *et al.*, 2018; McCallister *et al.*, 2021), taking advantage of the ability to inhale PFP over the course of several minutes. As knowledge of ^{19}F-MR ventilation imaging has evolved, there has been a corresponding shift in focus away from simply replicating existing measures (e.g. based on static HP-MRI methods) towards establishing new biomarkers of disease. The scan procedures outlined in Chapter 6 provide a platform on which to investigate this further, where the ability to monitor PFP wash-in and wash-out rates, as well as the association between them, may provide more clinically meaningful information than either one of these parameters alone.

It should be noted that, although different approaches to pulmonary MRI exist (as outlined in Chapter 1, Section 1.5), these do not have to be viewed as competing technologies; rather, it is prudent to consider the relative strengths of each technique in guiding the most appropriate clinical application. For instance, while ^{19}F-MRI offers potential advantages for evaluating airways disease through its ability to assess a range of dynamic ventilation properties, the capacity for higher resolution HP-MRI is (at present) likely better suited to report on static ventilation and global %VV measurements. The choice of technique may therefore be influenced by the specific clinical question, e.g. for a patient with COPD, HP-MRI may help to inform the *severity* of ventilation defect following a single breath, whereas PFP imaging may help to characterise regional ventilation *efficiency* (i.e. whether gas uptake is truly absent, or simply slow filling). Similarly, the avoidance of exogenous contrast agents entirely may make FD-MRI a more attractive option for investigating childhood disease (e.g. asthma, or CF), fostered by the ability to maintain relaxed breathing throughout. Importantly, a reliance on non-tidal (or forced) breathing and/or breath-hold manoeuvres may render some inhaled gas imaging techniques inappropriate for specific patient groups, such as those with significant breathlessness (which may be exacerbated lying supine). Moreover, a number of practical considerations exist relating to MRI in general, such that this modality may not be suitable for certain individuals (e.g. those with obesity, cardiac pacemakers and/or other implantable devices). The goal of this thesis is therefore not to disregard, or replace, other existing methods (including established clinical tests like CT and spirometry), but to highlight the potential of an additional tool to support the broader evaluation of pulmonary pathophysiology.

For ^{19}F-MRI, as with other MRI techniques, the path to clinical adoption is likely to be determined by several interdependent factors, including advances in hardware capabilities (e.g. improved RF coil performance), the development of simple and intelligible analysis tools, and standardisation of scan and breathing protocols. The present research represents an early phase within this developmental journey, heavily influenced by the systems and technologies currently available; at times, this has presented particular challenges to progress through the reliance on imperfect techniques and equipment (see Chapter 3, Section 3.2). As such, this work should not be viewed as the 'best possible' approach to ^{19}F-MR ventilation imaging, but rather a set of acceptable and workable procedures that form part of a wider iterative process. Fundamental to driving this process forward is the effective collaboration between MR physicists, engineers, clinicians and, crucially, patients. This approach has underpinned the work conducted over the course of my PhD, stressing the critical need to bring together experience and expertise across diverse fields to fulfil a common goal.

8.4 Conclusion

^{19}F-MRI of inhaled PFP represents a nascent area for human lung imaging. This thesis presents methods for performing static ^{19}F-MR ventilation imaging, focussing on the application of scan procedures to healthy volunteers, patients with asthma, and patients with CODP. In addition, novel approaches to the assessment of combined pulmonary ventilation and perfusion properties are described, utilising an established GBCA to extend the role of ^{19}F-MRI beyond pure ventilation imaging. This work builds upon an emerging literature base surrounding the use of inhaled PFP as a viable alternative to existing MRI techniques. As the field of pulmonary MRI continues to mature, the clinical relevance and utility of ^{19}F-MR ventilation imaging is likely to become more apparent. The methods outlined in this thesis provide an important contribution to this developmental process, with potential to complement and extend the existing armamentarium for the investigation of respiratory disease.

List of publications and presentations arising from this body of research

Publications

Pippard B.J., Neal M.A., Maunder A.M., *et al*. (2021) 'Reproducibility of ^{19}F-MR ventilation imaging in healthy volunteers', *Magnetic Resonance in Medicine*, 85, pp. 3343–3352.

Neal M.A.[*], **Pippard B.J.**[*], Simpson A.J. and Thelwall P.E. (2020) 'Dynamic susceptibility contrast ^{19}F-MRI of inhaled perfluoropropane: a novel approach to combined pulmonary ventilation and perfusion imaging', *Magnetic Resonance in Medicine*, 83, pp. 452–461. ([*]**joint first authors**)

Neal M.A., **Pippard B.J.**, Hollingsworth K.G., *et al*. (2019) 'Optimized and accelerated ^{19}F-MRI of inhaled perfluoropropane to assess regional pulmonary ventilation', *Magnetic Resonance in Medicine*, 82, pp.1301–1311.

Presented abstracts

Pippard B, Neal M, Forrest I, *et al*. Assessing bronchodilator response in patients with asthma and COPD using ^{19}F-MRI. *ERS International Congress, Sept 2020 (Virtual)*. **Poster presentation.**

Pippard B, Neal M, Maunder A, *et al*. Multicentre reproducibility of ^{19}F-MR ventilation imaging in healthy volunteers. *BTS Winter Meeting, Dec 2019 (London, UK)*. **Oral presentation**.

Pippard B, Neal M, Simpson AJ, Thelwall P. Assessing ventilation/perfusion properties with dynamic ^{19}F-MRI of inhaled perfluoropropane. *ERS International Congress, Sept 2019 (Madrid, Spain)*. **Poster presentation.**

Pippard B, Neal M, Maunder A, *et al*. Compressed sensing to reduce breath-hold duration in ^{19}F-MR ventilation imaging. *ERS International Congress, Sept 2019 (Madrid, Spain).* **Poster presentation.**

Pippard B, Neal M, Maunder A, *et al*. Assessing regional lung ventilation in patients and healthy volunteers using ^{19}F-MRI of inhaled perfluoropropane. *BTS Winter Meeting, Dec 2018 (London, UK).* **Oral presentation.**

Pippard B, Neal M, Simpson AJ, Thelwall P. Probing ventilation/perfusion properties using dynamic susceptibility contrast ^{19}F-MRI of inhaled perfluoropropane. *BTS Winter Meeting, Dec 2018 (London, UK).* **Oral presentation.**

Pippard B, Neal M, Simpson AJ, Thelwall P. Combined ventilation and perfusion imaging using dynamic susceptibility contrast ^{19}F-MRI of inhaled perfluoropropane. *British Chapter of the International Society for Magnetic Resonance in Medicine, Sept 2018 (Oxford, UK).* **Oral presentation.**

Pippard B, Neal M, Maunder A, *et al*. Assessing regional lung ventilation with ^{19}F-MRI of inhaled perfluoropropane. *ERS International Congress, Sept 2018 (Paris, France).* **Oral presentation.**

Pippard B, Neal M, Dutta P, Simpson AJ, Thelwall P. ^{19}F-MRI of inhaled perfluoropropane gas: a novel approach to ventilation imaging. *BTS Winter Meeting, Dec 2017 (London, UK).* **Poster presentation.**

Pippard B, Neal M, Dutta P, Simpson AJ, Thelwall P. Pulmonary ventilation imaging with ^{19}F-MRI of inhaled perfluoropropane gas. *British Chapter of the International Society for Magnetic Resonance in Medicine, Sept 2017 (Liverpool, UK).* **Oral presentation.**

Invited talk:

Functional MR imaging of the lung. *North East Cystic Fibrosis Club Annual Meeting, February 2020 (Centre for Life, Newcastle upon Tyne).*

List of awards relating to this body of research

GSK Sparrows SpR Symposium – First Place

ERS International Congress, Madrid, September 2019

North of England Thoracic Society – 'Golden Bronchoscope' Trainee Prize

Newcastle upon Tyne, November 2018

Institute of Cellular Medicine Director's Day – award for best poster

Newcastle University, Newcastle upon Tyne, September 2018

British Association for Lung Research Travel Award

BTS Winter Meeting, London, December 2019

British Thoracic Society Travel Grant

ERS International Congress, Madrid, September 2019

Newcastle University Travel Award

BTS Winter Meeting, London, December 2018

British Lung Foundation Travel Fellowship

ERS International Congress, Paris, September 2018

References

Adams, C.J., Capaldi, D.P.I., Di Cesare, R., McCormack, D.G. and Parraga, G. (2018) 'On the potential role of MRI biomarkers of COPD to guide bronchoscopic lung volume reduction', *Academic Radiology*, 25(2), pp. 159–168.

Adolphi, N.L. and Kuethe, D.O. (2008) 'Quantitative mapping of ventilation-perfusion ratios in lungs by 19F MR imaging of T1 of inert fluorinated gases', *Magnetic Resonance in Medicine*, 59(4), pp. 739–746.

Agarwal, R., Brunelli, S.M., Williams, K., Mitchell, M.D., Feldman, H.I. and Umscheid, C.A. (2009) 'Gadolinium-based contrast agents and nephrogenic systemic fibrosis: a systematic review and meta-analysis', *Nephrology Dialysis Transplantation*, 24(3), pp. 856–863.

Ajraoui, S., Lee, K.J., Deppe, M.H., Parnell, S.R., Parra-Robles, J. and Wild, J.M. (2010) 'Compressed sensing in hyperpolarized 3He lung MRI', *Magnetic Resonance in Medicine*, 63(4), pp. 1059–1069.

Albert, M.S., Haung, W., Lee, J.-H, Patlak, C.S. and Springer, C.S. (1993) 'Susceptibility changes following bolus injections', *Magnetic Resonance in Medicine*, 29(5), pp. 700–708.

Albert, M.S., Cates, G.D., Driehuys, B., Happer, W., Saam, B., Springer, C.S. and Wishnia, A. (1994) 'Biological magnetic resonance imaging using laser-polarized 129Xe', *Nature*, 370(6486), pp. 199–201.

Alger, J., Schaewe, T., Lai, T., Frew, A., Vespa, P., Etchepare, M., Liebeskind, D., Saver, J. and Kidwell, S. (2009) 'Contrast agent dose effects in cerebral dynamic susceptibility contrast magnetic resonance perfusion imaging', *Journal of Magnetic Resonance Imaging*, 29(1), pp. 52–64.

Altes, T.A., Johnson, M., Fidler, M., Botfield, M., Tustison, N.J., Leiva-Salinas, C., de Lange, E.E., Froh, D. and Mugler, J.P. (2017) 'Use of hyperpolarized helium-3 MRI to assess

response to ivacaftor treatment in patients with cystic fibrosis', *Journal of Cystic Fibrosis*, 16(2), pp. 267–274.

American College of Radiology (2020) *ACR Manual on Contrast Media*. Available at: http://www.acr.org/~/media/ACR/Documents/PDF/QualitySafety/Resources/Contrast Manual/2013_Contrast_Media.pdf. (Accessed: 22 December 2020).

Amis, T.C., Jones, H.A. and Hughes, J.M.B. (1984) 'Effect of posture on inter-regional distribution of pulmonary ventilation in man', *Respiration Physiology*, 56(2), pp. 145–167.

Asthma UK (2017) *Asthma facts and statistics.* Available at: http://www.asthma.org.uk/about/media/facts-and-statistics/ (Accessed: 22 December 2020).

Aurora, P., Gustafsson, P., Bush, A., Lindblad, A., Oliver, C., Wallis, C.E. and Stocks, J. (2004) 'Multiple breath inert gas washout as a measure of ventilation distribution in children with cystic fibrosis', *Thorax*, 59(12), pp. 1068–1073.

Bajc, M., Schümichen, C., Grüning, T., Lindqvist, A., Le Roux, P.Y., Alatri, A., Bauer, R.W., Dilic, M., Neilly, B., Verberne, H.J., Delgado Bolton, R.C. and Jonson, B. (2019) 'EANM guideline for ventilation/perfusion single-photon emission computed tomography (SPECT) for diagnosis of pulmonary embolism and beyond', *European Journal of Nuclear Medicine and Molecular Imaging*, 46(12), pp. 2429–2451.

Baraldo, S., Turato, G. and Saetta, M. (2012) 'Pathophysiology of the small airways in chronic obstructive pulmonary disease', *Respiration*, 84(2), pp. 89–97.

Bates, D., Maechler, M., Bolker, B. and Walker, S. (2014) 'lme4: linear mixed-effects models using Eigen and S4. *R package version 1.1-7*. Available at: http://CRAN.R-project.org/package=lme4.

Bauman, G., Puderbach, M., Deimling, M., Jellus, V., Chefd'hotel, C., Dinkel, J., Hintze, C., Kauczor, H.U. and Schad, L.R. (2009) 'Non-contrast-enhanced perfusion and ventilation assessment of the human lung by means of Fourier decomposition in proton MRI', *Magnetic Resonance in Medicine*, 62(3), pp. 656–664.

Bauman, G. and Eichinger, M. (2012) 'Ventilation and perfusion magnetic resonance imaging of the lung', *Polish Journal of Radiology*, 77(1), pp. 37–46.

Bauman, G., Scholz, A., Rivoire, J., Terekhov, M., Friedrich, J., De Oliveira, A., Semmler, W., Schreiber, L.M. and Puderbach, M. (2013) 'Lung ventilation- and perfusion-weighted Fourier decomposition magnetic resonance imaging: in vivo validation with hyperpolarized 3He and dynamic contrast-enhanced MRI', *Magnetic Resonance in Medicine*, 69(1), pp. 229–237.

Bayer (2020) *Summary of product characteristics: Gadovist 1.0 mmol/ml solution for injection.* Available at: https://www.medicines.org.uk/emc/product/2876/smpc#gref. (Accessed: 22 December 2020).

van Beek, E.J.R., Dahmen, A.M., Stavngaard, T., Gast, K.K., Heussel, C.P., Krummenauere, F., Schmiedeskamp, J., Wild, J.M., Søgaard, L.V., Morbach, A.E., Schreiber, L.M. and Kauczor, H.U. (2009) 'Hyperpolarised 3He MRI versus HRCT in COPD and normal volunteers: PHIL trial', *European Respiratory Journal*, 34(6), pp. 1311–1321.

Behzadi, A.H., Zhao, Y., Farooq, Z. and Prince, M.R. (2018) 'Immediate allergic reactions to gadolinium-based contrast agents: a systematic review and meta-analysis', *Radiology*, 286(2), pp. 471–482.

Bergin, C.J., Glover, G.H. and Pauly, J.M. (1991) 'Lung parenchyma: magnetic susceptibility in MR imaging', *Radiology*, 180(3), pp. 845-848.

Bianchi, A., Ozier, A., Ousova, O., Raffard, G. and Crémillieux, Y. (2013) 'Ultrashort-TE MRI longitudinal study and characterization of a chronic model of asthma in mice: inflammation and bronchial remodeling assessment', *NMR in Biomedicine*, 26(11), pp. 1451–1459.

Bickel, S., Popler, J., Lesnick, B. and Eid, N. (2014) 'Impulse oscillometry: interpretation and practical applications', *Chest*, 146(3), pp. 841–847.

BOC (2000) *Safety Data Sheet: Octafluoropropane (R218)*, *Material Safety Data Sheet*.

Available at: https://www.boconline.co.uk/en/products-and-supply/speciality-gas/pure-gases/perfluoropropane/perfluoropropane.html.

Bonini, M. and Usmani, O.S. (2015) 'The role of the small airways in the pathophysiology of asthma and chronic obstructive pulmonary disease', *Therapeutic Advances in Respiratory Disease*, 9(6), pp. 281–293.

Bossé, Y., Riesenfeld, E.P., Paré, P.D. and Irvin, C.G. (2009) 'It's not all smooth muscle: non-smooth-muscle elements in control of resistance to airflow', *Annual Review of Physiology*, 72, pp. 437–462.

Briscoe, W. and Dubois, A. (1958) 'The relationship between airway resistance, airway conductance, and lung volume in subjects of different age and body size', *The Journal of Clinical Investigation*, 37(9), pp. 1279–1285.

British Lung Foundation (2017) *Chronic obstructive pulmonary disease (COPD) statistics.* Available at: https://statistics.blf.org.uk/copd (Accessed: 22 December 2020).

British Thoracic Society (BTS)/Scottish Intercollegiate Guidelines Network (SIGN) (2014) 'British guideline on the management of asthma', *Thorax*, 69, pp. 1–192.

British Thoracic Society (BTS)/Scottish Intercollegiate Guidelines Network (SIGN) (2019) *SIGN 158: British guideline on the management of asthma.* Available at: https://www.brit-thoracic.org.uk/quality-improvement/guidelines/asthma/ (Accessed: 22 December 2020).

Bryan, A.C., Bentivoglio, L.G., Beerel, F., Macleish, H., Zidulka, A. and Bates, D.V. (1964) 'Factors affecting regional distribution of ventilation and perfusion in the lung', *Journal of Applied Physiology*, 19, pp. 395–402.

Callister, M.E.J., Baldwin, D.R., Akram, A.R., Barnard, S., Cane, P., Draffan, J., Franks, K., Gleeson, F., Graham, R., Malhotra, P., Prokop, M., Rodger, K., Subesinghe, M., Waller, D. and Woolhouse, I. (2015) 'British thoracic society guidelines for the investigation and management of pulmonary nodules', *Thorax*, 70, pp. ii1–ii54.

Capaldi, D.P.I., Sheikh, K., Eddy, R.L., Guo, F., Svenningsen, S., Nair, P., McCormack, D.G. and Parraga, G. (2017) 'Free-breathing functional pulmonary MRI: response to bronchodilator and bronchoprovocation in severe asthma', *Academic Radiology*, 24(10), pp. 1268–1276.

Carrero-González, L., Kaulisch, T. and Stiller, D. (2013) 'In vivo diffusion-weighted MRI using perfluorinated gases: ADC comparison between healthy and elastase-treated rat lungs', *Magnetic Resonance in Medicine*, 70(6), pp. 1761–1764.

Casanova, C., Cote, C., De Torres, J.P., Aguirre-Jaime, A., Marin, J.M., Pinto-Plata, V. and Celli, B.R. (2005) 'Inspiratory-to-total lung capacity ratio predicts mortality in patients with chronic obstructive pulmonary disease', *American Journal of Respiratory and Critical Care Medicine*, 171(6), pp. 591–597.

Cavalcanti, J.V., Lopes, A.J., Jansen, J.M. and Melo, P.L. (2006) 'Detection of changes in respiratory mechanics due to increasing degrees of airway obstruction in asthma by the forced oscillation technique', *Respiratory Medicine*, 100(12), pp. 2207–2219.

Chan, H.F., Stewart, N.J., Parra-Robles, J., Collier, G.J. and Wild, J.M. (2017) 'Whole lung morphometry with 3D multiple b-value hyperpolarized gas MRI and compressed sensing', *Magnetic Resonance in Medicine*, 77(5), pp. 1916–1925.

Chan, H.F., Weatherley, N.D., Johns, C.S., Stewart, N.J., Collier, G.J., Bianchi, S.M. and Wild, J.M. (2019) 'Airway microstructure in idiopathic pulmonary fibrosis: assessment at hyperpolarized 3He diffusion weighted MRI', *Radiology*, 291(1), pp. 223–229.

Chen, D.L., Cheriyan, J., Chilvers, E.R., Choudhury, G., Coello, C., Connell, M., Fisk, M., Groves, A.M., Gunn, R.N., Holman, B.F., Hutton, B.F., Lee, S., MacNee, W., Mohan, D., Parr, D., Subramanian, D., Tal-Singer, R., Thielemans, K., Van Beek, E.J.R., Vass, L., Wellen, J.W., Wilkinson, I. and Wilson, F.J. (2017) 'Quantification of lung PET images: challenges and opportunities', *Journal of Nuclear Medicine*, 58(2), pp. 201–207.

Chen, L., Liu, D., Zhang, J., Xie, B., Zhou, X., Grimm, R., Huang, X., Wang, J. and Feng, L. (2018) 'Free-breathing dynamic contrast-enhanced MRI for assessment of pulmonary lesions

using golden-angle radial sparse parallel imaging', *Journal of Magnetic Resonance Imaging*, 48(2), pp. 459–468.

Chon, D., Simon, B.A., Beck, K.C., Shikata, H., Saba, O.I., Won, C. and Hoffman, E.A. (2005) 'Differences in regional wash-in and wash-out time constants for xenon-CT ventilation studies', *Respiratory Physiology and Neurobiology*, 148(1-2), pp. 65–83.

Couch, M.J., Ball, I.K., Li, T., Fox, M.S., Littlefield, S.L., Biman, B. and Albert, M.S. (2013) 'Pulmonary ultrashort echo time 19F MR imaging with inhaled fluorinated gas mixtures in healthy volunteers: feasibility', *Radiology*, 269(3), pp. 903–909.

Couch, M.J., Ball, I.K., Li, T., Fox, M.S., Ouriadov, A.V., Biman, B. and Albert, M.S. (2014) 'Inert fluorinated gas MRI: a new pulmonary imaging modality', *NMR in Biomedicine*, 27(12), pp. 1525–1534.

Couch, M.J., Blasiak, B., Tomanek, B., Ouriadov, A.V., Fox, M.S., Dowhos, K.M. and Albert, M.S. (2015) 'Hyperpolarized and inert gas MRI: the future', *Molecular Imaging and Biology*, 17(2), pp. 149–162.

Couch, M.J., Fox, M.S., Viel, C., Gajawada, G., Li, T., Ouriadov, A.V. and Albert, M.S. (2016) 'Fractional ventilation mapping using inert fluorinated gas MRI in rat models of inflammation and fibrosis', *NMR in Biomedicine*, 29(5), pp. 545–552.

Couch, M.J., Ball, I.K., Li, T., Fox, M.S., Biman, B. and Albert, M.S. (2019a) '19F MRI of the lungs using inert fluorinated gases: challenges and new developments', *Journal of Magnetic Resonance Imaging*, 49(2), pp. 343–354.

Couch, M.J., Thomen, R., Kanhere, N., Hu, R., Ratjen, F., Woods, J. and Santyr, G. (2019b) 'A two-center analysis of hyperpolarized 129Xe lung MRI in stable pediatric cystic fibrosis: potential as a biomarker for multi-site trials', *Journal of Cystic Fibrosis*, 18(5), pp. 728–733.

Criée, C.P., Sorichter, S., Smith, H.J., Kardos, P., Merget, R., Heise, D., Berdel, D., Köhler, D., Magnussen, H., Marek, W., Mitfessel, H., Rasche, K., Rolke, M., Worth, H. and Jörres, R.A. (2011) 'Body plethysmography - its principles and clinical use', *Respiratory Medicine*,

105(7), pp. 959–971.

Cuenod, C.A. and Balvay, D. (2013) 'Perfusion and vascular permeability: basic concepts and measurement in DCE-CT and DCE-MRI', *Diagnostic and Interventional Imaging*, 94(12), pp. 1187–1204.

Currie, S., Hoggard, N., Craven, I.J., Hadjivassiliou, M. and Wilkinson, I.D. (2013) 'Understanding MRI: basic MR physics for physicians', *Postgraduate Medical Journal*, 89(1050), pp. 209–223.

Deninger, A.J., Eberle, B., Ebert, M., Großmann, T., Heil, W., Kauczor, H.U., Lauer, L., Markstaller, K., Otten, E., Schmiedeskamp, J., Schreiber, W., Surkau, R., Thelen, M. and Weiler, N. (1999) 'Quantification of regional intrapulmonary oxygen partial pressure evolution during apnea by 3He MRI', *Journal of Magnetic Resonance*, 141(2), pp. 207–216.

Diaz, S., Casselbrant, I., Piitulainen, E., Pettersson, G., Magnusson, P., Peterson, B., Wollmer, P., Leander, P., Ekberg, O. and Akeson, P. (2008) 'Hyperpolarized 3He apparent diffusion coefficient MRI of the lung: reproducibility and volume dependency in healthy volunteers and patients with emphysema', *Journal of Magnetic Resonance Imaging*, 27(4), pp. 763–770.

Dimitrov, I.E., Insko, E., Rizi, R. and Leigh, J.S. (2005) 'Indirect detection of lung perfusion using susceptibility-based hyperpolarized gas imaging', *Journal of Magnetic Resonance Imaging*, 21(2), pp. 149–155.

Doeing, D.C. and Solway, J. (2013) 'Airway smooth muscle in the pathophysiology and treatment of asthma', *Journal of Applied Physiology*, 114(7), pp. 834–843.

Dunham-Snary, K.J., Wu, D., Sykes, E.A., Thakrar, A., Parlow, L.R.G., Mewburn, J.D., Parlow, J.L. and Archer, S.L. (2017) 'Hypoxic pulmonary vasoconstriction: from molecular mechanisms to medicine', *Chest*, 151(1), pp. 181–192.

Ebner, L., Kammerman, J., Driehuys, B., Schiebler, M. L., Cadman, R. V. and Fain, S. B. (2017a) 'The role of hyperpolarized 129xenon in MR imaging of pulmonary function',

European Journal of Radiology, 86, pp. 343–352.

Ebner, L., He, M., Virgincar, R.S., Heacock, T., Kaushik, S.S., Freemann, M.S., McAdams, H.P., Kraft, M. and Driehuys, B. (2017b) 'Hyperpolarized 129Xenon magnetic resonance imaging to quantify regional ventilation differences in mild to moderate asthma: a prospective comparison between semiautomated ventilation defect percentage calculation and pulmonary function tests', *Investigative Radiology*, 52(2), pp. 120–127.

Eddy, R.L., Svenningsen, S., McCormack, D.G. and Parraga, G. (2018) 'What is the minimal clinically important difference for helium-3 magnetic resonance imaging ventilation defects?', *European Respiratory Journal*, 51(6), pp. 8–11.

Edelman, R.R., Hatabu, H., Tadamura, E., Li, W. and Prasad, P.V. (1996) 'Noninvasive assessment of regional ventilation in the human lung using oxygen-enhanced magnetic resonance imaging', *Nature Medicine*, 2(11), pp. 1236–1239.

Edelstein, W., Bottomley, P. and Pfeifer, L. (1984) 'A signal-to-noise calibration procedure for NMR imaging systems', *Medical Physics*, 11(2), pp. 180–185.

Essig, M., Shiroishi, M.S., Nguyen, T.B., Saake, M., Provenzale, J.M., Enterline, D., Anzalone, N., Dörfler, A., Rovira, À., Wintermark, M. and Law, M. (2013) 'Perfusion MRI: the five most frequently asked technical questions', *American Journal of Roentgenology*, 200(1), pp. 24–34.

Ester, M., Kriegel, H.-P., Sander, J. and Xu, X. (1996) 'A density-based algorithm for discovering clusters in large spatial databases with noise', *Proceedings of the Second International Conference on Knowledge Discovery and Data Mining (KDD-96)*, pp. 226–231.

Fain, S.B., Panth, S.R., Evans, M.D., Wentland, A.L., Holmes, J.H., Korosec, F.R., O'Brien, M.J., Fountaine, H. and Grist, T.M. (2006) 'Early emphysematous changes in asymptomatic smokers: detection with 3He MR imaging', *Radiology*, 239(3), pp. 875–883.

Fischer, A., Weick, S., Ritter, C.O., Beer, M., Wirth, C., Hebestreit, H., Jakob, P.M., Hahn,

D., Bley, T. and Köstler, H. (2014) 'SElf-gated Non-Contrast-Enhanced FUnctional Lung imaging (SENCEFUL) using a quasi-random fast low-angle shot (FLASH) sequence and proton MRI', *NMR in Biomedicine*, 27(8), pp. 907–917.

Fisher, A.J., Yadegarfar, M.E., Collerton, J., Small, T., Kirkwood, T.B.L., Davies, K., Jagger, C. and Corris, P.A. (2016) 'Respiratory health and disease in a UK population-based cohort of 85 year olds: the Newcastle 85+ study', *Thorax*, 71(3), pp. 255–266.

Fletcher, C. and Peto, R. (1977) 'The natural history of chronic airflow obstruction', *British Medical Journal*, 1(6077), pp. 1645–1648.

Fox, M.S., Gaudet, J.M. and Foster, P.J. (2015) 'Fluorine-19 MRI contrast agents for cell tracking and lung imaging', *Magnetic Resonance Insights*, 8(Suppl. 1), pp. 53–67.

Galvin, I., Drummond, G.B. and Nirmalan, M. (2007) 'Distribution of blood flow and ventilation in the lung: gravity is not the only factor', *British Journal of Anaesthesia*, 98(4), pp. 420–428.

Ginsburg, M.E., Thomashow, B.M., Yip, C.K., Dimango, A.M., Maxfield, R.A., Bartels, M. N., Jellen, P., Bulman, W.A., Lederer, D., Brogan, F.L., Gorenstein, L.A. and Sonett, J.R. (2011) 'Lung volume reduction surgery using the NETT selection criteria', *Annals of Thoracic Surgery*, 91(5), pp. 1556–1561.

Global Initiative for Asthma (GINA) (2020) *Global strategy for asthma management and prevention (2020 update)*. Available at: https://ginasthma.org/ (Accessed: 22 December 2020).

Global Initiative for Chronic Obstructive Lung Disease (GOLD) (2020) *Global strategy for the diagnosis, management, and prevention of chronic obstructive pulmonary disease (2020 report)*. Available at: https://goldcopd.org/ (Accessed: 22 December 2020).

Gono, H., Fujimoto, K., Kawakami, S. and Kubo, K. (2003) 'Evaluation of airway wall thickness and air trapping by HRCT in asymptomatic asthma', *European Respiratory Journal*, 22(6), pp. 965–971.

Goralski, J.L., Chung, S.H., Glass, T.M., Ceppe, A.S., Akinnagbe-Zusterzeel, E.O., Trimble, A.T., Boucher, R.C., Soher, B.J., Charles, H.C., Donaldson, S.H. and Lee, Y.Z. (2020) 'Dynamic perfluorinated gas MRI reveals abnormal ventilation despite normal FEV1 in cystic fibrosis', *JCI Insight*, 5(2), pp. e133400.

Gordon, Y., Partovi, S., Müller-Eschner, M., Amarteifio, E., Bäuerle, T., Weber, M.-A., Kauczor, H.-U. and Rengier, F. (2014) 'Dynamic contrast-enhanced magnetic resonance imaging: fundamentals and application to the evaluation of the peripheral perfusion.', *Cardiovascular diagnosis and therapy*, 4(2), pp. 147–164.

Goto, T., Nakata, Y., Ishiguro, Y., Niimi, Y., Suwa, K. and Morita, S. (2000) 'Minimum alveolar concentration-awake of xenon alone and in combination with isoflurane or sevoflurane', *Anesthesiology*, 93(5), pp. 1188–1193.

Gotway, M.B., Freemer, M.M. and King, T.E. (2007) 'Challenges in pulmonary fibrosis. 1: use of high resolution CT scanning of the lung for the evaluation of patients with idiopathic interstitial pneumonias', *Thorax*, 62(6), pp. 546–553.

Gulani, V., Calamante, F., Shellock, F.G., Kanal, E. and Reeder, S.B. (2017) 'Gadolinium deposition in the brain: summary of evidence and recommendations', *The Lancet Neurology*, 16(7), pp. 564–570.

Guo, B.J., Yang, Z.L. and Zhang, L.J. (2018) 'Gadolinium deposition in brain: current scientific evidence and future perspectives', *Frontiers in Molecular Neuroscience*, 11, pp. 335.

Gustafsson, P.M., De Jong, P.A., Tiddens, H.A.W.M. and Lindblad, A. (2008) 'Multiple-breath inert gas washout and spirometry versus structural lung disease in cystic fibrosis', *Thorax*, 63(2), pp. 129–134.

Gutberlet, M., Kaireit, T.F., Voskrebenzev, A., Lasch, F., Freise, J., Welte, T., Wacker, F., Hohlfeld, J.M. and Vogel-Claussen, J. (2018) 'Free-breathing dynamic19F gas MR imaging for mapping of regional lung ventilation in patients with COPD', *Radiology*, 286(3), pp. 1040–1051.

Gutberlet, M., Kaireit, T.F., Voskrebenzev, A., Kern, A.L., Obert, A., Wacker, F., Hohlfeld, J.M. and Vogel-Claussen, J. (2019) 'Repeatability of regional lung ventilation quantification using fluorinated (19F) gas magnetic resonance imaging', *Academic Radiology*, 26(3), pp. 395–403.

Halaweish, A.F., Moon, R.E., Foster, W.M., Soher, B.J., McAdams, H.P., MacFall, J.R., Ainslie, M.D., MacIntyre, N.R. and Charles, H.C. (2013a) 'Perfluoropropane gas as a magnetic resonance lung imaging contrast agent in humans', *Chest*, 144(4), pp. 1300–1310.

Halaweish, A., Foster, W., Moon, R., MacIntyre, N., MacFall, J. and Charles, H. (2013b) 'Dynamics of pulmonary ventilation distribution at steady state via 19Fluorine-enhanced MRI: initial experiences and future developments', *Procedings of the International Society for Magnetic Resonance in Medicine*, p. 4111.

Halaweish, A.F. and Charles, H.C. (2014) 'Physiorack: an integrated MRI safe/conditional, gas delivery, respiratory gating, and subject monitoring solution for structural and functional assessments of pulmonary function', *Journal of Magnetic Resonance Imaging*, 39(3), pp. 735–741.

Hall, E.J. and Brenner, D.J. (2008) 'Cancer risks from diagnostic radiology', *British Journal of Radiology*, 81(965), pp. 362–378.

Hamedani, H., Clapp, J.T., Kadlecek, S.J., Emami, K., Ishii, M., Gefter, W.B., Xin, Y., Cereda, M., Shaghaghi, H., Siddiqui, S., Rossman, M.D. and Rizi, R.R. (2016) 'Regional fractional ventilation by using multibreath wash-in 3He MR imaging', *Radiology*, 279(3), pp. 917–924.

Hammond, E., Sloan, C., Newell, J.D., Sieren, J.P., Saylor, M., Vidal, C., Hogue, S., De Stefano, F., Sieren, A., Hoffman, E.A. and Sieren, J.C. (2017) 'Comparison of low- and ultralow-dose computed tomography protocols for quantitative lung and airway assessment':, *Medical Physics*, 44(9), pp. 4747–4757.

Hanania, N.A., Celli, B.R., Donohue, J.F. and Martin, U.J. (2011) 'Bronchodilator reversibility in COPD', *Chest*, 140(4), pp. 1055–1063.

Harkness, L.M., Kanabar, V., Sharma, H.S., Westergren-Thorsson, G. and Larsson-Callerfelt, A.K. (2014) 'Pulmonary vascular changes in asthma and COPD', *Pulmonary Pharmacology and Therapeutics*, 29(2), pp. 144–155.

Harris, R.S., Winkler, T., Tgavalekos, N., Musch, G., Vidal Melo, M.F., Schroeder, T., Chang, Y. and Venegas, J.G. (2006) 'Regional pulmonary perfusion, inflation, and ventilation defects in bronchoconstricted patients with asthma', *American Journal of Respiratory and Critical Care Medicine*, 174(3), pp. 245–253.

He, M., Kaushik, S., Robertson, S., Freeman, M.S., Virgincar, R.S., McAdams, H.P. and Driehuys, B. (2014) 'Extending semi-automated ventilation defect analysis for hyperpolarized 129Xe ventilation MRI', *Academic Radiology*, 21(12), pp. 1530–1541.

Hogg, J.C. (2004) 'Pathophysiology of airflow limitation in chronic obstructive pulmonary disease', *Lancet*, 364(9435), pp. 709–721.

Hogg, J.C., Paré, P.D. and Hackett, T.L. (2017) 'The contribution of small airway obstruction to the pathogenesis of chronic obstructive pulmonary disease', *Physiological Reviews*, 97(2), pp. 529–552.

Hollingsworth, K.G. (2015) 'Reducing acquisition time in clinical MRI by data undersampling and compressed sensing reconstruction', *Physics in Medicine and Biology*, 60(21), pp. R297–R322.

Horn, F.C., Tahir, B.A., Stewart, N.J., Collier, G.J., Norquay, G., Leung, G., Ireland, R.H., Parra-Robles, J., Marshall, H. and Wild, J.M. (2014a) 'Lung ventilation volumetry with same-breath acquisition of hyperpolarized gas and proton MRI', *NMR in Biomedicine*, 27(12), pp. 1461–1467.

Horn, F.C., Deppe, M.H., Marshall, H., Parra-Robles, J. and Wild, J.M. (2014b) 'Quantification of regional fractional ventilation in human subjects by measurement of hyperpolarized 3He washout with 2D and 3D MRI', *Journal of Applied Physiology*, 116(2), pp. 129–139.

Horn, F.C., Marshall, H., Collier, G.J., Kay, R., Siddiqui, S., Brightling, C.E., Parra-Robles, J. and Wild, J.M. (2017a) 'Regional ventilation changes in the lung: treatment response mapping by using hyperpolarized gas MR imaging as a quantitative biomarker', *Radiology*, 284(3), pp. 854–861.

Horn, F.C., Rao, M., Stewart, N.J. and Wild, J.M. (2017b) 'Multiple breath washout of hyperpolarized 129Xe and 3He in human lungs with three-dimensional balanced steady-state free-precession imaging', *Magnetic Resonance in Medicine*, 77(6), pp. 2288–2295.

Horsley, A.R., Gustafsson, P.M., Macleod, K.A., Saunders, C., Greening, A.P., Porteous, D. J., Davies, J.C., Cunningham, S., Alton, E.W.F.W. and Innes, J.A. (2008) 'Lung clearance index is a sensitive, repeatable and practical measure of airways disease in adults with cystic fibrosis', *Thorax*, 63(2), pp. 135–140.

Horsley, A. (2009) 'Lung clearance index in the assessment of airways disease', *Respiratory Medicine*, 3(6), pp. 793–799.

Hosch, W., Schlieter, M., Ley, S., Heye, T., Kauczor, H.U. and Libicher, M. (2014) 'Detection of acute pulmonary embolism: feasibility of diagnostic accuracy of MRI using a stepwise protocol', *Emergency Radiology*, 21(2), pp. 151–158.

Hueper, K., Vogel-Claussen, J., Parikh, M.A., Austin, J.H.M., Bluemke, D.A., Carr, J., Choi, J., Goldstein, T.A., Gomes, A.S., Hoffman, E.A., Kawut, S.M., Lima, J., Michos, E.D., Post, W.S., Po, M.J., Prince, M.R., Liu, K., Rabinowitz, D., Skrok, J. *et al.* (2015) 'Pulmonary microvascular blood flow in mild chronic obstructive pulmonary disease and emphysema: the MESA COPD study', *American Journal of Respiratory and Critical Care Medicine*, 192(5), pp. 570–580.

Hughes, J., Glazier, J., Maloney, J. and West, J.B. (1968) 'Effect of lung volume on the distribution of pulmonary blood flow in man', *Respiration Physiology*, 4, pp. 58–72.

Hughes, J.M., Grant, B.J., Greene, R.E., Iliff, L.D. and Milic-Emili, J. (1972) 'Inspiratory flow rate and ventilation distribution in normal subjects and in patients with simple chronic bronchitis.', *Clinical Science*, 43(5), pp. 583–595.

Hughes, P.J.C., Horn, F.C., Collier, G.J., Biancardi, A., Marshall, H. and Wild, J.M. (2018) 'Spatial fuzzy c-means thresholding for semiautomated calculation of percentage lung ventilated volume from hyperpolarized gas and 1H MRI', *Journal of Magnetic Resonance Imaging*, 47(3), pp. 640–646.

Hughes, P.J.C., Smith, L., Chan, H.F., Tahir, B.A., Norquay, G., Collier, G.J., Biancardi, A., Marshall, H. and Wild, J.M. (2019) 'Assessment of the influence of lung inflation state on the quantitative parameters derived from hyperpolarized gas lung ventilation MRI in healthy volunteers', *Journal of Applied Physiology*, 126(1), pp. 183–192.

IEC 60601-2-33 (2010) *Particular requirements for the basic safety and essential performance of magnetic resonance equipment for medical diagnosis.* Available at: https://webstore.iec.ch/publication/2647. (Accessed: 22 December 2020).

Ingrisch, M., Maxien, D., Meinel, F.G., Reiser, M.F., Nikolaou, K. and Dietrich, O. (2016) 'Detection of pulmonary embolism with free-breathing dynamic contrast-enhanced MRI', *Journal of Magnetic Resonance Imaging*, 43(4), pp. 887–893.

IPCC (2013) *Climate Change 2013: The physical sceience basis. Contribution of working group I to the fifth assessment report of the Intergovernmental panel on climate change.* Available at: https://www.ipcc.ch/report/ar5/wg1/. (Accessed: 25 October 2021).

Iyer, R.S., Schopp, J.G., Swanson, J.O., Thapa, M.M. and Phillips, G.S. (2013) 'Safety essentials: acute reactions to iodinated contrast media', *Canadian Association of Radiologists Journal*, 64(3), pp. 193–199.

Jacob, R.E., Chang, Y.V., Choong, C.K., Bierhals, A., Hu, D.Z., Zheng, J., Yablonskiy, D.A., Woods, J.C., Gierada, D.S. and Conradi, M.S. (2005) '19F MR imaging of ventilation and diffusion in excised lungs', *Magnetic Resonance in Medicine*, 54(3), pp. 577–585.

Johns, C.S., Swift, A.J., Hughes, P.J.C., Ohno, Y., Schiebler, M. and Wild, J.M. (2017a) 'Pulmonary MR angiography and perfusion imaging - a review of methods and applications', *European Journal of Radiology*, 86, pp. 361–370.

Johns, C.S., Swift, A.J., Rajaram, S., Hughes, P.J.C., Capener, D.J., Kiely, D.G. and Wild, J.M. (2017b) 'Lung perfusion: MRI vs. SPECT for screening in suspected chronic thromboembolic pulmonary hypertension', *Journal of Magnetic Resonance Imaging*, 46(6), pp. 1693–1697.

Johnson, K.M., Fain, S.B., Schiebler, M.L. and Nagle, S. (2013) 'Optimized 3D ultrashort echo time pulmonary MRI', *Magnetic Resonance in Medicine*, 70(5), pp. 1241–1250.

Kaireit, T.F., Gutberlet, M., Voskrebenzev, A., Freise, J., Welte, T., Hohlfeld, J.M., Wacker, F. and Vogel-Claussen, J. (2018) 'Comparison of quantitative regional ventilation-weighted fourier decomposition MRI with dynamic fluorinated gas washout MRI and lung function testing in COPD patients', *Journal of Magnetic Resonance Imaging*, 47(6), pp. 1534–1541.

Kaireit, T.F., Voskrebenzev, A., Gutberlet, M., Freise, J., Jobst, B., Kauczor, H.U., Welte, T., Wacker, F. and Vogel-Claussen, J. (2019) 'Comparison of quantitative regional perfusion-weighted phase resolved functional lung (PREFUL) MRI with dynamic gadolinium-enhanced regional pulmonary perfusion MRI in COPD patients', *Journal of Magnetic Resonance Imaging*, 49(4), pp. 1122–1132.

Kakinuma, R., Moriyama, N., Muramatsu, Y., Gomi, S., Suzuki, M., Nagasawa, H., Kusumoto, M., Aso, T., Muramatsu, Y., Tsuchida, T., Tsuta, K., Maeshima, A.M., Tochigi, N., Watanabe, S.I., Sugihara, N., Tsukagoshi, S., Saito, Y., Kazama, M., Ashizawa, K. *et al.* (2015) 'Ultra-high-resolution computed tomography of the lung: image quality of a prototype scanner', *PLoS ONE*, 10(9), pp. e0137165.

Kaminsky, D.A. (2012) 'What does airway resistance tell us about lung function?', *Respiratory Care*, 57(1), pp. 85–99.

Kaminsky, D.A. (2019) 'What is a significant bronchodilator response?', *Annals of the American Thoracic Society*, 16(12), pp. 1495–1497.

Kandathil, A., Kay, F.U., Butt, Y.M., Wachsmann, J.W. and Subramaniam, R.M. (2018) 'Role of FDG PET/CT in the eighth edition of TNM staging of non-small cell lung cancer', *Radiographics*, 38(7), pp. 2134-2149.

Kaneko, K., Milic-Emili, J., Dolovich, M.B., Dawson, A. and Bates, D.V. (1966) 'Regional distribution of ventilation and perfusion as a function of body position', *Journal of Applied Physiology*, 21(3), pp. 767–777.

Katsoulis, K.K., Kostikas, K. and Kontakiotis, T. (2016) 'Techniques for assessing small airways function: possible applications in asthma and COPD', *Respiratory Medicine*, 119, pp. e2–e9.

Kaushik, S.S., Cleveland, Z.I., Cofer, G.P., Metz, G., Beaver, D., Nouls, J., Kraft, M., Auffermann, W., Wolber, J., McAdams, H.P. and Driehuys, B. (2011) 'Diffusion-weighted hyperpolarized 129Xe MRI in healthy volunteers and subjects with chronic obstructive pulmonary disease', *Magnetic Resonance in Medicine*, 65(4), pp. 1154–1165.

Kim, S.J., Lee, J., Park, Y.S., Lee, C.H., Yoon, H.I, Lee, S.M., Yim, J.J., Kim, Y.W., Han, S.K. and Yoo, C.G. (2015) 'Age-related annual decline of lung function in patients with COPD', *International Journal of COPD*, 11, pp. 51–60.

Kim, W.W., Lee, C.H., Goo, J.M., Park, S.J., Kim, J.H., Park, E.A. and Cho, S.H. (2012) 'Xenon-enhanced dual-energy CT of patients with asthma: dynamic ventilation changes after methacholine and salbutamol inhalation', *American Journal of Roentgenology*, 199(5), pp. 975–981.

Kirby, M., Mathew, L., Heydarian, M., Etemad-Rezai, R., McCormack, D.G. and Parraga, G. (2011) 'Chronic obstructive pulmonary disease: quantification of bronchodilator effects by using hyperpolarized 3He MR imaging', *Radiology*, 261(1), pp. 283–292.

Kirby, M., Svenningsen, S., Owrangi, A., Wheatley, A., Farag, A., Ouriadov, A., Santyr, G. E., Etemad-Rezai, R., Coxson, H.O., McCormack, D.G. and Parraga, G. (2012a) 'Hyperpolarized 3He and 129Xe MR imaging in healthy volunteers and patients with chronic obstructive pulmonary disease', *Radiology*, 265(2), pp. 600–610.

Kirby, M., Heydarian, M., Svenningsen, S., Wheatley, A., McCormack, D. G., Etemad-Rezai, R. and Parraga, G. (2012b) 'Hyperpolarized 3He magnetic resonance functional imaging semiautomated segmentation', *Academic Radiology*, 19(2), pp. 141–152.

Kirby, M., Heydarian, M., Wheatley, A., McCormack, D.G. and Parraga, G. (2012c) 'Evaluating bronchodilator effects in chronic obstructive pulmonary disease using diffusion-weighted hyperpolarized helium-3 magnetic resonance imaging', *Journal of Applied Physiology*, 112(4), pp. 651–657.

Kirby, M., Svenningsen, S., Kanhere, N., Owrangi, A., Wheatley, A., Coxson, H.O., Santyr, G.E., Paterson, N.A.M., McCormack, D.G. and Parraga, G. (2013) 'Pulmonary ventilation visualized using hyperpolarized helium-3 and xenon-129 magnetic resonance imaging: differences in COPD and relationship to emphysema', *Journal of Applied Physiology*, 114(6), pp. 707–715.

Kirby, M., Eddy, R.L., Pike, D., Svenningsen, S., Coxson, H.O., Sin, D., McCormack, D.G. and Parraga, G. (2017) 'MRI ventilation abnormalities predict quality-of-life and lung function changes in mild-to- moderate COPD: longitudinal TINCan study', *Thorax*, 72(5), pp. 475–478.

Kirby, M., Tanabe, N., Tan, W.C., Zhou, G., Obeidat, M., Hague, C.J., Leipsic, J., Bourbeau, J., Sin, D.D., Hogg, J.C. and Coxson, H.O. (2018) 'Total airway count on computed tomography and the risk of chronic obstructive pulmonary disease progression', *American Journal of Respiratory and Critical Care Medicine*, 197(1), pp. 56–65.

Kiselev, V.G. (2005) 'Transverse relaxation effect of MRI contrast agents: a crucial issue for quantitative measurements of cerebral perfusion', *Journal of Magnetic Resonance Imaging*, 22(6), pp. 693–696.

Kluge, A., Luboldt, W. and Bachmann, G. (2006) 'Acute pulmonary embolism to the subsegmental level: diagnostic accuracy of three MRI techniques compared with 16-MDCT', *American Journal of Roentgenology*, 187(1), p. W7-14.

Kolsum, U., Borrill, Z., Roy, K., Starkey, C., Vestbo, J., Houghton, C. and Singh, D. (2009) 'Impulse oscillometry in COPD: identification of measurements related to airway obstruction, airway conductance and lung volumes', *Respiratory Medicine*, 103(1), pp. 136–143.

Kong, X., Sheng, H.X., Lu, G.M., Meinel, F.G., Dyer, K.T., Schoepf, U.J. and Zhang, L.J. (2014) 'Xenon-enhanced dual-energy CT lung ventilation imaging: techniques and clinical applications', *American Journal of Roentgenology*, 202(2), pp. 309–317.

Konstantellou, E., Papaioannou, A.I., Loukides, S., Patentalakis, G., Papaporfyriou, A., Hillas, G., Papiris, S., Koulouris, N., Bakakos, P. and Kostikas, K. (2015) 'Persistent airflow obstruction in patients with asthma: characteristics of a distinct clinical phenotype', *Respiratory Medicine*, 109(11), pp. 1404–1409.

Kraft, M., Pak, J., Martin, R.J., Kaminsky, D. and Irvin, C.G. (2001) 'Distal lung dysfunction at night in nocturnal asthma', *American Journal of Respiratory and Critical Care Medicine*, 163(7), pp. 1551–1556.

Kruger, S.J., Nagle, S.K., Couch, M.J., Ohno, Y., Albert, M. and Fain, S.B. (2016) 'Functional imaging of the lungs with gas agents', *Journal of Magnetic Resonance Imaging*, 43(2), pp. 295–315.

Kuethe, D.O., Caprihan, A., Fukushima, E. and Waggoner, R.A. (1998) 'Imaging lungs using inert fluorinated gases', *Magnetic Resonance in Medicine*, 39(1), pp. 85–88.

Kuethe, D.O., Behr, V.C. and Begay, S. (2002) 'Volume of rat lungs measured throughout the respiratory cycle using 19F NMR of the inert gas SF6', *Magnetic Resonance in Medicine*, 48(3), pp. 547–549.

de Lange, E.E., Patrie, J.T., Mugler, J. and Platts-mills, T.A. (2009) 'Changes in regional airflow obstruction over time in the lungs of patients with asthma', *Radiology*, 250(2), pp. 567–575.

Ley, S. (2015) 'Lung imaging', *European Respiratory Review*, 24(136), pp. 240–245.

Lilburn, D.M.L., Pavlovskaya, G.E. and Meersmann, T. (2013) 'Perspectives of hyperpolarized noble gas MRI beyond 3He', *Journal of Magnetic Resonance*, 229, pp. 173–186.

Lomauro, A. and Aliverti, A. (2018) 'Sex differences in respiratory function', *Breathe*, 14(2), pp. 131–140.

Lowery, E.M., Brubaker, A.L., Kuhlmann, E. and Kovacs, E.J. (2013) 'The aging lung', *Clinical Interventions in Aging*, 8, pp. 1489–1496.

Ma, W., Sheikh, K., Svenningsen, S., Pike, D., Guo, F., Etemad-Rezai, R., Leipsic, J., Coxson, H.O., McCormack, D.G. and Parraga, G. (2015) 'Ultra-short echo-time pulmonary MRI: evaluation and reproducibility in COPD subjects with and without bronchiectasis', *Journal of Magnetic Resonance Imaging*, 41(5), pp. 1465–1474.

Macleod, K.A., Horsley, A.R., Bell, N.J., Greening, A.P., Lnnes, J.A. and Cunningham, S. (2009) 'Ventilation heterogeneity in children with well controlled asthma with normal spirometry indicates residual airways disease', *Thorax*, 64(1), pp. 33–37.

Marshall, H., Parra-Robles, J., Deppe, M.H., Lipson, D.A., Lawson, R. and Wild, J.M. (2014a) '3He pO2 mapping is limited by delayed-ventilation and diffusion in chronic obstructive pulmonary disease', *Magnetic Resonance in Medicine*, 71(3), pp. 1172–1178.

Marshall, H., Kiely, D.G., Parra-Robles, J., Capener, D., Deppe, M.H., Van Beek, E.J.R., Swift, A.J., Rajaram, S., Hurdman, J., Condliffe, R., Elliot, C.A. and Wild, J.M. (2014b) 'Magnetic resonance imaging of ventilation and perfusion changes in response to pulmonary endarterectomy in chronic thromboembolic pulmonary hypertension', *American Journal of Respiratory and Critical Care Medicine*, 190(5), pp. e18–e19.

Marshall, H., Horsley, A., Taylor, C.J., Smith, L., Hughes, D., Horn, F.C., Swift, A.J., Parra-Robles, J., Hughes, P.J., Norquay, G., Stewart, N.J., Collier, G.J., Teare, D., Cunningham, S., Aldag, I. and Wild, J.M. (2017) 'Detection of early subclinical lung disease in children with cystic fibrosis by lung ventilation imaging with hyperpolarised gas MRI', *Thorax*, 72(8), pp. 760–762.

Martinez, F.D. and Vercelli, D. (2013) 'Asthma', *The Lancet*, 382(9901), pp. 1360–1372.

Mathew, L., Evans, A., Ouriadov, A., Etemad-Rezai, R., Fogel, R., Santyr, G., McCormack,

D.G. and Parraga, G. (2008) 'Hyperpolarized 3He magnetic resonance imaging of chronic obstructive pulmonary disease. reproducibility at 3.0 Tesla', *Academic Radiology*, 15(10), pp. 1298–1311.

Mathew, L., Wheatley, A., Castillo, R., Castillo, E., Rodrigues, G., Guerrero, T. and Parraga, G. (2012) 'Hyperpolarized 3He magnetic resonance imaging: comparison with four-dimensional X-ray computed tomography imaging in lung cancer', *Academic Radiology*, 19(12), pp. 1546–1553.

Maunder, A., Rao, M., Robb, F. and Wild, J.M. (2019) 'Optimization of steady-state free precession MRI for lung ventilation imaging with 19F C3F8 at 1.5T and 3T', *Magnetic Resonance in Medicine*, 81(2), pp. 1130–1142.

Maunder, A., Chan, H.F., Hughes, P.J.C., Collier, G., Norquay, G., Rodgers, O., Thelwall, P., Robb, F., Rao, M. and Wild, J.M. (2021) 'MR properties of 19F C3F8 gas in the lungs of healthy volunteers: T2∗ and apparent diffusion coefficient at 1.5T and T2∗ at 3T', *Magnetic Resonance in Medicine*, 85(3), pp. 1561–1570.

McCallister, A., Chung, S.H., Antonacci, M., Powell, M.Z., Ceppe, A.S., Donaldson, S.H., Lee, Y.Z., Branca, R.T. and Goralski, J.L. (2020) 'Comparison of single breath hyperpolarized 129Xe MRI with dynamic 19F MRI in cystic fibrosis lung disease', *Magnetic Resonance in Medicine*, 85, pp. 1028–1038.

McCollough, C.H., Leng, S., Yu, L. and Fletcher, J.G. (2015) 'Dual-and multi-energy CT: principles, technical approaches, and clinical applications', *Radiology*, 276(3), pp. 637–653.

Milic-Emili, J., Henderson, J.A., Dolovich, M.B., Trop, D. and Kaneko, K. (1966) 'Regional distribution of inspired gas in the lung', *Journal of Applied Physiology*, 21(3), pp. 749–759.

Miller, M.R., Hankinson, J., Brusasco, V., Burgos, F., Casaburi, R., Coates, A., Crapo, R., Enright, P., van der Grinten, C.P.M., Gustafsson, P., Jensen, R., Johnson, D.C., MacIntrye, N., McKay, R., Navajas, D., Pedersen, O.F., Pellegrino, R., Viegi, G. and Wagner, J. (2005) 'Standardisation of spirometry', *European Respiratory Journal*, 26(2), pp. 319–338.

Mills, G.H., Wild, J.M., Eberle, B. and Van Beek, E.J.R. (2003) 'Functional magnetic resonance imaging of the lung', *British Journal of Anaesthesia*, 91(1), pp. 16–30.

Mirsadraee, M., Boskabady, M.H. and Attaran, D. (2013) 'Diagnosis of chronic obstructive pulmonary disease earlier than current Global Initiative for Obstructive Lung Disease guidelines using a feasible spirometry parameter (maximal-mid expiratory flow/forced vital capacity)', *Chronic Respiratory Disease*, 10(4), pp. 191–196.

Mitchell, A.M., Jones, A.E., Tumlin, J.A. and Kline, J.A. (2010) 'Incidence of contrast-induced nephropathy after contrast-enhanced computed tomography in the outpatient setting', *Clinical Journal of the American Society of Nephrology*, 5(1), pp. 4–9.

Moore, A.J.E., Wachsmann, J., Chamarthy, M.R., Panjikaran, L., Tanabe, Y. and Rajiah, P. (2018) 'Imaging of acute pulmonary embolism: an update', *Cardiovascular Diagnosis and Therapy*, 8(3), pp. 225–243.

Morris, D.G. and Sheppard, D. (2006) 'Pulmonary emphysema: when more is less', *Physiology*, 21(6), pp. 396–403.

Mugler, J.P. and Altes, T.A. (2013) 'Hyperpolarized 129Xe MRI of the human lung', *Journal of Magnetic Resonance Imaging*, 37(2), pp. 313–331.

Mühle, J., Ganesan, A.L., Miller, B.R., Salameh, P.K., Harth, C.M., Greally, B.R., Rigby, M., Porter, L.W., Steele, L.P., Trudinger, C.M., Krummel, P.B., O'Doherty, S., Fraser, P.J., Simmonds, P.G., Prinn, R.G. and Weiss, R.F. (2010) 'Perfluorocarbons in the global atmosphere: tetrafluoromethane, hexafluoroethane, and octafluoropropane', *Atmospheric Chemistry and Physics*, 10(11), pp. 5145–5164.

Müller, C.J., Schwaiblmair, M., Scheidler, J., Deimling, M., Weber, J., Löffler, R.B. and Reiser, M.F. (2002) 'Pulmonary diffusing capacity: assessment with oxygen-enhanced lung MR Imaging—preliminary findings', *Radiology*, 222(2), pp. 499–506.

Musch, G., Layfield, J.D.H., Harris, R.S., Melo, M.F.V., Winkler, T., Callahan, R.J., Fischman, A.J., Venegas, J.G., Layfield, J.D.H., Har, R.S., Melo, M.F.V., Winkler, T., Cal,

R.J., Fischman, A.J. and Topo, J.G.V. (2002) 'Topographical distribution of pulmonary perfusion and ventilation, assessed by PET in supine and prone humans', *Journal of Applied Physiology*, 93(5), pp. 1841–1851.

Nagao, M., Ichiki, T., Sakai, S., Yasuhara, Y. and Ikezoe, J. (2000) 'Quantitative analysis of Technegas SPECT: evaluation of regional severity of emphysema', *Journal of Nuclear Medicine*, 41(4), pp. 590–595.

Nakagawa, T., Sakuma, H., Murashima, S., Ishida, N., Matsumura, K. and Takeda, K. (2001) 'Pulmonary ventilation-perfusion MR imaging in clinical patients', *Journal of Magnetic Resonance Imaging*, 14(4), pp. 419–424.

National Institute for Health and Care Excellence (NICE) (2017) 'Asthma: diagnosis, monitoring and chronic asthma management', *NICE guideline 80*, pp.1-38. Available at: www.nice.org.uk/guidance/ng80. (Accessed: 22 December 2020).

Neal, M. (2017) '[19]F-MRI of inhaled perfluoropropane for quantitative imaging of pulmonary ventilation', PhD thesis, Newcastle University, Newcastle upon Tyne.

Neal, M.A., Pippard, B.J., Hollingsworth, K.G., Maunder, A., Dutta, P., Simpson, A.J., Blamire, A.M., Wild, J.M. and Thelwall, P.E. (2019) 'Optimized and accelerated 19F-MRI of inhaled perfluoropropane to assess regional pulmonary ventilation', *Magnetic Resonance in Medicine*, 82(4), pp. 1301–1311.

Neal, M.A., Pippard, B.J., Simpson, A.J. and Thelwall, P.E. (2020) 'Dynamic susceptibility contrast 19F-MRI of inhaled perfluoropropane: a novel approach to combined pulmonary ventilation and perfusion imaging', *Magnetic Resonance in Medicine*, 83(2), pp. 452–461.

Niles, D.J., Kruger, S.J., Dardzinski, B.J., Harman, A., Ruddy, M., Nagle, S.K. and Fain, S.B. (2013) 'Exercise-induced bronchoconstriction:reproducibility of hyperpolarized 3He MR imaging', 266(2), pp. 618–625.

O'Donnell, C.R., Bankier, A.A., Stiebellehner, L., Reilly, J.J., Brown, R. and Loring, S.H. (2010) 'Comparison of plethysmographic and helium dilution lung volumes: which is best for

COPD?', *Chest*, 137(5), pp. 1108–1115.

O'Sullivan, B., Couch, M., Roche, J.P., Walvick, R., Zheng, S., Baker, D., Johnson, M., Botfield, M. and Albert, M.S. (2014) 'Assessment of repeatability of hyperpolarized gas MR ventilation functional imaging in cystic fibrosis', *Academic Radiology*, 21(12), pp. 1524–1529.

Ochs, M., Nyengaard, J.R., Jung, A., Knudsen, L., Voigt, M., Wahlers, T., Richter, J. and Gundersen, H.J.G. (2004) 'The number of alveoli in the human lung', *American Journal of Respiratory and Critical Care Medicine*, 169(1), pp. 120–124.

Ohno, Y., Hatabu, H., Takenaka, D., Adachi, S., Van Cauteren, M. and Sugimura, K. (2001) 'Oxygen-enhanced MR ventilation imaging of the lung: preliminary clinical experience in 25 subjects', *American Journal of Roentgenology*, 177(1), pp. 185–194.

Ohno, Y., Hatabu, H., Takenaka, D., Van Cauteren, M., Fujii, M. and Sugimura, K. (2002) 'Dynamic oxygen-enhanced MRI reflects diffusing capacity of the lung', *Magnetic Resonance in Medicine*, 47(6), pp. 1139–1144.

Ohno, Y., Iwasawa, T., Joom, B.S., Koyama, H., Takahashi, H., Oh, Y.M., Nishimura, Y. and Sugimura, K. (2008) 'Oxygen-enhanced magnetic resonance imaging versus computed tomography: multicenter study for clinical stage classification of smoking-related chronic obstructive pulmonary disease', *American Journal of Respiratory and Critical Care Medicine*, 177(10), pp. 1095–1102.

Østergaard, L. (2005) 'Principles of cerebral perfusion imaging by bolus tracking', *Journal of Magnetic Resonance Imaging*, 22(6), pp. 710–717.

Ouriadov, A.V., Fox, M.S., Couch, M.J., Li, T., Ball, I.K. and Albert, M.S. (2015) 'In vivo regional ventilation mapping using fluorinated gas MRI with an x-centric FGRE method', *Magnetic Resonance in Medicine*, 74(2), pp. 550–557.

Park, E.A., Goo, J.M., Park, S.J., Lee, H.J., Lee, C.H., Park, C.M., Yoo, C.G. and Kim, J.H. (2010) 'Chronic obstructive pulmonary disease: quantitative and visual ventilation pattern

analysis at xenon ventilation CT performed by using a dual-energy technique', *Radiology*, 256(3), pp. 985–997.

Parraga, G., Mathew, L., Etemad-Rezai, R., McCormack, D.G. and Santyr, G.E. (2008) 'Hyperpolarized 3He magnetic resonance imaging of ventilation defects in healthy elderly volunteers: initial findings at 3.0 Tesla', *Academic Radiology*, 15(6), pp. 776–785.

Pasteur, M.C., Bilton, D. and Hill, A.T. (2010) 'British thoracic society guideline for non-CF bronchiectasis', *Thorax*, 65(Suppl. 1), pp. i1–58.

Peinado, V.I., Pizarro, S. and Barbera, J.A (2008) 'Pulmonary vascular involvement in COPD', *Chest,* 134(4), pp. 808–814.

Pellegrino, R., Viegi, G., Brusasco, V., Crapo, R.O., Burgos, F., Casaburi, R., Coates, A., van der Grinten, C.P.M., Gustafsson, P., Hankinson, J., Jensen, R., Johnson, D.C., MacIntyre, N., McKay, R., Miller, M.R., Navajas, D., Pedersen, O.F. and Wanger, J. (2005) 'Interpretative strategies for lung function tests', *European Respiratory Journal*, 26(5), pp. 948–968.

Pérez-Sánchez, J.M., de Alejo, R.P., Rodríguez, I., Cortijo, M., Peces-Barba, G. and Ruiz-Cabello, J. (2005) 'In vivo diffusion weighted 19F MRI using SF6', *Magnetic Resonance in Medicine*, 54(2), pp. 460–463.

Perisinakis, K., Seimenis, I., Tzedakis, A. and Damilakis, J. (2014) 'Perfusion scintigraphy versus 256-slice CT angiography in pregnant patients suspected of pulmonary embolism: comparison of radiation risks', *Journal of Nuclear Medicine*, 55(8), pp. 1273–1280.

Petersson, J., Sánchez-Crespo, A., Larsson, S.A. and Mure, M. (2007) 'Physiological imaging of the lung: single-photon-emission computed tomography (SPECT)', *Journal of Applied Physiology*, 102(1), pp. 468–476.

Petersson, J. and Glenny, R.W. (2014) 'Gas exchange and ventilation-perfusion relationships in the lung', *European Respiratory Journal*, 44(4), pp. 1023–1041.

Petousi, N., Talbot, N.P., Pavord, I. and Robbins, P.A. (2019) 'Measuring lung function in airways diseases: current and emerging techniques', *Thorax*, 74(8), pp. 797–805.

Pike, D., Kirby, M., Guo, F., McCormack, D.G. and Parraga, G. (2015) 'Ventilation heterogeneity in ex-smokers without airflow limitation', *Academic Radiology*, 22(8), pp. 1068–1078.

Prince, M.R., Lee, H.G., Lee, C.H., Youn, S.W., Lee, I.H., Yoon, W., Yang, B., Wang, H., Wang, J., Shih, T.T.F., Huang, G.S., Lirng, J.F. and Palkowitsch, P. (2017) 'Safety of gadobutrol in over 23,000 patients: the GARDIAN study, a global multicentre, prospective, non-interventional study', *European Radiology*, 27(1), pp. 286–295.

de Prost, N., Sasanelli, M., Deux, J.F., Habibi, A., Razazi, K., Galactéros, F., Meignan, M., Maître, B., Brun-Buisson, C., Itti, E. and Dessap, A.M. (2015) 'Positron emission tomography with 18F-Fluorodeoxyglucose in patients with sickle cell acute chest syndrome', *Medicine*, 94(18), pp. e821.

Qing, K., Mugler, J.P., Altes, T.A., Jiang, Y., Mata, J.F., Miller, G.W., Ruset, I.C., Hersman, F.W. and Ruppert, K. (2014) 'Assessment of lung function in asthma and COPD using hyperpolarized 129Xe chemical shift saturation recovery spectroscopy and dissolved-phase MRI', *NMR in Biomedicine*, 27(12), pp. 1490–1501.

Qing, K., Tustison, N.J., Mugler, J.P., Mata, J.F., Lin, Z., Zhao, L., Wang, D., Feng, X., Shin, J.Y., Callahan, S.J., Bergman, M.P., Ruppert, K., Altes, T.A., Cassani, J.M. and Shim, Y.M. (2019) 'Probing changes in lung physiology in COPD using CT, perfusion MRI, and hyperpolarized Xenon-129 MRI', *Academic Radiology*, 26(3), pp. 326–334.

Quanjer, P.H., Stanojevic, S., Cole, T.J., Baur, X., Hall, G.L., Culver, B.H., Enright, P.L., Hankinson, J.L., Ip, M.S.M., Zheng, J., Stocks, J. and Schindler, C. (2012) 'Multi-ethnic reference values for spirometry for the 3-95-yr age range: the global lung function 2012 equations', *European Respiratory Journal*, 40(6), pp. 1324–1343.

R Core Team (2015) *R: a language and environment for statistical computing*, R Foundation for statistical computing, Vienna, Austria.

Rabe, K.F. and Watz, H. (2017) 'Chronic obstructive pulmonary disease', *The Lancet*, 389(10082), pp. 1931–1940.

Rayment, J.H., Couch, M.J., McDonald, N., Kanhere, N., Manson, D., Santyr, G. and Ratjen, F. (2019) 'Hyperpolarised 129Xe magnetic resonance imaging to monitor treatment response in children with cystic fibrosis', *European Respiratory Journal*, 53(5), pp. 180-188.

Rhodes, C.G. and Hughes, J.M.B. (1995) 'Pulmonary studies using positron emission tomography', *European Respiratory Journal*, 8(6), pp. 1001–1017.

Rinck, P., Peterson, S., Heidelberger, E., Acuff, V., Reinders, J., Bernardo, M., Hedges, L. and Lauterbur, P. (1984) 'NMR ventilation imaging of the lungs using perfluorinated gases', *Magnetic Resonance in Medicine*, 1(2), p. 237.

Roach, P.J., Schembri, G.P. and Bailey, D.L. (2013) 'V/Q scanning using SPECT and SPECT/CT', *Journal of Nuclear Medicine*, 54(9), pp. 1588–1596.

Robinson, P.D., Latzin, P., Verbanck, S., Hall, G.L., Horsley, A., Gappa, M., Thamrin, C., Arets, H.G.M., Aurora, P., Fuchs, S.I., King, G.G., Lum, S., Macleod, K., Paiva, M., Pillow, J.J., Ranganathan, S., Ratjen, F., Singer, F., Sonnappa, S., Stocks, J., Subbarao, P., Thompson, B.R. and Gustafsson, P.M. (2013) 'Consensus statement for inert gas washout measurement using multiple- and singlebreath tests', *European Respiratory Journal*, 41(3), pp. 507–522.

Royal College of Radiologists (2015) *Standards for intravascular contrast agent administration to adult patients (Third Edition), RCR Guidelines*. Available at: https://www.rcr.ac.uk/sites/default/files/Intravasc_contrast_web.pdf. (Accessed: 22 December 2020).

Sakao, S., Voelkel, N.F. and Tatsumi, K. (2014) 'The vascular bed in COPD: pulmonary hypertension and pulmonary vascular alterations', *European Respiratory Review*, 23(133), pp. 350–355.

Sarkar, M., Niranjan, N. and Banyal, P.K. (2017) 'Mechanisms of hypoxemia', *Lung India,*

34(1), pp. 47–60.

Schenck, J.F. (1996) 'The role of magnetic susceptibility in magnetic resonance imaging: MRI magnetic compatibility of the first and second kinds', *Medical Physics*, 23(6), pp. 815–850.

Scholz, A.W., Wolf, U., Fabel, M., Weiler, N., Heussel, C.P., Eberle, B., David, M. and Schreiber, W.G. (2009) 'Comparison of magnetic resonance imaging of inhaled SF6 with respiratory gas analysis', *Magnetic Resonance Imaging*, 27(4), pp. 549–556.

Schönfeld, C., Cebotari, S., Voskrebenzev, A., Gutberlet, M., Hinrichs, J., Renne, J., Hoeper, M.M., Olsson, K.M., Welte, T., Wacker, F. and Vogel-Claussen, J. (2015) 'Performance of perfusion-weighted Fourier decomposition MRI for detection of chronic pulmonary emboli', *Journal of Magnetic Resonance Imaging*, 42(1), pp. 72–79.

Schreiber, W.G., Eberle, B., Laukemper-Ostendorf, S., Markstaller, K., Weiler, N., Scholz, A., Bürger, K., Heussel, C.P., Thelen, M. and Kauczor, H.U. (2001) 'Dynamic 19F-MRI of pulmonary ventilation using sulfur hexafluoride (SF6) gas', *Magnetic Resonance in Medicine*, 45(4), pp. 605–613.

Sciurba, F.C., Ernst, A., Herth, F.J.F., Strange, C., Criner, G.J., Marquette, C.H., Kovitz, K. L., Chiacchierini, R.P., Goldin, J. and McLennan, G. (2010) 'A randomized study of endobronchial valves for advanced emphysema', *New England Journal of Medicine*, 363(13), pp. 1233–1244.

Sciurba, F.C., Criner, G.J., Strange, C., *et al*. (2016) 'Effect of endobronchial coils vs usual care on exercise tolerance in patients with severe emphysema: the renew randomized clinical trial', *Journal of the American Medical Association*, 315(20), pp. 2178–2189.

Sergiacomi, G., Taglieri, A., Chiaravalloti, A., Calabria, E., Arduini, S., Tosti, D., Citraro, D., Pezzuto, G., Puxeddu, E. and Simonetti, G. (2014) 'Acute COPD exacerbation: 3T MRI evaluation of pulmonary regional perfusion - preliminary experience', *Respiratory Medicine*, 108(6), pp. 875–882.

Shah, M.K., Shin, W., Parikh, V.S., Ragin, A., Mouannes, J., Bernstein, R.A., Walker, M.T., Bhatt, H. and Carroll, T.J. (2010) 'Quantitative cerebral MR perfusion imaging: preliminary results in stroke.', *Journal of magnetic resonance imaging,* 32(4), pp. 796–802.

Sheikh, K., Coxson, H.O. and Parraga, G. (2016) 'This is what COPD looks like', *Respirology*, 21(2), pp. 224–236.

Sheikh, K., Guo, F., Capaldi, D.P.I., Ouriadov, A., Eddy, R.L., Svenningsen, S. and Parraga, G. (2017) 'Ultrashort echo time MRI biomarkers of asthma', *Journal of Magnetic Resonance Imaging*, 45(4), pp. 1204–1215.

Smith, L.J., Collier, G.J., Marshall, H., Hughes, P.J.C., Biancardi, A.M., Wildman, M., Aldag, I., West, N., Horsley, A. and Wild, J.M. (2018) 'Patterns of regional lung physiology in cystic fibrosis using ventilation magnetic resonance imaging and multiple-breath washout', *European Respiratory Journal*, 52(5), pp. 1–12.

Sorkness, R.L., Bleecker, E.R., Busse, W.W., Calhoun, W.J., Castro, M., Chung, K.F., Curran-Everett, D., Erzurum, S.C., Gaston, B.M., Israel, E., Jarjour, N.N., Moore, W.C., Peters, S.P., Teague, W.G. and Wenzel, S.E. (2008) 'Lung function in adults with stable but severe asthma: air trapping and incomplete reversal of obstruction with bronchodilation', *Journal of Applied Physiology*, 104(2), pp. 394–403.

Stein, P.D., Freeman, L.M., Sostman, H.D., Goodman, L.R., Woodard, P.K., Naidich, D.P., Gottschalk, A., Bailey, D.L., Matta, F., Yaekoub, A.Y., Hales, C.A., Hull, R.D., Leeper, K. V., Tapson, V.F. and Weg, J.G. (2009) 'SPECT in acute pulmonary embolism', *Journal of Nuclear Medicine*, 50(12), pp. 1999–2007.

Stewart, N.J., Chan, H.F., Hughes, P.J.C., Horn, F.C., Norquay, G., Rao, M., Yates, D.P., Ireland, R.H., Hatton, M.Q., Tahir, B.A., Ford, P., Swift, A.J., Lawson, R., Marshall, H., Collier, G.J. and Wild, J.M. (2018) 'Comparison of 3He and 129Xe MRI for evaluation of lung microstructure and ventilation at 1.5T', *Journal of Magnetic Resonance Imaging*, 48(3), pp. 632–642.

Stockley, J.A., Ismail, A.M., Hughes, S.M., Edgar, R., Stockley, R.A. and Sapey, E. (2017)

'Maximal mid-expiratory flow detects early lung disease in α1-antitrypsin deficiency', *European Respiratory Journal*, 49(3), pp. 1–10.

Subramanian, D.R., Gupta, S., Burggraf, D. *et al.* (2016) 'Emphysema- and airway-dominant COPD phenotypes defined by standardised quantitative computed tomography', *European Respiratory Journal*, 48(1), pp. 92–103.

Svenningsen, S., Kirby, M., Starr, D., Leary, D., Wheatley, A., Maksym, G.N., McCormack, D.G. and Parraga, G. (2013) 'Hyperpolarized 3He and 129Xe MRI: differences in asthma before bronchodilation', *Journal of Magnetic Resonance Imaging*, 38(6), pp. 1521–1530.

Svenningsen, S., Kirby, M., Starr, D., Coxson, H.O., Paterson, N.A.M., McCormack, D.G. and Parraga, G. (2014) 'What are ventilation defects in asthma?', *Thorax*, 69(1), pp. 63–71.

Svenningsen, S., Nair, P., Guo, F., McCormack, D.G. and Parraga, G. (2016) 'Is ventilation heterogeneity related to asthma control?', *European Respiratory Journal*, 48(2), pp. 370–379.

Svenningsen, S., McIntosh, M., Ouriadov, A., Matheson, A.M., Konyer, N.B., Eddy, R.L., McCormack, D.G., Noseworthy, M.D., Nair, P. and Parraga, G. (2020) 'Reproducibility of Hyperpolarized 129Xe MRI ventilation defect percent in severe asthma to evaluate clinical trial feasibility', *Academic Radiology*, S1076-6332(20), pp. 30237-3. E-pub ahead of print.

Swanney, M.P., Ruppel, G., Enright, P.L., Pedersen, O.F., Crapo, R.O., Miller, M.R., Jensen, R.L., Falaschetti, E., Schouten, J.P., Hankinson, J.L., Stocks, J. and Quanjer, P.H. (2008) 'Using the lower limit of normal for the FEV1/FVC ratio reduces the misclassification of airway obstruction', *Thorax*, 63(12), pp. 1046–1051.

Swift, A.J., Telfer, A., Rajaram, S., Condliffe, R., Marshall, H., Capener, D., Hurdman, J., Elliot, C., Kiely, D.G. and Wild, J.M. (2014) 'Dynamic contrast-enhanced magnetic resonance imaging in patients with pulmonary arterial hypertension', *Pulmonary Circulation*, 4(1), pp. 61–70.

Tantucci, C., Bottone, D., Borghesi, A., Guerini, M., Quadri, F. and Pini, L. (2016) 'Methods for measuring lung volumes: is there a better one?', *Respiration*, 91(4), pp. 273–280.

Theilmann, R.J., Arai, T.J., Samiee, A., Dubowitz, D.J., Hopkins, S.R., Buxton, R.B. and Prisk, G.K. (2009) 'Quantitative MRI measurement of lung density must account for the change in T2* with lung inflation', *Journal of Magnetic Resonance Imaging*, 30(3), pp. 527–534.

Thilmann, O., Larsson, E.M., Björkman-Burtscher, I.M., Ståhlberg, F. and Wirestam, R. (2005) 'Comparison of contrast agents with high molarity and with weak protein binding in cerebral perfusion imaging at 3 T', *Journal of Magnetic Resonance Imaging*, 22(5), pp. 597–604.

Thomas, E.T., Guppy, M., Straus, S.E., Bell, K.J.L. and Glasziou, P. (2019) 'Rate of normal lung function decline in ageing adults: a systematic review of prospective cohort studies', *BMJ Open*, 9(6), pp. e028150.

Trivedi, A., Hall, C., Hoffman, E.A., Woods, J.C., Gierada, D.S. and Castro, M. (2017) 'Using imaging as a biomarker for asthma', *Journal of Allergy and Clinical Immunology*, 139(1), pp. 1–10.

Turato, G., Zuin, R., Miniati, M., Baraldo, S., Rea, F., Beghé, B., Monti, S., Formichi, B., Boschetto, P., Harari, S., Papi, A., Maestrelli, P., Fabbri, L.M. and Saetta, M. (2002) 'Airway inflammation in severe chronic obstructive pulmonary disease: relationship with lung function and radiologic emphysema', *American Journal of Respiratory and Critical Care Medicine*, 166(1), pp. 105–110.

Verbanck, S., Schuermans, D., Van Muylem, A., Melot, C., Noppen, M., Vincken, W. and Paiva, M. (1998) 'Conductive and acinar lung-zone contributions to ventilation inhomogeneity in COPD', *American Journal of Respiratory and Critical Care Medicine*, 157(5), pp. 1573–1577.

Vidal Melo, M.F., Layfield, D., Harris, R.S., O'Neill, K., Musch, G., Richter, T., Winkler, T., Fischman, A.J. and Venegas, J.G. (2003) 'Quantification of regional ventilation-perfusion ratios with PET', *Journal of Nuclear Medicine*, 44(12), pp. 1982–1991.

Vidal Melo, M.F., Winkler, T., Harris, R.S., Musch, G., Greene, R.E. and Venegas, J.G.

(2010) 'Spatial heterogeneity of lung perfusion assessed with 13N PET as a vascular biomarker in chronic obstructive pulmonary disease', *Journal of Nuclear Medicine*, 51(1), pp. 57–65.

Vignaud, A., Maître, X., Guillot, G., Durand, E., De Rochefort, L., Robert, P., Vivès, V., Santus, R. and Darrasse, L. (2005) 'Magnetic susceptibility matching at the air-tissue interface in rat lung by using a superparamagnetic intravascular contrast agent: influence on transverse relaxation time of hyperpolarized helium-3', *Magnetic Resonance in Medicine*, 54(1), pp. 28–33.

Virgincar, R.S., Cleveland, Z.I., Kaushik, S.S., Freeman, M.S., Nouls, J., Cofer, G.P., Martinez-Jimenez, S., He, M., Kraft, M., Wolber, J., Mcadams, H.P. and Driehuys, B. (2013) 'Quantitative analysis of hyperpolarized 129Xe ventilation imaging in healthy volunteers and subjects with chronic obstructive pulmonary disease', *NMR in Biomedicine*, 26(4), pp. 424–435.

Vogel-Claussen, J., Schönfeld, C.O., Kaireit, T.F., Voskrebenzev, A., Czerner, C.P., Renne, J., Tillmann, H.C., Berschneider, K., Hiltl, S., Bauersachs, J., Welte, T. and Hohlfeld, J.M. (2019) 'Effect of indacaterol/glycopyrronium on pulmonary perfusion and ventilation in hyperinflated patients with chronic obstructive pulmonary disease (CLAIM). A double-blind, randomized, crossover trial', *American Journal of Respiratory and Critical Care Medicine*, 199(9), pp. 1086–1096.

Voskrebenzev, A., Gutberlet, M., Klimeš, F., Kaireit, T.F., Schönfeld, C., Rotärmel, A., Wacker, F. and Vogel-Claussen, J. (2018) 'Feasibility of quantitative regional ventilation and perfusion mapping with phase-resolved functional lung (PREFUL) MRI in healthy volunteers and COPD, CTEPH, and CF patients', *Magnetic Resonance in Medicine*, 79(4), pp. 2306–2314.

Walker, T.G. and Happer, W. (1997) 'Spin-exchange optical pumping of noble-gas nuclei', *Reviews of Modern Physics*, 69(2), pp. 629–642.

Wang, H., Naghavi, M., Allen, C., *et al.* (2016) 'Global, regional, and national life expectancy, all-cause mortality, and cause-specific mortality for 249 causes of death, 1980–

2015: a systematic analysis for the Global Burden of Disease Study 2015', *The Lancet*, 388(10053), pp. 1459–1544.

Wang, J.M., Robertson, S.H., Wang, Z., He, M., Virgincar, R.S., Schrank, G.M., Smigla, R.M., O'Riordan, T.G., Sundy, J., Ebner, L., Rackley, C.R., McAdams, P. and Driehuys, B. (2018) 'Using hyperpolarized 129Xe MRI to quantify regional gas transfer in idiopathic pulmonary fibrosis', *Thorax*, 73(1), pp. 21–28.

Wanger, J., Clausen, J.L., Coates, A., Pedersen, O.F., Brusasco, V., Burgos, F., Casaburi, R., Crapo, R., Enright, P., van der Grinten, C.P.M., Gustafsson, P., Hankinson, J., Jensen, R., Johnson, D.C., MacIntyre, N., McKay, R., Miller, M.R., Navajas, D., Pellegrino, R. and Veigi, G. (2005) 'Standardisation of the measurement of lung volumes', *European Respiratory Journal*, 26(3), pp. 511–522.

Washko, G.R., Hoffman, E. and Reilly, J.J. (2008) 'Radiographic evaluation of the potential lung volume reduction surgery candidate', *Proceedings of the American Thoracic Society*, 5(4), pp. 421–426.

Washko, G.R. and Parraga, G. (2018) 'COPD biomarkers and phenotypes: opportunities for better outcomes with precision imaging', *European Respiratory Journal*, 52(5), pp. 1–11.

Weatherley, N.D., Stewart, N.J., Chan, H.F., Hughes, P.J.C., Marshall, H., Austin, M., Smith, L., Collier, G., Rao, M., Norquay, G., Renshaw, S., Bianchi, S.M. and Wild, J.M. (2018) 'Probing diffusion and perfusion in idiopathic pulmonary fibrosis with hyperpolarised xenon and dynamic contrast-enhanced magnetic resonance imaging', *Thorax*, 73(Suppl. 4), p. A44-45.

Weatherley, N.D., Stewart, N.J., Chan, H.F., Austin, M., Smith, L.J., Collier, G., Rao, M., Marshall, H., Norquay, G., Renshaw, S.A., Bianchi, S.M. and Wild, J.M. (2019) 'Hyperpolarised xenon magnetic resonance spectroscopy for the longitudinal assessment of changes in gas diffusion in IPF', *Thorax*, 74(5), pp. 500–502.

Weibel, E.R. (2009) 'What makes a good lung? The morphometric basis of lung function', *Swiss Medical Weekly*, 139(27–28), pp. 375–386.

West, J.B. and Dollery, C.T. (1960) 'Distribution of blood flow and ventilation-perfusion ratio in the lung, measured with radioactive carbon dioxide', *Journal of applied physiology*, 15, pp. 405–410.

West, J.B. (1962) 'Regional differences in gas exchange in the lung of erect man', *Journal of Applied Physiology*, 17(6), pp. 893–898.

West, J.B. and Luks, A.M. (2016) *West's pulmonary physiology: the essentials*. (10th Ed.), Philadelphia: Wolters Kluwer.

Wild, J.M., Marshall, H., Bock, M., Schad, L.R., Jakob, P.M., Puderbach, M., Molinari, F., van Beek, E.J.R. and Biederer, J. (2012) 'MRI of the lung (1/3): Methods', *Insights into Imaging*, 3(4), pp. 345–353.

Wild, J.M. (2018) 'Imaging pathophysiological changes in the lungs in IPF with xenon magnetic resonance imaging', *Thorax*, 73(1), p. 1.

Wolf, U., Scholz, A., Heussel, C.P., Markstaller, K. and Schreiber, W.G. (2006) 'Subsecond fluorine-19 MRI of the lung', *Magnetic Resonance in Medicine*, 55(4), pp. 948–951.

Wolf, U., Scholz, A., Terekhov, M., Muennemann, K., Kreitner, K., Werner, C., Dueber, C. and Schreiber, W.G. (2008) 'Fluorine-19 MRI of the lung: first human experiment', *Proceedings of the International Society for Magnetic Resonance in Medicine,* 16, p. 3207.

Wolf, U., Scholz, A., Terekhov, M., Koebrich, R., David, M. and Schreiber, L.M. (2010) 'Visualization of inert gas wash-out during high-frequency oscillatory ventilation using fluorine-19 MRI', *Magnetic Resonance in Medicine*, 64(5), pp. 1478–1483.

World Health Organisation (2020) *Global health estimates: the top 10 causes of death.* Available at: https://www.who.int/news-room/fact-sheets/detail/the-top-10-causes-of-death. (Accessed: 22 December 2020).

Xu, J., Moonen, M., Johansson, Å., Gustafsson, A. and Bake, B. (2001) 'Quantitative analysis of inhomogeneity in ventilation SPET', *European Journal of Nuclear Medicine*,

28(12), pp. 1795–1800.

Yablonskiy, D.A., Sukstanskii, A.L. and Quirk, J.D. (2017) 'Diffusion lung imaging with hyperpolarized gas MRI', *NMR in Biomedicine*, 30(3), EPub:10.1002/nbm.3448.

Yii, A.C.A., Tan, G.L., Tan, K.L., Lapperre, T.S. and Koh, M.S. (2014) 'Fixed airways obstruction among patients with severe asthma: findings from the Singapore General Hospital-severe asthma phenotype study', *BMC Pulmonary Medicine*, 14(1), pp. 191.

Yushkevich, P.A., Piven, J., Hazlett, H.C., Smith, R.G., Ho, S., Gee, J.C. and Gerig, G. (2006) 'User-guided 3D active contour segmentation of anatomical structures: significantly improved efficiency and reliability', *NeuroImage*, 31(3), pp. 1116–1128.

Zhang, L.J., Zhou, C.S., Schoepf, U.J., Sheng, H.X., Wu, S.Y., Krazinski, A.W., Silverman, J.R., Meinel, F.G., Zhao, Y.E., Zhang, Z.J. and Lu, G.M. (2013) 'Dual-energy CT lung ventilation/perfusion imaging for diagnosing pulmonary embolism', *European Radiology*, 23(10), pp. 2666–2675.

Zhang, L., Tang, M., Min, Z., Lu, J., Lei, X. and Zhang, X. (2016) 'Accuracy of combined dynamic contrast-enhanced magnetic resonance imaging and diffusion-weighted imaging for breast cancer detection: a meta-analysis', *Acta Radiologica*, 57(6), pp. 651–660.

Zhang, W.J., Niven, R.M., Young, S.S., Liu, Y.Z., Parker, G.J.M. and Naish, J.H. (2015) 'Dynamic oxygen-enhanced magnetic resonance imaging of the lung in asthma - initial experience', *European Journal of Radiology*, 84(2), pp. 318–326.